Three Dimensional Control of a Diode Based Laser Cutter

Prepared by:

Phillip John Lowne Frost

FRSPHI001

Department of Electrical Engineering
University of Cape Town

Prepared for:

Samuel Ginsberg

ELECTRICAL ENGINEERING
University of Cape Town

February 2014

Submitted to the Department of Electrical Engineering at the University of Cape Town in partial fulfilment of the academic requirements for a Master of Science Degree in **ELECTRICAL ENGINEERING**.

Key Words: **Laser cutter, Laser diode, Infrared, Phase detector, Optical Distance Measurement, Arduino, MATLAB, x-y gantry.**

Declaration

1. I know that plagiarism is wrong. Plagiarism is to use another's work and pretend that it is one's own.
2. I have used the IEEE convention for citation and referencing. Each contribution to, and quotation in this masters report from the work(s) of other people, has been attributed and has been cited and referenced.
3. This report is my own work.
4. I have not allowed, and will not allow, anyone to copy my work with the intention of passing it off as their own work or part thereof.

Name: **Phillip John Lowne Frost**

Signature: _____ **Date:** 24 May 2014

Acknowledgements

God – for leading me throughout this project

Samuel Ginsberg (my supervisor) – for advice, guidance and always being available

My girlfriend – for understanding and listening

My parents – for encouragement and support

My colleagues in the Tomography lab – for all those late nights and interest in my progress

National Research Foundation – for Scarce Skills Development funding

Abstract

Laser cutting is a widely used technology in many areas of industry and research. Conventional laser cutters only offer control of two axes and either cut through a material or rudimentary control of the third dimension is possible by varying the power, pulse rate and travel rate of the laser beam. These rudimentary three-dimensional systems (often called 2.5D laser cutters) do not incorporate any feedback mechanism to control the depth of cut.

The idea of measuring distance using diode lasers (and other laser technologies) is a relatively mature technology and is common to various consumer and industrial products. Recently diode lasers have become powerful enough to perform as laser cutters allowing a merger of these technologies.

The aim of this project is to verify the concept of using a laser diode to achieve both material processing and distance measurement. This would allow the creation of a full three-dimension laser-cutting machine that is capable of accurate material processing in all three dimensions. This would also offer the ability to cut non-homogenous materials, such as timber, which current '2.5D' laser cutters are unable to cut with any accuracy.

A gantry system was designed and constructed, which was able to move the laser cutting toolhead in the x-y plane, using stepper motors and a belt-driven drive system. A 2W single emitter laser diode was used for both laser cutting and distance measurement. Optics were designed and assembled that focused the laser onto the workpiece and directed light reflected back from the workpiece onto a photodiode. Laser driver circuitry was constructed to control the DC current of the laser and to modulate the laser power at the high frequencies required for accurate phase shift measurements. A photodetector and phase shift measurement circuit was designed, simulated and constructed. The phase shift circuit amplified the signal from the light reflected off the workpiece and then compared that signal to a reference signal in order to determine the phase shift between the two. An *Atmel*® ATmega2560 microcontroller was used to control the gantry, laser driver circuitry and to measure the phase shift output of the phase detector circuitry. Software written in *MATLAB*® was used to command the microcontroller and to interpret the data received from the microcontroller.

The photo sensor circuit was not sensitive enough to detect the weak signals that were present when the workpiece had a low reflectivity but was able to be tested using reflective tape. On the other hand the laser diode was not powerful enough to cut reflective tape as it absorbs very little energy from the laser. Nevertheless, the same laser diode was used, without changing any configuration other than the workpiece material, to measure distance and to cut materials.

Testing of both the materials processing ability and the distance measurement ability were carried out. Many aspects of each of these major functions were tested, individually and together, in order to determine the areas that performed well and those that need more research.

In conclusion, this project was able to verify the concept of a three-dimensionally controlled diode powered laser cutter. Future work will be needed before a practical and useful laser cutter can be built but this project should prove a good starting point for any such future work.

Table of Contents

List of Figures

List of Illustrations

List of Tables

Nomenclature

AC	– **A**lternating **C**urrent
ADC	– **A**nalogue to **D**igital **C**onverter
AEL	– **A**ccessible **E**mission **L**imit
CAD	– **C**omputer **A**ssisted **D**esign
CCD	– **C**harge-**C**oupled **D**evice
CNC	– **C**omputer **N**umerically **C**ontrolled
DAC	– **D**igital to **A**nalogue **C**onverter
DC	– **D**irect **C**urrent
DOF	– **D**egree **O**f **F**reedom
EERPOM	– **E**lectrically **E**rasable **P**rogrammable **R**ead-**O**nly **M**emory
FFT	– **F**ast **F**ourier **T**ransform
FM	– **F**requency **M**odulated
FMCW	– **F**requency **M**odulated **C**ontinuous-**W**ave
FWHM	– **F**ull **W**idth at **H**alf **M**aximum
GBWP	– **G**ain-**B**and**W**idth **P**roduct
GPIO	– **G**eneral **P**urpose **I**nput **O**utput
GUI	– **G**raphical **U**ser **I**nterface
HMI	– **H**uman **M**achine **I**nterface
IC	– **I**ntegrated **C**ircuit
IDE	– **I**ntegrated **D**evelopment **E**nvironment
IEC	– **I**nternational **E**lectrotechnical **C**ommission
IIC	– **I**nter-**I**ntegrated **C**ircuit
LASER (or laser)	– **L**ight **A**mplification by **S**timulated **E**mission of **R**adiation
LCD	– **L**iquid **C**rystal **D**isplay
LED	– **L**ight **E**mitting **D**iode
LSB	– **L**east **S**ignificant **B**it
LVDS	– **L**ow-**V**oltage **D**ifferential **S**ignalling
LVPECL	– **L**ow-**V**oltage **P**ositive **E**mitter-**C**oupled **L**ogic
MSB	– **M**ost **S**ignificant **B**it
NA	– **N**umeric **A**perture
Nd:YAG	– **N**eodymium-**d**oped **Y**ttrium **A**luminium **G**arnet
PCB	– **P**rinted **C**ircuit **B**oard
PIN	– **P**-type **I**ntrinsic **N**-type photodiode
PWM	– **P**ulse **W**idth **M**odulated
RC	– **R**esistor - **C**apacitor
RF	– **R**adio **F**requency
SCI	– **S**erial **C**ommunications **I**nterface
SMA	– **S**ub**M**iniature version **A**
SPI	– **S**erial **P**eripheral **I**nterface
SSI	– **S**imple **S**erial **I**nterface
UART	– **U**niversal **A**synchronous **R**eceiver/**T**ransmitter

1. Introduction

1.1 Background to the Study

Industrial grade laser cutters have been available since 1971 when the first flatbed cutter was introduced by Laser Work AG [1, p. 23]. Most laser cutters are either 2-dimensional or 2.5-dimensional laser cutters where they can cut in an 'x'-'y' plane but only have rudimentary control of the 'z' plane. This control is usually achieved by specifying the material to be cut. By using predefined properties of that material, the cutter can predict how deep a specific cut will be. There is no feedback mechanism and therefore not much depth control of the cut. This method works very badly on non-homogeneous materials such as wood.

1.2 Objectives of this Study

The aim of this project is to verify the concept and build a three-dimensional laser cutter.

The requirements are to build a 2-dimensional laser cutter using a laser diode. Research into the z-axis control mechanism will be performed and evaluated.

The laser cutter will be small enough to fit on a desktop and will have a working volume of about 300x220x50 mm. It will also be safe to operate without any personal protective equipment, as the laser will be fully enclosed.

1.2.1 Problems to be investigated

The major problem to be investigated is the achievable distance accuracy with a laser modulated at 100MHz using phase shift measurement to measure the distance. Many challenges will be faced while investigating this problem; problems that are expected to arise are modulating a high-powered laser diode at these high frequencies, the optical control of this laser radiation and receiving signals reflected from the workpiece in order to measure the phase shift.

A mechanically simple and robust apparatus also needs to be constructed; this apparatus will be required to move the laser in the horizontal plane similarly to the movement of conventional laser cutters.

1.3 Motivation

Being able to laser cut with full control of the z-plane would be very important in the design and manufacture process, as it could be used in almost every application where conventional 3-dimensional printers and CNC milling machines are used. A three dimensional laser cutter could also be used in industry to replace conventional milling machines as the non-contact nature of laser cutting makes it a lot more reliable and repeatable.

Many designers do not have a quick, accurate and cheap way of converting 3-dimensional computer models into physical parts. Most designers use 3-dimensional printers or CNC milling machines to do this but these machines are either costly or inaccurate.

1.4 Scope

In order to build a functioning 3-dimensional laser cutter many aspects of the laser cutter's design have to be taken into account. Initially a standard 2-dimensional laser cutter will need to be built, then distance measuring ability will be added and finally software will be written to control the cutting and testing procedure.

The scope of this project is to verify that all the aspects required to build a functioning 3-dimensional laser cutter are possible. A fully functional 3-dimensional laser cutter is not required although all design work should be performed with the goal being to build a fully functional 3-dimensional laser cutter.

This aim of this project is to achieve the following goals:

- A comprehensive literature review of the physical theory of lasers, mechanical systems, electronics, optics and distance measurement techniques. This will include detailed research findings on the advantages and disadvantages of all the different possibilities in each of the research areas.

- Design and construct the mechanical frame to both move the laser in an x-y plane and to prevent any direct or incident laser radiation escaping the laser cutter while running.

- Design and construct the optical system involved in laser cutting including the laser housing, lenses to focus the beam, mirrors to direct the beam and a photodetector to detect the reflected radiation.

- Design and implement electronics used to drive the motors, power the laser, compare the laser beam phase with the phase of the reflected beam and calculate the distance, process the software and communicate with a PC.

- Design a suitable and accurate test rig in order to verify the accuracy of the distance measurement.

- Test the accuracies of the abovementioned components.

- Test the cutting ability of a 2W laser diode on different materials.

- Draw conclusions from the work done, comment on the feasibility of such a system and make recommendations on future work required.

1.5 Limitations

Due to the nature of this project and physical limitations, a number of limitations were identified and accepted.

These include:

- A lower powered laser diode will have to be used because of the safety issues and high prices associated with higher-powered laser diodes. A 2W diode should be able to prove that the concept is possible.

- Simpler optics will be employed as optical elements are very expensive and reasonable results should be achievable without the levels of sophistication required in high performance cutters.

- Frequencies above 100MHz were not explored, as this would require high frequency and RF components, board layout and many other issues experienced in RF electronics.

1.6 Plan of Development

Mechanical and electrical design will be completed within the first 4 months including CAD drawings and construction methods.

Mechanical construction will be carried out followed by photodetector circuitry construction and testing with a CD drive laser. Constant and modulated current laser driver circuitry will then be designed, implemented and tested allowing the optical phase of the project to commence. The optics will then be assembled and tested. All these components will be combined and tested together. Software will need to be developed throughout this process, as it will be required to test all of the components individually as well as the final assembly. Testing and analysis will then be done for a month and the final project write up should be completed before February 2014.

Most of the equipment needed to manufacture the laser cutter is available at UCT. A lot of materials and components will need to be purchased and are available from various South African retailers. Personal protective equipment such as laser goggles will need to be purchased for use during the construction of the project and these are available both locally and internationally.

This document will consist of 15 chapters as can be seen in the table of contents. These follow roughly the same chronological order that the project was completed in: '*Introduction*', '*Literature Review*', '*Design Specification*', '*Preliminary Design*', '*Mechanical Design*', '*Optics*', '*Laser Driver*', '*Photo Sensor and Phase Detector*', '*Miscellaneous Circuitry*', '*Software*', '*Final Testing, Results and Discussion*', '*Conclusions*', '*Recommendations*', '*List of References*' and '*Appendices*'. Each of these chapters describe, in detail, the processes that were followed and the decisions made throughout the project.

2. Literature Review

This chapter contains research into relevant books, articles, papers and other forms of publication that were consulted during the design and development of this project. The project was divided into various sections for the purpose of the literature review with each section being thoroughly researched.

2.1 Laser Definition and Characteristics

"A laser can be considered as a source of a narrow beam of monochromatic, coherent light in the visible, infrared, or ultraviolet parts of the spectrum" [2, p. 2]. Continuous wave lasers range from milliwatts to megawatts and pulsed lasers can reach powers in the terawatt range although only for very short pulse durations. [2, p. 2]

2.2 History of Lasers

The name LASER is an acronym for "Light Amplification by Stimulated Emission of Radiation". [3] Lasers are a relatively new technology when compared to many other similar technologies although they have been developed at a substantial rate since their invention.

2.2.1 Laser theory

The theory behind lasers involves the idea of stimulated emission. Stimulated emission is when a photon interacts with an atom in an excited energy state and causes that atom to drop to a lower energy level and emit a photon with identical properties to the first. "The idea of stimulated emission originated with Albert Einstein in 1916" [2, p. 14]. "Einstein formulated the concept of stimulated emission by combining Planck's law and Boltzmann statistics. Einstein's discovery of stimulated emission provided essentially all of the theory necessary to describe the physical principal of the laser" [4, p. 2]. Stimulated emission is unlikely in the real word as atoms are usually in lower energy levels at thermodynamic equilibrium. This means that the majority of photons are absorbed rather than stimulate emission. The first evidence for stimulated emission was demonstrated by Ladenburg in 1928. [2, p. 14]

2.2.2 MASER

The MASER was the predecessor of the laser in that it operates by the same principals but in the microwave region. MASER is an acronym for "Microwave Amplification by the Stimulated Emission of Radiation" [3]. The first successful maser was developed by Charles Townes and Arthur Schawlow at Bell Labs in the 1950s. [5, p. 10] "In 1959 Gould introduced the acronym LASER, for Light Amplification by Stimulated Emission of Radiation" [5, p. 10].

2.2.3 Laser construction

The first laser was presented by Theodore Maiman in May 1960 and a simplified view of its construction can be seen in Figure 2-1 [6]. "Maiman used a flash lamp to pump a synthetic ruby crystal to produce red light at a wavelength of 694nm." [5, p. 11]. This laser was only capable of pulsed

operation. The first gas laser, a helium and neon (He-Ne), laser was built in 1961 by Ali Javan, William Bennet and Donald Herriot, which operated at a wavelength of 1150 nm. [5, p. 11]

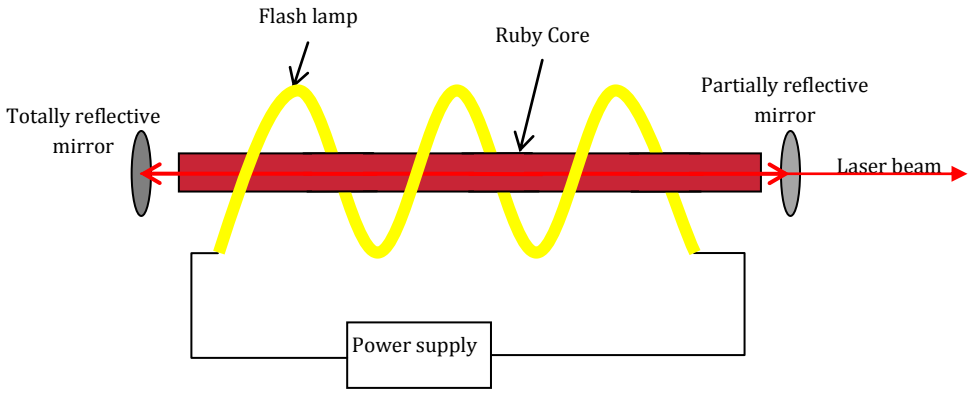

Figure 2-1. A simplified view of the ruby laser built by Theodore Maiman. [2]

2.2.4 *Laser diodes*

"The first injection laser diode used gallium arsenide (GaAs) and emitted radiation at 850nm" [5, p. 11]. This laser was built by Robert Hall in September 1962 and was based on the work done by Nikolai Basov's group at the Laser Physics Institute in Moscow. The first heterojunction laser diodes were developed in the 1970s independently by both Izuo Hayashi and Morton Panish of Bell labs and Zhores Alferov; these were the first lasers capable of operating at room temperatures. [5, p. 11]. Diode lasers are now the most common form of laser in the world used extensively in fibre-optic communications and CD/DVD/Blu-ray drives amongst others.

2.2.5 *Laser materials processing*

It was soon realised that lasers would become vital in the manufacturing sector due to their ability to work materials without making physical contact with them. Ruby lasers were the first to be used in manufacturing but this soon spread to other more powerful laser types as they were discovered. [2, p. 19]. The majority of materials processing is currently carried out by either gas (e.g. CO_2) or pumped solid state (e.g. Nd:YAG) lasers.

2.3 Different Types of Lasers

Commercially available lasers can generally be divided into 3 categories namely; solid-state lasers, gas lasers and laser diodes. Their fundamental differences, major uses and their properties are discussed here.

2.3.1 *Solid state lasers*

The first working laser was a ruby laser, built by Theodore Maiman in May 1960 [6]. This was an example of a solid-state laser and it was constructed with a flashbulb coiled around a ruby core, the visible light from the flash bulb excited chromium atoms in the ruby moving them to a higher energy state. If one of the atoms spontaneously emitted a photon this would cause stimulated emission in another chromium atom producing two photons. These photons then induce stimulated emission in two other chromium atoms producing four photons and so on. This is how all solid state lasers operate

although, of course, they have different cores, they can be excited (or optically pumped) by different radiation sources and different types of atoms (ions) can produce the lasing effect. [7]

Solid-state lasers consist of a host material that is doped with various ions. The host material needs to be transparent at both the optical pumping frequency and the lasing frequency and have good mechanical and thermal properties. The dopants are trivalent and divalent rare earth metals and transition metals. The trivalent neodymium (Nd^{3+}) "was known to exhibit a satisfactorily long fluorescence lifetime and narrow fluorescence line widths in crystals with ordered structures" and "continuous wave operation at room temperature was readily feasible" [4, p. 29]. Suitable hosts for neodymium were not found at first but finally Yttrium Aluminium Garnet (YAG) was discovered to be superior to all other host materials. Nd:YAG lasers are now one of the most common solid state lasers.

2.3.2 Gas lasers

In gas lasers "a light emitting vapour is confined inside a hollow tube with mirrors on either end. Passing an electric discharge through the gas excites the gas atoms to states in which they can generate stimulated emission" [7]. Gas lasers can achieve very large power outputs and are commonly used in manufacturing because of their lower cost and high output powers. Gas lasers need a very high voltage, typically in the order of 1000 – 1500V DC. [8]

2.3.3 Laser diode

Laser diodes are a form of solid-state diode but differ "by their stimulation principle: While other solid-state laser media have to be pumped optically, semiconductor lasers are directly pumped by supplying electrical current" [9, p. 163]. The electrical characteristics of a laser diode are similar to those of normal electrical diodes. Laser diodes achieve high efficiencies of 50 to 70% and the average power per area of active material is very high. [9, p. 164] "On the other hand the technological principals limit the size of the active volume". "Therefore, despite very high-power densities achieved in the active medium, only absolute output power of a few watts can be extracted from a single laser diode. For this reason, typically laser diode arrays – also called laser diode bars – are employed when high output power is required" [9, p. 164].

2.4 The Physics of Laser Radiation

Considering an ideal material, that has only two nondegenerate energy levels E_1 and E_2, all atoms will be in one of these two energy levels. For an atom to transition from state E_1 to E_2 it needs to absorb energy and to transition from E_2 to E_1 it will need to emit energy. [4, p. 4] This energy is absorbed and emitted as a photon. Emission can be either spontaneous or stimulated. Figure 2-1 shows the three possible different interactions that can cause an atom to change state. In "spontaneous emitting atoms there is no phase relationship between the individual emission processes; the quanta emitted are incoherent" [4, p. 5]. In stimulated emission, one photon stimulates an atom to drop to a lower energy state emitting another photon. "Stimulated emission provides a phase-coherent amplification mechanism for the applied signal. The signal extracts from the atoms a response that is directly proportional to, and phase coherent with, the electric field of the stimulating signal" [4, p. 7]. "The stimulated emission is, in fact, completely indistinguishable from the stimulating radiation field." [4, p. 7]. Meaning that, "the stimulated emission has the same directional properties, same polarization, same phase, and same spectral characteristics as the stimulation emission." [4, p. 7]. These are the reasons behind the high levels of coherence that are found in lasers.

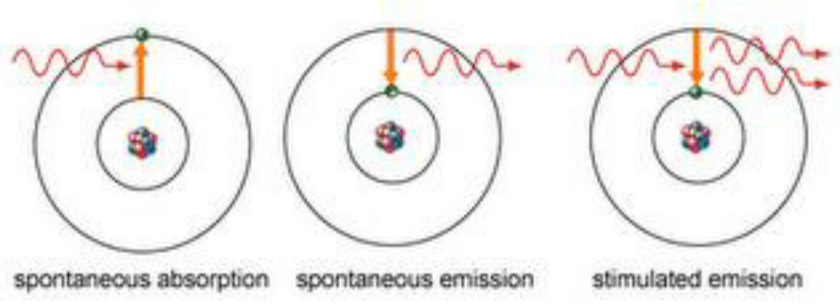

Figure 2-2. Showing the three possible interactions of electrons and photons. [10]

Only the simplest lasers, such as the ammonia laser, have two energy states. Most lasers have 3 or 4 energy states. In three state lasers, the electrons are excited to a high-energy state where they spontaneously drop to a more stable lower energy state, or metastable state. Stimulated emission then occurs emitting photons and dropping the atoms back to the lowest energy state. The fact that atoms in the ground state will absorb photons from nearby emissions means that three level lasers are generally limited to pulsed operation. In four state lasers, there is another state between the metastable state and the ground state meaning that these lasers are usually capable of continuous wave operation. [11]

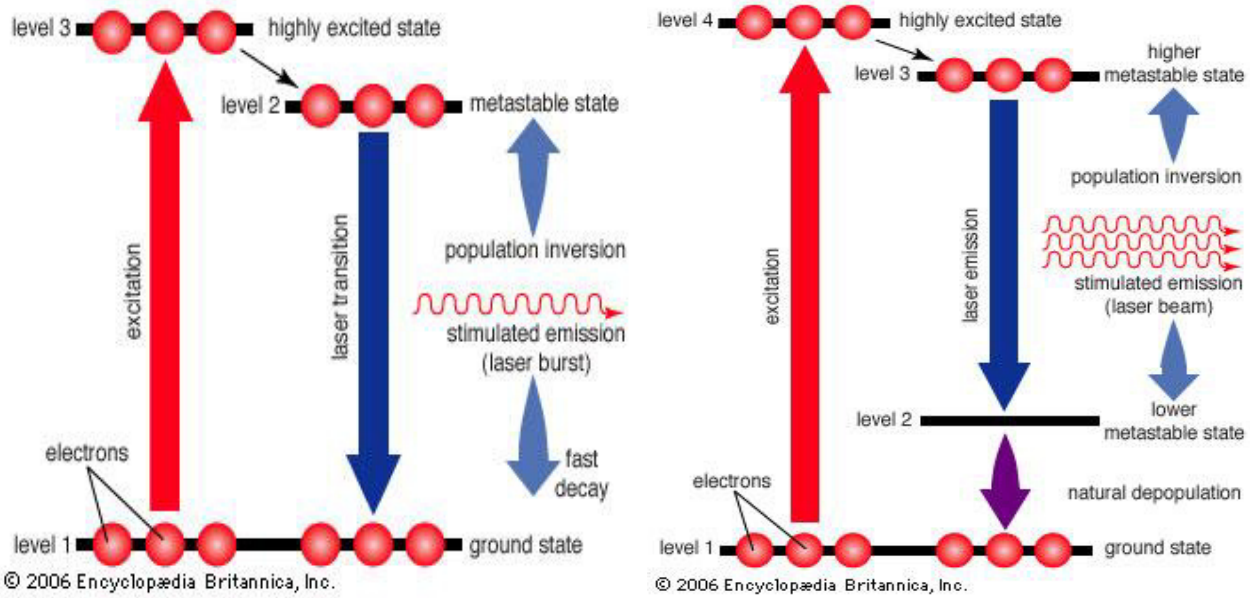

Figure 2-3. Three and four energy level laser mediums. [11]

2.5 Single Emitters, Bars or Stacks.

"Despite very high-power densities achieved in the active medium, only absolute output power of a few watts can be extracted from a single laser diode" [9, p. 164]. For this reason, many high-powered single emitters are often arranged in such a way that their laser beams can be combined to form a very high-powered device; this can be seen in Figure 2-4. Compared to other high-powered laser sources, multi-element diode lasers also achieve the very high efficiencies and power densities single emitters do. Each of the single emitters that make up the laser need their own optical element (which may be combined into a single piece but has multiple different lensing regions. i.e. A single lens that contains many smaller lenses, this looks a little like bubble wrap) in order to combine the beam into a single

focusable laser beam. This makes laser combinations a lot more complicated optically, although advances in both optics and diode lasers mean we are seeing more and more multi-element lasers in industry for high powered material processing work.

The highest-powered single emitters that could be found during market research were 10W laser diodes from Laser2000 [12] and the highest-powered stack was a 4.5kW stack from Coherent Inc. [13]. 4.5kW is well within the materials processing region in Figure 2-5 below.

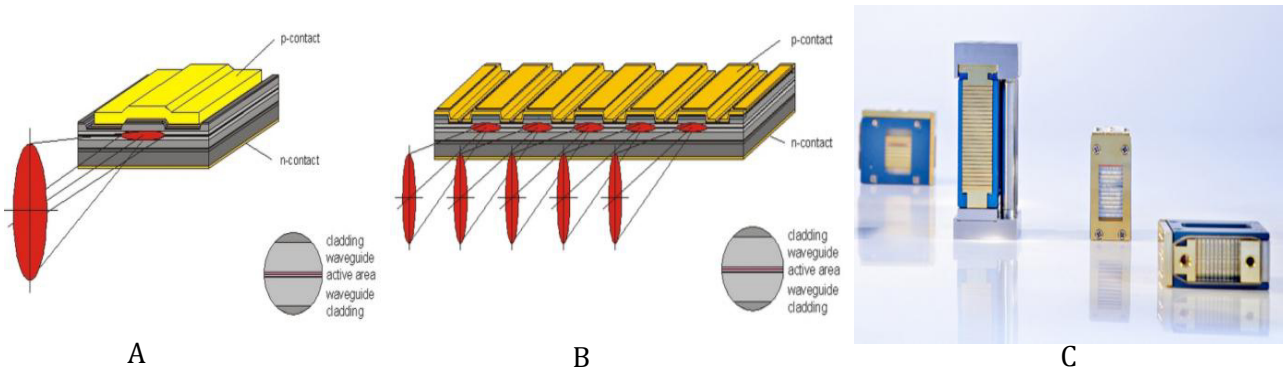

Figure 2-4. Showing a single emitter 'A', a laser bar made up of single emitters 'B' and a laser stack made up of several bars. [14] [15]

2.6 Properties and Uses of Different Laser Radiation

All lasers emit light at a very specific wavelength within a very narrow band of frequencies. This wavelength is defined by the properties of the laser itself and stems from the properties of the atoms that undergo stimulated emission. These atoms each have a range of possible wavelengths and the optical design of the laser determines which of these wavelengths are emitted. [7]

2.6.1 Possible commercially available wavelengths and powers

Lasers are available in a range of wavelengths ranging most of the electromagnetic spectrum. "Lasers normally operate in the infrared, visible and ultraviolet parts of the spectrum. Masers operate at microwave frequencies" [7]. "A few lasers have operated at the long-wavelength edge of the X-ray spectrum" [7].

The following figure, Figure 2-5, shows a graphic of different laser types and their power and wavelength properties. These are overlaid on a background indicating the uses of these lasers, namely; communications, measurement and material processing. This graphic has been edited to include "high power diode lasers in the range of tens of watts (that) were introduced in the late 1990s" [16, p. 1]. These high-powered laser diodes have started to become commercially available in the last 3 years making laser diodes suitable for low powered material processing. An example of this would be a 10W single emitter laser diode at a wavelength of 808nm made by Apollo Instruments [17]. This would move single emitter laser diodes into the bottom of the material processing region.

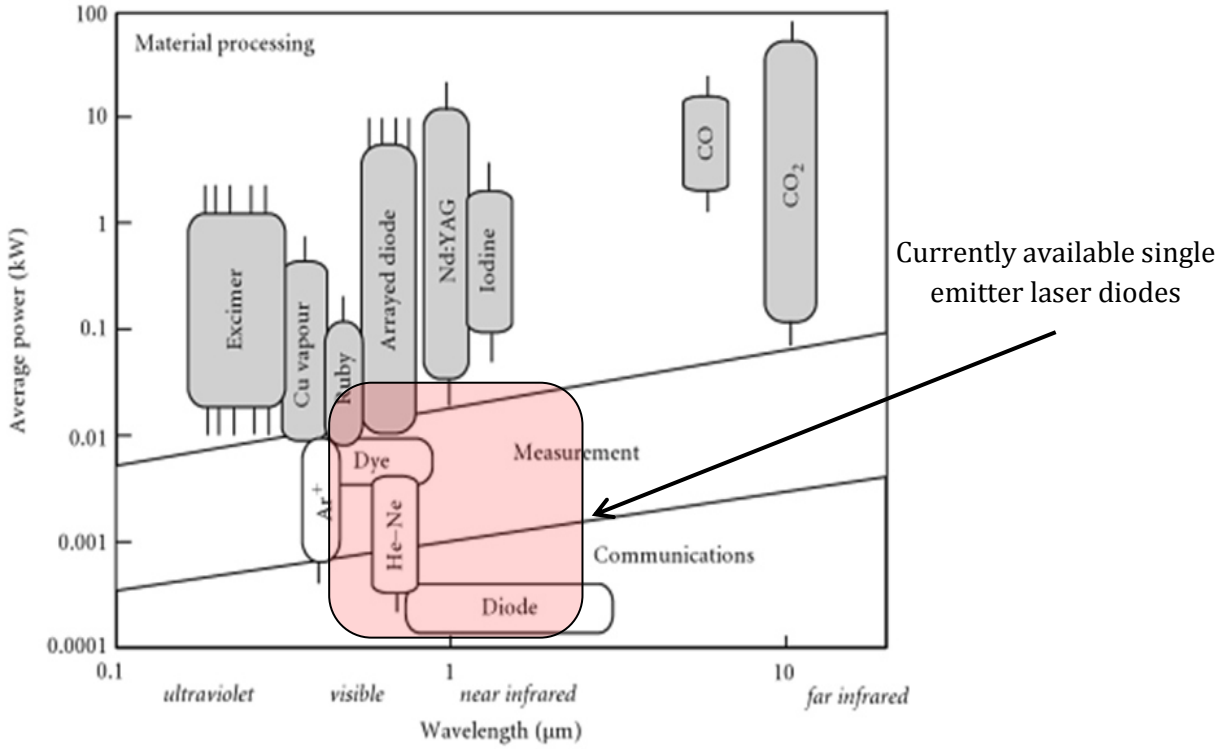

Figure 2-5. Showing the ranges of possible laser wavelengths and the powers that can be achieved, the background shows regions of different uses depending on the power and wavelength. [18, p. 72]

2.6.2 Wavelengths in material processing and manufacturing

Different wavelengths are absorbed differently by different materials. One classic example is that Perspex is easily cut buy a 10μm CO_2 laser but it is transparent and colourless to the naked eye (absorbs very little visible light) and hence does not cut with visible wavelength lasers.

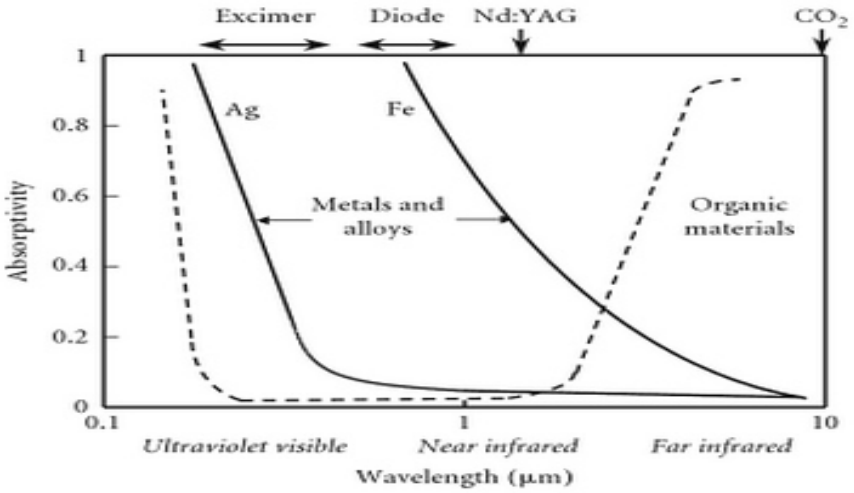

Figure 2-6. Variation of absorptivity with wavelength of metals and organic materials. [1, p. 169]

2.6.3 *Absorption of laser radiation*

All materials have a specific absorptivity where "the absorptivity is the ratio of power that is deposited within the workpiece and the power of incident radiation:" [19]

$$A = \frac{P_{abs}}{P}$$ **Equation 2-1** [19]

where A – Absorptivity (from 0 to 1)
P_{abs} – The power absorbed by the workpiece (W)
P – The incident radiation power (W)

"The absorbed radiation energy is in general transformed to heat energy. The absorption of laser radiation can for example lead to the dissociation of molecules. Before transformation of the absorbed energy to heat energy, the dissociated molecules can be removed. In that case the material is ablated." [19]

The incident radiation is defined by the laser beam itself and the absorptivity of a material depends on many properties of that material at a specific wavelength including; the index of refraction, the index of absorption, electric conductivity and specific heat. Some other effects on the absorptivity of the workpiece include; laser properties such as wavelength and polarization, ambient conditions, surface properties, workpiece dimensions and the local changes to these aforementioned factors caused by the laser. [19] All these complexities require specific situations to be studied depending on the properties of laser used, the workpiece and many other factors.

2.7 Laser Safety

"The two major concerns are exposure to the beam (which presents much more danger to the eyes than the rest of the body) and high voltages within the laser and power supply" [2, p. 8]. Laser diodes have low operating voltages so do not pose the normal high voltage risks associated with gas lasers. This said, the laser beam itself will pose the same risks in all lasers. Two other hazards encountered when laser cutting are the toxic fumes produced when some materials are processed and the possibility of fires.

2.7.1 *Hazards*

Three major hazards are present when operating a laser cutter; Exposure of the eyes, possible toxic fumes and fire. These are discussed below.

i. Exposure of the eyes

"The property of lasers that is of primary concern with regard to the eye hazards is their high radiance, i.e. the combination of high power density and directionality. The latter property causes the lens to focus the parallel beam emitted form a laser to a tiny spot on the retina" [4, p. 698]. In certain conditions and when focused "even lasers having power outputs of only a few milliwatts will produce power densities of kilowatts per square centimetre on the retina" [4, p. 699]. These high power densities will cause permanent damage to the retina.

"The maximum permissible exposure of laser radiation to the eye depends on the wavelength and is dependent on the spectral transmission of the eye" [4, p. 699]. The most sensitive and irreparable part of the eye is the retina and is therefore the part of the eye that should have the most protection. "Retinal damage is possible from exposure to laser energy in the wavelength region between 400 and 1400nm" [4, p. 699]. Some absorption does occur within the eye for wavelengths longer than 700nm. Below 315nm and above 1400 nm radiation is absorbed by the cornea and between 315 and 400nm it is absorbed by the lens. These regions are shown in Figure 2-7. [4, p. 699]

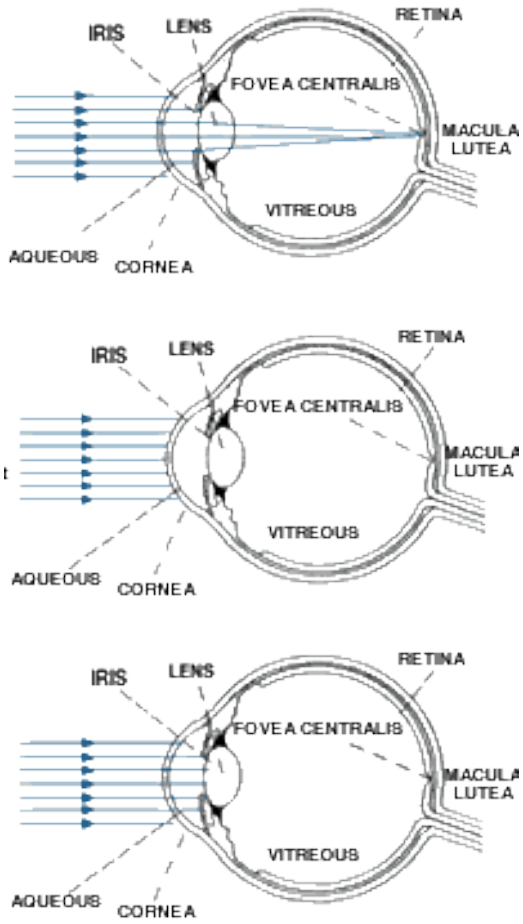

Between 400nm and 1400nm. Little absorption by the eye, most radiant energy reaches and is focused onto the retina

Below 315nm and above 1400nm. Most radiant energy is absorbed by the cornea

Between 315nm and 400nm. Most radiant energy is absorbed by the lens.

Figure 2-7. How different wavelengths penetrate the eye. [20]

ii. Possible toxic fumes

When laser cutting, particles are released into the atmosphere. These particles depend on the material being cut and therefore pose different risks. Table 2-1 shows the risks posed by laser cutting some materials; this list is to demonstrate some of the risks associated with laser cutting and by no means aims to cover all the risks posed by specific materials or all the materials that can be laser cut. The Material Safety Data Sheet (MSDS) for a specific material should always be consulted before laser cutting.

Table 2-1. A table to show the toxic fumes produced by and risks associated with lasing some materials.

Material	Toxic Fumes	Risk
Steel	Chromium, Nickel	Carcinogenic [21]
Polyvinyl Chloride (PVC)	Hydrogen chloride, dioxin, ethylene dichloride, vinyl chloride, phosgene	Cancer, neurological, reproductive and immune system damage. [21] [22]
Polyethylene	Formaldehyde	Cancer, asthma and allergies [21]
Plastics, Rubbers	Benzene, a Volatile Organic Compounds (VOC)	Death, low white blood cell count, anaemia and cancer [21]
Wood	None	Irritation
Glass	None	Irritation
ceramic	None	Irritation

iii. Fire

Class 4 lasers can ignite flammable and combustible materials. For this reason laser beams should be terminated with non-combustible materials. [23] "The three components required for a fire to start are: a combustible material, an oxidizing agent and a source of ignition. Therefore, to reduce the risk of fire in laser applications, great care should be taken to keep these components separated" [24]. Extreme caution should be taken when laser cutting combustible materials.

2.7.2 Precautions

The following safety precautions are recommended by Walter Koechner in his book Solid State Laser Engineering: [4, p. 700]

- Wear safety glasses that have a sufficient attenuation at the wavelength present.
- Never look directly into the laser or scattered light from any reflective sources.
- Set up the laser and all optical components below eye level.
- Use an infrared viewing scope when infrared wavelengths are present.
- Operate the laser in bright light conditions; a smaller iris means less radiation enters the eye.
- Post appropriate warnings including a flashing red light.
- Provide interlocks to prevent the laser being fired accidently or when the housing is open.

Other safety precautions would include displaying a list of materials that can be cut by the specific laser cutter and a carbon dioxide fire extinguisher should be present and accessible at all times.

2.7.3 Standards

In international standards, such as the IEC 60825-1, the hazard classification of a laser is classified based on the laser's wavelength and pulse duration called the Maximum Permissible Exposure (MPE). [25, p. 209] There are two major classification bodies (although many others do exist); the International Electrotechnical Commission (IEC) and the American National Standards Institute (ANSI). These standards classify lasers into four classes, and some subclasses, which indicate the hazard they pose.

Class 1: “Lasers that are safe under reasonably foreseeable conditions of operation.” [26]

Class 1M: “Lasers emitting in the wavelength range from 302.5 nm to 4 000 nm which are safe under reasonably foreseeable conditions of operation, but may be hazardous if the user employs optics within the beam.” [26]

Class 2: “Lasers that emit visible radiation in the wavelength range from 400 nm to 700 nm where eye protection is normally afforded by aversion responses, including the blink reflex.” [26]

Class 2M: The same classification as Class 2 “however, viewing of the output may be more hazardous if the user employs optics within the beam.” [26]

Class 3R: “Lasers that emit in the wavelength range from 302.5 nm to 10^6 nm where direct intrabeam viewing is potentially hazardous.” [26] “The Accessible Emission Limit [AEL] is within five times the AEL of Class 2 in the wavelength range from 400 nm to 700 nm and within five times the AEL of Class 1 for other wavelengths.” [26]

Class 3B: “Lasers that are normally hazardous when direct intrabeam exposure occurs.” “Viewing diffuse reflections is normally safe.” [26]

Class 4: “Lasers that are also capable of producing hazardous diffuse reflections.” [26]

Almost all lasers used in material processing would be classed as Class 4 lasers.

2.8 Optics

Optics will be used in focusing and directing the laser beam. Some of the different optical aspects that will be used in the project are discussed here.

2.8.1 What is infrared radiation

Infrared radiation is electromagnetic radiation with wavelengths between wavelength of 0.7µm and 1mm. This is further divided into near (0.75-1.4µm), short-wavelength (1.4-3µm), mid-wavelength (3-8µm), long-wavelength (8-15µm) and far infrared (15µm-1mm) [27, pp. 21-22] .

2.8.2 Viewing infrared radiation

Light with wavelengths longer than 700nm is invisible to the naked eye. This implies that in order to view infrared light some other viewing method is required. One method is using an infrared-to-visible (an example is manufactured by Alphas [28]) light converter. Another is to use a CCD camera with appropriate filters as CCD sensors can sense wavelengths from 400nm to 1050nm [29].

A common and cheap way is to use a standard CCD webcam and replace the infrared filtering window with another widow that is transparent to infrared but opaque to visible light. Two commonly available materials for such a window are exposed photographic/x-ray film or the magnetic storage medium from stiffy disks.

2.8.3 *Absorptivity and reflectivity*

Some materials absorb radiation more effectively than others do. “Absorptivity is a measure of a materials ability to absorb radiation while minimising losses due to reflection. As a result white and light colors are poor absorber colors” [30, p. 234].

Reflectivity is defined as “the ratio of power reflected per unit area to the power incident per unit area.” [5, p. 76]

Therefore by definition:

$$\boldsymbol{Reflectivity + Absorptivity = 1} \qquad \textbf{Equation 2-2}$$

2.8.4 *Lens transmission*

Lens transmission is made up of three properties, namely; reflectance, transmittance and absorptivity. They are related by the following formula:

$$\boldsymbol{r + t + a = 1} \qquad \textbf{Equation 2-3 } [31]$$

where: r is the reflectance.
t is the transmittance.
a is the absorptivity [31, p. 5].

Transmittance can be calculated from the following equation:

$$\boldsymbol{T_a = e^{-\delta x}} \qquad \textbf{Equation 2-4 } [31]$$

where: T_a is the transmittance.
δ is the absorption coefficient.
x is the distance travelled through the optical element [31, p. 5].

Reflectance can be calculated from the following equation:

$$\boldsymbol{r = \frac{(n-1)^2}{(n+1)^2}} \qquad \textbf{Equation 2-5 } [31]$$

where: r is the uncoated reflection loss per surface.
n is the index of refraction of optical material [31, p. 6].

2.8.5 *Focusing the lens*

The lens equation can be expressed as follows:

$$\frac{1}{f} = \frac{1}{l'} - \frac{1}{l}$$

Equation 2-6 [31]

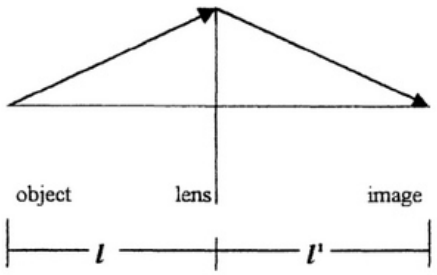

Figure 2-8. Showing a graphical representation of the lens equation. [31]

where: f is the effective focal length.

The lens equation can be used to calculate the focal points of a laser beam if the effective focal length is known.

2.8.6 *Optical aberrations*

Optical aberrations fall into two broad categories; these are either monochromatic or chromatic aberrations. Chromatic aberrations only appear when using light made up of various wavelengths. Laser radiation is by definition monochromatic; this means that chromatic aberrations will have no effect in a laser system. For this reason, only monochromatic aberrations are discussed here.

"Monochromatic aberrations are aberrations that arise due to geometrical deviations from paraxial (Gaussian) theory" [32]. There are "five primary or Seidel aberrations: spherical aberration, coma, astigmatism, field curvature, and distortion" [32].

i. Spherical aberration

"It is the aberration resulting from the deviation of spherical surfaces from the ideal shape" [32]. This can be seen in Figure 2-9 below and it causes the focal point of the outermost rays to be shorter than the paraxial rays. Aspheric spherical aberration corrected lensed can be purchased. [33] When mounting lenses "if an aspheric lens is being used to collimate the light from a point source or laser diode, the side with the greater radius of curvature (i.e., the flatter surface) should face the point source or laser diode" [33].

ii. Coma

"Coma is an aberration which causes rays from an off-axis point of light in the object plane to create a trailing "comet-like" blur directed away from the optic axis" [34]. In this design the laser will be placed on the optical axis so should not experience a coma aberration. Any coma aberration observed will be seen as an indication of poor optical alignment and will be corrected.

iii. Astigmatism

"Astigmatism is due to the asymmetry between the rays in the meridional (major axis) and sagittal (minor axis) planes. The meridional rays intercept the lens at a larger angle than the sagittal rays, so they are bent more" [32]. The image can be focused for either axis but "the image degenerates into a line in each (focal) plane" [32].

iv. Field curvature

This is only an issue with off axis point source, which is not expected in this design.

v. Distortion

"This results in a magnification that depends upon the cube of the distance of the object from the axis. This will cause the shape of an extended object to become distorted" [32]. Since a laser is generally placed on the optical axis this form of aberration is not often considered in laser application.

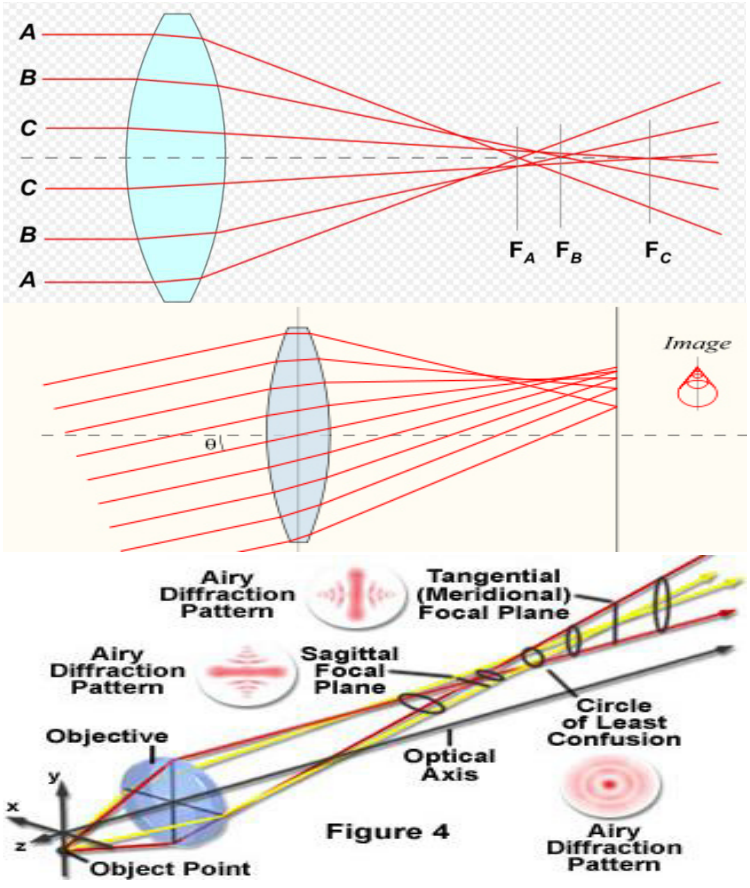

Spherical aberration

Coma aberration

Astigmatic aberration

Figure 2-9. Showing the three primary aberrations. [35] [36] [37]

2.9 Distance Measurements with Lasers

There are a few different ways to measure distances using light or lasers and these are discussed below.

2.9.1 *Interferometry*

"Interferometers allow distance measurements with accuracies related to the wavelength of the light source" [38, p. 70]. Interferometry uses the wave nature of light and the interference caused by superimposed coherent waves to measure the distance travelled. This provides an ambiguous result, as waves are periodic. "Measurement accuracy inside a cycle being at subnanometer level" [38, p. 71].

2.9.2 *Time of flight*

There are three common means of realising time of flight measurements which are each used for different types of applications. These are very similar to Radar systems and are thus often called lidar; "a device, similar in operation to radar, that uses pulses of laser light" [39].

i. Phase shift

The power of a laser is modulated and transmitted to a target. The reflected light is then received and the phases of the received and transmitted signals are compared. The distances measured are ambiguous because of the cyclic nature of the phase shift between two signals. Generally, only distances up to a single wavelength can be measured unambiguously.

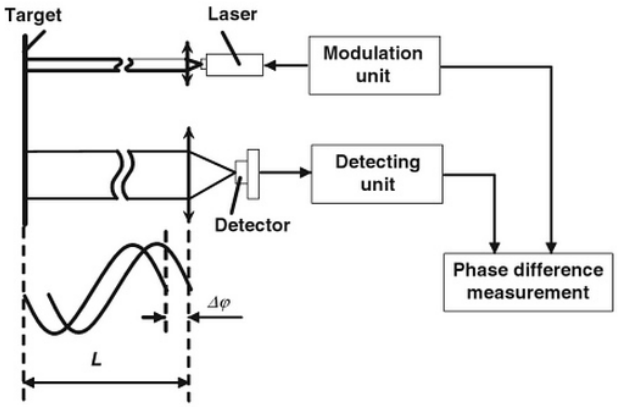

Figure 2-10. Showing how phase shift method for distance measurement works. [38, p. 71]

$$L = \frac{\theta * c}{2 * 2\pi f}$$ **Equation 2-7** [38]

Where: θ is the phase shift in radians
c is the speed of light ≈ 300×10^6 ms^{-1}
f is the modulation frequency
L is the distance from the laser and detector to the target

Equation 2-7 is used to calculate the distance from the relative phase shift.

Considering a reasonable situation where the modulation frequency = 100MHz and the phase shift resolution is 0.24° an accuracy of 1mm is achievable over a theoretical unambiguous range of 1.5m.

2.9.3 AD8302 phase shift and magnitude detection IC.

The AD8302 was chosen as the phase detector for this project because it is simple to use and tolerant to a wide input voltage range. “The AD8302 is a fully integrated system for measuring gain/loss and phase in numerous applications”. “The outputs provide an accurate measurement of either gain or loss over a ± 30 dB range scaled to 30mV/db, and of phase over a 0°-180° range scaled to 10mV/degree.”

The AD8302 contains multiple internal functional blocks but the major components are the logarithmic amplifiers and the phase detectors. “The AD8302 comprises a closely matched pair of demodulating logarithmic amplifiers, each having a 60 dB measurement range.” “The AD8302 includes a phase detector of the multiplier type, but with precise phase balance driven by the fully limited signals appearing at the outputs of the two logarithmic amplifiers. Thus, the phase accuracy measurement is independent of signal level over a wide range.”

The AD8302 is intended to be used in a 50Ω environment and can detect signals from DC to 2.7GHz. It is accurate to 1 degree. Please see the AD8302 datasheet for a more detailed description.

ii. Frequency Modulated Continuous Wave (FMCW)

"Compared to continuous wave phase shift method in this case the frequency of the sinusoidal modulate pulsed beam will be modulated by some function" [38, p. 72], this function will normally be a saw tooth function. The frequency shift between the transmitted and received signals is then measured and the distance is a function of this. A measurement range of about 0.2mm can be realised. [38, p. 73]

This system uses the Doppler Effect and measures the difference on frequencies of the transmitted and received signals.

$$\boldsymbol{L = \frac{2*c*T*\Delta f}{(f_2 - f_1)}}$$ **Equation 2-8** [40]

Where: f_2 is the maximum frequency of the transmitted signal
f_1 is the minimum frequency of the transmitted signal
T is the period between f_1 and f_2, or the period of the modulating signal
c is the speed of light
Δf is the difference between transmitted and received frequencies

iii. Pulsed system

A pulsed "system measures the round trip time between a light pulse emission and the return of the pulse echo from the object" [38, p. 73]. Standard physics is then used to measure the distance by multiplying the velocity of light and the roundtrip time remembering to divide this answer by two as the light travelled to and from the object. For 10mm accuracies, this system would need to be able to detect 66.7ps time intervals. This method gives unambiguous distance measurements.

2.10 Microcontroller

"A microcontroller is a computer-on-chip used to control electronic devices" [41, p. 1]. The microcontroller in this project will be used to coordinate the movement of the motors, control the laser cutting and modulation, read the indicated phase shift and magnitude ratios and communicate with a PC running either MATLAB or other custom software. Both of the following were available to and well understood by the author.

2.10.1 *Arduino™ MEGA 2560*

The *Arduino™* Mega 2560 is a microcontroller development board based on the ATmega2560 which is a "High Performance, Low Power *Atmel*® *AVR*® 8-Bit Microcontroller" [42]. Useful aspects include; 5V supply, 16 MHz clock frequency, 54 general purpose input/output pins, a 10 bit ADC multiplexed onto 16 pins, three SCIs, an SPI and a two wire Interface compatible with IIC.

2.10.2 *Freescale™ MC9S08GT16A*

The MC9S08GT16A is a microcontroller made by Freescale Semiconductor. It is an 8-bit microcontroller that has 16K Flash and 2K RAM. It has 34 general-purpose input/output pins. It also has a 10 bit ADC, two SCIs, an SPI and an IIC module. [43]

2.10.3 Stepper motor controller and drivers

"The L297 integrates all the control circuitry required to control bipolar and unipolar stepper motors. Used with a dual bridge driver such as the L298, forms a complete microprocessor-to-bipolar stepper motor interface." [44] This combination of chips allows easy control of a stepper motor by a microcontroller. It has the following inputs: step clock, half/full step, direction, enable, chopper mode, reset and two digital outputs namely, home and sync (synchronise). It outputs four lines to drive a bipolar stepper motor with voltages up to 36V. This is a well-known and robust circuit for driving stepper motors. [44] Two tested and working L297/L298 circuits were available from a previous project in which they were built by the author.

There are many other smaller, more efficient and more powerful stepper motor controllers on the market such as the DRV8818 from Texas instruments and the L6208 from ST Microelectronics. These both offer microstepping, higher efficiencies, a smaller surface mount footprint and a much-reduced external component count. [45] [46]

2.11 Software

As with all CNC machines, some sort of software running on either a microcontroller or PC is needed to integrate the many different components and ensure that they operate as needed. Some common programming languages that were considered for this project have been reviewed here.

2.11.1 MATLAB®

"MATLAB is a mathematical and graphical software package with numerical, graphical and programming capabilities. It has built-in functions to perform many operations, and there are toolboxes that can be added to augment these functions" (e.g. signal processing). [47, p. 4] MATLAB is a high-level language in which "many operations are generally combined into one program statement" [48, p. 975]. This makes it easier to program and more portable from one processor to another. MATLAB is relatively easy to use when it comes to mathematical operations using matrices as all variables in MATLAB are defined as a matrix (even if only a 1x1 matrix). The toolbox that is most relevant to this project is the Image Processing Toolbox™, which "provides a comprehensive set of reference-standard algorithms and graphical tools for image processing, analysis, visualization and algorithm development." [49]

2.11.2 C - Programming language

"C is a 'higher-level language,' yet it provides capabilities that enable the user to 'get in close' with the hardware and deal with the computer on a much lower level" [50]. Programming a microcontroller in C is a lot easier and less time consuming than programming in Assembly or machine language although some control of the actual operations on the microcontroller is lost and the program may be less efficient. This depends a lot on the compiler and some compilers produce less efficient code, which can use unnecessary resources on the microcontroller. C is the most popular language for most microcontrollers. [51]

2.12 Motors and Actuators

"Mechatronic systems employ actuators or drives that are part of the physical process being controlled" [52, p. 211].

There are many different types of motors available and can be classified into AC and DC motors. Electric motors are used to convert electrical energy in the form of command signals into mechanical kinetic energy. [52, p. 211] Examples of AC motors are induction and synchronous motors. Examples of DC motors are commutator, brushless and stepper motors. For the purpose of this project only DC motors with inherent position control will be reviewed.

2.12.1 Permanent magnet stepper motor

Stepper motors are classified in many different ways by different references. Some classify them as AC motors [52, p. 214], as digital actuators [48, p. 675] and most commonly as DC motors because they run off DC power supplies. "The stepper motor is an actuator that translates electrical pulses into precise, equally spaced angular movements of the rotor in the form of steps. The rotor is positioned by magnetically aligning the rotor and stator teeth" [52, p. 214]. Permanent magnet stepper motors have permanent magnet rotors. Stepper motors require circuitry to drive them, which controls when to step and the direction of the step. The speed of a stepper motor is controlled by the frequency of the input step signal that is controlling the stepper driver circuitry. Stepper motors step in steps as small as 1.8° (which can then be further reduced by gearing) but have poor torque, efficiency and size characteristics. Stepper motors are brushless and therefore very reliable. They are extremely well suited for operation in open loop situations [52, p. 214].

2.12.2 Servomotor

The servomotors discussed here are all either brushed or brushless DC motors that have some sort of position control. "In a DC servomotor system both angular position and speed might be measured (using shaft encoders, tachometers, resolvers, RVDTs, potentiometers, etc.) and then compared with a desired position and speed." [48, p. 788] Servomotors have similar speed, torque and size characteristics to both brushed and brushless DC motors but are usually highly geared to achieve better position and speed control. The accuracy of the speed and position control is very dependent on the controller and the infrared sensor used to measure speed and position.

2.13 Design Materials

Plexiglas™ (Perspex), aluminium and hardboard are easily available at UCT in sheets that range in thickness. These three materials are thus reviewed in further detail.

2.13.1 Plexiglas™ (Perspex)

Plexiglas™ (or Perspex as it is known in South Africa) is chemically known as polymethyl methacrylate (PMMA) [53, p. 709]. This rigid acrylic material is used in a variety of applications. Perspex is slightly heavier than hardboard and it is stronger than hardboard. It is a brittle material meaning that it will shatter if subjected to large stresses. Perspex is available in 2mm, 3mm, 5mm and 10mm sheets at UCT and it is easily cut with a laser cutter.

2.13.2 Aluminium

Aluminium sheets are available at UCT in 2mm and 3mm sheets. Aluminium is a light and very workable metal. It is also very malleable, meaning it can be easily bent into different shapes with the correct equipment. Being a metal, it is electrically conductive. The laser cutter at UCT is not able to cut aluminium.

2.13.3 Hardboard

Hardboard is a compressed form of exploded wood fibres that have been compressed into boards. Hardboard is lighter than both Perspex and aluminium but also not as strong. Hardboard is not brittle but will snap when bent too far.

Hardboard is available in 3mm and 5mm sheets at UCT and it is easily cut with the laser cutter. It is also the cheapest of the reviewed materials.

After completion of any necessary research and the literature review, the design and implementation stages of the project commenced. The following chapter, 'Design Specification', outlines the different requirements for the project and how the project will be tested against these requirements.

2.14 Market Review

A brief market review of some products with similar applications.

2.14.1 3-dimensional printers

There are many 3-dimensional printers on the market. These employ a multitude of printing technologies and printing materials. They vary in price form open source projects to cheap $1300 desktop printers such as the popular MakerBots [54] to industrial printers [55]. The major disadvantage of most of these printers are that the materials they print are can be expensive and the print times are very long for larger parts (industrial printers often print multiple parts in parallel). A 3-dimensional laser cutter would not necessarily have expensive materials as with the depth control it could cut any material that the laser beam is powerful enough to cut. The cut times would potentially be a lot shorter. Maintenance on a laser cutter is also considerably lower than that of most 3-dimensional printer technologies.

2.14.2 '3-dimensional' or higher laser cutters

There are laser cutters on the market that offer 3-dimensional or even 5-dimensional laser cutting. These products are all fundamentally different to this laser cutter in that they do not have any way to measure the cut depth. These products work similarly to conventional 2-dimensional laser cutters in that they cut all the way through a workpiece. The only difference between these products is that they are able to lift and rotate the cutting head. Wieser is just one of many companies that offer such a laser cutter [56]. Similar applications are when a laser end effector is attached to a robotic arm; these are often used in the automotive industry to either cut or weld bodywork where the laser would need to follow the contours of the workpiece [57].

3. Design Specification

This brief chapter expands on the 'Scope' above giving more details on the requirements of each of the different aspects of the project.

3.1 Specification

This section describes the details of the specifications set out by the project brief, which were then discussed, in order to make them more specific, and agreed upon by my supervisor and myself. These were expanded from the terms of reference when it was discovered a more detailed 'Specification' would be needed.

It was then agreed that the laser cutter should conform to the following design specifications:

- be able to move a laser cutting toolhead in a 2-dimensional x-y plane
- be able to move over a range of 200x250mm which will make up the workbed
- have a step size that is smaller than 0.1mm in both directions
- be able to move at a speed of $0.1ms^{-1}$
- be able to measure cut depth to within 1mm over a range of 50mm
- to have a minimum cutting spot size smaller than 0.1mm and a maximum spot size no bigger than 2mm
- should be controllable by a PC although an LCD display panel on the laser cutter would be advantageous
- be of an acceptable size to fit on a desk top, have a footprint smaller than 500x500mm

It was also decided that this is a proof of concept design and therefore does not need to be designed for large-scale manufacture or for sale to the public.

These specifications were referred to throughout the design and implementation process in order to make decisions about mechanical design, component selection and the overall operation of the thermal imager. The specifications will also be used to determine whether the imager is ultimately a success by analysing its performance with regard to these specifications.

3.2 Acceptance Test

Each aspect of the project was tested individually to ensure that it operated as designed. The final laser cutter was tested against all of the above specifications.

- The workbed size was tested by commanding the toolhead platform to move from one corner to the other across both diagonals. The displacement in the x and y directions were measured.
- The step size should be measured with a calliper and verified throughout the workbed.
- The speed should be verified by moving a set distance and measuring the time taken. This should be done while maintaining position control and accuracy.
- A specific test platform should be built to verify the depth measurement.

The results to all these tests can be found in the relevant chapters below and final testing in the 'Final Testing, Results and Discussion' chapter.

These tests were intended to prove that the laser cutter met all the requirements as set out in the 'Specification' chapter.

The design specification described what needed to be achieved by this project and the laser cutter as a whole. Chapter 4, 'Preliminary Design', describes the initial design stages of each component of the project. The preliminary design was carried out before any detailed design to ensure that the basics of each component would work together and that no major difficulties in the following sections would be created by careless design of a previous section.

4. Preliminary Design

This chapter aims to give a general overview of the design process and how different components and systems work together to create a 3-dimensional laser cutter. This preliminary design was carried out at the beginning of the project, mostly in the form of rough sketches, in order to better understand the expected challenges that were to follow. The next 6 chapters describe all the different sections of the design process in detail.

4.1 Mechanical Design

In order to construct the two-dimensional cutting part of the laser cutter a mechanical gantry would need to be designed and built. For safety reasons, an enclosure for the whole laser cutter would need to be built in order to prevent the operator being exposed to any direct or diffused laser radiation and to provide protection for the laser cutter.

The following sketch, Figure 4-1, shows what the gantry system is expected to look like. This system is belt-driven but can be easily modified for a leadscrew setup if required.

The laser cutter gantry will consist of a mechanism that is able to move the laser cutting tool head in ‘x’ (red arrows) and ‘y’ (green arrows) directions in a horizontal plane. This would make up a 2 Degree Of Freedom (DOF) system and hence would require two motors with some sort of position control to achieve this. As per the ‘Design Specifications’ the accuracy of this system, after any gearing, should be 0.1mm.

It was decided that a system with a fixed work bed would be best for this design, as the work bed is much larger than the cutting tool. Having a fixed work bed would allow the laser cutter to be physically smaller for a certain sized work area.

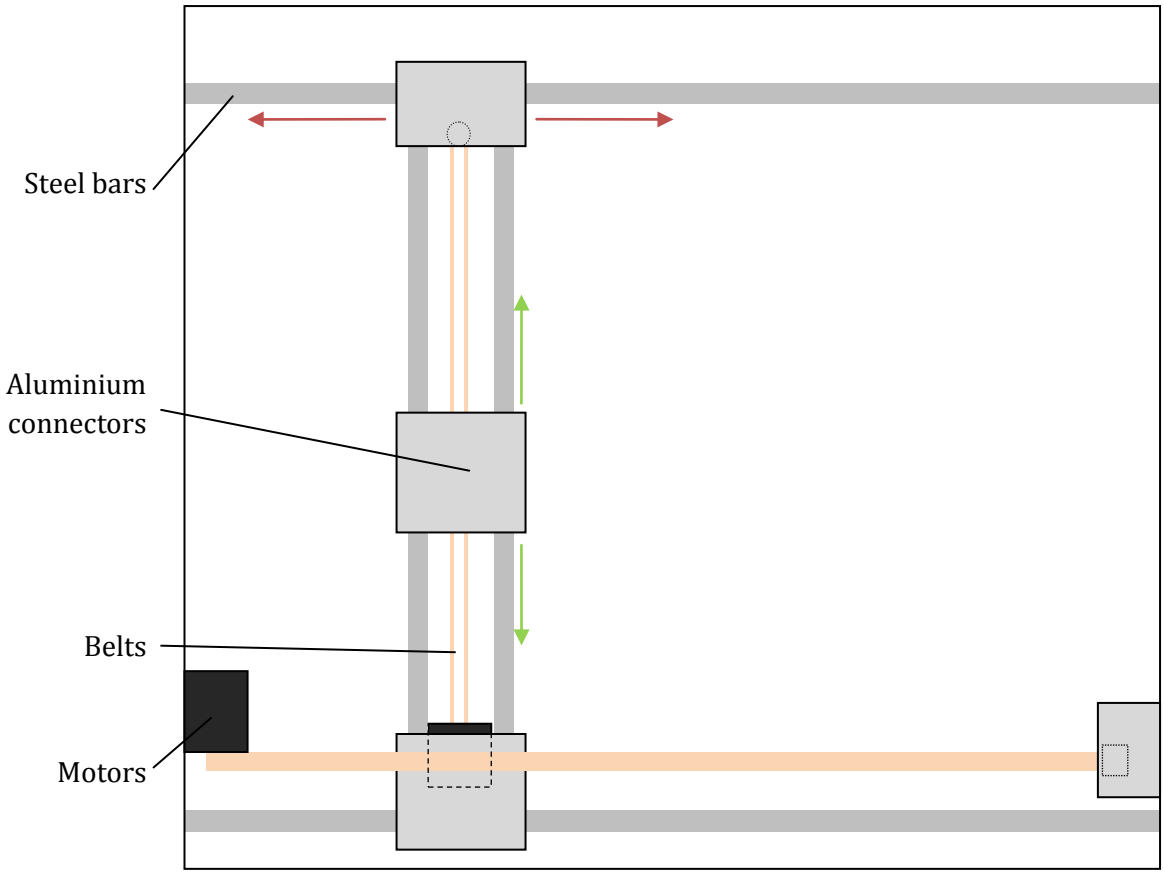

Figure 4-1. Showing a top view of the preliminary mechanical design.

The housing should be designed in a way that will not allow any laser radiation to escape and to provide structural rigidity. It should also be easy to construct and inexpensive. A housing using 5mm Masonite and 25mm aluminium angle was designed and can be seen in Figure 5-4.

4.2 Optical Design

The optics of the laser cutter need to be designed in a way to allow the laser beam to be focused to a small point for cutting and then have the light reflected off the workpiece received by a photodetector of some sort.

Three different optical configurations were considered in the preliminary optical design and these can be seen in Figure 4-2. All three configurations only require a single photodetector and configurations 'A' and 'C' allow for a second in order to measure both the transmitted and received beams. Configuration 'B' allows all of the laser power to reach the workpiece without the beam being split; this configuration does however require a third lens in order to focus the 'field of view' of the photodetector to the cutting point.

Dynamically adjustable optics, in order to adjust the focal distance, were considered to be outside the scope of this project although a system that could be adjusted during assembly would be preferable in order to adjust for mathematical and mechanical inaccuracies.

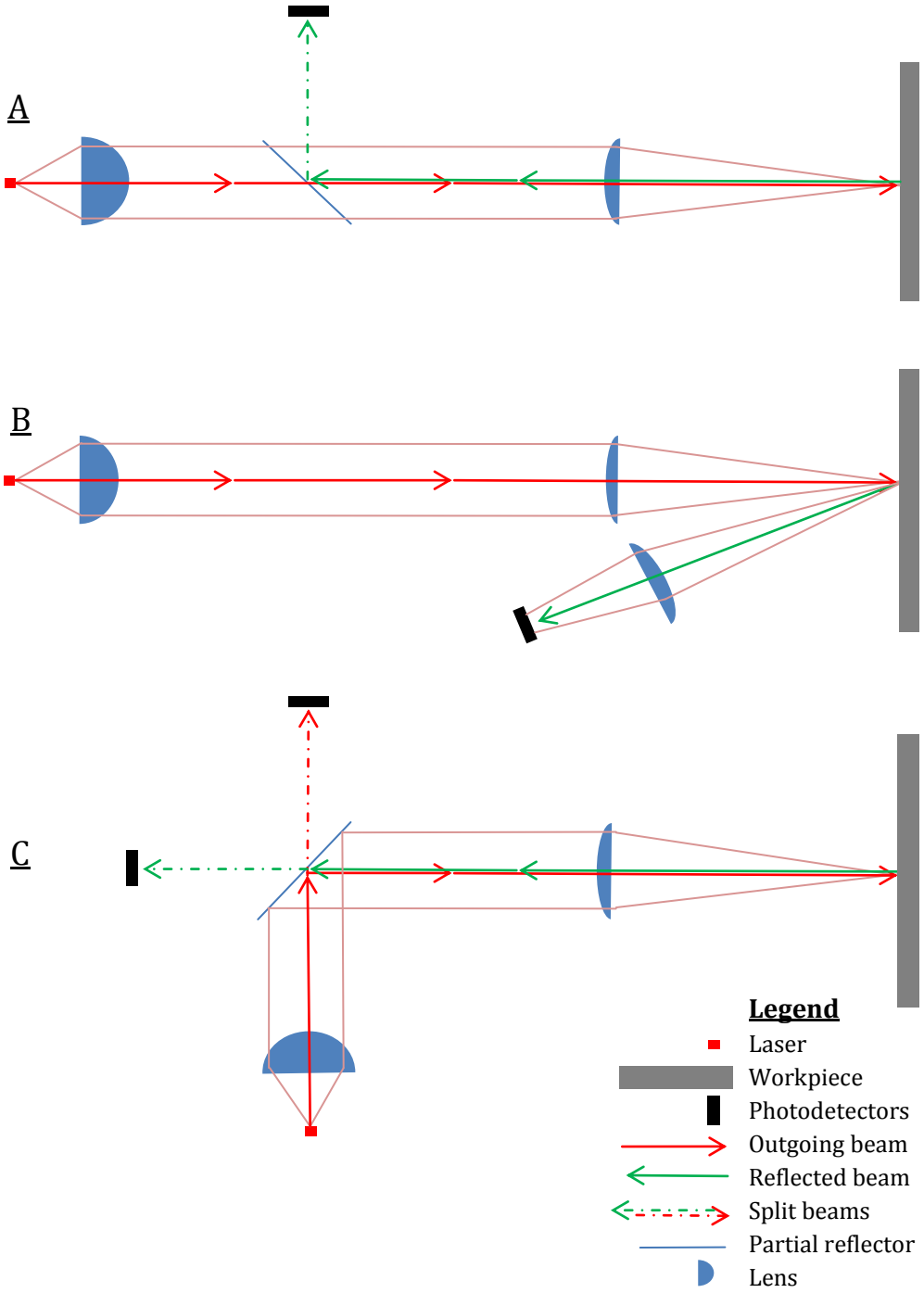

Figure 4-2. Showing the three different optical configurations considered.

4.3 Electronic Hardware Considerations

This project will have three major electronic systems; namely the laser driver, phase detector and digital communications. Figure 4-3 shows the overall system design which will then be expanded upon.

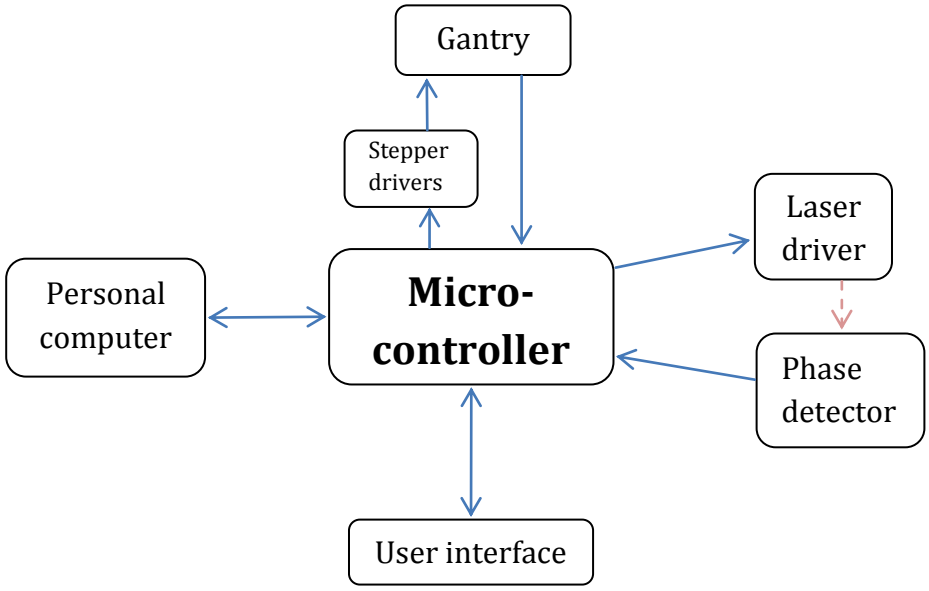

Figure 4-3. Showing the overall electrical system preliminary design.

4.3.1 Laser driver design

The laser driver will need to power and modulate a 2W laser. A laser diode should be current controlled, as the output power of the laser is proportional to current [58]. The laser will also need to be modulated at high frequency. Preferably, both the current and frequency should be able to be controlled digitally by the microcontroller. Figure 4-4 shows a design that would be able to perform the abovementioned tasks. This should all be implemented on a single PCB. The high frequency generator and buffer will inject an alternating current into the constant current system allowing the laser to have a controlled DC bias current keeping it in the 'on' state at all times. The frequency generator would be an AC voltage source with a series resistor to create a modulated AC current.

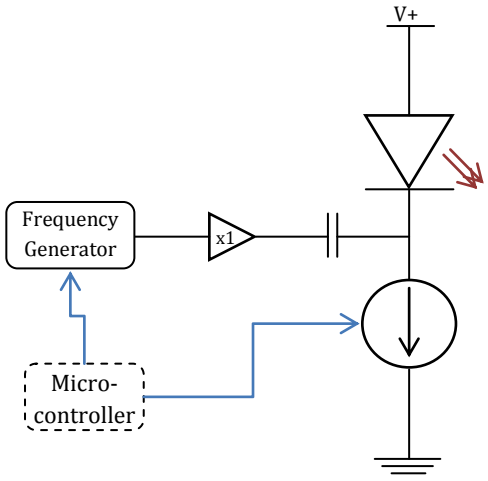

Figure 4-4. Showing the laser driver and modulator preliminary design.

4.3.2 *Photodetector and phase detector design*

The photodetector and phase detector will be responsible for converting the received optical signals into a signal that represents the phase shift between these two signals. From this relative phase shift, the cutting distance can be calculated. Figure 4-5 shows a preliminary design for this circuit. Depending on the optical design selected, either one or two photodetector channels will be needed but this does not affect the preliminary design. The photodetectors will feed into a transimpedance amplifier and then a filter stage before the phase shift is detected. The phase shift output will be conveyed to the microcontroller via either analogue or digital signals.

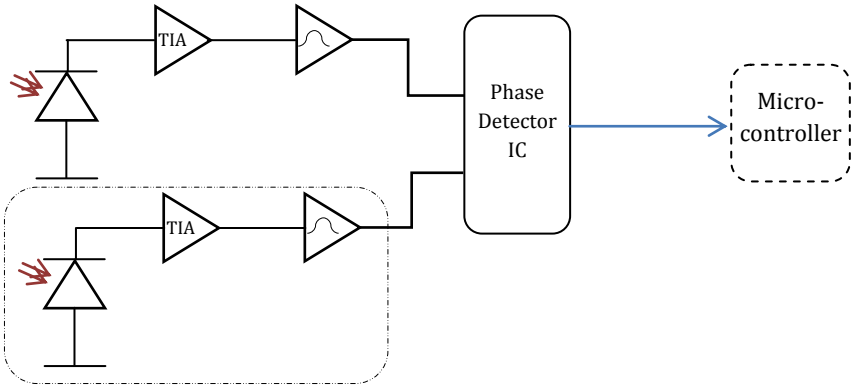

Figure 4-5. Photodetector and phase detector preliminary design.

4.3.3 *Digital communications and wiring*

The digital communications and wiring will depend on the IC's used and careful consideration when designing the peripheral systems should be taken in order for that peripheral to communicate with the microcontroller.

The following should be considered when doing the preliminary communications and wiring:

- Serial UART should be used for PC communication preferably over USB.
- Wiring to the moving toolhead should be minimised for a reliable and robust design.
- Multi stranded, thin (and preferably shielded), wiring should be used for the toolhead in order to maximise mobility and reduce noise pickup.
- Communications to the toolhead should be digital as there will be a lot of electrical noise radiated by the stepper motors and laser driver.
- Communications to the toolhead should also be serial to minimise wiring.
- Stepper motor and gantry signals can be either serial or parallel as wiring considerations are not as stringent on non-moving parts.
- Both of the microcontroller development boards considered have an on board LCD screen.

4.4 Software

The complete software used to control a 3-dimensional laser is not part of the scope of this project but software will have to be written in order to do testing and demonstrate some of the abilities of the finished system. This software will need to be edited in order to perform specific tasks and tests but where possible reusable functions should be used.

A GUI will be written in MATLAB and used to send commands to the microcontroller via UART. Where possible these commands will follow standard G-code commands. The software on the microcontroller will interpret the MATLAB commands, perform the required operations and reply with the results of the operations performed.

4.5 Testing Considerations

All of the abovementioned components will need to be tested individually before they can be combined into the complete system. Some testing considerations for each of the individual components are discussed here. Complete testing of each subsystem can be found in the relevant chapters and final testing on the system as a whole can be found in chapter 11 'Final Testing, Results and Discussion'

4.5.1 Mechanical testing

The mechanical set up will be tested for accuracy, speed and repeatability as these are all important aspects when it comes to designing an operational laser cutter. Step accuracy and repeatability will be measured with a digital calliper, which has a resolution of 0.01mm and is accurate to 0.03mm. This is 3 times more accurate than the 'Design Specification' requirement for the mechanics of 0.1mm. The speed will be tested by commanding the mechanical setup to move to a distant point and back and whilst being timed using the microcontroller. The repeatability will be tested by commanding the mechanical setup to cover a certain toolpath at high speed a number of times, its final position will then be measured and compared to the expected final position.

4.5.2 Optical testing

The optics will be tested for spot size and that light that is reflected off the workpiece is present at the photodetector. Spot size testing will be done by cutting a material and measuring the cut width. This should be repeated throughout the 50mm cut depth range as due to the focusing nature of light this will vary depending on the distance of the material from the laser. Testing for the presence of reflected light will be performed by shining the laser onto a mirror and then 'visually' observing the presence of this reflected light where the photodetector will be placed (observations will be carried out with a camera as infrared light is invisible).

4.5.3 Electronic hardware

Each aspect of the electronic design will be tested thoroughly to verify any simulations performed and expected performance.

The constant current supply will be verified by reading the voltage across the sense resistor using an oscilloscope at various set currents. The accuracy and ripple introduced by the current supply will be monitored. The modulation component of the laser driver will be tested by monitoring the AC current

through a small resistor in the modulation current path. This will show both the waveform and the magnitude of the modulation current. The modulation frequency will also be checked at this point.

The photodetector will be tested using a lower powered DVD laser diode connected to a signal generator. This poses a lower risk of eye damage and the lower power allows the diode to be powered by a signal generator, which typically drive higher impedance loads. The accuracy of the phase shift detection will also be tested using a 2-channel signal generator where relative phase shift can be controlled.

4.5.4 System testing

The complete system will be tested both for cutting ability and distance measurement ability. To test cutting ability materials with various different properties will be cut and the results observed and discussed. To test the distance measurement ability of the system a test rig, in which a portion of a workpiece can be moved back and forth accurately, will be constructed. The workpiece will then be set at different distances and the phase output measured and compared to the expected results.

5. Mechanical Design

The mechanical design of the gantry system is integral to the design of the other components and it was decided that this should be done first as it will have the most influence on other aspects of the project. The mechanical housing was also designed at the beginning of the project although this was not implemented during the course of the project. All mechanical designs were modelled and simulated in *SolidWorks*® before being constructed. This chapter aims to describe, in detail, the design process used to create the mechanics of the gantry system and explains why certain choices were made during the design process.

5.1 Conceptual Designs

There are many ways to design a 2-dimensional system that would be able to meet the requirements set out. Polar co-ordinate based systems were ruled out as a system such as this will not benefit from the inherent advantage it provides when cutting circles. After observing current laser cutters, milling machines and 3-dimensional printers, it was decided to explore two possible conceptual designs further. Both of these designs operate on the same x-y co-ordinate system.

5.1.1 Moving workpiece

This system would be one in which the toolhead remains stationary while the workbed (and workpiece) moves in the horizontal x-y plane. Rails would need to be fixed to the housing for a cross arm, containing another set of rails, to run along. The actual workbed would then move along this cross arm. This would require one motor to be fixed to the housing while the other is mounted to the gantry cross arm.

Advantages of this system are that the toolhead is stationary and therefore the complications of wiring and coupling a moving toolhead are eliminated.

The major disadvantage is that with a relatively large workbed area of 190x250mm this system would require the laser cutter to be at least twice the length and breadth of this in order for the workbed to move completely from one corner to another. Another disadvantage is that one motor needs to be mounted to the cross arm and therefore will be moving.

This design is one that is commonly used in milling machines and 3-dimensional printers, as the toolhead is usually large and heavy. These toolheads require geared coupling in the case of a milling machine or electrical and printing material in the case of a typical 3-dimensional printer.

5.1.2 Moving toolhead

This system would be similar to the 'Moving workpiece' design above although in this system both the workpiece and workbed remain stationary while the toolhead moves in the horizontal x-y plane. Rails would need to be fixed to the housing for a cross arm, containing another set of rails, to run along. The actual toolhead would then move along this cross arm. This would also require one motor to be fixed to the housing while the other is mounted to the gantry cross arm.

Advantages and disadvantages of this system are the converse to those above. It will produce an overall smaller system. With a moving toolhead, the complications of wiring and coupling would need to be overcome. One of the drive motors will need to be moving as in the design above.

This system is often used in commercial flatbed laser cutters as they require no electronics, materials supply or mechanical coupling for the toolhead which normally only contains a mirror and focusing lens.

5.1.3 Hybrid design

In the hybrid design both the workbed and toolhead move perpendicularly to each other. A set of rails for both the toolhead and workpiece would be fixed to the housing, as would their respective drive motor. This would allow the workbed to move in the 'x' direction and the toolhead to move in the 'y' direction allowing the complete x-y plane to be covered.

The major advantage of this system over the other two are that both motors are fixed to the housing and do not need to move. Not having a cross arm will also simplify construction and improve accuracies.

The disadvantages of this system are that the toolhead still needs to move and hence complications of wiring and coupling would need to be overcome. This system would also need to be twice as wide in the 'x' dimension in order to accommodate the workbed movements.

This system is used in specialised cases where the motors are large or very fine accuracies are needed.

5.1.4 Design selection

The 'Moving toolhead' design was decided upon for this project. The major reason for this was that the laser cutter is intended to be able to fit on a 'desk top' as set out in the 'Specification'. This design is smaller than the other two options. Other factors in the decision were that the toolhead will only need electrical coupling of digital and DC signals so coupling would not be a major problem and that the motors selected would be light and having one of them on a cross arm would not be an issue. Figure 2-1 shows the preliminary design and the final design can be seen in Figure 5-2 below.

5.2 Drive Type

Two major drive systems are employed to achieve translational motion in designs such as those mentioned above; these being either leadscrew or belt-driven systems and they are briefly discussed here. Both of these systems could easily be designed into all three of the aforementioned systems.

5.2.1 Leadscrew

In a leadscrew system, the motor shaft is attached to a long threaded rod, which has a non-rotating nut that travels along this rod as the rod is rotated by the motor. The object or platform to be translated would then be mounted to this nut.

The major advantage of a leadscrew drive in this design is that very high translational accuracies are achievable as very high effective gearing ratios are inherent to the system. For example, a 1.8° stepper motor with a 1mm pitch single start leadscrew has a theoretical single step distance of 0.005mm.

The major disadvantage in this design would be speed. Leadscrews generally have high friction and very small translational distance per revolution (equal to the number of starts multiplied by the thread pitch) when designed for higher accuracies.

5.2.2 Belt-driven

In a belt-driven system, the motor shaft is attached to a pulley and another pulley is attached to the far side of the translation range. A belt is then looped around these two pulleys and the object or platform to be translated would be mounted to this belt. For position accurate systems such as this, a toothed belt and pulley system is used to prevent slippage.

Belt-driven systems are a lot more efficient than leadscrew systems and they are a lot faster as one revolution of the drive motor causes a translational distance of π*d metres (where d is the diameter of the pulley in metres).

The disadvantage of a belt-driven system is that it is less accurate. For example, a 1.8° stepper motor with a 10mm diameter pulley has a theoretical step distance of 0.157mm.

The design specification states that the system be able to achieve mechanical accuracies of 0.1mm and a 'fast' feedrate ('3.1 Specification'). For these reasons, it was decided that a belt-driven system would be more suitable for this design. A 5mm wide T2.5 belt and 16mm diameter pulleys were chosen.

5.3 Motor Selection

In this design, the motors require accurate position control and the ability to rotate fully. There are two common methods of achieving this; these are stepper motors and closed loop controlled DC motors. The requirements of these motors will be discussed here and then a motor type, and finally a motor, will be selected.

5.3.1 Required speed and torque

The speed requirements of each motor will be the same as the gantry is expected to move the same speed in each direction; however, the torque requirements will not be the same as the 'x' direction motor will also need to drive the extra mass of the cross arm (this can be seen in Figure 4-1).

i. Speed and acceleration

The design specifications state that the mechanical system should be 'fast' ('Design Specification'). It was decided that this would mean that the mechanics should in no way limit the speed of cutting which should only be limited by the optical output power and hence cutting speed of the laser diode. For this reason, a target speed of $0.5ms^{-1}$ was set. It was decided that this speed should be reached in 0.1s giving an acceleration of $5ms^{-2}$. These values were used in the required torque calculation below. With a 40mm radius pulley, the motor would need to rotate at 12.5 rotations/second or 25π rad/s.

ii. Torque

The 'x' direction motor will need to drive the cross arm and therefore require more torque; thus these calculations only concern the 'x' direction motor.

The required torque will comprise of two sources, the first being the torque required to overcome friction and the other being the torque required for acceleration. The system is horizontally orientated therefore; no torque will be needed in order to overcome gravity.

Torque due to friction:

$$\boldsymbol{F_{fric} = \mu N}$$ **Equation 5-1** [59]

Where: F_{fric} is the frictional force
μ is the coefficient of friction
N is the normal force

The mass of the cross arm and toolhead system is estimated to be less than 1kg.

The coefficient of friction is assumed to be 0.1 as linear ball bearings running on hard steel are used. As no data was provided for the bearings purchased similar bearings' datasheets were consulted and in no situation was the quoted coefficient of friction higher than 0.1.

$F_{fric} = 0.1 * 1 * 9.81$
$F_{fric} = 0.981\ N$
Therefore $\tau_{Fric} = 7.848\ mN.m$

Torque due to Inertia:

$$\boldsymbol{\tau_{inert} = m * r * a}$$ **Equation 5-2** [60]

Where: τ_{inert} is the torque due to inertia
m is the mass
r is the radius of the pulley
a is the acceleration of the toolhead and gantry

The required linear acceleration is 5ms^{-2} at a pulley radius of 8mm.
$\tau_{inert} = 1 * 0.008 * 5$
Therefore $\tau_{inert} = 40\ mN.m$

Therefore, the total torque required is 47.9mN.m or about 0.05N.m.

5.3.2 Position accuracy

The resultant position is calculated by Equation 5-3 and shown in Figure 5-1, which shows that in a belt-driven system there are three factors that influence the position accuracy; namely, the rotational accuracy of the motor, the number of teeth on the pulley and the spacing of the teeth on the belt.

$$\boldsymbol{Step\ Distance = \frac{teethNum * toothspacing * \theta}{360}}$$ **Equation 5-3**

Where: θ is the step angle of the stepper motor

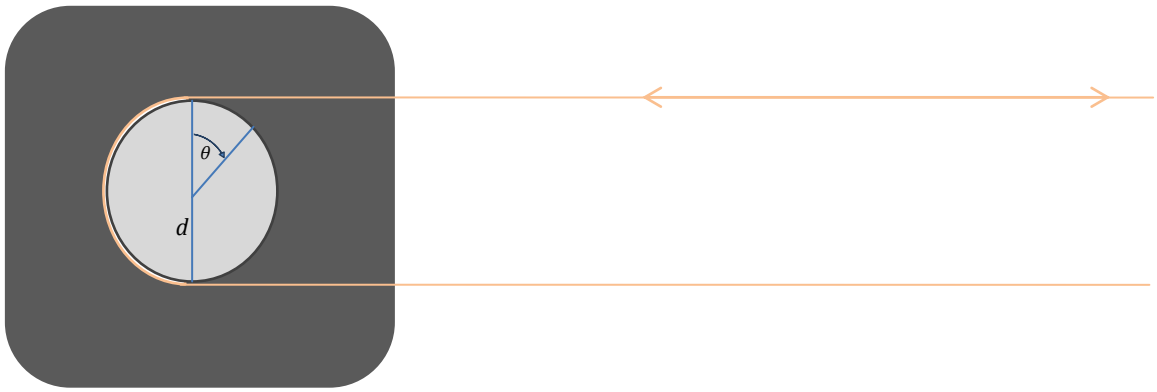

Figure Error! No text of specified style in document.**-1. Showing where the step angle and diameter are measured.**

The number of teeth on the pulley is 16, the tooth spacing is 2.5mm and step distance must be less than 0.1mm therefore θ can be calculated as follows:

$$\theta = \frac{0.0001 * 360}{16 * 0.0025} = 0.9°$$

This means that the motor must have a resolution of 0.9°. In the case of stepper motors, they can be fractionally stepped. Meaning a half stepped 1.8° motor would suffice.

5.3.3 Motor selection

Considering the above calculations and requirements it was decided that a stepper motor would perform best for this project. The low torque requirements of the motors mean that the major advantage of a closed loop controlled DC motor is not required. Stepper motors also require less processing power from the microcontroller allowing the microcontroller more time to perform other tasks.

After some market research, motors supplied by MANTECH Electronics [61] were found to be suitable. These motors are manufactured by Changzhou Fulling Motor Co. and the part number is FL42STH33-1334A [62]. These motors provides a step size of 1.8°, a torque of about 1000 g.cm or about 0.1Nm and a speed of 25π rad/s. These motors are also relatively small and light for their torque output relative to other stepper motors.

5.4 Choice of Materials

The choice of materials used for construction is very important. It was decided that with the high accuracy requirement of the gantry system that the materials should be rigid but light.

The sliding rods that the system runs on are made of hard steel as they will support the weight of the gantry and must not warp in any way.

The linear bearings are linear ball bearings. This is both to reduce friction, hence increasing speed, and to reduce wear that would occur on other friction bearings such as nylon bushes.

The machined components that act to hold the cross arm in place and as the toolhead mounting platform are all machined from aluminium. This is because aluminium is light and easily machined on a CNC milling machine.

The housing was designed with aluminium angle to provide the structure and hardboard to full the sides. Hardboard is relatively cheap, easily laser cut and will prevent any laser radiation escaping the housing.

5.5 Final Gantry Design

The gantry and housing were modelled in SolidWorks. The parts needing machining were machined in the UCT Mechanical Engineering department, and other parts were made or laser cut in the Electrical

Engineering department. Figure 5-2 to Figure 5-4 show screenshots of the assembly. Individual part drawings can be found in 'Gantry' in the appendix and SolidWorks .asm, .prt and .drw files can be found on the attached CD.

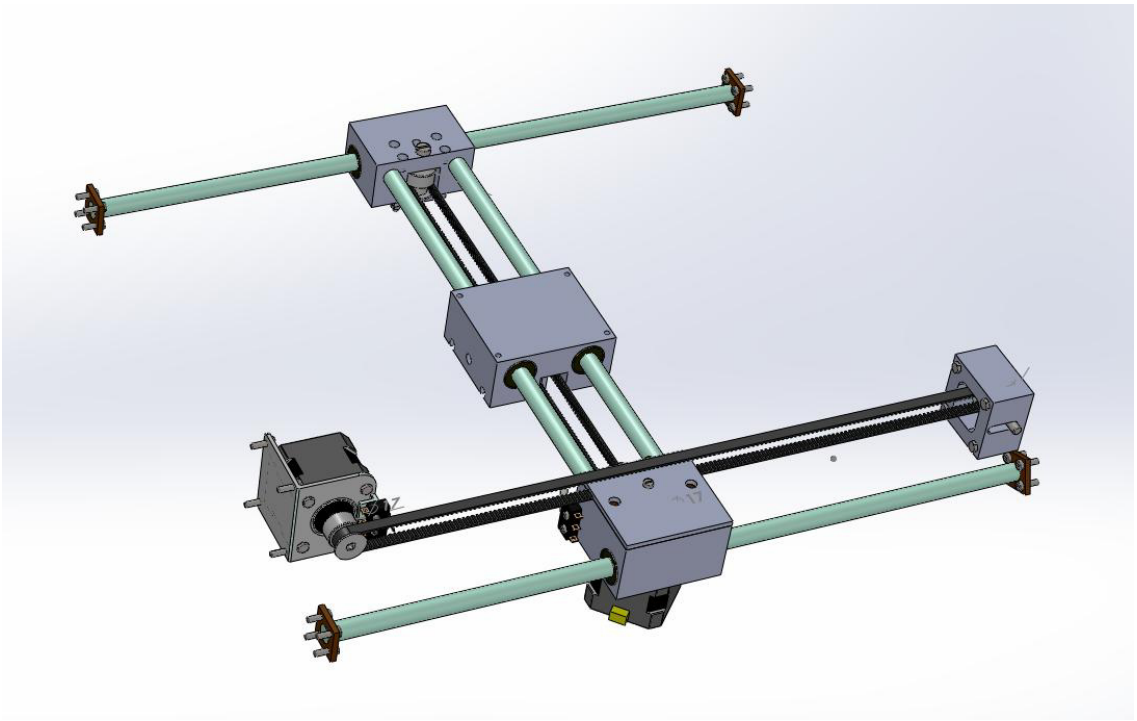

Figure 5-2. Showing the gantry system as modelled using SolidWorks. Green bars are stainless steel; grey is aluminium and brown is hardboard. The belts are shown in black. The two homing limit switches are also visible.

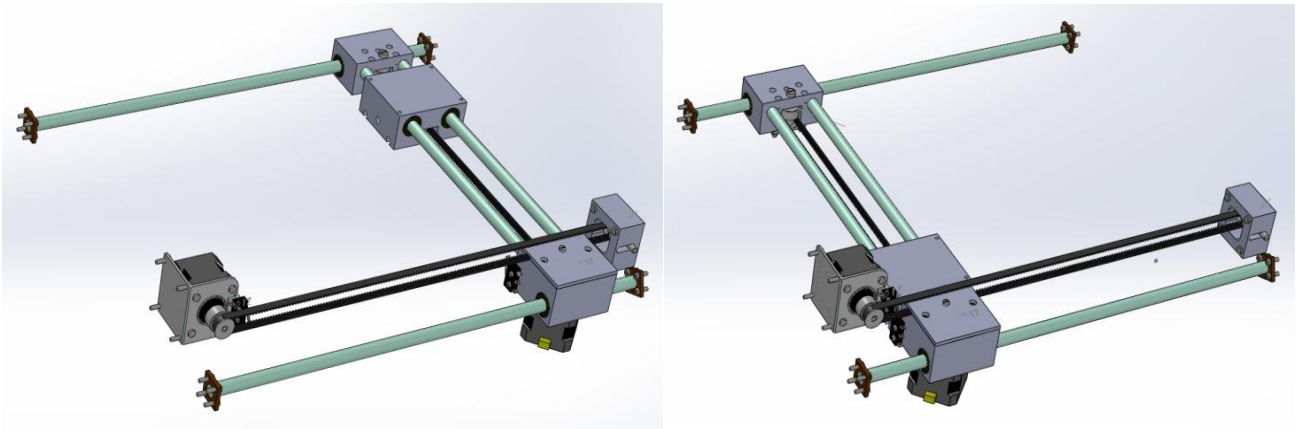

Figure 5-3. Showing the gantry system when the toolhead is positioned at either extreme of the workbed.

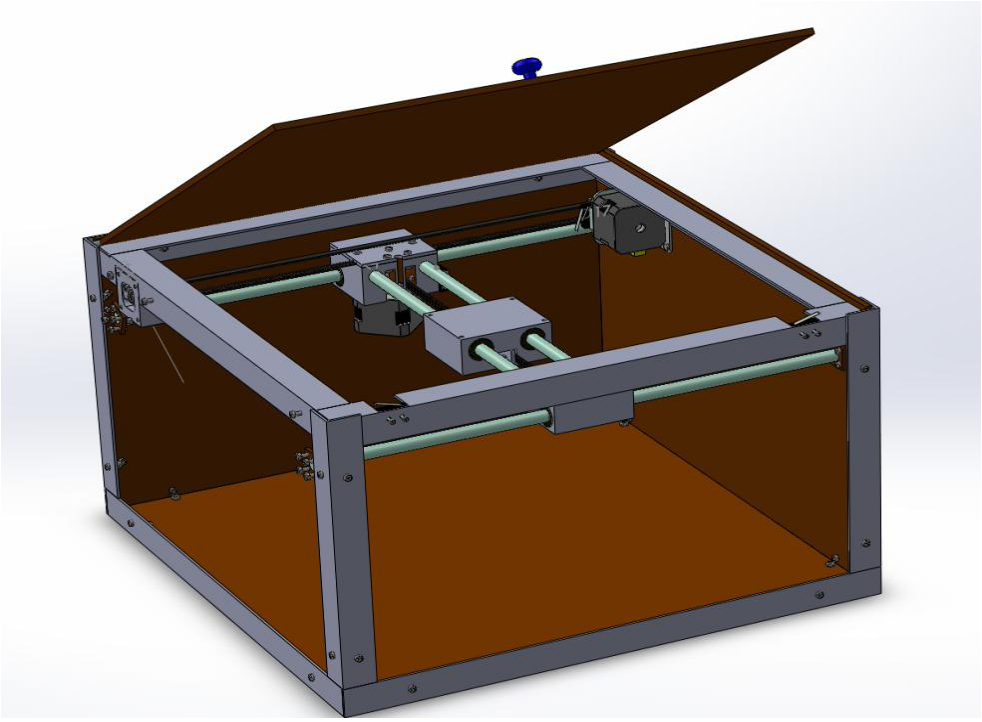

Figure 5-4. Showing the gantry within the housing. Two sides and the cutting bed have been hidden for clarity. The electronics would be located underneath the cutting bed. Two micro-switches can also be seen on the top of the housing, these would be used as safety switches to shut off the laser in case the lid is opened during operation.

5.6 Construction and Verification

The machined gantry parts were initially printed on a prototyping 3-dimensional printer to ensure that all the dimensions were correct and that parts would fit together as expected. Some minor adjustments were then made before milling the parts. One of these parts can be seen in Figure 5-5. Once all the parts were acquired and constructed they were assembles as per the design. A crude but structurally sound support system was built for gantry testing purposes, as it would be difficult to perform testing inside a closed housing. The constructed gantry and the support system can be seen in Figure 5-5.

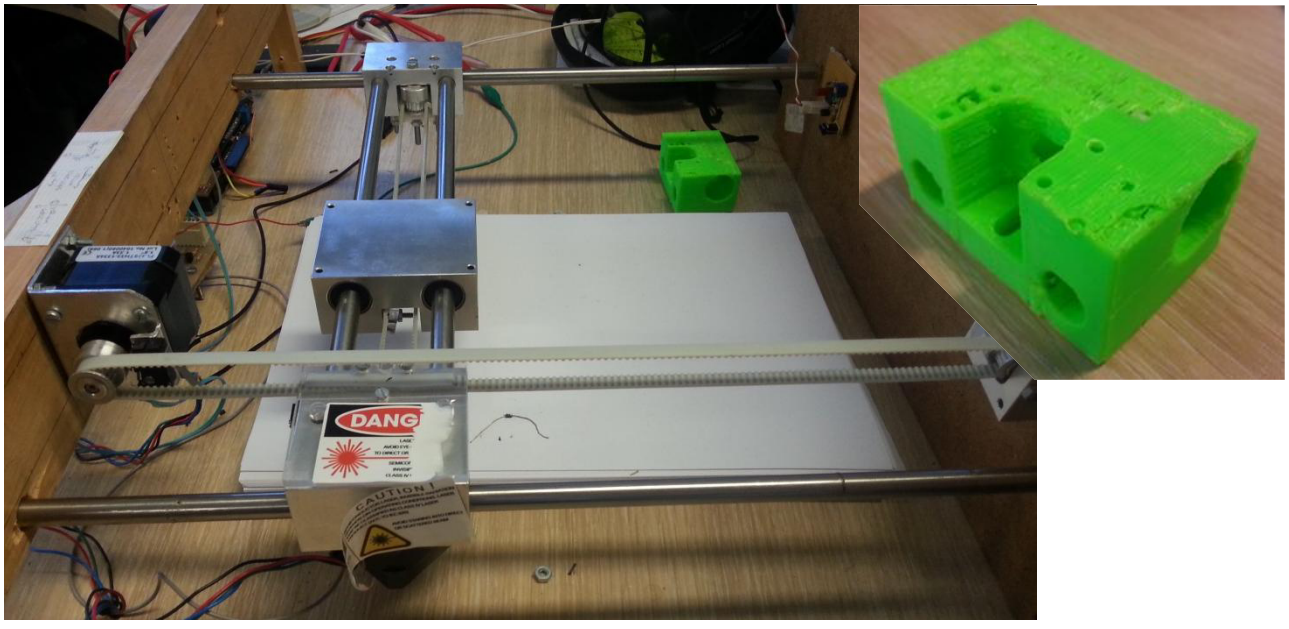

Figure 5-5. Showing a photograph of the gantry (LEFT) and a 3-dimensionally printed part (TOP RIGHT).

5.6.1 *Testing step size*

In order to test the step size a digital calliper was initially placed between the toolhead platform and one end of the cross arm. It was later placed between the cross arm and housing in order to test the other direction. The microcontroller was programmed to command the motors to step a half step and the stepped distance was measured; this was repeated 10 times over the full range of motion. These results were recorded and tabulated in Table 5-1. These verify that the step size meets the requirements set out in the design specification (3.1 'Specification'). The resolution of the calliper used is 0.01mm and this would apply to all the results meaning that the average step size in both directions would be 0.1±0.01mm.

Table 5-1. Showing the results from step testing.

Reading number	'x' direction (mm)	'y' direction (mm)
1	0.12	0.11
2	0.10	0.11
3	0.10	0.09
4	0.10	0.11
5	0.9	0.08
6	0.11	0.11
7	0.11	0.09
8	0.9	0.1
9	0.10	0.1
10	0.8	0.1
Average	**0.10**	**0.10**
Standard deviation	0.0115	0.01

5.6.2 *Testing speed*

In order to test the speed of movement the microcontroller commanded the motors to move to a far distance and back as fast as possible without missing any steps. This was timed using an oscilloscope. To check that no steps were missed the digital calliper was placed in similar positions to those mentioned above and the readings before and after were checked to be the same. A mass approximately the same as the toolhead was attached to the tooling platform in order to simulate the toolhead inertia.

The maximum speed that was achieved without missing steps was 1667 steps/s or 0.1667 ms^{-1} in the 'x' direction and 2500 steps/s or 0.25 ms^{-1} in the 'y' direction. Although no steps were missed at this speed, it is recommended that when accuracy is important a speed of 1000 steps/s or 0.1 ms^{-1} not be exceeded. Speeds of up to 10 000 steps/s or 1ms^{-1} could be, and were, used for homing and free-jogging functions but steps were missed when changing direction. These results met the requirements set out in the 'Design Specification'.

5.6.3 *Testing repeatability*

Repeatability was tested to some extent in the above two tests as no steps were missed and the standard deviation of the step size was calculated. A final test for repeatability was nevertheless performed where the gantry was commanded to go to the home position then move in a 'pizza slice'

route encompassing most of the workbed 100 times. It was then commanded to move back to where it expected 10 steps away from home in both axes to be. It then moved slowly counting the number of steps required to reach the home position, as this would indicate the number of missed steps in each direction. A 'pizza slice' route was chosen as it includes straight line, diagonal and circular movements. After repeating this 5 times and not a single missed step recorded, it was concluded that the system meets all repeatability specifications.

5.7 Toolhead Design

The toolhead will be responsible for mounting the optical assembly, laser driver PCB and the photo sensor PCB. This is necessary, because both of the PCBs need to be physically close to the laser for best results. The position of the optics assembly and the laser driver PCB will be fixed relative to each other and need not be adjusted at any stage but the position of the photo sensor PCB will need to be adjustable in all three dimensions in order to ensure that the SHF2701 photodiode is in the correct position relative to the optics.

The toolhead configuration was designed after the optical assembly, laser driver PCB and the photo sensor PCB. The toolhead mounting block was designed toward the beginning of the project. The PCBs would need to be mounted on a nonconductive platform that is then attached to the mounting holes that were included on the toolhead mounting block. It was decided to use Perspex as the platform because it is available, rigid and easily laser cut. The laser driver PCB and the optical assembly were fixed to this Perspex platform and the photo sensor PCB was mounted to a movable and adjustable gripper that would hold it in place. This gripper clamped onto the optics assembly and could be swivelled around or moved up and down on this grip; there were two slots in the gripper which allowed the distance of the photo sensor PCB from the optics assembly to be adjusted. The clamped grip onto the photo sensor PCB itself allowed it to be adjusted vertically and horizontally.

The whole toolhead assembly is attached and detached from the toolhead mounting block by four M3 screws; this was in order to make testing and repair work a lot easier. The complete toolhead assembly can be seen in Figure 5-6 with the toolhead mounting block in black. Individual part drawings can be found in 'Toolhead' in the appendix and SolidWorks .asm, .prt and .drw files can be found on the attached CD.

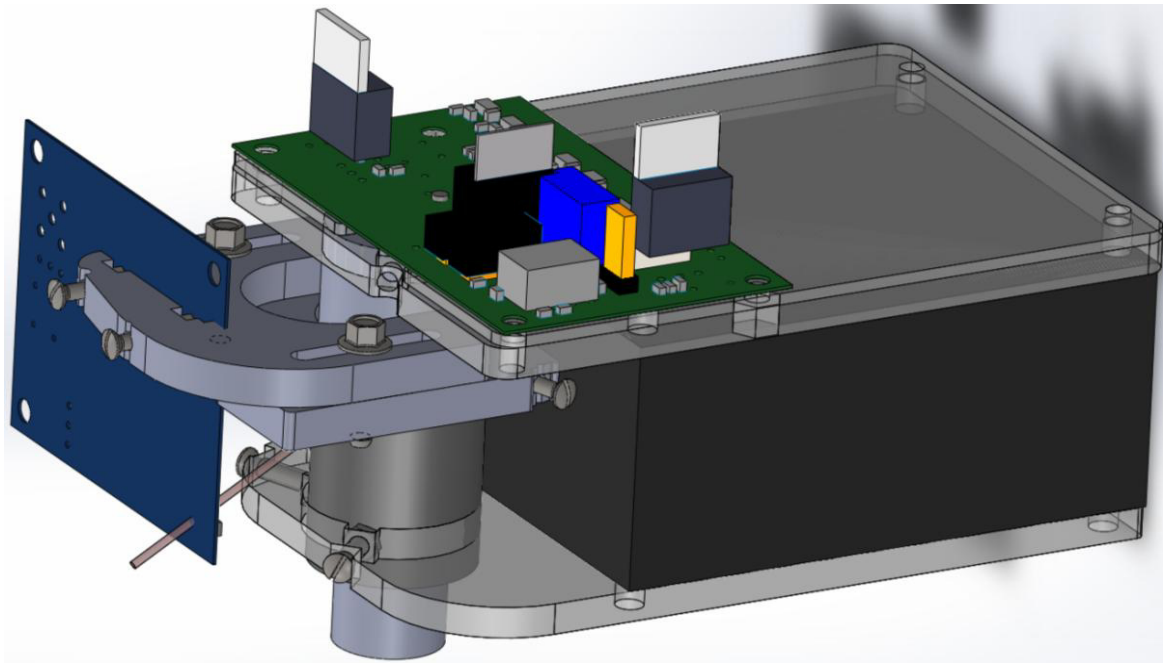

Figure 5-6. Showing the final toolhead assembly.

5.8 Testing Rig

A testing rig was designed and built, on which the toolhead could be mounted horizontally along with a digital calliper positioned in such a way as to measure the distance between the laser and an object attached to the calliper. The toolhead was attached to the test rig by the same four M3 bolts that attach it to the toolhead mounting block, which allowed the toolhead to be moved from the gantry to the test rig easily. A photograph of the test rig can be seen in Figure 5-7. Individual part drawings can also be found in 'Test Rig' the appendix and SolidWorks .asm, .prt and .drw files can be found on the attached CD.

Figure 5-7. Showing a photograph of the test rig.

6. Optics

This chapter discusses the optics that were considered, tested and finally implemented during the design of the laser cutter. All laser systems need some sort of optical system in order to manipulate the laser in such a way that it is useful. The optics in this system had two broad tasks to accomplish; these being to focus the laser onto the workpiece and to direct the reflected laser radiation onto the sensor. Accurate optics are inherently expensive because of their precision so a design would need to be as cost effective as possible.

6.1 Laser Diode

In order to design the optics with any accuracy the laser that was going to be used in the final design had to be selected and then purchased. A 2W continuous optical power, 802nm, C-mount laser diode produced by Osram Opto Semiconductors [58] (part number: SPL_CG_81_2S) was selected as this was one of the higher optical powered single emitters available at the time. This laser is not sold with any optics.

Notable characteristics of the laser, in terms of optical design, are that it has a wavelength centred about 808nm with a 6nm maximum spectral width. This is in the near infrared range and is therefore invisible and extremely dangerous to eyesight. It also does not radiate in a round beam pattern meaning the beam will have a major and minor axis. The shape of the light leaving the laser can be seen in Figure 6-1 but is treated as either elliptical or circular in subsequent calculations, depending on whether the beam shape has any affect in those calculations. The major consequence of this is that the optics will have a different effect on each of these axes. The major axis also has a very large beam divergence of 38° FWHM (or 60° for 92.8% of the total power as calculated in Figure 6-2, this was used during design) meaning that the optics would need to capture and collimate this wide divergence. This is an expected divergence for a standard broad area laser. [16, p. 38] Figure 6-2 and Equation 6-1 show the relative intensity, I_{rel}, at various angles; the integral of this gives power. I_{rel}, in Equation 6-1, is a best-fit graph because the true Gaussian curve is not given in the datasheet. Other optical characteristics of this laser can be seen in the datasheet [58].

$$\boldsymbol{I_{rel} = 100 * e^{-0.0018x^2}} \qquad \textbf{Equation 6-1}$$

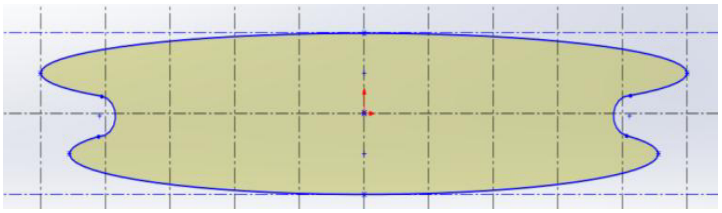

-Each line represents 5° from axis centre
-Major axis horizontal
-Minor axis vertical

Figure 6-1. Showing the shape of the beam as it leaves the laser.

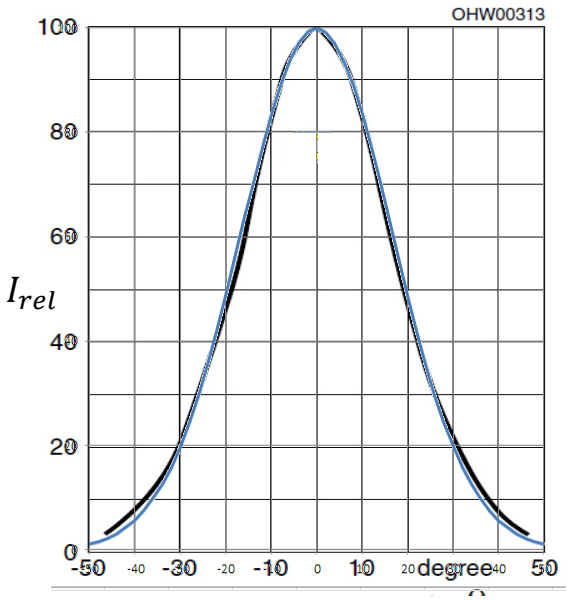

$$\frac{\int_{-30}^{30} I_{rel}}{\int_{-\infty}^{\infty} I_{rel}} = \frac{3877.5}{4177.71} = 0.928$$

Figure 6-2. Showing major axis beam distribution given in datasheet overlaid with approximate major axis beam distribution function (blue).

6.2 Preliminary Designs

During the preliminary design phase, the laser was considered a circular beam and standard geometric optical calculations were used. Three preliminary physical setups were considered and these were briefly discussed in 4.2 'Optical Design' and can be seen in Figure 4-2.

6.2.1 Selecting a Physical Configuration

It was noted that configurations 'A' and 'C', in Figure 4-2, were very similar but are distinguishable in that, configuration 'C' would be used if the laser was stationary and mirrors were used to direct the beam to the toolhead. This configuration would then need two optical sensors, both on the toolhead, in order to mitigate the distance travelled by the gantry. Configuration 'B' allows all the optical power to reach the workpiece but also requires a third lens and would need to be a lot more precise in order to ensure that the optical sensor is receiving light reflected from the cutting point and not alongside it. Due to this added complexity configuration 'B' was ruled out early in the design process although it should be considered in future work.

Following some design and research it was realised that the optics and laser drive circuitry could be made small enough to be carried on the gantry's toolhead platform and that configuration 'A' would therefore be both the simplest, most accurate and easiest configuration to implement.

6.3 Initial CD/DVD Optics Testing

Early on in the optical design phase of this project it was realised that there are many similarities between CD/DVD drive optics and this project, with the main difference being the power of the laser. For this reason, optical elements from a CD drive were used for much of the early testing of both the optics and photodetectors.

6.3.1 *Preliminary design configuration testing*

In a CD drive, a 780nm diode laser shines onto the surface of a CD and the reflected laser beam is detected by a photodetector. These optics can be seen in Figure 6-3. Showing the optics in a CD drive which also shows the path of the laser both to the CD and reflected from the CD (the collimating lens is below the 'complete reflector'). This system is optically very similar to configurations 'A' and 'C' in Figure 4-2.

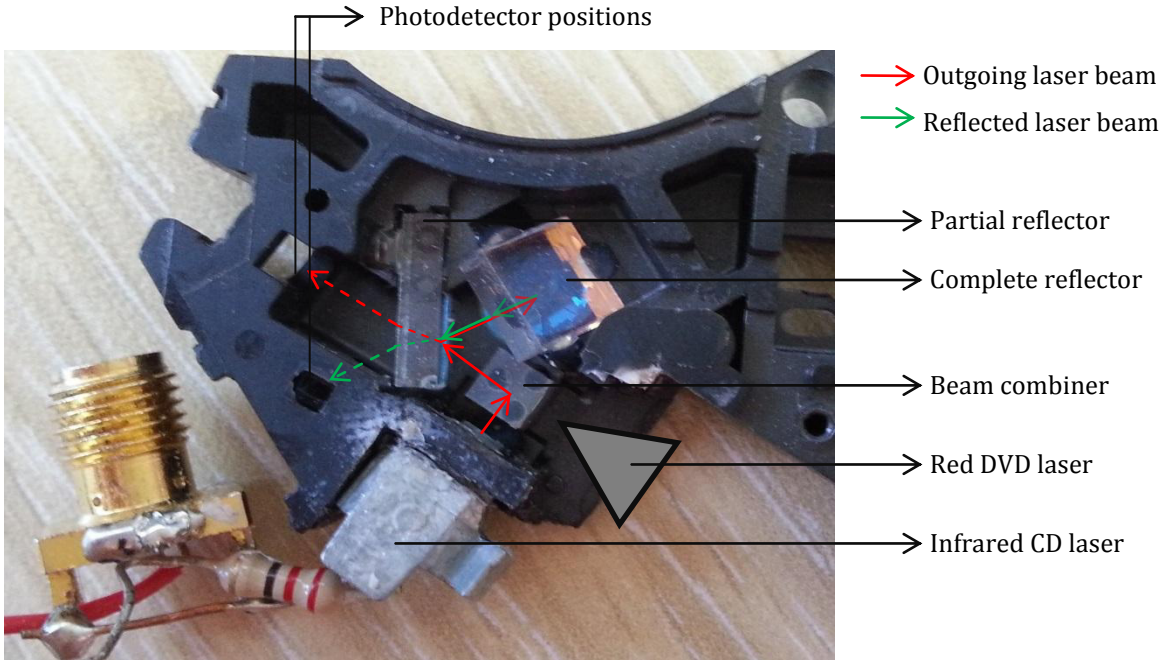

Figure 6-3. Showing the optics in a CD drive.

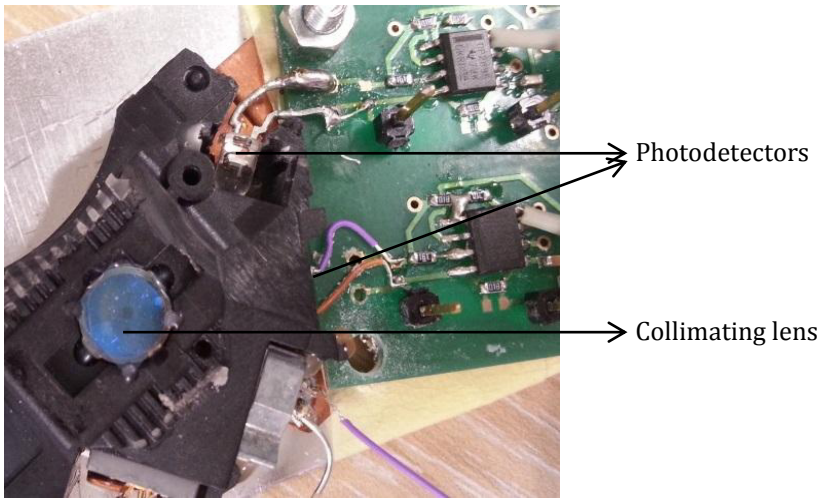

Figure 6-4. Showing the other side of the CD drive optics with the photodetectors and phase shift circuitry in place.

The CD laser was driven at 10MHz using a signal generator and the signals received by the photodetectors were monitored with an oscilloscope. When a reflective object was placed in front of the collimating lens at various heights, a signal was detected on both photodetector channels whereas when no reflector was present a signal was only detected on a single channel. The phase between the signals was also monitored and found to shift proportionally to the height of the reflective object as predicted Equation 2-7 above. This proved that the preliminary design would perform as expected.

6.4 Final Design and Assembly

The mechanical components of the optics were designed in SolidWorks whereas the mathematical calculations were performed by hand.

6.4.1 *Design requirements*

Figure 6-5 shows a modified version of configuration 'A', from Figure 4-2. This is how the optics were designed and implemented.

Notable differences, requirements and reasons are:

- Minimise d_1. | This will allow a smaller collimating lens to be used, which is cheaper and smaller lenses are generally able to achieve higher numerical apertures.
- Allow d_2 to be adjustable by moving the focusing lens. | This will allow the focal distance, d_3, to be adjusted.
- Place the partial reflector at a 60° angle. | This will minimise optical noise from the outgoing beam.
- Use a small focusing lens. | This will allow a smaller spot size over focal range.
- Ensure that beam is slightly divergent in d_2. | This will focus the reflected signals onto the photodetector.

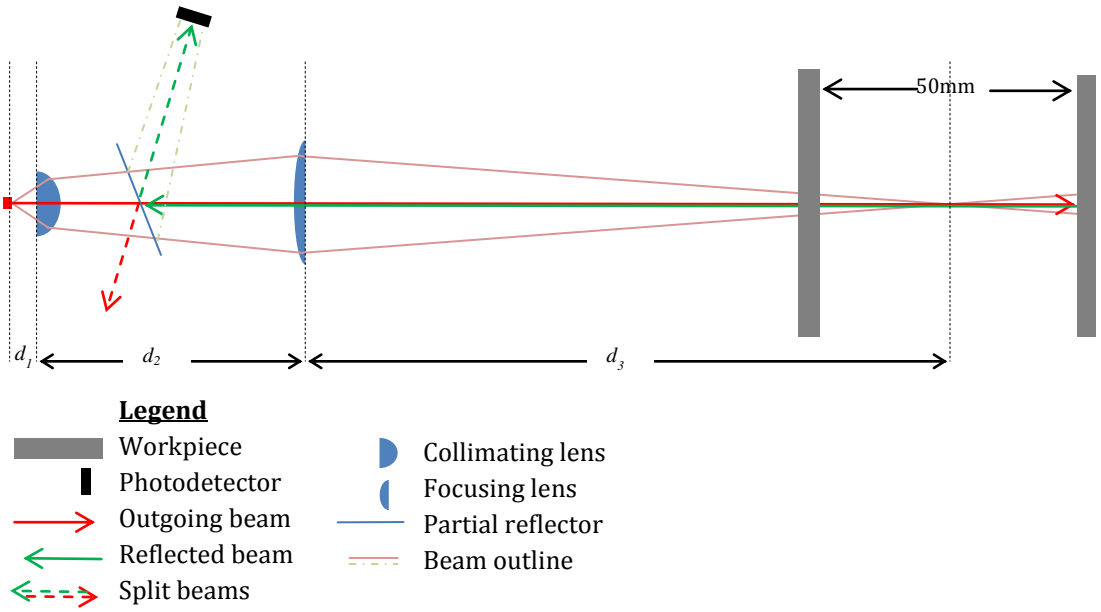

Figure 6-5. Showing a representation of the optical design.

6.4.2 *Mathematical calculations*

For the optical mathematics, the laser was assumed to be a circular beam. The beam divergence exiting the laser was considered 60°.

i. Collimating lens

The Numerical Aperture (NA) of a lens must be greater than that of the laser beam entering it in order for the lens to affect the whole laser beam. The NA is calculated as follows:

$$\boldsymbol{NA = n * sin\theta} \qquad \textbf{Equation 6-2 } [63, \text{p. } 137]$$

where: NA – Numerical Aperture
n – refractive index (= 1 for air)
θ – half-angle of the lens

NA is defined for both the laser and the optical elements and Equation 6-2 is derived from Snell's Law. The NA is a simple way to relate focal length and lens aperture.

For the laser θ = 30°, NA = 0.5.

This implies that the NA of the collimating lens should be 0.5 or greater.

ii. Focusing lens

Assuming that the beam divergence before the lens is 5° and that d_3 = 40mm the focusing lens needs a focal length of about 25.6mm. This was found using Equation 2-6.

$$\frac{1}{f_1'} + \frac{1}{f_2'} = \frac{1}{fl}$$

$$f_1' = \frac{D_2}{2\tan\theta_2} = 71.23mm. \;|\; f_2' = d_3 = 40mm. \;|\; fl = 25.6mm.$$

If the diameter of the collimating lens is D_1 = 3.6mm, the beam divergence exiting it is θ_2 = 5° and d_2 = 30mm then the diameter of the focusing lens, D_2, must be 6.22mm as seen in Figure 6-6.

$$D_2 = D_1 + 2 * d_2 \tan\theta_2 \;|\; 3.6 + 2 * 30\, tan(2.5) = 6.22mm.$$

d_2 will be adjustable to correct for any mechanical errors.

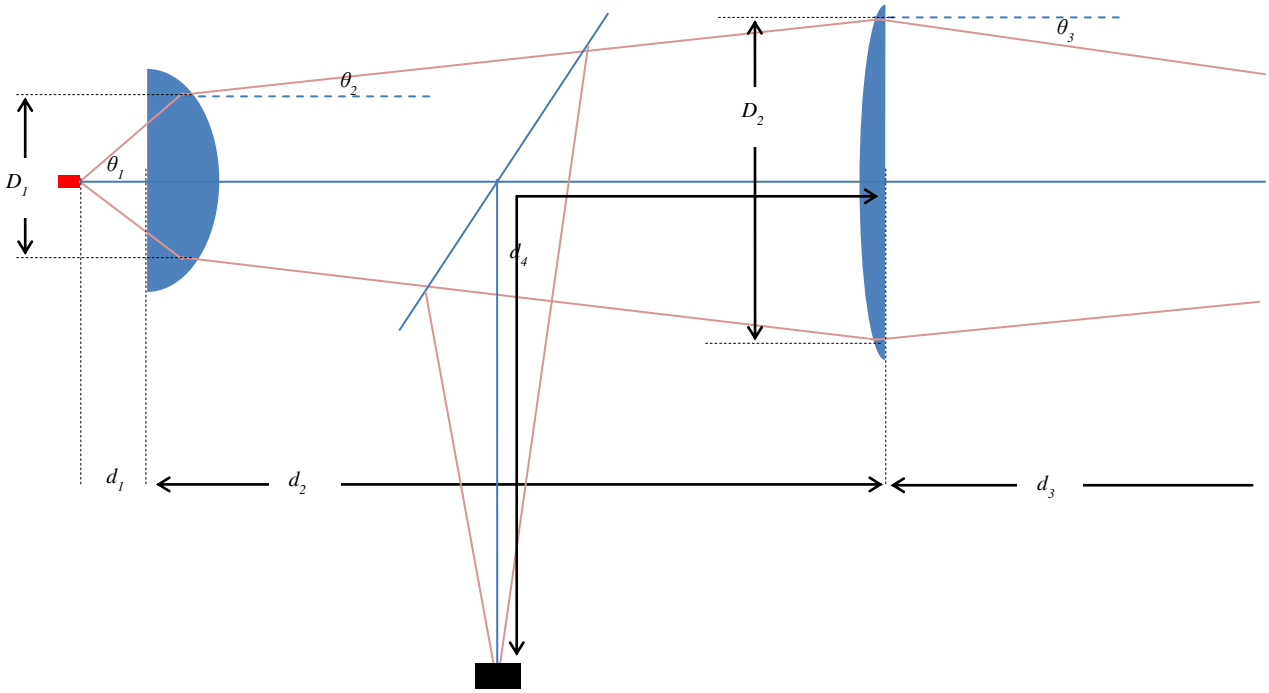

Figure 6-6. Showing mathematical references on the optics.

iii. Distance to photodetector

The distance to the photodetector, d_4, is simply the distance from the focusing lens to its focal point. This can be calculated as follows: $\frac{D_2}{2\tan\theta_2} = 71.23mm$. In fact, the photodetector used has a sensitive area that is 0.6x0.6mm large. This means that at a 5° beam convergence the photodetector can be placed 7mm on either side of the focal point (on axis) and still receive all the reflected optical power.

6.4.3 Optical elements

The most critical element in the optics is the collimating lens as it has a small diameter and short focal length, hence a high NA. This high NA means that optical aberrations arising from this lens would be most pronounced. For this reason astigmatism and coma corrected glass aspheric lens produced by ThorLabs (part number: 355392-B, [33]) was selected and ordered. This lens is similar to those used in CD drives for focusing but clouding of the lenses occurred because these plastic lenses were not able to handle the high power densities in this design.

The focusing lens used was from a CD drive. As it was a salvaged lens, no details about this lens were known. CD drives operate at 780nm so it is reasonable to assume that the coatings used would not have any major effect at 808nm. This was also tested by measuring the optical signal from the laser with and without the lens directly in from of the photodetector; no noticeable differences in optical power were detected. The aperture was measured to be 6.5mm, which is greater than the 6.22mm required. The focal length was measured, by shining collimated light through the lens, to be 24mm. This lens in the arrangement aforementioned will focus the laser at a distance of 36.2mm from the said lens. This is 3.8mm shorter than initially intended but will be able to be corrected for by adjusting d_2 manually.

The partial reflector is a small, thin, flat and clear piece of glass with a high transmittance in order to allow most of the laser power to reach the workpiece. It measures 6 x 8 mm making it large enough not to obstruct the laser beam.

6.4.4 Optical Mechanical design

The optics were designed and modelled in SolidWorks. One part was turned on a lathe while the other parts were laser cut.

Figure 6-7 shows an exploded view of the optical assembly. The laser mount and heat-sink (transparent to show laser) was turned on a lathe in the Mechanical Engineering Department; this was made from aluminium and is reasonably thick in order to act as a heat-sink for the laser. The collimating lens mount was designed so that the back/flat side of the lens was flush with the mount. This mount then pressed against the laser mount, which has a small flange to hold the lens mount at the correct distance (some rings of paper were used between the lens mount and flange to correct for slight machining errors, rings of copper shim would have been preferable but were not available at the time of construction). Some spacers were inserted between the collimating lens and casing; one of which was a compressible rubber designed to hold everything in place when the casing is screwed in. The partial reflector was set at a 60° angle in a wooden mount. The reflection from the laser beam traveling to the workpiece is absorbed by highly absorbent black rubber foam and a black paper window was glued to either side to reduce optical noise/reflections. The casing has a small hole for the reflected light to exit at a 60° angle. The collimating lens was mounted in a piece that screwed into the casing, this allowed the distance of this lens from the laser to be adjusted. Figure 6-8 shows the assembly of the optics.

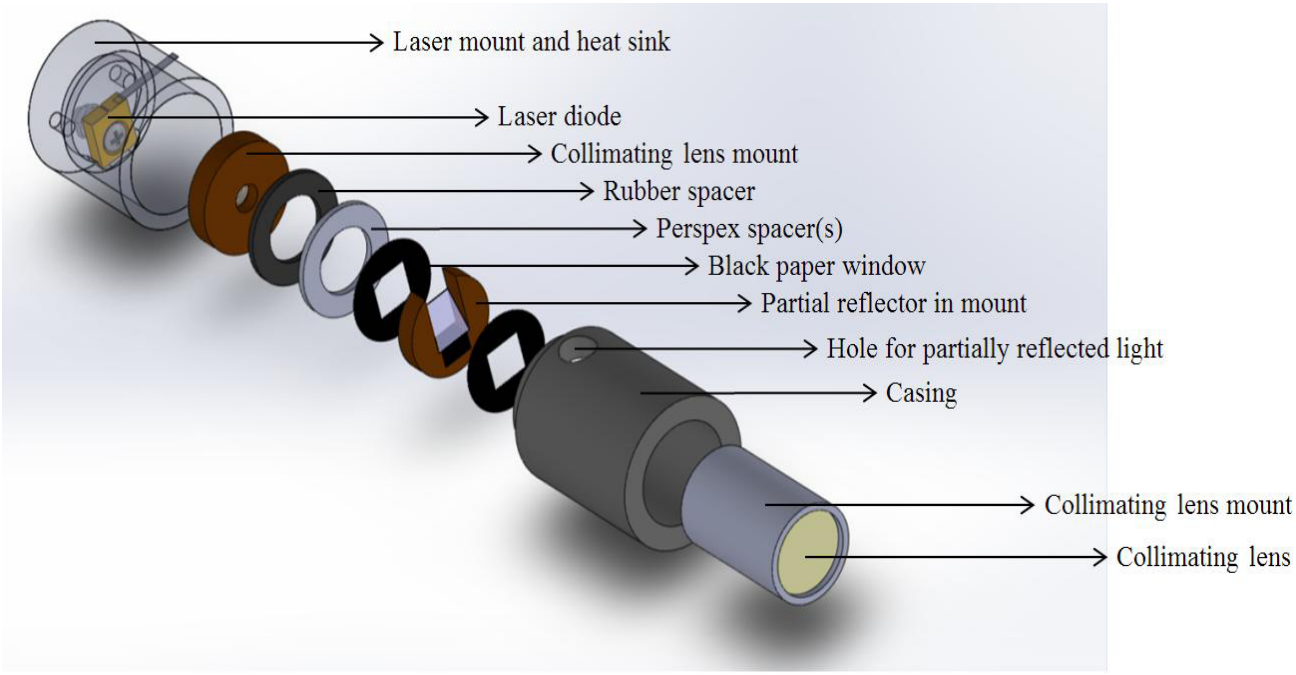

Figure 6-7. Shows an exploded view of the optical assembly.

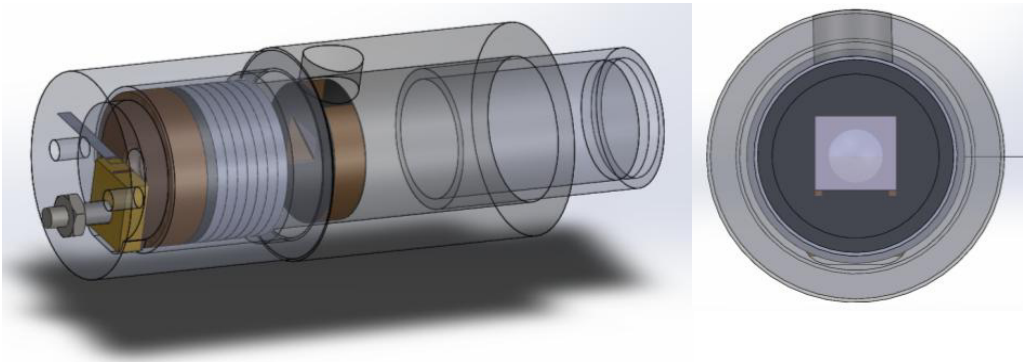

Figure 6-8. Shows a projection of the assembled optics and an end view into the optics.

6.5 Testing

The three major elements of the optics; namely, the collimating lens, focusing lens and reflector were tested and verified to be operating as predicted.

6.5.1 Collimating lens

The collimating lens was mounted in place as expected without either of the other optical elements and the beam divergence was measured. Two rings of 0.09mm thick pieces of paper needed to be placed between the collimating lens mount (increasing d_1 by 0.18mm) and the laser mount in on order to achieve the required beam divergence.

The laser beam was directed onto a piece of black paper, with grid markings, set at three different distances as seen in Figure 6-9. The diameter in both the major and minor axes were measured and recorded in Table 6-1. Appropriate calculations show that the divergence in the major axis is 6.8° and in the minor axis is 4°. This was larger than expected but should be able to be corrected by the focusing lens. Adding a third piece of paper, hence increasing d_1 by a further 0.09mm, caused the collimating lens to focus the laser. This would be undesirable, as the focusing lens would not serve to focus the light reflected off the workpiece onto the photodetector.

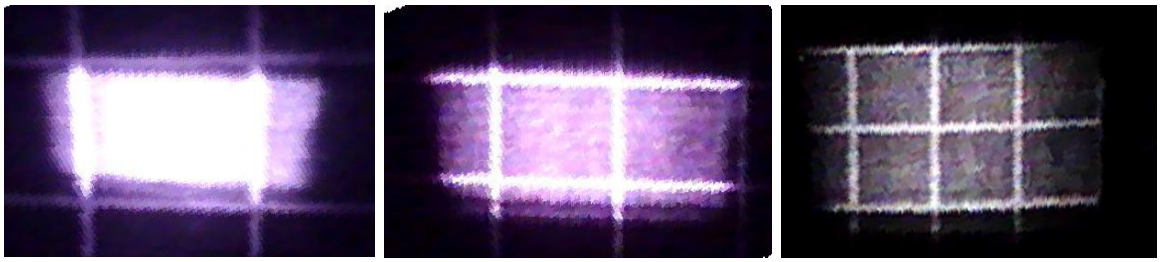

Figure 6-9. Laser beam directed onto black paper with 10mm grid markings at a distance of 100, 200 and 300mm respectively.

Table 6-1. Showing the results obtained when testing beam divergence.

Distance (mm)	X(mm)	Y (mm)	Θ_x (°)	Θ_y (°)
100	1.24	0.68	7.08	3.89
200	2.27	1.39	6.48	3.98
300	3.67	2.14	6.97	4.08
	Average divergence:		**6.84°**	**3.98°**

6.5.2 *Focusing lens*

The focus of the laser was then tested by using it to burn a black plastic ruler, with short pulse durations to prevent excessive melting, at eleven set distances (seen in Figure 6-10). The nine burn marks (making up a 40mm depth range) were then measured in both axes and recorded in Table 6-2, the initial '0mm' reading was made 20mm from the focusing lens. This distance allowed the designed focal point of 40mm to be at the centre of the testing range.

From these results, it can be seen that the focal distances in the x-direction (major axis) and y-direction (minor axis) are not the same. The major axis has a focal point at about 35mm from the focusing lens and the minor axis is focused about 60mm from the focusing lens. It is also observed that the change in the major axis dimension is larger than expected due to it having a larger beam cross section throughout.

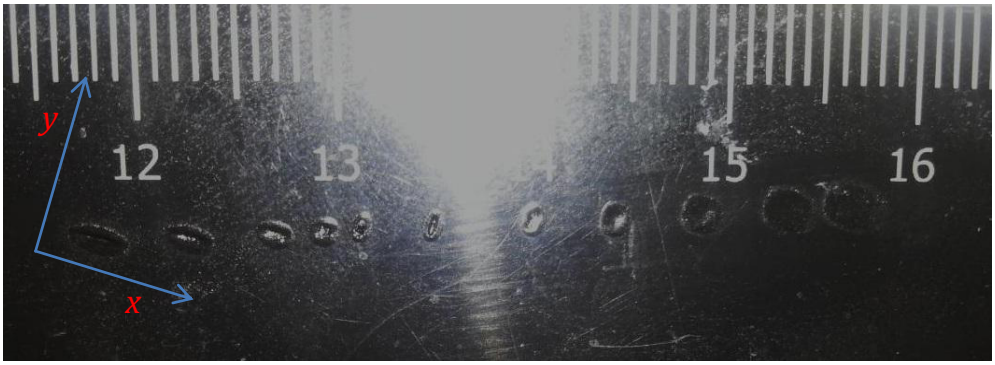

Figure 6-10. Showing burn marks in a ruler, each is 5mm further from the focusing lens.

Table 6-2. Showing the measured cut dimensions shown in Figure 6-10. (all measurements in mm).

Δ distance	40	35	30	25	20	15	10	5	0
x	2.5	2.08	1.25	0.83	0.42	0.21	0.42	0.63	1.25
y	0.21	0.31	0.63	0.83	0.83	1.04	1.25	1.25	1.46

6.5.3 *Reflector*

In order to test the reflector the laser was shone onto a reflective surface and a bright spot appeared on a piece of paper set where the photodetector would be. This spot then disappeared when the reflective material was removed. The said spot can be seen in Figure 6-11 and was observed using a webcam with optical filters.

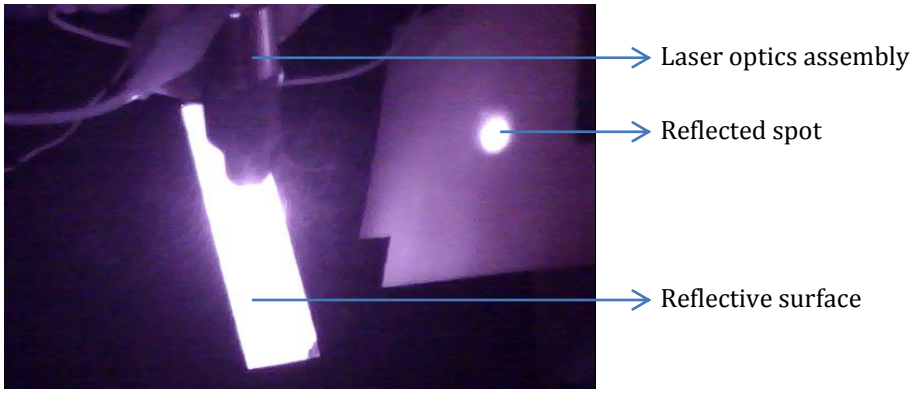

Figure 6-11. Showing the expected operation of the reflector.

6.5.4 *Optical aberration discussion*

As can be seen in Figure 6-10, the laser is not focused to an elliptical spot that only changes size as distance changes but the axis of the laser beam with a larger diameter also changes from horizontal to vertical. This is because the laser beam exiting the laser is elliptical and has a different back focal point for each axis [64, pp. 3, 5](meaning the source of the laser appears to be different depending on the axis it is viewed in). This causes the optical elements to have a slightly different effect on each axis. This, in turn, causes two different focal points, one for each the major and minor axis. This is a form of optical astigmatism as discussed in 'Astigmatism'.

In applications such as this where a small round laser spot is required, there are three common ways to reduce astigmatic aberrations; to use a cylindrical lens to collimate each axis separately [65], to use pair of prisms to increase the beam width in one axis and produce a circular shaped beam [66] or to place a thick piece of glass at an angle in the beam path to reduce the beam width in one axis [67]. ThorLabs recommends the use of an Anamorphic Prism Pair such as PS879-A [68]. This was deemed both too expensive and too complex for a proof of concept project such as this.

The reflector was placed in such a way that the major axis of the laser was in the same plane as the reflected beam. Theoretically, this would help to reduce the width of the major axis [67], and hence the difference in width of the two axes, but this effect was too small to be measured with the equipment available.

The collimating lens was aspheric and aberration corrected. Coma, field curvature and distortion aberrations were all mitigated by the fact that the laser and all the optics were placed on the same optical axis.

6.6 Optical Sensors

The optical sensor plays an integral role as it will be used to detect the laser beam that is reflected off the workpiece. Some elements of photodetectors are discussed here.

6.6.1 *Sensor type*

There are four types of optical sensors that were considered for this project and they are discussed here. Their positive and negative points have been noted using '+' and '-' symbols.

Standard P-N photodiode [69]

+ most common way to measure any form of light
+ readily available
+ well understood and easy to implement
– slow response time
– not very sensitive

Avalanche photodiode [70]

+ very sensitive to small amounts of light
+ internal gain due to avalanche effect
+ very fast
– high, and potentially dangerous, voltages required

Phototransistor

+ sensitive to small amounts of light
+ internal gain due to h_{fe} of transistor
− longer response times

PIN photodiode [71]

+ common in fibre-optic networks
+ very fast response times especially in photoconductive mode
− less sensitive than avalanche photodiode or phototransistor
− small reverse voltage required

6.6.2 Sensor requirements

The major requirement for the optical sensor in this project was that it be able to measure signals at frequencies of hundreds of megahertz. Internal gain was not seen as a requirement as the optical output from the laser is very high and the reflected signal should be large enough to be received by any of the aforementioned photodetectors.

i. Expected reflected power

Assuming the transmittance of the optical elements is negligible, the reflectivity of the reflector is μ and the retro-reflectivity of the workpiece is α.

The power at the photodetector, assuming no other significant losses occur and well-focused optics, is calculated as follows:

$$\boldsymbol{P_r = P_{laser} * (\mu.\alpha - \mu^2.\alpha)} \qquad \textbf{Equation 6-3}$$

Assuming reasonable values for μ and α are 0.1 and 0.2. The modulated laser power when measuring distance is $P_{laser} = 0.5W$.

Therefore:

$P_r = 9mW$

The design allowed for a worst case of 90% of this expected power to be lost in inefficiencies and inaccuracies leaving 1mW of optical power.

6.6.3 Selected sensor

For the reasons listed above it was decided that a PIN photodiode would be best in this application. Two photodiodes were considered, the BPW43 from Vishay Telefunken [72] and the SFH2302 from Osram Opto Semiconductor [73]. Assuming a reverse voltage of 10V, the BPW43 offers a switching time of 4ns and a junction capacitance of 1.3pF, whereas the SFH2302 offers a switching time of 1.6ns and a junction capacitance of 1.9pF. Both have a high relative sensitivity at 808nm and both are packaged in standard through-hole LED packages. After searching the SFH2302 from Osram Opto Semiconductor website the SFH2701 [74], a surface mounted version of the SFH2302, was discovered. This has very similar characteristics but being surface mounted there will be less stray capacitance

and inductance caused by the leads of the SFH2302. For this reason, the SFH2302 was selected and used as the photodetector in this design.

The response time and junction capacitance of the SFH2701 were deemed satisfactory. The spectral sensitivity is marked as 0.5A/W and at an expected received power of 9mW; this should produce 5mA of photocurrent (or a worst case of 500μA of photocurrent). This is more than the maximum photocurrent the SFH2701 can produce and the SFH2701 is therefore sensitive enough.

7. Laser Driver

This chapter aims to describe the circuitry that was designed in order to drive the laser. Some of the design decisions that were made during this process are also explained here.

7.1 Electrical Properties of Laser Diodes

Laser diodes are constant current devices and operate similarly to standard diodes or light emitting diodes (LEDs). A 2W continuous optical power laser produced by Osram Opto Semiconductors [58] was selected due to its optical characteristics. Some of this laser's electrical characteristics are discussed here.

The optical output power is proportional to the current through the laser as can be seen in Figure 7-1. There is also a threshold voltage and current. The threshold voltage is 0.7V; this is when the laser starts to conduct current although no lasing occurs at this voltage. The threshold current is when the laser diode transitions from LED operation to laser operation meaning that the total photon energy is enough to cause stimulated emission. The lasing threshold current is 0.6A [75].

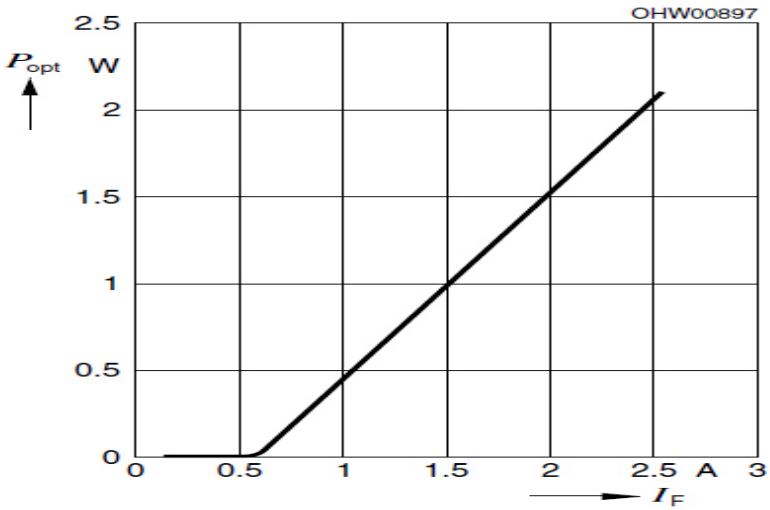

Figure 7-1. Optical Output Power vs. Forward Current. [75]

Other electrical properties to take note of are; the low reverse voltage of 3v, operating current of 2.35A (maximum of 2.6A), a differential efficiency of 1.15A/W and a forward operating voltage of 1.9V [75].

7.2 Laser Driver Requirements

The laser driver circuitry will need to fulfil two major roles; firstly to drive the laser with a constant current and secondly to provide a high frequency modulated current in order to modulate the output of the laser. It would also need to do both of these concurrently.

The constant current should also be able to be controlled externally and the frequency should be variable. It would be preferable if these can also be controlled by the microcontroller as it would allow for more flexibility when testing and trouble shooting.

The frequency should be controllable over a range of 10 to 100MHz. The reason for the low 10MHz requirement is that available signal generators can generate signals up to 15MHz and this will allow testing of other circuitry with the signal generator and laser driver at the same frequency. This will eliminate unknowns in the initial testing stage. The 100MHz frequency was set as a target after calculations in 'Time of flight' showed that at 100MHz a 1mm accuracy could be achieved given an accurate phase detector circuit and sampling techniques.

It was decided that a modulation current of ±400mA would provide enough optical modulation to be reliably received by the photodetector. This number would result in an optical power range of 700mW, which is reasonably high, and greater than the power used in calculations in 'Expected reflected power'.

7.3 Constant Current Source

The DC current source will need to provide a very reliable regulated current up to 3A with very little ripple or other noise. For this reason, a linear current regulator circuit topology was selected. With a supply voltage of 7 volts, the maximum power that will need to be dissipated by the current source will be 12W. The laser cutter need not be energy efficient and is not battery powered so 12W is acceptable but it will need correct heat sinking.

7.3.1 Prototype current source

Since the current source is DC, components with poor high frequency responses can be used. Such components were available in the UCT component store. A prototype was initially milled on the UCT PCB milling machine and a similar design was then implemented on the final laser driver PCB. The schematic, PCB and a photograph of this first prototype can be seen in Figure 7-2. This circuit includes variable voltage and current limiting allowing the power of the laser to be controlled by current or voltage. This driver circuit was used for initial collimating optics testing.

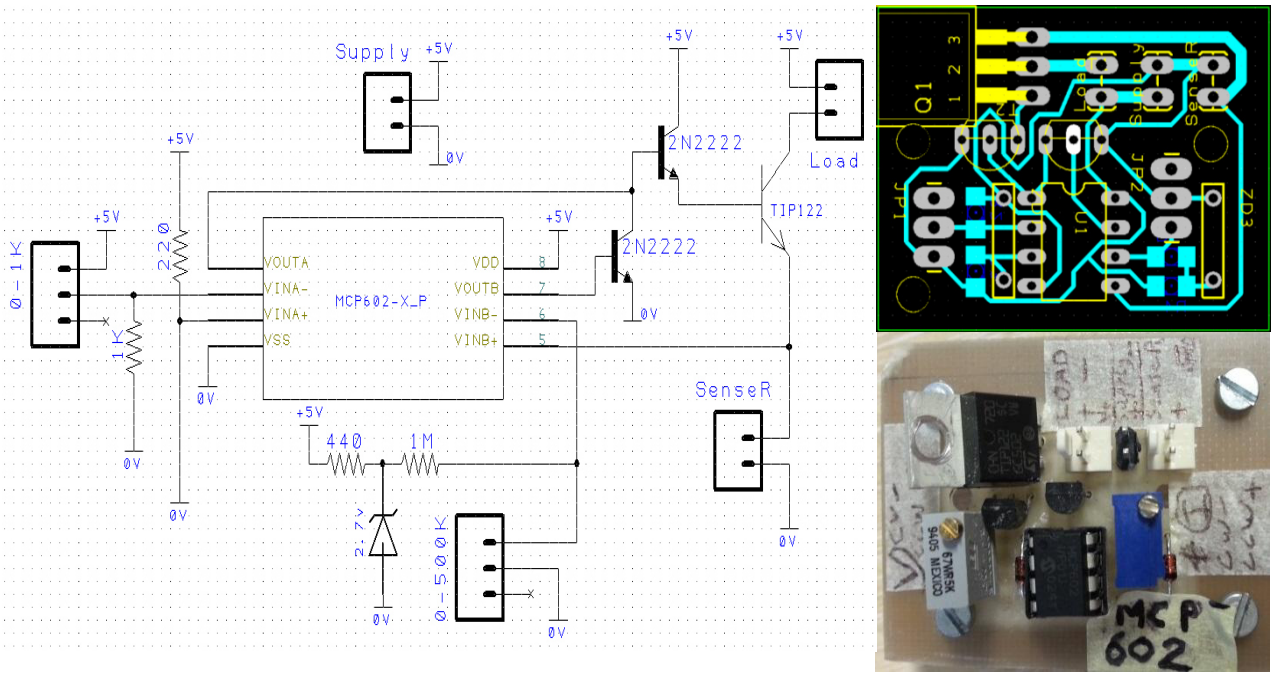

Figure 7-2. Showing the first prototype current source.

7.3.2 *Final constant current source*

After testing the laser with the prototype current source it was decided that voltage control was not necessary. A current source without voltage control was designed and the simplified schematic can be seen in Figure 7-3.

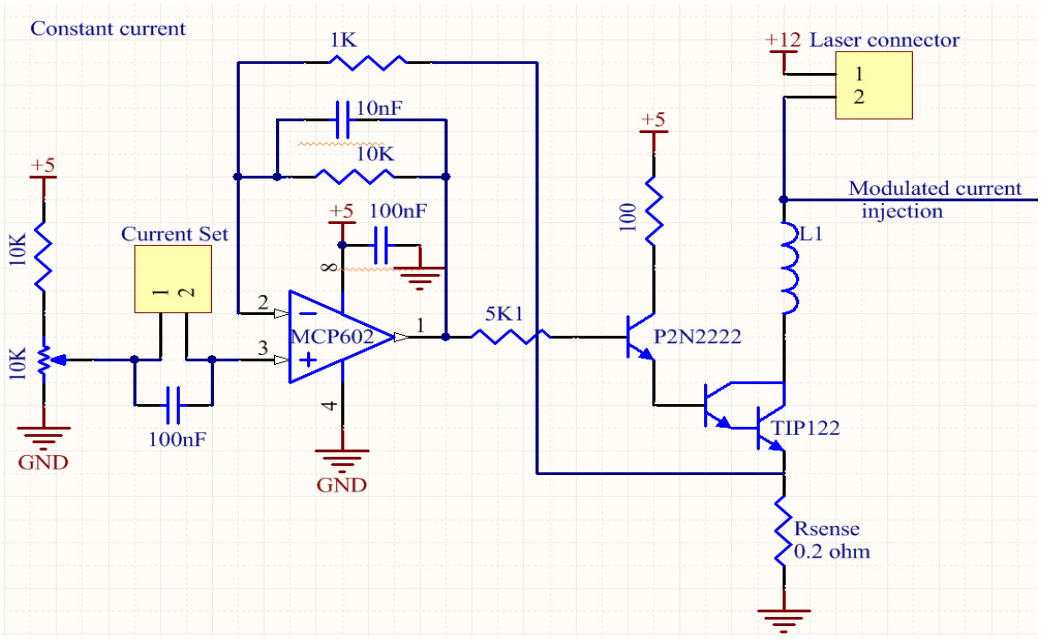

Figure 7-3. Showing the final constant current source schematic.

The current is set by an analogue reference voltage that is either provided by the on-board multi-turn potentiometer (using a jumper across 'Current Set') or provided externally by a microcontroller via a DAC when the potentiometer is grounded. A 1.6kHz low pass filter is implemented on the operational amplifier in order to filter out any high frequency and digital noise. A 1µH inductor was also included in line with the laser in order to prevent the current source trying to compensate for the high frequency modulation.

For a maximum current of 2.6A, the voltage across R_{sense} will be 0.52V.

The transfer function of the operational amplifier can be calculated as follows:

$$V_{out} = 2.25R_{p-} - 10V_{sense}$$

where: V_{out} is the output voltage of the MCP602 operational amplifier (V_{out} proportional to current)
R_{p-} is the resistance on the potentiometer
V_{sense} is the voltage across R_{sense} (V_{sense} is proportional to current)

It can be further calculated that only the lower 4 kilo-Ohm range of the potentiometer is used. This was satisfactory as a multi-turn potentiometer was used providing good current control. This also means that any DAC input should only be in a range from 0V to 1V.

The constant current source circuitry operates on a single 7V to 15V supply although the higher the voltage supply the more power needs to be dissipated by the pass transistor. A LM317 linear voltage regulator was used to provide the 5V supply.

7.4 High Frequency Generator

The laser driver is responsible for modulating the laser beam at a high frequency in order for the phase detector to measure the phase shift in the transmitted signal. A 100MHz signal is required that can preferably be set digitally within a range from 10 to 100MHz. After some market research, the CDCE421A from Texas Instruments [76] was selected. This crystal oscillator clock generator can generate LVDS or LVPECL digital signals from 10.9MHz to 1.1GHz. It has a proprietary SSI that allows the frequency and output type to be controlled by a microcontroller over a single wire. It also has a digital Chip Enable (CE) pin which allows the modulation to be turned on and off over a second digital link. Its frequency settings are stored in non-volatile EEPROM.

The high frequency generator circuitry schematic can be seen in Figure 7-4 . This contains an LM317 regulator to provide the 3.3V supply. The value of the 32.768MHz crystal clock, which is multiplied up or down by the CDCE421A, is not critical as the exact frequency that is used to measure distance is not critical as long as it is known and stable. Logic level shifting resistors are included as the microcontroller operates on 5V logic and the CDCE421A on 3.3v. Two 100Ω terminating resistors were used to terminate the CDCE421A, as this is required for operation in LVDS mode. The CDCE421A is decoupled with two ceramic capacitors, one a 1µF capacitor with an X5R dielectric and the other a 10nF capacitor with a C0G/NP0 dielectric both in 0603 packages. This decoupling scheme was employed in order to remove both low and high frequency ripple from the supply line. The LM317 circuit was also placed physically close to the CDCE421A also to ensure that as little noise as possible is picked up from the higher powered circuitry on the same PCB. A green LED is used to indicate when the CDCE421A is enabled and therefore the laser is being modulated.

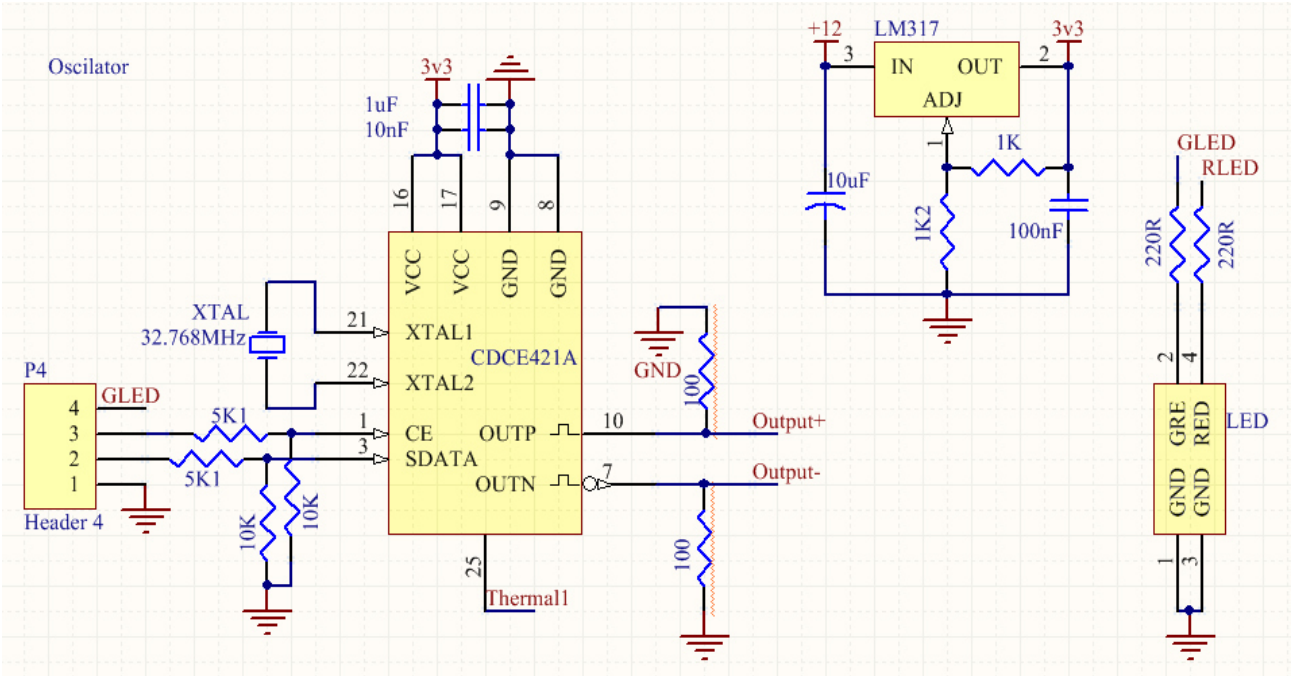

Figure 7-4. The high frequency generator circuit schematic.

This circuit was not tested on a prototype board as the CDCE421A is housed in a VQFN24 package, this pitch is too small to be reliably milled on the UCT milling machine. The software used to program the CDCE421A over SSI can be seen in '10.1.3-Communications with, and control of CDCE421A'.

7.5 Reference Signal

The reference signal would be fed into the phase detector circuit in order for the phase shift detection IC to have a signal to compare to the phase of the detected signal. The phase properties of this signal relative to the modulation signal need not be preserved, as only the change in phase will be measured. This being said, the frequency of the two signals needs to be the same for accurate results. For this reason, the inverted signal from the CDCE421A was used as the reference signal.

The signal from the CDCE421A was AC coupled and then amplified by the unused stage of an OPA2695 current feedback operational amplifier before being transmitted via impedance matched coaxial cable to the phase detector.

Figure 7-5 below shows the schematic of the reference signal amplification and the signal acquired by an oscilloscope at the output of the operational amplifier. The gain of the amplifier is set to 8 using resistor values recommended in the OP2695 datasheet [77, p. 27]. This gain allowed a higher powered, $8V_{pp}$, and therefore more noise immune, signal to be transmitted to the phase detector IC. The OPA2695 is decoupled with three ceramic capacitors, two 1µF capacitors with an X5R dielectric on each supply rail to ground and the other a 10nF capacitor with a C0G/NP0 dielectric across the supply pins all in 0603 packages and physically close to the IC.

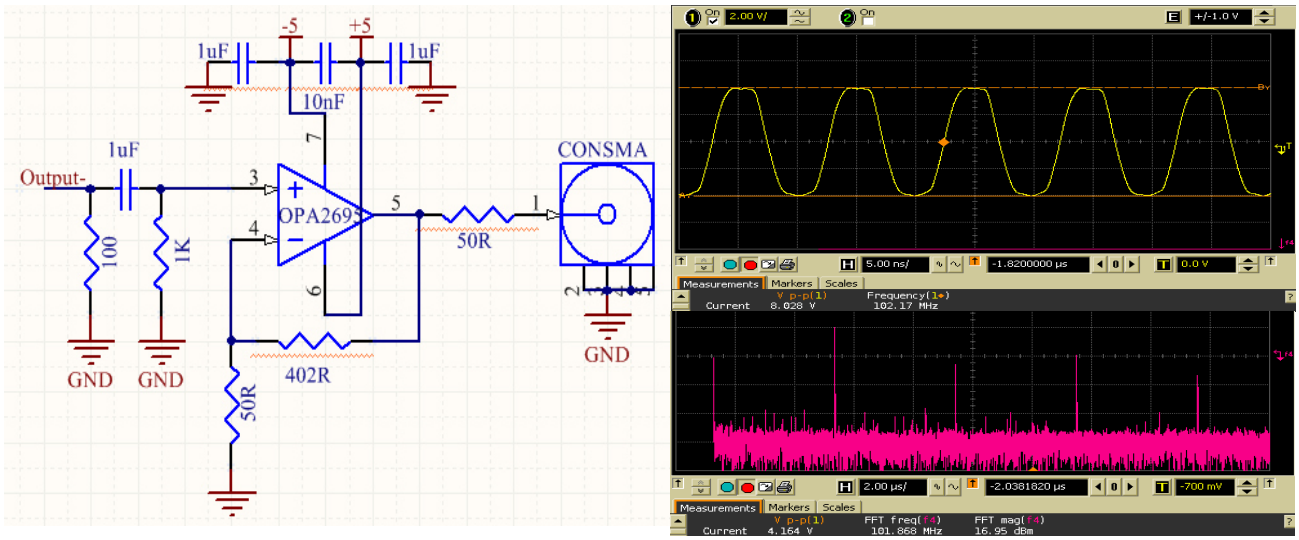

Figure 7-5. Reference signal schematic and oscilloscope acquired signals.

7.6 Modulated Current Source

The modulated current source part of the laser driver circuitry will take a voltage signal provided by the CDCE421A and convert it into a current signal that injects ±400mA into the laser. This current will be injected into the DC bias current and will modulate the optical output power of the laser.

The other signal from the CDCE421A was AC coupled and then amplified by an OPA2695 current feedback operational amplifier this was then transmitted to 5 parallel BUF602 high speed buffers [78] in order to achieve the required current output.

Figure 7-6 below shows the schematic for the final design of the modulated current source. It is made up of a voltage amplification stage and then a current amplification stage before being injected via AC coupling into the laser. The different aspects of this circuit are discussed below.

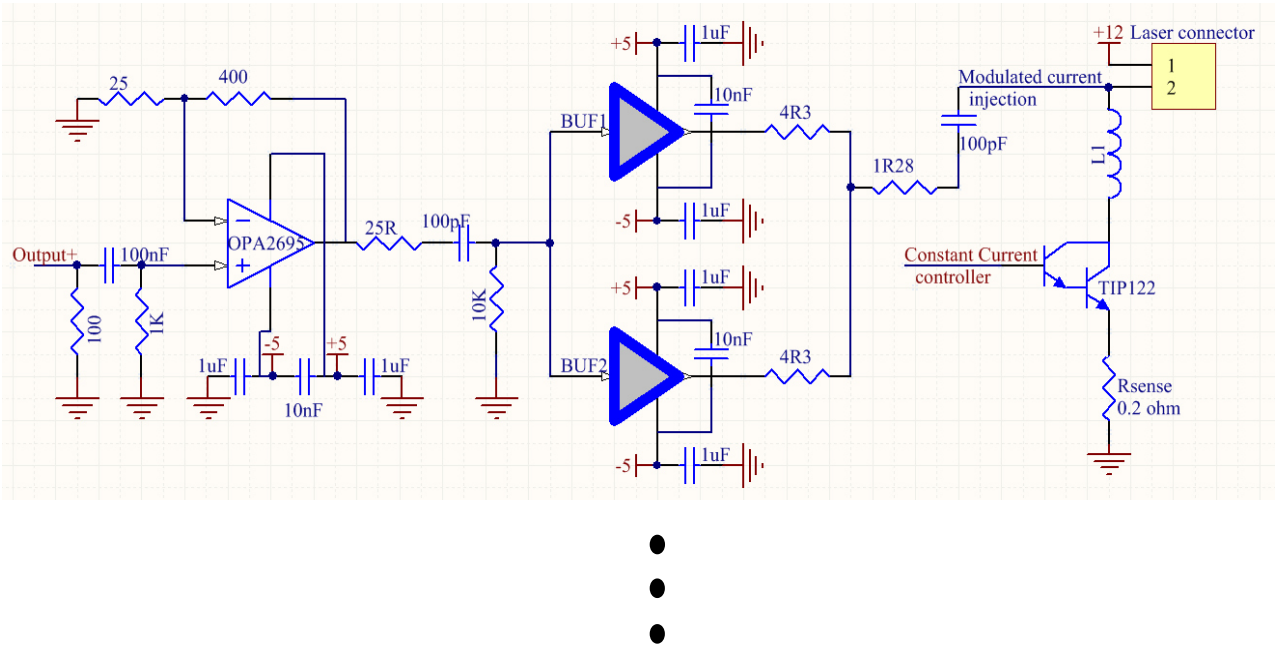

Figure 7-6. Showing the modulated current source schematic.

The output from the CDCE421A is AC coupled into the OPA2695. This signal has a voltage between 400mV$_{pp}$ and 1V$_{pp}$ and therefore needs to be amplified before driving the buffers. This is achieved using a high-speed OPA2695 current feedback operational amplifier. The OPA2695 was chosen because of its high gain capabilities at frequencies well above 100MHz and an output voltage swing of ±4.1V [77, p. 1]. In the schematic shown in Figure 7-6, the operational amplifier is set at a gain of 17 which will multiply the input from the CDCE421A to a voltage between ±3.4V and the maximum swing of ±4.1V. The highest output voltage of the buffers is ±3.7V [78, p. 4]. This OPA2695 channel is housed within the same IC packaging as that shown above and therefore the same decoupling discussed in 7.5 decouples both operational amplifier channels.

A 25Ω resistor (R$_{source}$) is used on the output of the OPA2695 as the inputs of the BUF602s have a parallel capacitance of 10.5pF and a 30Ω output resistor is recommended in the datasheet [77, p. 9]. 25Ω was used to account for a small amount of stray capacitance.

There is an AC coupling / high-pass RC filter pair set with a 3dB frequency of 160kHz in order to prevent any lower frequency signals being amplified by the buffers.

Five buffers were used in parallel in order to achieve the required current to be injected into the laser (only two are shown in Figure 7-6 for simplicity). Each of these buffers were decoupled in much the same way as the OPA2695. The buffer output impedance at 100MHz is in the order of 10Ω [78, p. 9]. There are 4.3Ω resistors on the output of each buffer in order to limit thermal runaway, which would occur in parallel ICs with bipolar transistor output stages [78, p. 15]. Four 5.1Ω resistors are then placed in parallel, due to power dissipation constraints, to form the 1.28Ω resistor shown in Figure 7-6. This 1.28Ω resistor helps to limit the output current and was set experimentally during testing.

Due to the high output power of each BUF602, thermal analysis needs to be carried out and is calculated below:

$$\boldsymbol{T_J = T_A + \theta_{JA} * (P_{DQ} + V_s^2/(4 * R_L)}$$ **Equation 7-1** [78, p. 15]

where: T_J is the junction temperature (should not exceed 150°C)

T_A is the maximum ambient temperature (assumed to be less than 80°C)

θ_{JA} is the thermal resistance and equals 150°C/W for the SOT23-5 package BUF602

P_{DQ} is the quiescent power dissipated (=10V*0.0058A = 58mW)

V_s is the supply voltage (5V)

R_L is the load resistance (5.58Ω)

Therefore:

$$T_J = 80 + 150 * \left(0.058 + \frac{5^2}{4 * 5.58}\right) = 256.7°C$$

This is well above the maximum operating temperature of 150°C and therefore correct heat-sinking will be required to dissipate this power.

This signal is then AC coupled and injected into the laser's constant current path either increasing the current by 400mA or decreasing it by 400mA.

The modulated current source was constructed using 0603 inch components and laid out on the PCB as compactly as possible to minimise parasitic effects. This proved to be successful except large parasitic inductances affected the link from the buffers to the lasers this is discussed below in 'Simulating Parasitic Inductance'.

7.7 Simulations

Only the DC current source component of the laser driver circuit was able to be constructed and tested before designing the complete board, due to the small footprint sizes found in the other parts of the circuit. Simulations were carried out on all sub-circuits in order to verify the design intentions and calculations. These simulations were also used as a reference point when testing the circuit. Most of the major components used (such as the OPA2695, BUF602 and CDCE421A) were manufactured by Texas Instruments and this was the reason that the *TINA-TI*® simulation platform was used.

7.7.1 Reference signal simulations

The simulations of the reference signal were very similar to the results seen in Figure 7-5 above; the simulated signal can be seen in Figure 7-7 below.

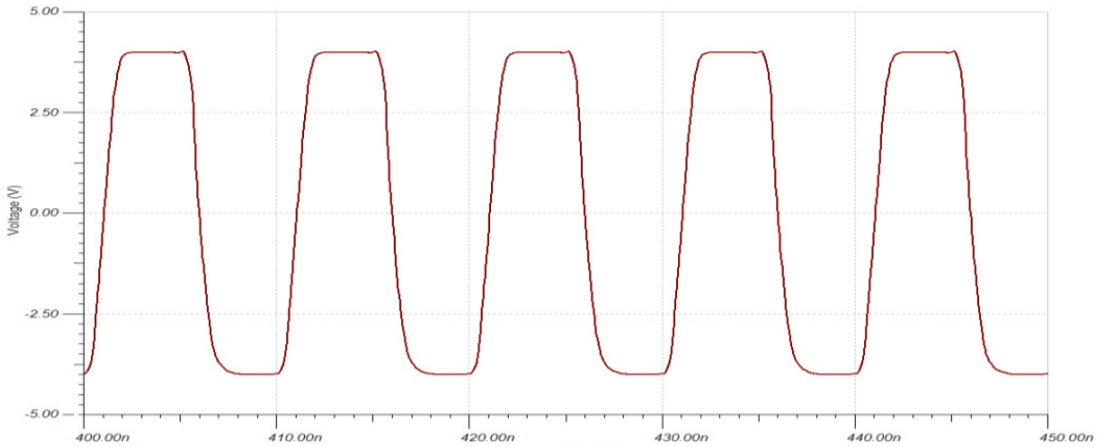

Figure 7-7. Shows the simulated reference signal.

7.7.2 *Modulated current simulations*

The modulated current circuit, shown in Figure 7-6, was modelled with a goal of $1A_{peak\ to\ peak}$ of modulation and the largest possible buffer output voltage swing in order to minimise the power dissipation of the buffers. As can be seen in Figure 7-8 a $1A_{pp}$ modulation current was achievable whilst maintaining a ±3.5V output from the buffers. The current through the laser is a square wave but parasitic effects on the constructed PCB are expected to remove higher frequency harmonics leaving a more sinusoidal current wave (the shape of the waveform should not affect the phase shift measurement). This simulation was carried out with the 1.28Ω resistor, this was replaced by a 5.1Ω resistor during initial testing but inductive parasitic effects meant that this value was changed to 1.28Ω after testing.

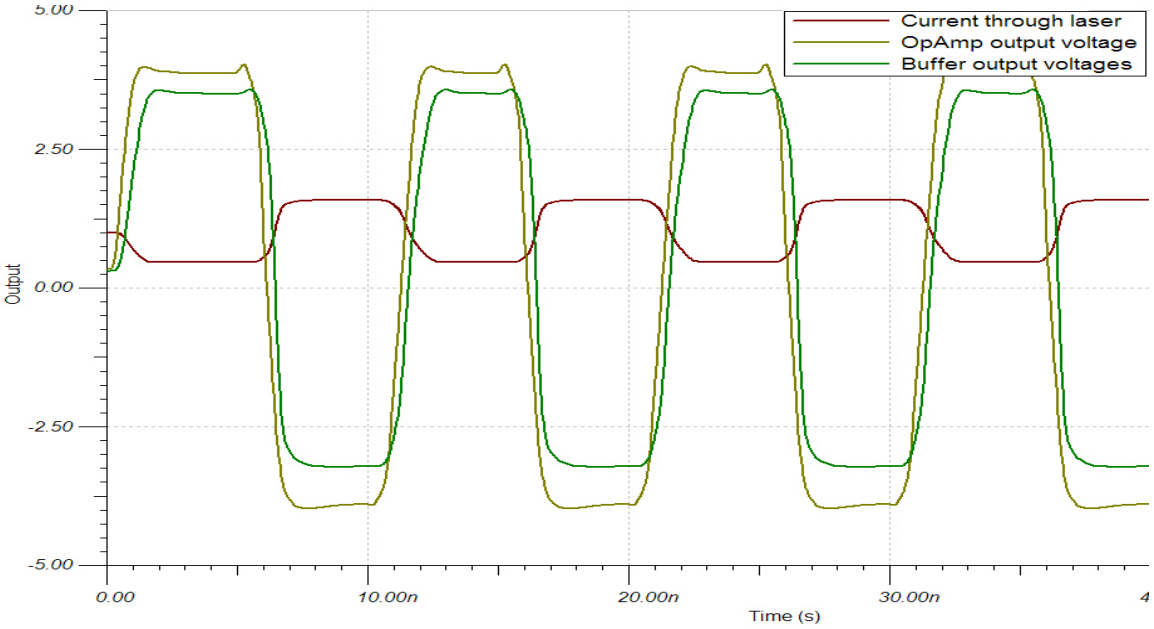

Figure 7-8. Showing the modulated current circuit simulations.

7.8 Complete Design

The schematic of the complete laser driver design can be found on the attached CD; this is a combination of the abovementioned components and includes voltage regulation and any other components omitted above for simplification purposes. The final PCB layout can be seen in Figure 7-9 and Figure 7-10, and photographs of both the bare and fully assembled PCB can be seen in Figure 7-12 (the buffers' heat-sink is not present in this photograph). The PCB was soldered by hand and each major section of the circuit was tested to make sure that components were soldered correctly and no short circuits were present before moving on to the section.

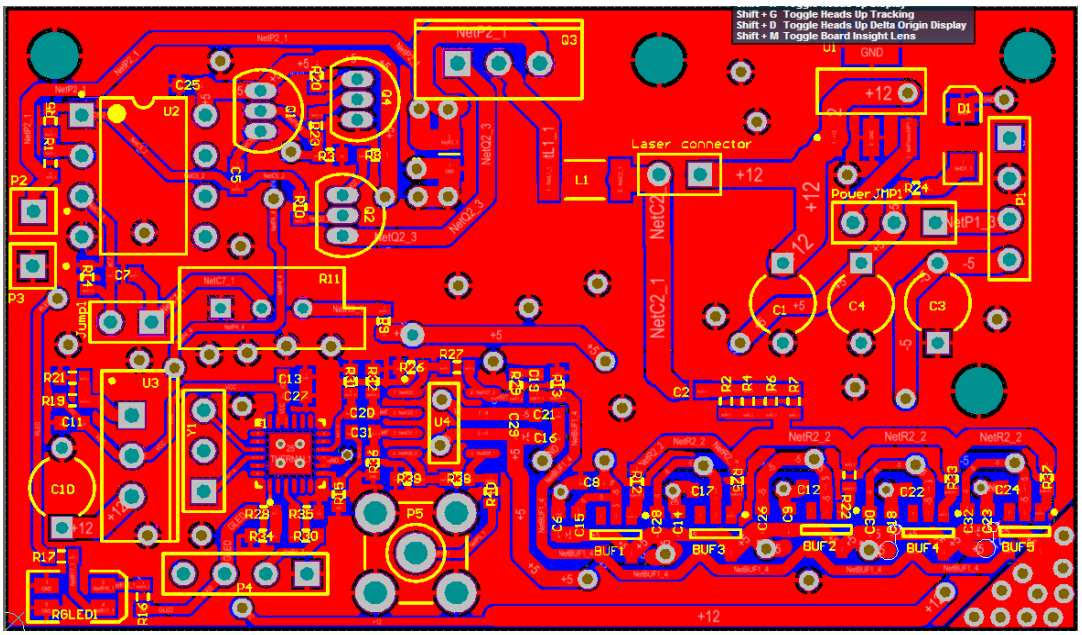

Figure 7-9. Showing the top layer of the final PCB layout.

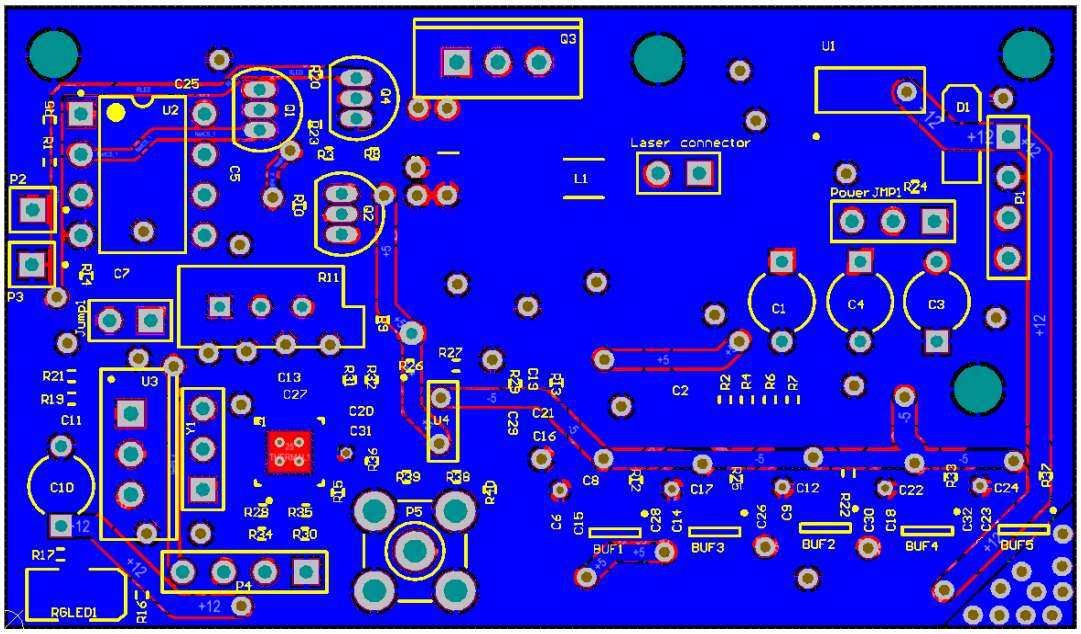

Figure 7-10. Showing the bottom layer of the final PCB layout.

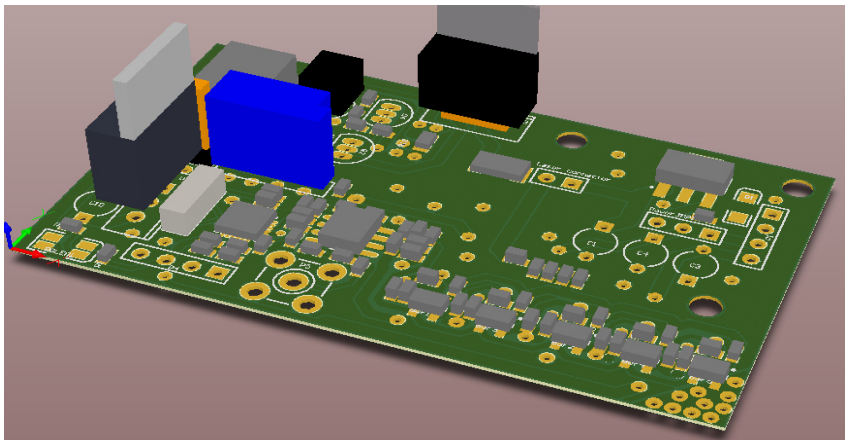

Figure 7-11. Showing a three dimensional view of the final PCB layout.

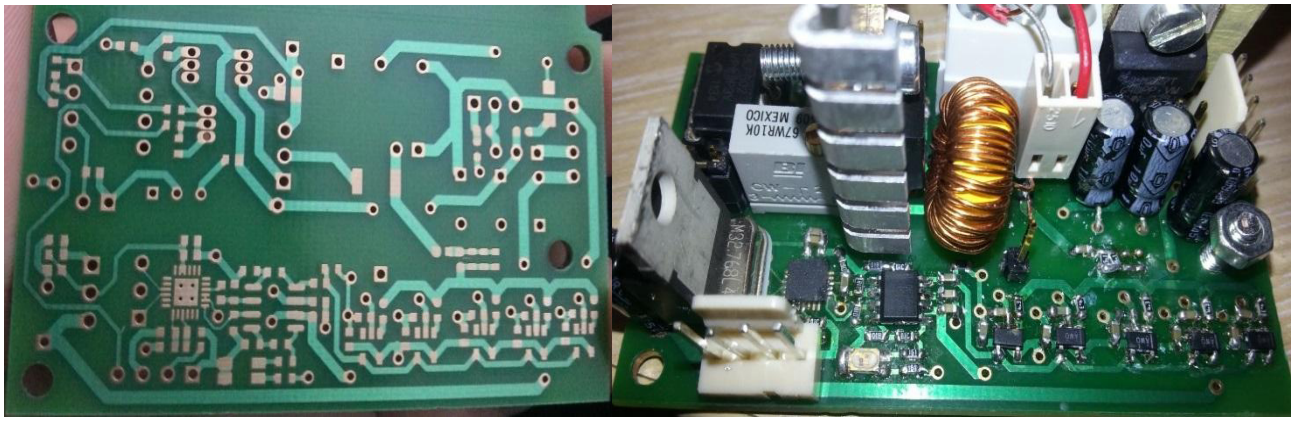

Figure 7-12. Showing photographs of both the bare and fully assembled laser driver PCB.

The PCB seen in Figure 7-12 is the PCB that was used in testing but the PCB layout in Figure 7-9 and Figure 7-10 has slight changes made. These changes either were errors or omitted in the initial design. These changes and errors were not major and were thought not to affect the operation of the laser driver circuit; for this reason, a new PCB was designed but not produced.

Some of these changes included:

- adding passive components
- adding an SMA connector for reference signal
- changing the 5V regulator from a LM317 to a LM340
- moving the TIP122 to the board edge for easier heat-sinking
- rerouting some connections
- adding some on-board heat-sink areas to the buffers
- moving test pins
- adding a top ground plane
- pulling the copper pours away from the edges by 0.2mm to prevent accidental exposed copper contact

7.9 Testing

The circuit was initially tested using three 1N4004 diodes in series, as these closely resemble the electrical characteristics of a laser diode. This was done for two reasons; firstly, these diodes were cheap and readily available meaning there was no risk of damaging an expensive laser if the laser driver did not work as planned and secondly, there is no dangerous infrared laser radiation emitted by these diodes. This testing verified the operation of the laser driver and allowed testing using the SPL_CG_81_2S laser diode.

The voltage regulation circuits were constructed first and all the supply voltages were verified before any other circuitry was soldered onto the board. Then all other components were added and tested systematically to ensure no short circuits were present.

7.9.1 Constant current circuit testing

After assembly, the constant current source was tested with the three 1N4004 diodes. This was done with the CDCE421A disabled and hence no modulation current was present. It was found that the

current through the diodes could be smoothly varied over a range of 0 to 4 amps and with a supply voltage of 7 to 15 volts (higher values may be achievable but were not tested to prevent damage as this test had surpassed the requirements). The higher the voltage and current the more power the TIP122 pass transistor had to dissipate causing it to heat up considerably, for this reason a heat-sink was attached and it was decided to operate the circuit off an 8V supply.

The current could be controlled either by the on-board potentiometer or via a DAC output from the microcontroller when the potentiometer was set to 0Ω. The voltage across the sense resistor, proportional to current, was observed with an oscilloscope and found to have a ripple below the noise floor of the oscilloscope. The noise over the 0Hz to 200MHz range was below -80dBm and with -70dBm FM radio noise being received from 90MHz to 110MHz and a single -65dBm signal at 125MHz. These measurements can be seen in Figure 7-13 where the blue signal shows the operational amplifier output and the green signal the signal across R_{sense}. The white/pink signals are the FFT of both signals above overlaid (causing it to be white). It can be seen that about 1.03A is flowing through the 0.2Ω $R_{sense,}$ as the average voltage is 205.3mV. Noise levels did not change throughout the current range.

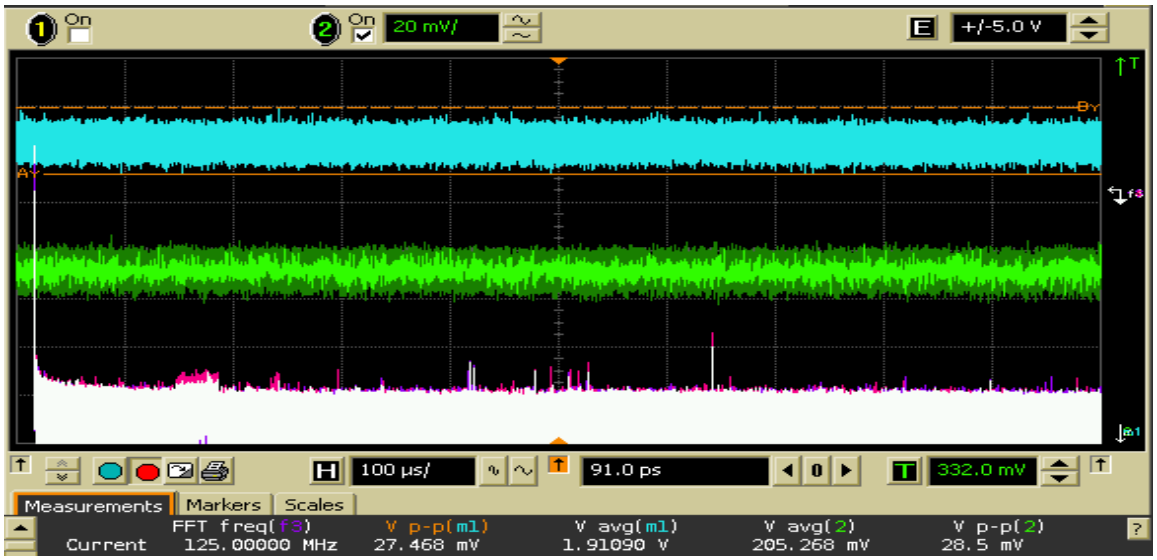

Figure 7-13. Showing the noise across the sense resistor and on the operational amplifier output.

7.9.2 High frequency generator testing

The AC coupling capacitors between the CDCE421A and the OPA2695 were not initially installed in order to isolate the two components. After some issues with programming the SSI, it was found that the CDCE421A and its peripherals were operating as intended. The signals were monitored with an oscilloscope and these can be seen in Figure 7-14 with 100MHz, 50MHz and 10MHz signals from top to bottom respectively (the time per division is not accurate as it applies to the green signal off-screen, all the signals shown were saved in memory). The EEPROM was programmable and the frequency could be varied in a range from 10MHz to upwards of 250MHz, well beyond the requirements. The amplitude of the output voltage was observed to be 1.02 V for LVPECL. When the frequency was set to 100 MHz it was measured to be 101.93MHz, this will be used in distance calculations. From the FFT (pink) peaks at 101.93 and 305.79MHz were observed, the 305.79MHz peak is expected, as it is an odd harmonic, which should be present in a square wave. The overshoot and slight ringing are thought to be either due to incorrect termination or because of inaccuracies in the oscilloscope probing techniques. Using 50Ω resistors instead of 100Ω resistors should address the termination issue. Similar signals were observed for both the outputs of the CDCE421A.

Figure 7-14. Showing the output signals of the frequency generator set at 10, 50 and 100MHz.

7.9.3 Reference signal testing

The reference signal observed on the oscilloscope, shown in Figure 7-5 (page 57), was generated with the CDCE421A set at 101MHz; harmonics of this are present in the FFT but will be filtered out on the phase detector board later on in the signal chain. At lower frequencies, the signal appeared to be a lot more like a square wave. It can be seen that although there is overshoot and ringing present on CDCE421A output, the reference signal circuitry filters this out and amplifies the signal as expected.

7.9.4 Modulated current testing

Initially the AC coupling capacitor between the OPA2695 and the BUF602 network was not installed in order to isolate the two components. This allowed the correct operation of the OPA2695 to be verified. The AC coupling capacitor was then installed but the 1.28Ω current limiting resistor was not installed in order to verify the correct voltage output of the BUF602 network with no current being drawn. These results were as expected and the modulated current source was tested as a whole. Signals along various parts of the signal path can be seen in Figure 7-15. The oscillations seen in these signals are thought to be primarily due to the oscilloscope probing techniques used and therefore can be ignored to some extent (more about oscilloscope probing techniques in 'The effect of different oscilloscope probes.' below). It can be seen that the voltage on the OPA2695 output has an amplitude of 8.85V. This verifies that the gain stage of this operational amplifier is working correctly although there is some distortion, in that the duty cycle is about 60%. This is due to the capacitive loading at the input of the BUF602 network. This could be corrected by using a larger R_{source} although this will lengthen the rise time on the BUF602 inputs. The current through the 1.28Ω resistor was also measured by subtracting the signal on the input from the signal on the output; this gave an 855mV_{pp} signal and when divided by 1.28 gives a 670mA_{pp} or ±334mA. This is lower than the designed for ±400mA and is due to the parasitic inductance in the wiring to the laser as explained in 7.10. Again, the poor quality of this signal is attributed to errors in the oscilloscope probing and the fact that the difference signal is scaled up by a factor of 10 to make it visible.

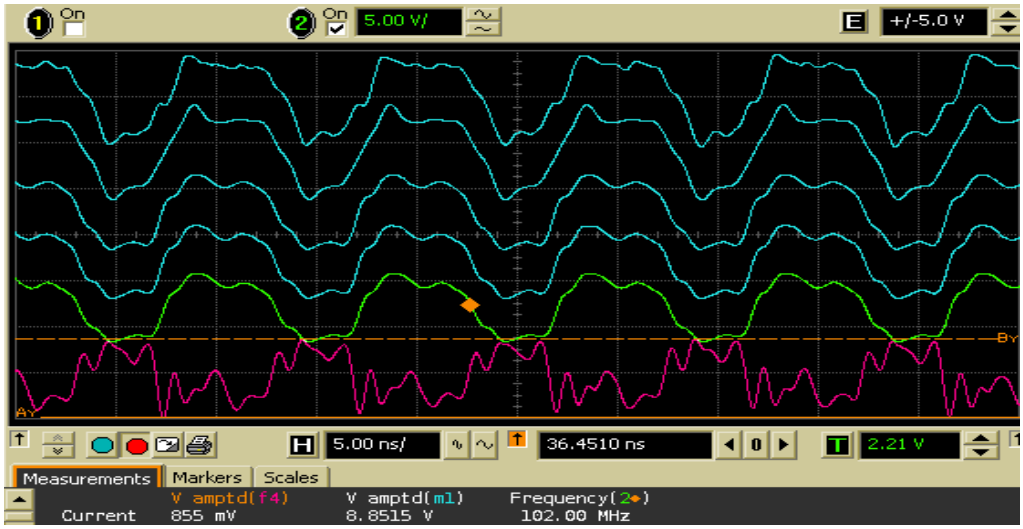

Figure 7-15. Showing signals along the modulated current path.

i. The effect of different oscilloscope probes.

At high frequencies, the oscilloscope probe one uses can have a profound effect on the results obtained when monitoring a signal. The signal monitored below was the reference signal. This signal has a frequency of 100MHz and has an amplitude of $8V_{pp}$. The top signal was acquired using an active probe with 45mm long tweezers to grip onto IC pins (shown in Figure 7-16 on the right). The middle signal was acquired by the same active probe, as above, with a short pin on the signal line and a short wire for grounding. These were pressed onto the device to be measured. The bottom (yellow) signal was acquired using a matched coaxial cable soldered onto the reference signal output pin. It is impractical to solder a coaxial cable onto every point that is to be tested and hence this method was only used when the two methods above did not yield satisfactory results. The tweezer type grippers were the most convenient to use as they did not need to be held in place by hand. Hence this method was used most often and small irregularities in signals were ignored, such as in Figure 7-15 above. The effect on large signals such as these is small but on smaller signals, 10s to 100s of millivolts, these effects begin to swamp the signal.

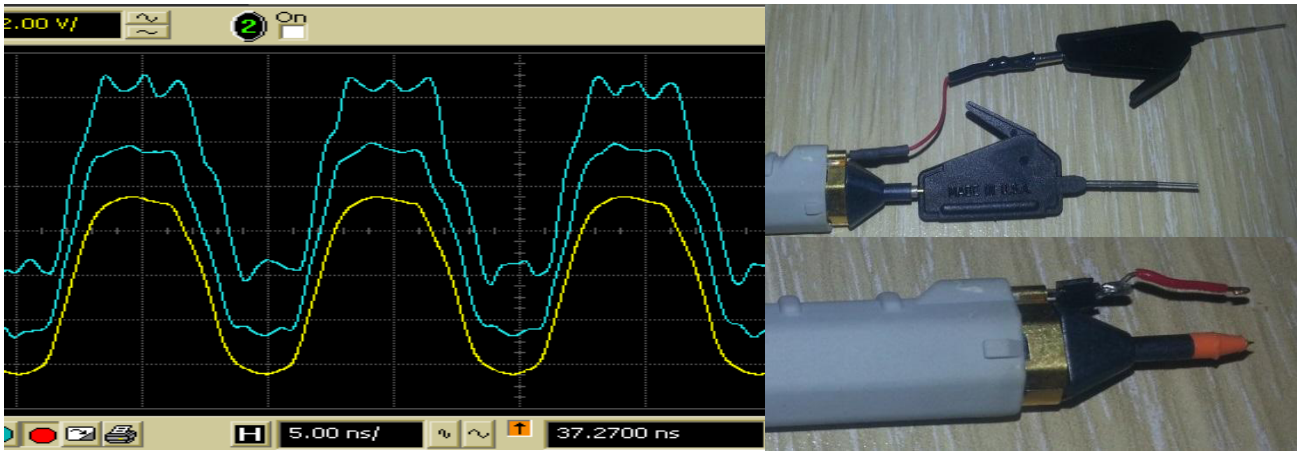

Figure 7-16. LEFT: Showing the same signal monitored with three different oscilloscope-probing techniques. RIGHT: the techniques used to acquire the top and middle signal respectively.

7.10 Simulating Parasitic Inductance

During testing of the modulated current circuitry, it was found that even though the voltage on the output of the individual BUF602s was relatively square the current through the laser was 'shark fin' shaped. The reason for this was thought to be due to parasitic inductances. The buffers have an 8Ω internal output impedance at 100MHz but only a 1.5Ω internal output impedance at 10MHz [78, p. 9], meaning that the internal output impedance has less of an effect at 10MHz; for this reason the parasitic inductance effects were measured and simulated at 10MHz.

The voltages on either side of the 1.28Ω resistor were measured and subtracted from each other. The results, along with the simulated signals, can be seen in Figure 7-17. The two yellow signals were the voltage before the resistor, the blue/green signals are after the resistor. The purple/maroon signals are the current through the resistor and hence the modulated portion of the current through the laser (the spikes on the purple signal are due to a slight frequency mismatch as the signals could not be measured at the same time because only one active robe was available therefore one signal had to be stored in memory). The voltage signals in other parts of the modulated current and laser path were also measured. The simulation was then modified to add inductances, and a small 0.2Ω resistor, between the laser and the supply voltage and between the laser and the modulated current injection point. The combination, shown in Figure 7-17, was able to model the observed results as closely as possible. This added up to a 50nH inductance, which presents significant inductive impedance at 100MHz; this reduced the modulating current drastically.

This parasitic inductance is thought to be caused mainly by the approximately 60mm of PCB tracks and wiring in the current path. This could be reduced by changing the physical setup of the Laser driver PCB and laser optical housing in order to minimise track lengths.

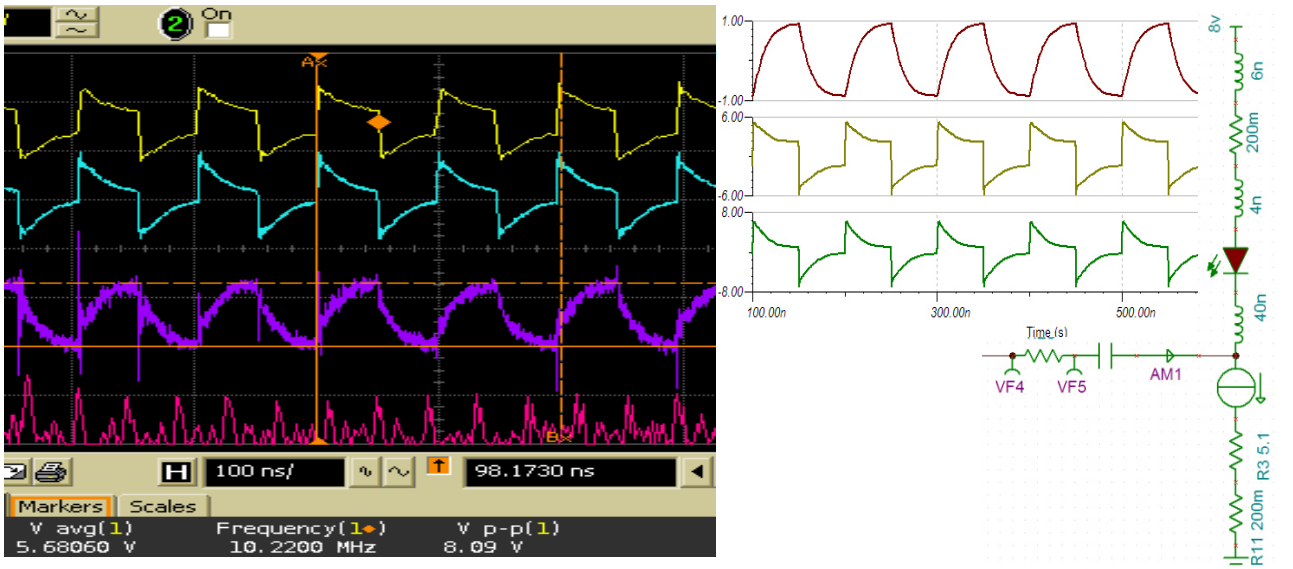

Figure 7-17. Showing measured (LEFT) and simulated (RIGHT) current through and voltage across 1.28Ω resistor with parasitic inductance modelled.

7.11 Miscellaneous Laser Driver Circuits

Two circuits were built after designing the laser driver PCB; these were the TLV5618 DAC and a circuit to provide an extra layer of overcurrent protection.

7.11.1 TLV5618 digital to analogue converter circuit

It was initially thought that the Arduino microcontroller's on-board PWM signal could be used to set the constant current of the laser driver but there was a lot of low frequency digital PWM noise present on the constant current signal. It was decided to build a small standalone DAC circuit that could be mounted close to the laser driver circuit in order to produce a signal with less noise and more precision. The TLV5618 was selected, as this is a common, robust and relatively cheap IC from Texas Instruments. The features include 12-bit resolution, SPI serial programmable, rail to rail output, chip select pin (output enable) and an analogue reference input for output scaling [79]. The schematic of this circuit can be seen in Figure 7-18. This circuit's voltage supply was drawn from the microcontroller, which can provide 40mA; this was sufficient for correct operation. This also eliminated noise created by the laser driver circuit on the supply rails. This circuit operated as expected and the potentiometer allowed the maximum output voltage to be controlled. The software used to program the TLV5618 can be found in 'Communications with and control of TLV5618'.

7.11.1 Over current protection circuit

As an extra layer of protection, an overcurrent circuit was built to monitor the power supply to the laser driver. This circuit also included power on and off pushbuttons to ensure that the laser was definitely off when intended; this reduced the risk of accidentally exposing one's eyes to laser radiation. This circuit included an L272 power operational amplifier [80], a current sense resistor, a current limit setting potentiometer and two relays for switching purposes in order to provide complete electrical isolation. This circuit schematic can be seen in Figure 7-18 (RIGHT). The circuit operated as designed and the power on/off pushbuttons proved invaluable during testing.

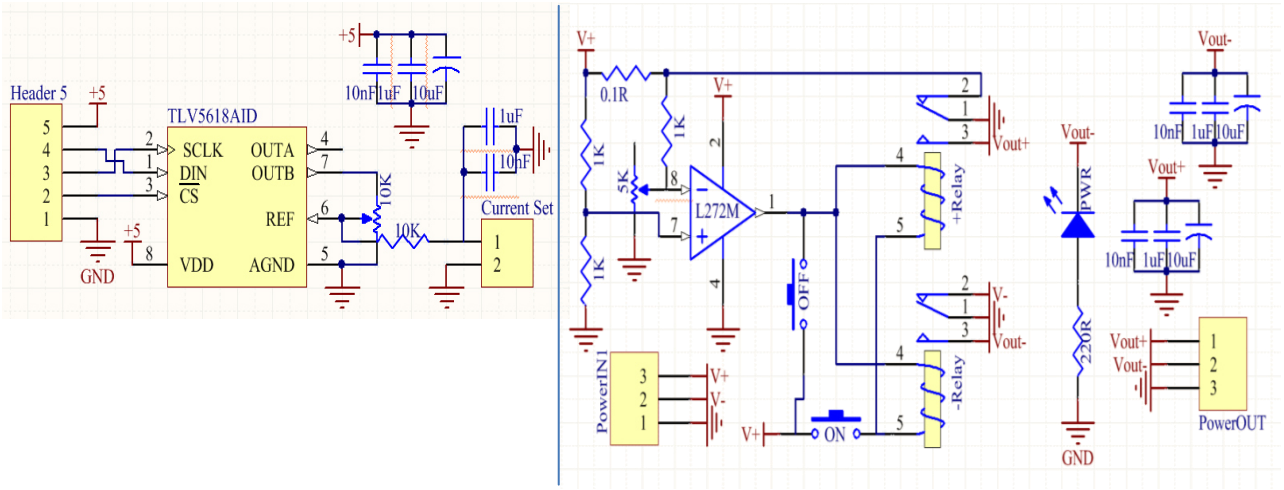

Figure 7-18. Showing miscellaneous circuit schematics. LEFT: TLV5618 DAC circuit. RIGHT: over current protection circuit.

8. Photo Sensor and Phase Detector

This chapter aims to describe the circuitry that was designed in order to sense the reflected laser radiation and then to measure the phase difference between the transmitted and received signals in order to calculate the depth of cut. This chapter also describes some of the design decisions that were made and previous testing that was carried out during this process.

8.1 Photo Sensor and Phase Detector Requirements

The photo sensor and phase detector circuit has two major roles; namely, the detection of the reflected laser signal and then the phase shift detection. The signal that the photo sensor needs to detect will be a modulated infrared signal with a frequency between 10MHz and 100MHz and an optical power of 1mW (see 'Expected reflected power' on page 51). This signal will then need to be amplified to a level detectable by the phase detector. The phase detector circuit will need to detect the phase difference between the received signal and the reference signal and provide an output that corresponds to phase shift and can be interpreted by a microcontroller. This relative change in phase shift will be used to determine the depth of cut.

8.2 Initial Photodiode Sensor Testing

Initially two PIN photodiodes were tested to determine which would be more suitable for use in this application. These two sensors were connected to the same amplification circuit with the same laser stimulation source and were both operated in photoconductive mode. A 10MHz signal supplied by a workbench signal generator was used for initial testing as the laser driver circuit had not yet been constructed and this was the highest frequency possible (with decent modulation depth although the signal generator was rated to 15MHz) with the said signal generator. The signal on the output of the amplification circuit for each photodiode was observed and can be seen in Figure 8-1 where the left hand image shows the results with an OP950 PIN photodiode and the right hand image shows the results with an SFH2307. It can be seen that amplitude of the output signal for the SFH2307 was about 6 times larger than that of the OP950 and that the slew rate is much higher (note the time scaling differences). Both sensitivity and speed are major concerns for this application and for this reason, the SFH2307 was selected; although in future designs the SFH2701 was used, as this is simply a surface mounted package of the same PIN photodiode.

Figure 8-1. Showing PIN photodiode testing. LEFT: OP950. RIGHT: SFH2307.

8.3 Electrical Properties of the SFH2701 PIN Photodiode

The SFH2701 PIN photodiode was selected as the most suitable photodiode. Some of the electrical characteristics that were influential in the design of the photo detector circuit are summarised here:

- Peak relative spectral sensitivity – 820nm

The SPL_CG81_2S, the 2W laser used has a wavelength of 810nm at which the SFH2701 is very sensitive.

- Spectral sensitivity – 0.5A/W

Alternatively, 500µA/mW and therefore sensitive enough.

- Photocurrent – 1.4µA
- Dark current – 0.05nA
- Rise and fall time - 2ns
- Capacitance – 3pF

Fast rise and fall time and low capacitance lead to higher operation frequencies and simpler amplification circuit design.

- Recommended reverse voltage – 5V

Low recommended reverse voltage means that a separate voltage source is not needed and all circuitry can operate on a single split supply.

PIN photodiodes can operate in both photovoltaic and photoconductive modes and these are both discussed below.

i. Photovoltaic mode

In photovoltaic operation, the photodiode is zero biased. In this mode the photodiode operates similarly to a photovoltaic solar cell generating a voltage that is proportional (although not directly) to the incident radiation. Photovoltaic mode reduces the bandwidth of a photodiode, this can be seen in the SFH2701 datasheet [81, p. 4] where, at 0V bias, the junction capacitance 3pF and the response time is longer than 8ns. This mode does minimise dark current and noise; it is normally used in low speed high sensitivity environments. [82]

ii. Photoconductive mode

In photoconductive operation, the photodiode is subjected to a reverse bias voltage where the anode is driven to a negative voltage with respect to the cathode. The current through the photodiode is directly proportional to the power of the incident radiation. “Applying a reverse bias increases the width of the depletion junction producing an increased responsivity with a decrease in junction capacitance and produces a very linear response” [82]. This decrease in junction capacitance allows shorter response times and therefore faster operating frequencies. This mode of operation does produce a larger dark current, which in turn increased the noise output. This is the more commonly used mode for photodiodes and due to the faster response times, this mode of operation was selected for use in this design.

8.4 Voltage Feedback vs Current Feedback Operational Amplifier

Two major operational amplifier topologies exist; these are voltage feedback and current feedback operational amplifiers. Both amplifier topologies were explored in the design phase and some of the notable differences are discussed below.

8.4.1 Advantages of voltage feedback operational amplifiers [83]

- The major advantage of voltage feedback amplifiers is that they are well understood and therefore dominate the operational amplifier market.
- They also have much more flexible feedback networks allowing them to be used in a myriad of different applications including many active filter designs.
- Variable feedback gain resistor, which can be in the MΩ or even GΩ range allowing for high transimpedance gains although, the frequency is limited by GBWP.
- They have low input bias currents and therefore do not load input circuitry significantly.
- Very low noise voltage feedback operational amplifiers are available.

8.4.2 Advantages of current feedback operational amplifiers [83]

- Bandwidth is constant and ranges to higher frequencies before dropping off steeply.
- GBWP is not constant allowing higher gains to be achieved without influencing bandwidth.
- High slew rates allow for high frequency operation without significant signal distortion.
- Sallen-Key active filter topology is possible.
- The effects of input capacitance in transimpedance applications are reduced due to low inverting input impedance.

From the advantages of each operational amplifier topology seen above a simple rule of thumb is to use a voltage feedback operational amplifier in lower frequency and high gain circuits and a current feedback operational amplifier in circuits where high frequency at higher gain is a major requirement. Both operational amplifier topologies were initially tested but it was found that the constant GBWP of voltage feedback operational amplifiers limited the frequencies at which the photodetector circuit could operate.

This can be supported by relevant calculations for the LMH6609 [84] with a transimpedance gain of 1.82kΩ, this was the value used in the final current feedback amplifier. Higher transimpedance gains would result in a poorer frequency response:

$$f_{(-3dB)} = \sqrt{\frac{GBWP}{4\pi * R_f * (C_{diode} + C_{input})}}$$ **Equation 8-1** [82]

$$f_{(-3dB)} = \sqrt{\frac{900 * 10^6}{4\pi * 1820 * ((3 + 1.2) * 10^{-12})}}$$

$$= 96.8\text{MHz}$$

At 96.8MHz, only half the amplitude of the amplified signal will actually be output by the amplifier. This was deemed unacceptable and it was decided to use a current feedback operational amplifier. The OPA2695 was thus selected.

8.5 Transimpedance Amplification

A transimpedance amplifier is an amplifier that converts current to voltage. Such an amplifier will be needed in a situation such as this because the output signal of a PIN photodiode used in photoconductive mode is a current signal.

8.5.1 Theory and simulations

Transimpedance amplifiers are normally constructed using voltage feedback operational amplifiers as there is no restriction on the range of the feedback (transimpedance gain) resistor and resistor values of 10s of mega-ohms are common. The value of the feedback resistor does however limit the frequency response as predicted by Equation 8-1.

Transimpedance amplifiers can be constructed using current feedback operational amplifiers in situations where high transimpedance amplification is not necessary but high frequency response is. Current feedback operational amplifiers are limited by the range of the possible feedback (transimpedance gain) resistor and a higher value of this resistor will reduce the -3dB frequency of the amplifier circuit.

Simulations to show the effects of different feedback resistors when used in conjunction with the SFH2701 PIN photodiode are shown in **Figure 8-2**. With transimpedance gains below 1.2kΩ gain peaking occurred above the targeted 100MHz but it can be seen that as the resistance values were increased this peaking was minimised and finally absent from the 1.5kΩ plot. Increasing this resistor yields a higher gain at 100MHz even though the gain has begun to roll off. It was found that a transimpedance gain of 4.8kΩ had the highest gain for a frequency of 100MHz but that there was little difference between this and a 5.1kΩ transimpedance gain.

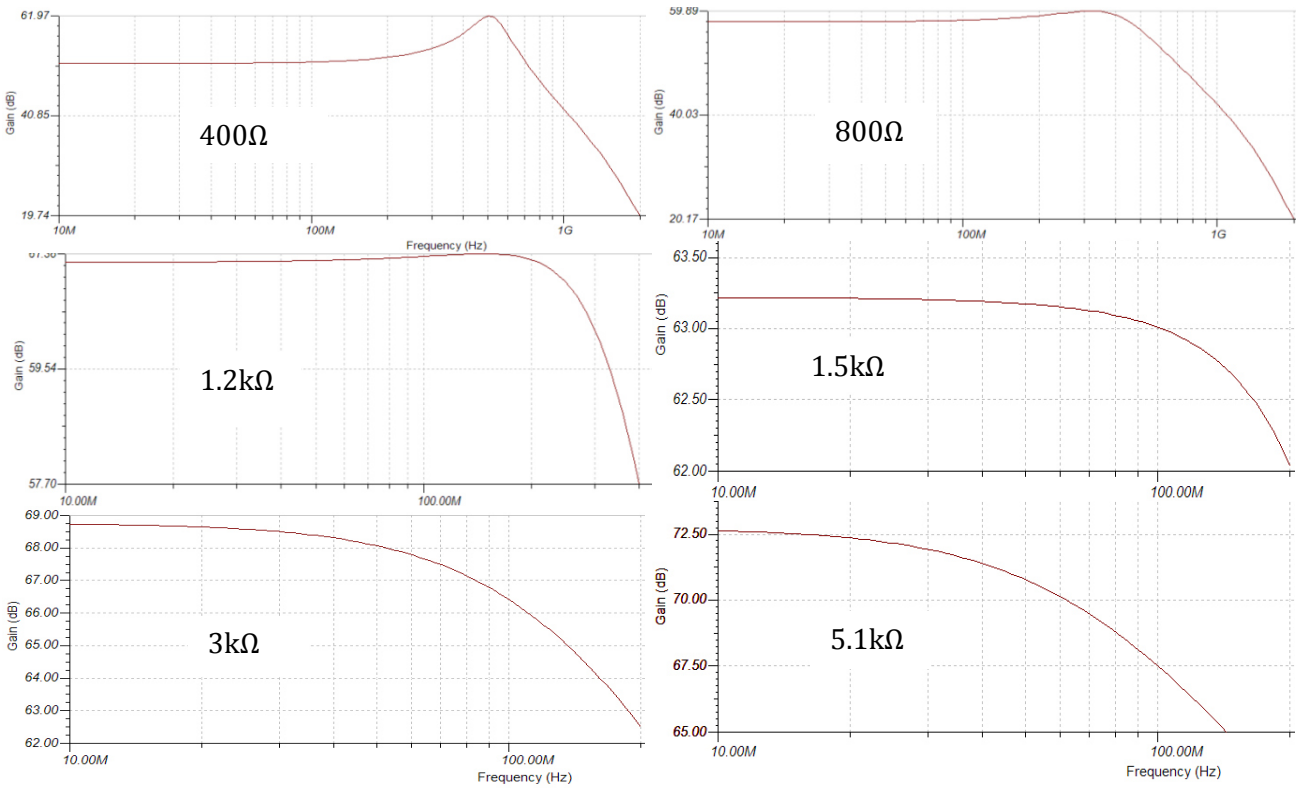

Figure 8-2. Showing the effect of increasing feedback resistor (transimpedance gain) on the frequency response of the OPA2695 (note scaling differences).

8.5.2 *Circuit design*

The transimpedance stage was designed with the aforementioned considerations taken into account. Initially both voltage feedback and current feedback transimpedance amplifiers were tested and it soon became evident that the calculations above held true. After this a transimpedance amplifier stage was designed and built using the lessons learnt from the prototype circuit to construct a more accurate and sensitive circuit. This circuit can be seen in Figure 8-3. The OPA2695 IC contains two current feedback operational amplifiers; the first was used as the transimpedance stage and the second as a non-inverting amplification stage with a gain of four. All power supply decoupling capacitors used had a C0G/N0P dielectric for high frequency operation. The signals between amplifier stages were AC coupled with RC high-pass filters with a -3dB frequency of 1.6MHz in order to filter low frequency noise and remove any DC bias. During board layout, the SFH2701 was placed as close to the OPA2695 as possible, all other PCB tracks were kept as short as possible and 0603 sized passive components were used throughout the circuit board to reduce parasitic effects. The 510Ω and 160Ω feedback resistors in the gain stage were as per recommendation of the datasheet.

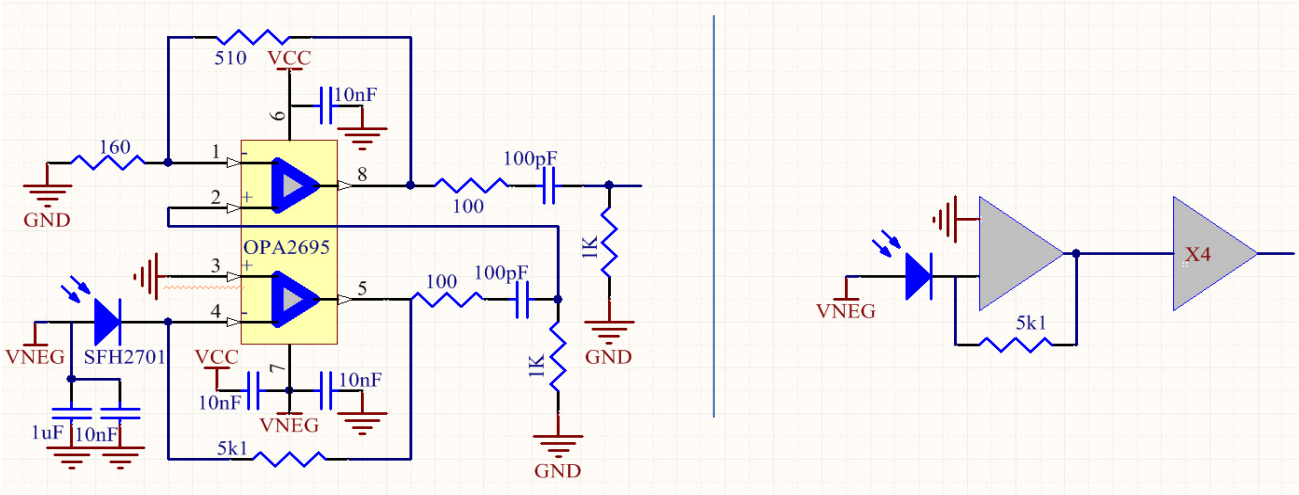

Figure 8-3. LEFT: complete transimpedance amplifier circuit schematic. RIGHT: simplified transimpedance amplifier circuit schematic.

8.6 Signal Conditioning and Filter Circuits

Following the initial transimpedance amplification stage described above, the signal passed through two active filters. These being a low-pass and high-pass stage in order to create a band-pass filter. These were both Sallen-Key filter topologies as this is the only active filter type that can be successfully implemented using current feedback operational amplifiers.

The schematic of the signal conditioning circuit can be seen in Figure 8-4. The filters were designed in such a way as to produce a second order band-pass filter with a pass-band between 33MHz and 256MHz. The high-pass cut-off frequency was initially set at 11MHz by using 1.2kΩ resistors in place of the 402Ω resistors; these were changed when the circuit was found to be operating as expected at higher frequencies. Both gain stages were set with a gain of two in order to negate the losses of the filter and provide some extra signal gain. 1.6MHz high pass filters were again used to couple the active filter stages in order to remove DC bias voltages and other low frequency noise.

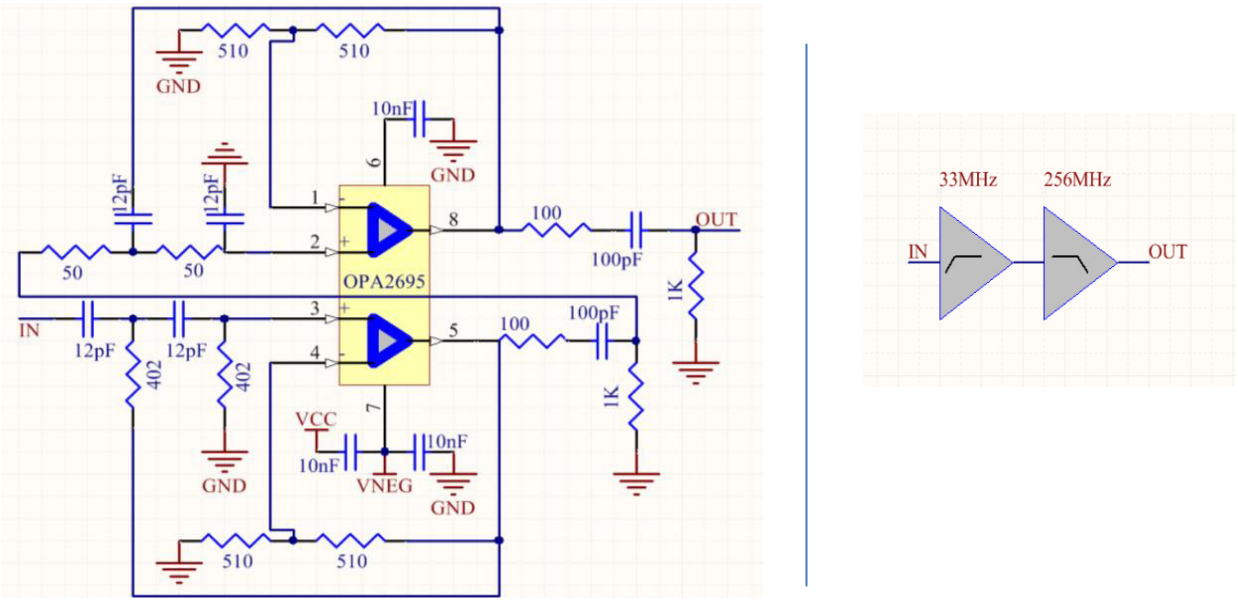

Figure 8-4. LEFT: Complete signal conditioning circuit. Right: Simplified signal conditioning circuit.

8.7 Photodetector and Signal Conditioning Simulations

Both the transimpedance amplification and the signal conditioning circuits shown above were simulated in TINA-TI in order to ensure that all the different components interacted as planned. The SFH2701 was modelled as a current source with a 3pF capacitor in parallel; this is the standard way to model PIN photodiodes. No shunt or series resistance figures were given and therefore not modelled although the dark current was included as a DC offset in the current source.

The results of the simulations can be seen in Figure 8-5. The outputs of all four amplifiers, which have been monitored for both transient and AC transfer characteristics, are shown. The amplitude of the output signal (blue) was measured and found to be 99.38mV, which is -7.1dBm into a 50Ω load and within the 0dBm to -60dBm signal range required by the phase detector IC. The gain at 100MHz was simulated to be 88.91dB, which is an equivalent transimpedance gain of 27.9kΩ. The filtering was designed to create a peak gain at about 80MHz as this allowed the circuit to be tested at lower frequencies initially. The plot of AC transfer characteristics shows the effect of the two Sallen-Key filters each creating the 40dB/decade roll-off, expected in a second order filter, in turn. The phase shift at 100MHz (not shown) was predicted to be 183°; this is inconsequential, as only the relative change in phase will be measured.

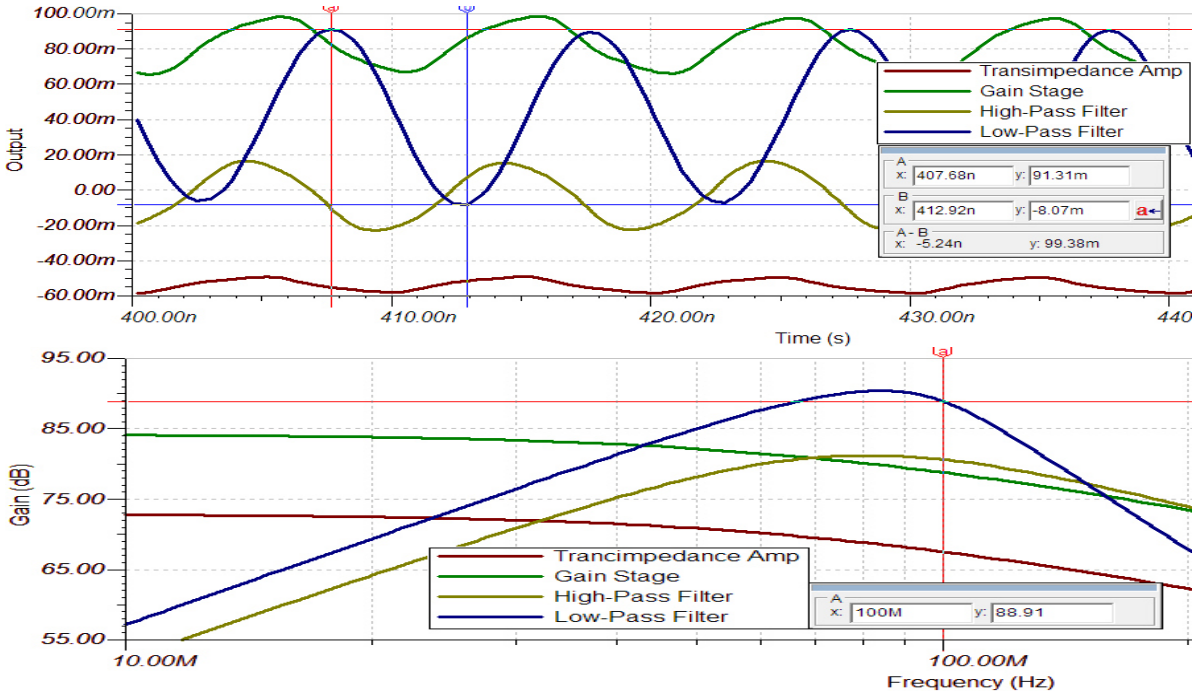

Figure 8-5. Showing simulation results for transimpedance amplification and the signal conditioning circuits.

8.8 Reference Signal Conditioning

The reference signal that is transmitted from the laser driver circuit is a 100MHz, $8V_{pp}$ quasi-square wave (Figure 7-5). The input signal range of the phase detector IC is 0dBm to -60dBm (50Ω environment) which works out to be $630mV_{pp}$ to $0.63mV_{pp}$. For this reason, the reference signal needs to be reduced by a factor of 14 or more and this is done with a simple resistor divider circuit. A Shottkey diode pair is also used to clamp the signal and prevent damage to the phase detector IC. The reference signal conditioning schematic and the measured signal can be seen in Figure 8-6. The dotted line shows the boundary of the phase detector IC and this is where the signal was observed using an oscilloscope. The BAS70 Shottkey diodes have a 3pF capacitance and this in conjunction with the transmission network produces a 530MHz low-pass filter. A resistor network divides the signal by fifteen and correctly terminated the transmission line. The 100pF capacitor is a compulsory AC couple capacitor but also acts as a 0.8MHz low pass filter with the input impedance of the phase detector IC. From the measured reference signal is can be seen that the frequency is 102.05MHz and the amplitude is $16.3mV_{pp}$, or -26dBm, and well within the required range.

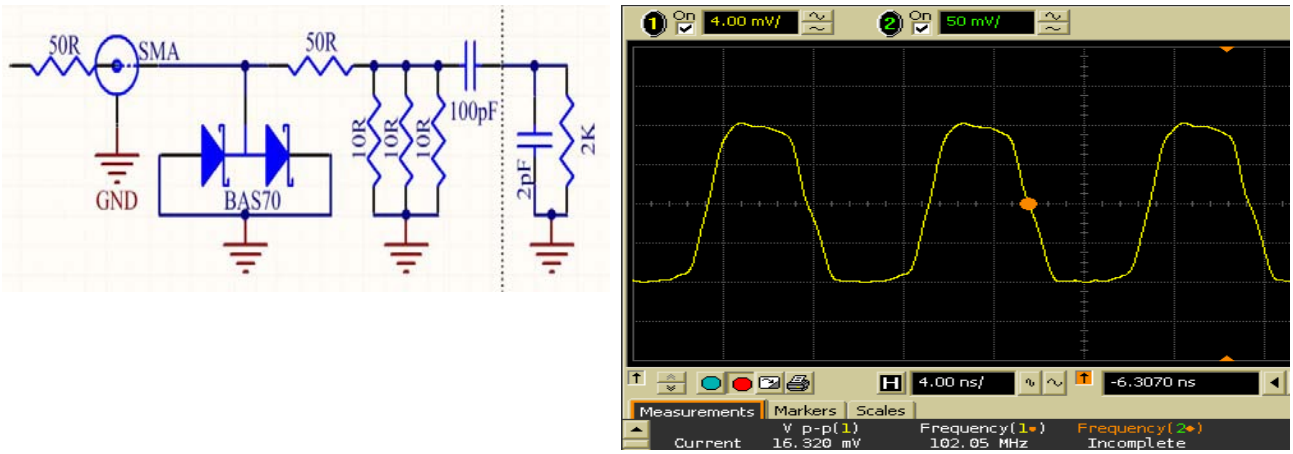

Figure 8-6. Showing the reference signal conditioning circuit (LEFT) and the measured reference signal at the input to the phase detector IC (RIGHT).

8.9 Phase and Magnitude Detection Circuit

The IC that was chosen to carry out the phase and magnitude detection was the AD8302 [85]. This IC was chosen because of its wide input range both in terms of magnitude and in terms of frequency; less that 1° nonlinearity and because it gives a magnitude ratio output. The schematic of the phase and magnitude detection circuit can be seen in Figure 8-7 below.

i. Inputs

The input pins (INPA and INPB) are high input impedance pins with nominal 2kΩ||2pF impedance at 100MHz. These pins must be AC coupled and are done so with 100pF capacitors.

ii. Offset compensation filters

The offset compensation filter pins (OFSA and OFSB) allow the offset compensation filter corner frequency to be set using a single capacitor to ground. This sets the cut-off frequency of the internal high pass filter acting on the input signals.

This corner frequency can be set by the following formula:

$$f_{-3dB} = \frac{0.002}{C_f + 1\times10^{-11}}$$ **Equation 8-2** [85, p. 17]

where: f_{-3dB} is the corner frequency (Hertz)
C_f is the capacitor value (Farads)

The 10nF capacitors used on the OFSA and OFSB pins created a 200kHz corner frequency although using 400pF capacitors may have been more suitable and would produce a 4.9MHz corner frequency.

iii. Low-pass filter

The low pass filter terminals for the outputs (PFLT and MFLT) are pins that allow the internal low-pass filter corner frequency to be set. These low pass filters act on the output signals and can be calculated by Equation 8-3 as follows:

$$f_{-3dB} = \frac{1}{19800*(C_{AVE} + 1.5\times10^{-12})}$$ **Equation 8-3** [85, p. 16]

where: f_{-3dB} is the corner frequency (Hertz)
C_{AVE} is the capacitor value (Farads)

The low-pass filter corner frequency was set at 500kHz with 100pF capacitors.

iv. Output signals

The PSET and MSET pins are used to modify the slope and centre point of the output signals VPHS and VMAG respectively. This was not needed in this design so the control signals were simply connected to the relevant output pins as described in the datasheet. [85, p. 18]

The range of the output signals, VPHS and VMAGs, is 0V to 1.8V but the analogue to digital converter on board the Arduino microcontroller converts voltages in a range from 0V to 5v. This can be modified on the Arduino itself both in software and in hardware but the HMI uses 0V to 5V analogue signals and converting from one range to another is timely and possibly inaccurate [42, p. 275]. For this reason, and to improve noise immunity in the long cables linking the phase detector IC outputs to the Arduino, it was decided to include an operational amplifier to boost the 1.8V signals to 4.4V signals. For this task TLV2372 voltage feedback operational amplifier was selected; this operational amplifier has rail-to-rail inputs and outputs, 3MHz GBWP, and 5V supply operation. The TLV2372 was set as a non-inverting amplifier with a gain of 2.4V/V.

The phase output of the AD8302 can be calculated using the following equation that is derived from the AD8302 datasheet and the TLV2372 scaling factor:

$$\boldsymbol{V_{PHS} = 2.4 * (0.01(|\theta_A - \theta_B| - 90°) + 0.9)}$$ **Equation 8-4** [85, p. 16]

where: V_{PHS} is the output voltage proportional to phase

$\theta_A - \theta_B$ is the phase difference between the signals

The magnitude output of the AD8302 can be calculated using the following equations that are derived from the AD8302 datasheet and the TLV2372 scaling factor:

$$\boldsymbol{V_{MAG} = 2.4 * (0.03 * \log \frac{V_A}{V_B} + 0.9)}$$ **Equation 8-5** [85, p. 16]

Or

$$\boldsymbol{V_{MAG} = 2.4 * (\frac{0.03}{20} * (P_A - P_B) + 0.9)}$$ **Equation 8-6** [85, p. 16]

where: V_{MAG} is the output voltage proportional to magnitude

V_A and V_B are the voltages of the input signals

P_A and P_B are the powers of the input signals in dBm.

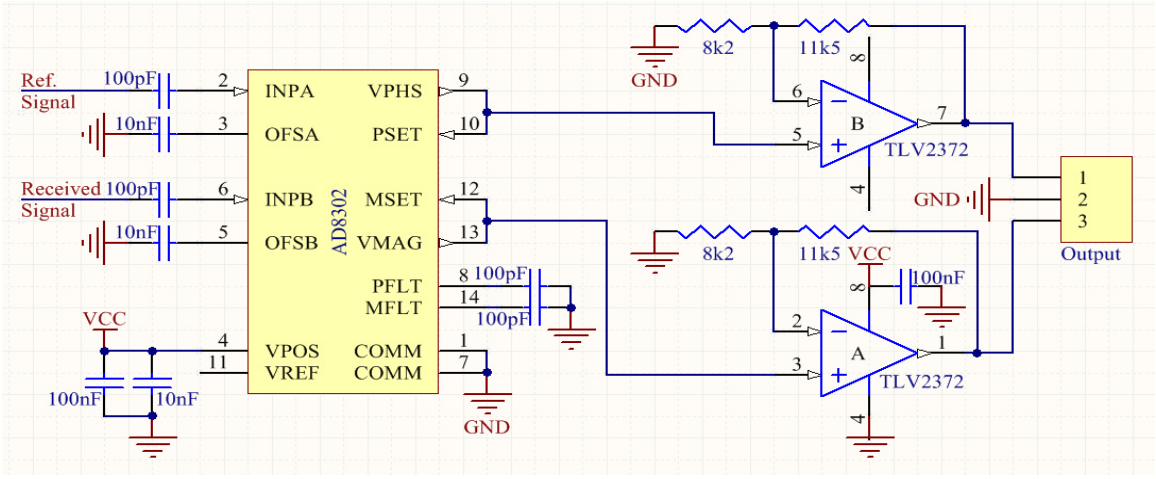

Figure 8-7. Showing the schematic of the phase and magnitude detection circuit.

8.10 Complete Photo Sensor and Phase Detector Circuit Design

The schematic of the complete Photo Sensor and Phase Detector Circuit can be found on the attached CD; this is a combination of the abovementioned components and includes voltage regulation and some other components omitted above for simplification purposes. The final PCB layout can be seen in Figure 8-8 and Figure 8-9 and a photograph of the board can be seen in Figure 8-10. The circuit was assembled by hand and tested after the completion of all major assembly stages.

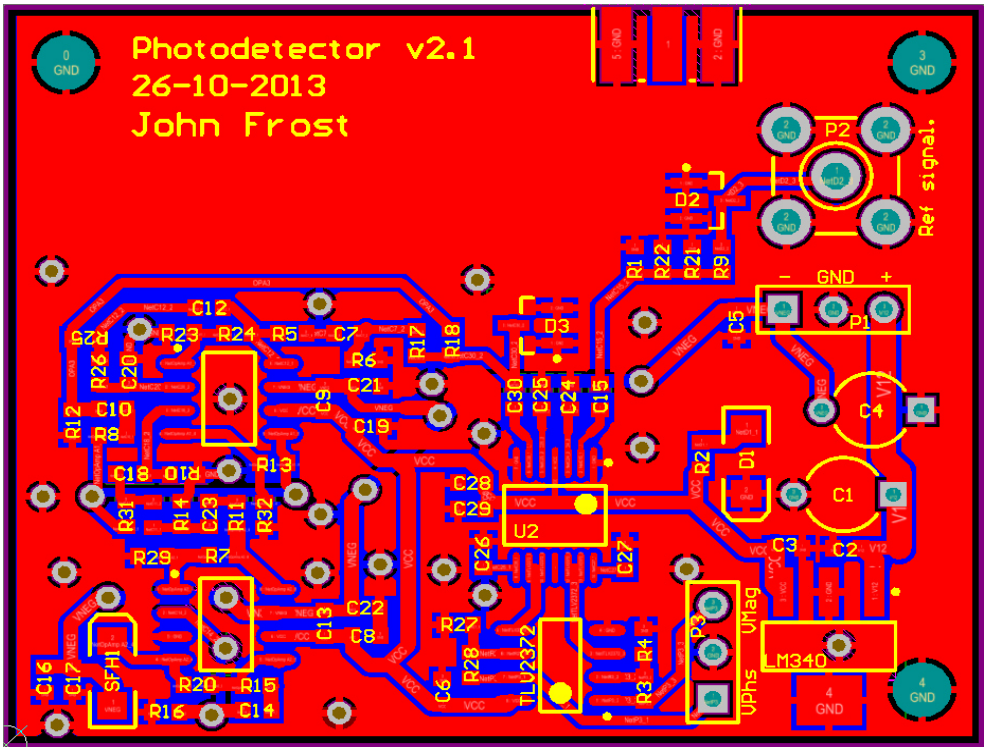

Figure 8-8. Showing the top side of the final photo sensor and phase detector circuit PCB.

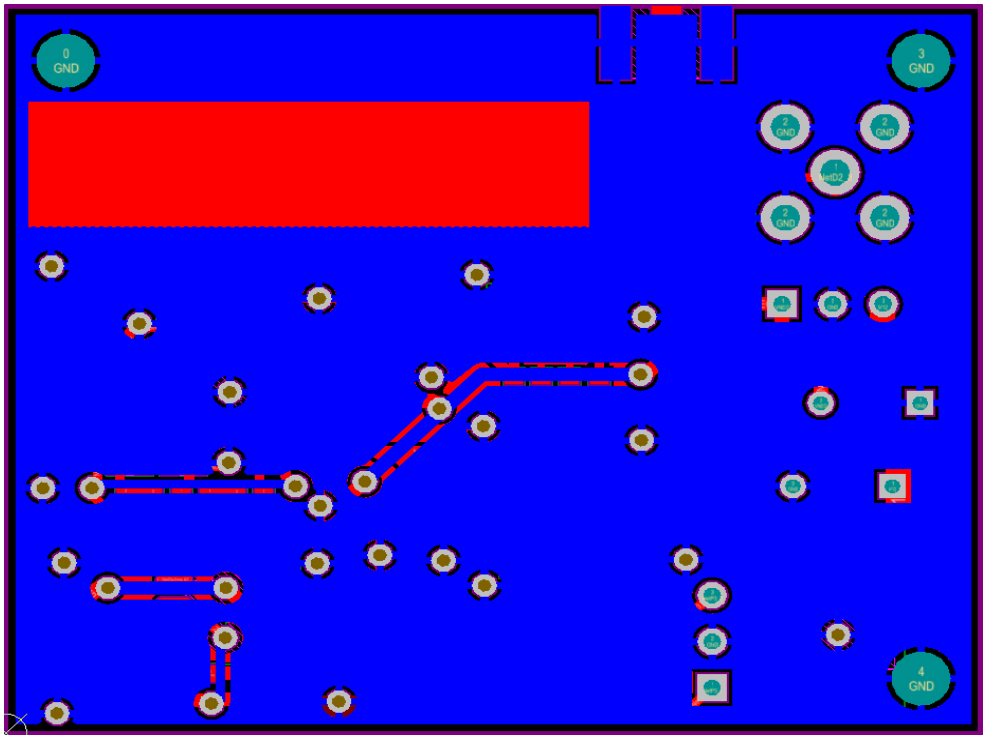

Figure 8-9. Showing the bottom side of the final photo sensor and phase detector circuit PCB.

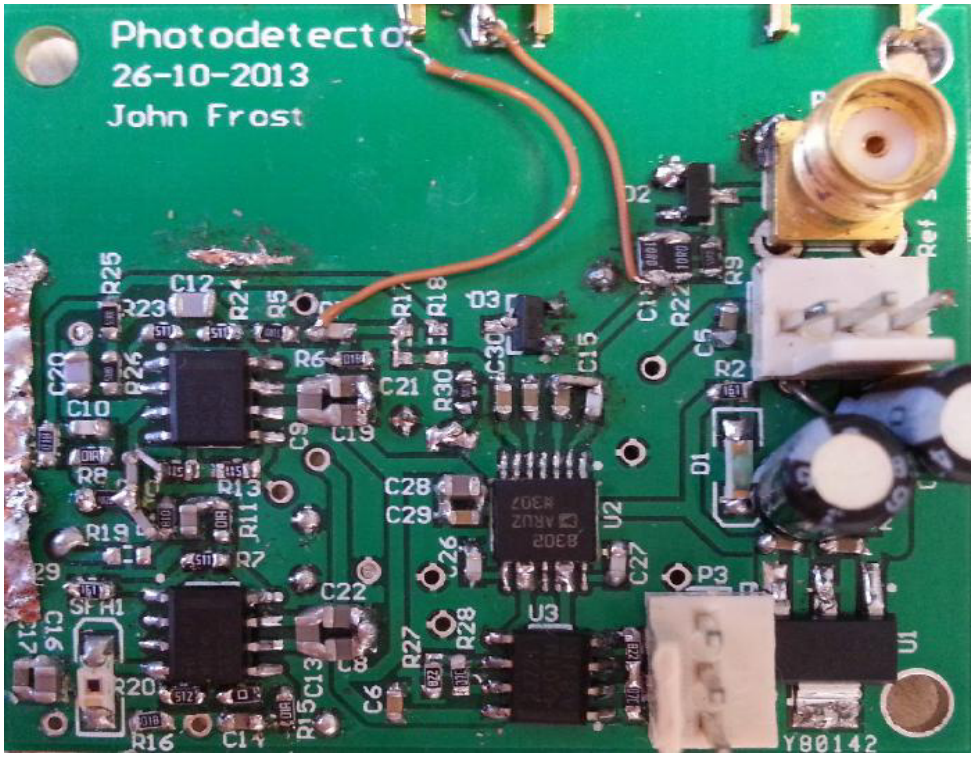

Figure 8-10. Showing a photograph of the top side of the final photo sensor and phase detector circuit PCB after assembly.

The PCB seen in Figure 8-10 is the PCB that was used in testing but the PCB layout in Figure 8-8 and Figure 8-9 has slight changes made that were either errors or omitted in the initial design. These changes and errors were not major and were thought not to affect the operation of the photo sensor and phase detector circuit; for this reason, a new PCB was designed but not produced.

Some of these changes included:

- adding passive components, especially adding high pass Sallen-Key filtering (seen implemented on PCB between other components)
- adding an SMA connectors to the top edge for monitoring with an oscilloscope
- rerouting some connections and moving some components for a better fit
- Adding a strip of bare copper above the filtering circuitry for shield mounting (seen as scratched area in Figure 8-10)

During PCB design, all trace lengths were kept as short as possible in order to reduce parasitic effects and eliminate the need to apply transmission like theory when routing. All tracks were made reasonably wide to reduce inductance on signal lines and resistance on power lines. All passive components were 0603 surface mount components also to reduce track lengths and other parasitic effects. 10nF ceramic decoupling capacitors and all AC coupling capacitors had an N0P/C0G dielectric for improved frequency response.

8.11 Noise Analysis

Noise is often a major problem for a circuit like this as there is a lot of high-speed amplification all of which is carried out by current feedback operational amplifiers, which are inherently noisy. Major noise sources were identified and attempts were made to reduce or mitigate these noise sources.

The amplification of the entire signal chain is quite large being 89dB (or 28kΩ transimpedance). Most of this gain is on the initial transimpedance amplifier and therefore the noise originating from this operational amplifier is dominant. The OPA2695 datasheet shows an input voltage noise of 2.7nV/√Hz and an inverting input current noise of 26pA/√Hz [77, p. 3]. This noise source is unavoidable and the best way to reduce the noise on the output is by reducing the overall circuit gain and the number of operational amplifiers used in the signal chain. It was realised that the 4V/V gain operational amplifier was unnecessary, as this gain could have been included within the filtering stages.

It was found that a lot of RF noise was being emitted by the laser driver circuit and then picked up by the phase detector circuit due to its close proximity. A shield was then placed over the transimpedance and filtering stages in order to minimise this RF noise; this was found to be a very successful way of mitigating this noise source.

The noise at the output of the last OPA2695 was measured using an oscilloscope with only the power connection connected to the PCB and the SFH2701 completely covered so as no light would be received. Figure 8-11 shows this signal and its corresponding FFT. The signal has a peak-to-peak voltage of 33mV and the FFT, which is centred at 100MHz, has maximum amplitude of -62dBm at 40MHz. This noise level is slightly below the -60dBm minimum input signal for the AD8302.

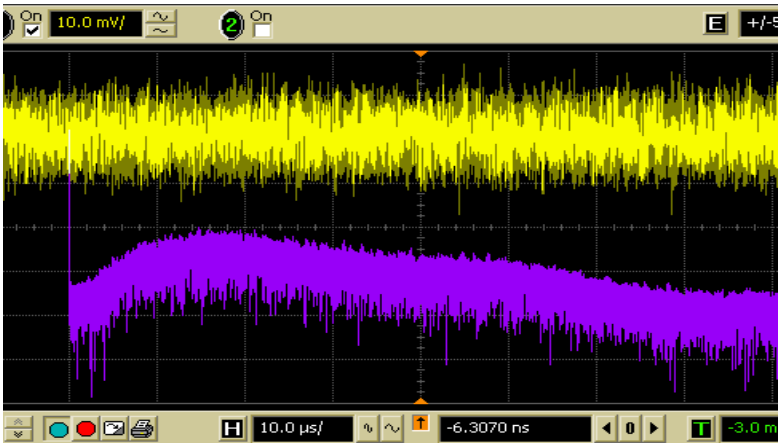

Figure 8-11. Showing the noise signal and FFT.

8.12 Testing Photo Sensor Circuit

In order to test the photo sensor circuit the circuit was placed in front of the laser with the focusing lens removed in order to provide a diffused illumination of the SFH2701 at a distance that was thought to receive a similar optical power per area as would be when measuring the distance of a typical material.

8.12.1 Transimpedance amplification testing

In order to test the transimpedance amplification, the output of the 4V/V amplifier was monitored with an oscilloscope and the results can be seen in Figure 8-12. It can be seen that a 102MHz 107mV$_{pp}$ signal is output shown in yellow. From the FFT it can be seen that some harmonics of this signal are present, but do drop off quickly, indicating that this is not a perfect sine wave. The magnitude of the 100MHz signal spike on the FFT is -15dBm. This signal is about twice as large as that predicted by the simulations but this could be because the photo sensor was illuminated with more optical power than expected. The transimpedance amplification stage worked as expected.

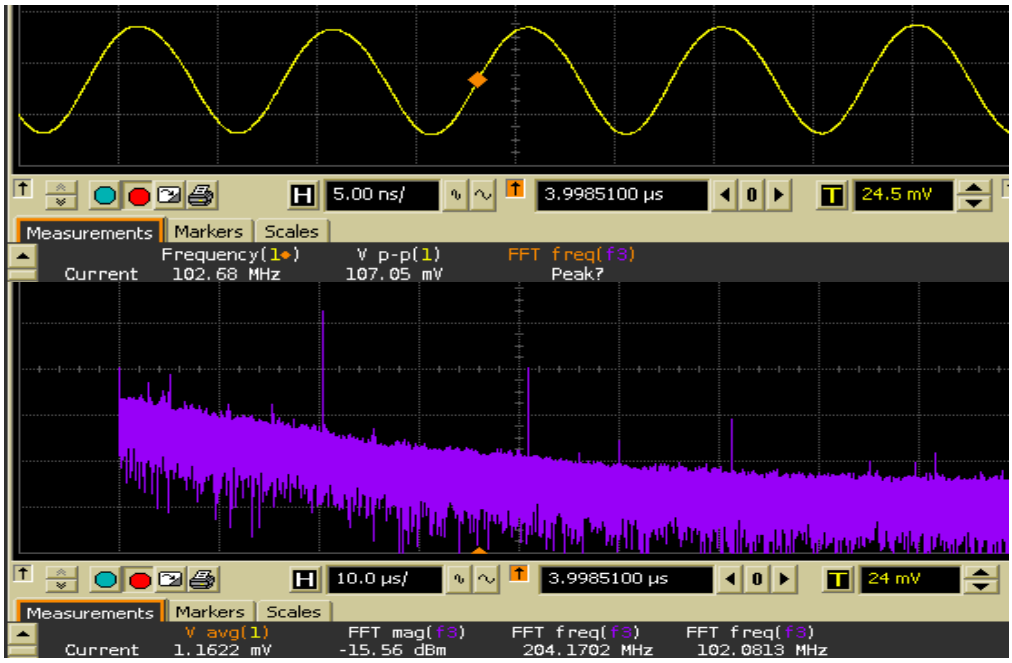

Figure 8-12. Showing the signal output from the 4V/V amplifier.

8.12.2 *Signal conditioning testing*

In order to test the signal conditioning the output of the low-pass filter was monitored with an oscilloscope and the results can be seen in Figure 8-13. It can be seen that a 102MHz 97.6mV$_{pp}$ signal is output this is shown in yellow. From the FFT it can be seen that the first harmonic of this signal is present but is smaller in magnitude when compared to the 4V/V amplifier output stage. The magnitude of the signal is as predicted during simulations. The effects of the two Sallen-Key filters are evident when comparing the noise floor of this signal to that shown above in Figure 8-12. The high-pass filter has the effect of reducing the noise for frequencies up to about 30MHz as designed and the low-pass filter stage increases the roll-off rate of frequencies between 80MHz and 200MHz, after which the oscilloscope's noise floor is reached, as predicted by the simulations. The highest noise levels are those between 30MHz and 80MHz, which reach levels of -45dBm.

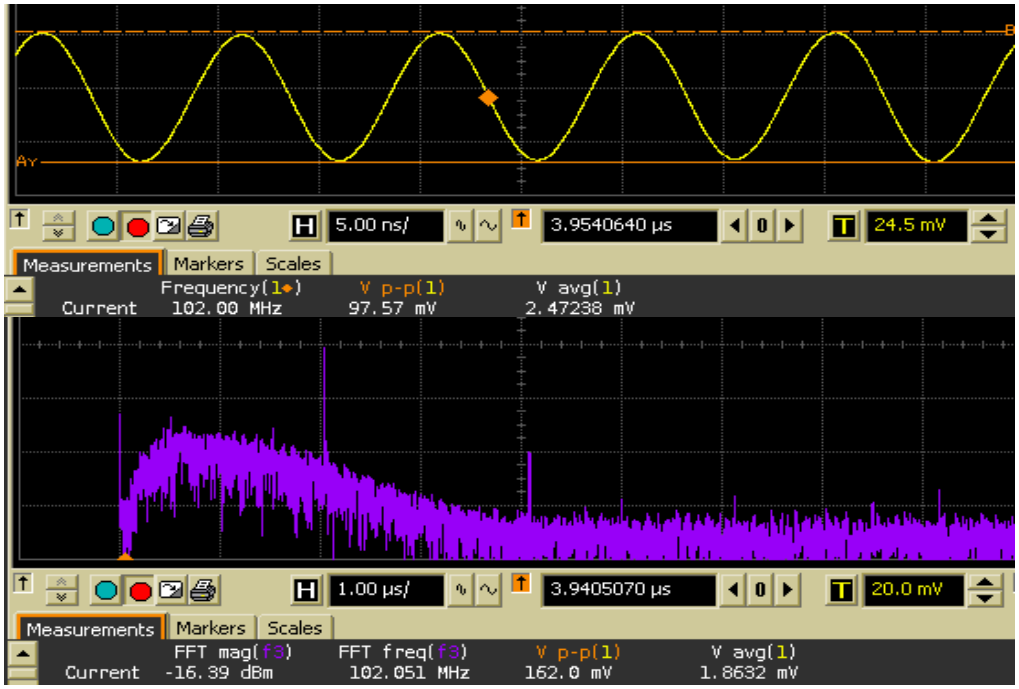

Figure 8-13. Showing the signal output from the low-pass filter.

8.12.3 *Phase shift detection testing*

In order to test the phase shift portion of the circuit a signal from a signal generator was fed into the AD8302's AC coupling capacitor on the optical channel and a second signal was fed into the reference channel. These signals were sine waves both set at -10dBm into 50Ω. (The signal seen in Figure 8-14, in yellow, is the signal into the reference channel before being divided by the reference signal conditioning resistor network; at the time of measurement, the 3.3Ω resistor was a 10Ω resistor.) One of the signals was set at 30MHz while the other was set at 29.96MHz.

The phase output of the TLV2372 was then monitored with an oscilloscope and is shown in Figure 8-14 as the green signal. This signal is a triangle wave as expected and has a frequency of 40kHz, as this is the difference between the input signal frequencies. It can be seen that the magnitude of the phase output is 4V$_{pp}$, which shows that the TLV2372 is operating as expected. This test proved that the AD8302 was operating correctly. More testing was carried out where different magnitude signals were used and the performance was much the same for signals in a range of -52dBm to 5dBm; it is thought that below -52dBm the signal became swamped by noise and testing above 5dBm was not conducted

for fear of damaging the AD8302. The magnitude ratio output was also verified and found to be correct although did not perform well for signals with more than 30dBm power difference.

Figure 8-14. Showing the phase output of the TLV2372 operational amplifier.

9. Miscellaneous Circuitry

Some other circuits were constructed during this project and these are discussed further here.

9.1 Stepper Drivers

The stepper motor drive circuits used were from a previous project that was completed by the author. These circuits took three inputs, 'step clock', 'enable' and 'direction' and had a jumper on the board to control half or full stepping. They consisted of an L297-L298 (stepper motor controller and dual H-bridge) IC combination. Two of these circuits were constructed, one for each stepper motor, and these had been thoroughly tested previously and further testing was not regarded as part of the scope of this project.

Stepper driver ICs are now available that are able to step bipolar stepper motors in increments as small as 1/32 steps (such as the DRV8825 from Texas Instruments). If circuitry with this level of fractional stepping had been substituted for the current half stepping drivers a theoretical step size of 6.25µm would be possible. These ICs are also more efficient, smaller, surface mount and a lot more reactive. It is therefore advised that any future designs use this more modern circuitry.

9.2 Dynamically Adjustable Optics

Before the optics that were used in the final design were implemented some testing was done using the servomechanism used to focus the laser within optical storage drives. It was hoped that the focal distance of the laser could be changed dynamically by the microcontroller in order to achieve the best cutting performance. Circuitry was constructed using two L298 H-bridges. The major problem with this circuitry was that a 400Hz PWM output from the microcontroller was used to control the voltage on each coil. The combination of low PWM frequency and very light actuated parts meant that the focusing lens seemed to vibrate distorting the focal point. This worked as expected to some extent but it was soon realised that this was not part of the scope of the project and would require more thought and design work. It is advised that this or a similar method be investigated more thoroughly on future optical designs.

9.3 Crowbar Circuit

In order to test the laser driver circuitry a 'crowbar circuit' was built and connected in parallel with the laser. This circuit comprised of a thyristor, a 2.7V Zener diode and a resistor. This circuit was designed in such a way that when a voltage greater than 3.4V was present across the laser diode the thyristor would conduct current and clamp the laser driver output voltage to 1.4V and turning the laser off (the laser diode has a threshold voltage of 1.7V) until power was removed. This circuit worked well during the initial testing phase. It was believed to be redundant once the laser driver testing had shown that no voltage spikes with potential to damage the laser were present.

9.4 Dummy Load

A very simple dummy load circuit to test the laser driver without damaging the laser was constructed out of three 1N4004 diodes in series. These diodes were very similar to the laser diode electrically (at DC). They presented a forward voltage drop of 2.1V and were able to sink the high currents the laser would sink. This circuit was used because it was cheaper that the laser diode to replace had something not worked correctly and because it posed no safely hazard to one's eyes.

9.5 Arduino Shield

A small Arduino shield PCB was designed and milled on the UCT PCB machine. This board plugged into the available header pins on the Arduino alongside the HMI board. It provided a neat and robust way to connect all the cabling to the Arduino, a power supply for the DAC and a Molex connector for safety switches on the lid.

10. Software

After the hardware was selected and the circuitry was designed, software design commenced. Most of the software written was done in order to conduct testing and was adapted slightly for different tests. Software was written for the Arduino microcontroller that communicated with MATLAB running on a PC. This chapter is broken up into these two broad chapters. There were two program pairs written, a pair consists of one program on both MATLAB and the Arduino that work together. One pair was written for gantry testing and then used for laser cutting testing while the other pair was written for distance measurement testing. Many functions were similar in each program pair and therefore all the functions are described individually while the two distinct programs' main loops are described independently below. This chapter aims to summarise and describe the software used as simply and concisely as possible; full copies of the software can be found on the attached CD.

10.1 Arduino Functions

The Arduino had many tasks to perform, most of which were to control the hardware of the laser cutter. The Arduino microcontroller was selected because it has simple prototyping development abilities although register manipulation is still possible. The Arduino MEGA 2560 development board provides multiple interface pins that were used for all the functions needed.

The Arduino had to perform the following tasks:

- communicate with MATLAB on the PC via serial communications
- control the stepper motor driver circuitry via GPIO pins
- communicate with the CDCE421A via a proprietary Simple Serial Interface implemented in software on GPIO ports
- communicate with the TLV5618 DAC via a SPI
- measure the voltage output of the AD8302 (via the TLV2372) using the ADC
- communicate with the HMI, which consisted of a screen and 5 buttons, via serial and analogue channels
- monitor two micro switches that indicate the home position

Each major task that had to be performed is described in more detail below. The headings of each chapter correspond to the function-calling name in the code and, where possible, follow a similar order to that above. The *setup* and *main* loop for gantry testing and phase and magnitude testing can be seen below the function descriptions.

10.1.1 MATLAB communications

MATLAB was used to control the Arduino via the serial port. Most communications were done in the form of G-code and G-code standards were followed were possible. The functions shown in Figure 10-1 and discussed below are used to set up communications with MATLAB and decode the commands received from MATLAB. The software running in the MATLAB environment on a PC can be seen in 'Software Running in MATLAB'.

i. establishContact()

This function is a loop that is run when the Arduino starts up. This function is used either to confirm communications between the Arduino and MATLAB or to detect that a button has been pressed. It then sets a variable to indicate whether the Arduino is under MATLAB or HMI control. It prints '*A*' to the serial port until either MATLAB responds or a button is pressed on the HMI.

ii. GCodeReader ()

This function is called in order to read G-code that is transmitted by MATLAB over serial communications. It is able to read G-codes 1, 3, 5 and 28. 'G1' is used to transmit positioning information and is made up of 'x', 'y' and 'z' coordinates that indicate the position to be moved to, as well as the feed rate (speed) that the unit should move. 'G3' and 'G5' are to turn the laser on and off respectively, these two commands are normally used to start and stop the spindle on a conventional milling machine. 'G28' commands the gantry to move to the home position. This function only reads the received command and sets the appropriate global variables when 'G1' is received.

iii. GCodeExecute()

This function is called to translate the position and feed-rate data transmitted by MATLAB when the 'G1' code is received. This function checks that the incoming positions are within the allowed ranges and then calculates a distance, direction and time between steps for each axis. These are calculated from the difference between the current position and the new position and from the received feed-rate. This function then calls *Motor()* to move the motors, displays the new position on the LCD and then responds to MATLAB when the position has been reached.

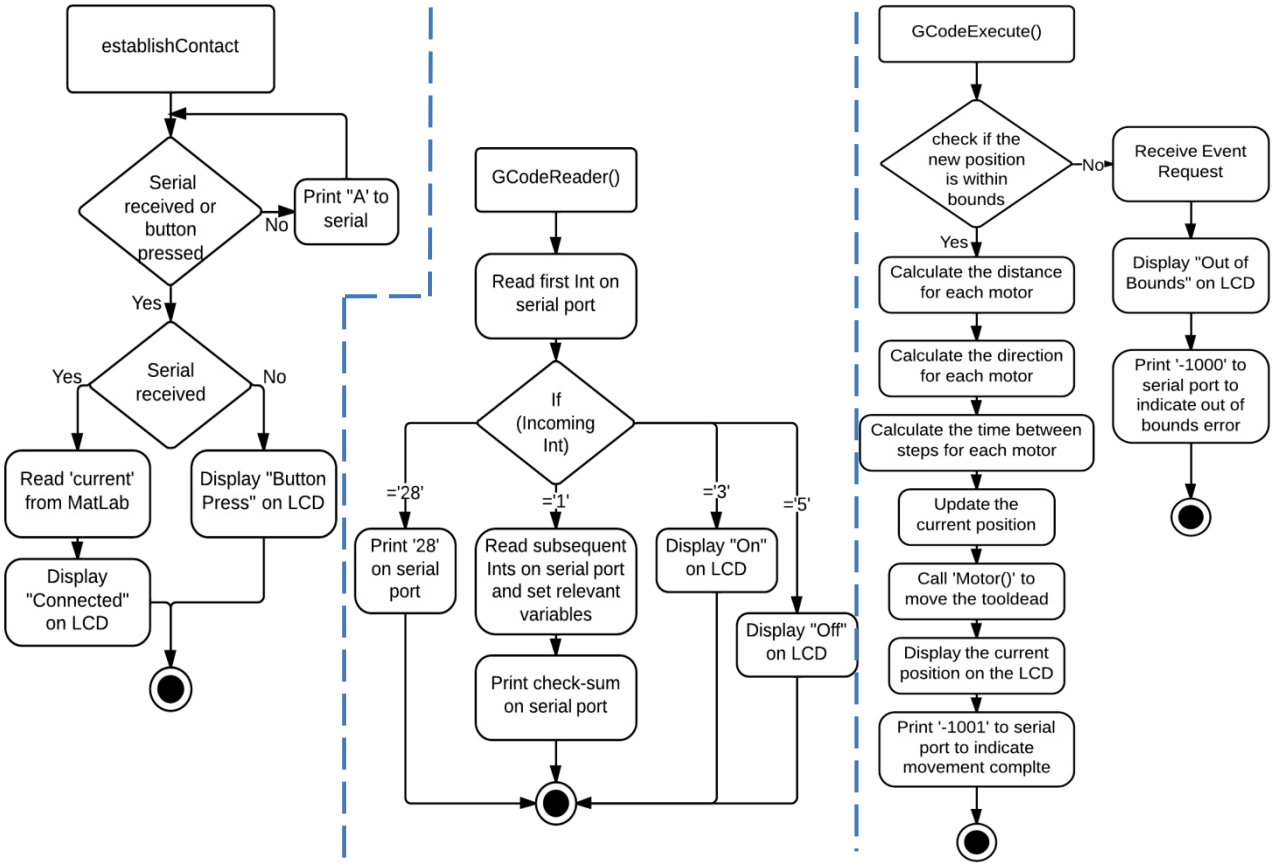

Figure 10-1. Showing MATLAB communications functions.

10.1.2 Stepper motor control

The following three functions are used to control the movements of the stepper motors via GPIO pins that control two stepper driver circuits. Figure 10-2 below shows these functions used to control the stepper motor.

i. Home()

This function is called to move the toolhead to the home position. It enables both stepper motors and moves the toolhead toward the home position quickly until both home switches are depressed (if one is depressed then it ceases to move in that direction). It then moves the toolhead back out 5mm in both directions and then back towards the home position, using deceleration code; this is to mitigate any overrun steps during the initial fast homing. Finally, this function resets the current position, displays a message on the LCD and communicates to MATLAB that homing is complete.

ii. Motor()

The *Motor()* function is used to move the motors simultaneously, a certain number of steps in a certain direction, at a specified speed. This function takes three inputs for each motor; namely, '*MillisBetweenSteps*', '*Direction*' and '*steps*'. This function enables the stepper motor drivers and checks that the direction input is valid. It then steps the motors simultaneously by running through a loop that continuously compares the current CPU time to that of the last step. When the difference exceeds '*MillisBetweenSteps*' it steps the corresponding motor one step. This stepping ceases when the correct number of steps for both motors has been reached (this will be at the same time for both motors as '*GCodeExecute()*' calculated the time between steps for each motor in order for each motor to reach the final point at the same time). This function uses either milliseconds or microseconds in order to achieve a broader and more accurate range of feed-rates, this is not shown in Figure 10-2 for simplicity but can be seen in the software attached.

iii. setup_Motor()

This function sets the motor GPIOs as outputs and disables the motor. It also enables internal pull-up resistors for the 'HomeSwitch' pins connected to the micro-switches.

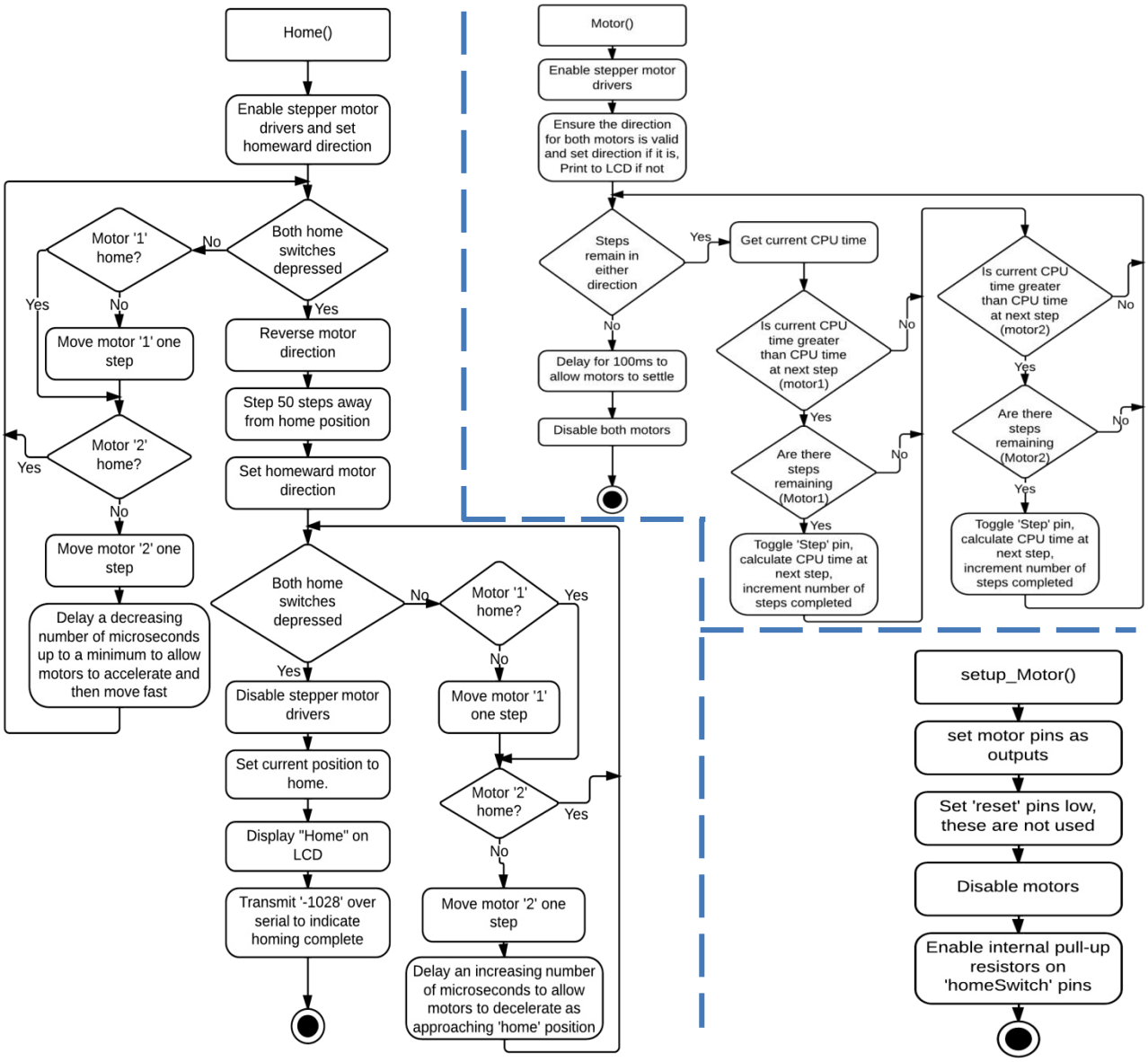

Figure 10-2. Showing stepper motor control functions.

10.1.3 Communications with, and control of CDCE421A

The CDCE421A is used to generate the frequency that modulates the laser. This IC multiplies (or divides) a crystal oscillator to achieve the desired frequency. This frequency output and output logic levels can be set by writing to specific registers within the CDCE421A's flash memory. This IC is communicated with via propriety SSI which is a single wire communications protocol developed by Texas Instruments. This communications protocol had to be written in software as this is not natively supported by microcontrollers and hence there are a large number of functions for this seemingly simple task. The values of the CDCE421A's registers can also be read via the output lines.

i. setup_CDCE421()

This function sets the two GPIO pins, which are used to communicate with the CDCE421A, as outputs. It also disables the CDCE421A and sets a Boolean variable to record that the CDCE421A is disabled.

ii. SetFreq()

This function has a single integer input and uses this to set the frequency. It enables the CDCE421A and calls '*SSIEnterProgramming()*'. It then writes the data corresponding to the frequency to the CDCE421A's frequency register and standard settings to the next five registers on the CDCE421A by calling '*SSIWriteWord_1to5()*'. It then saves this setting to the CDCE421A's built in EEPROM and after communications are complete it disables the CDCE421A. Finally, it displays the frequency that was set to the LCD panel.

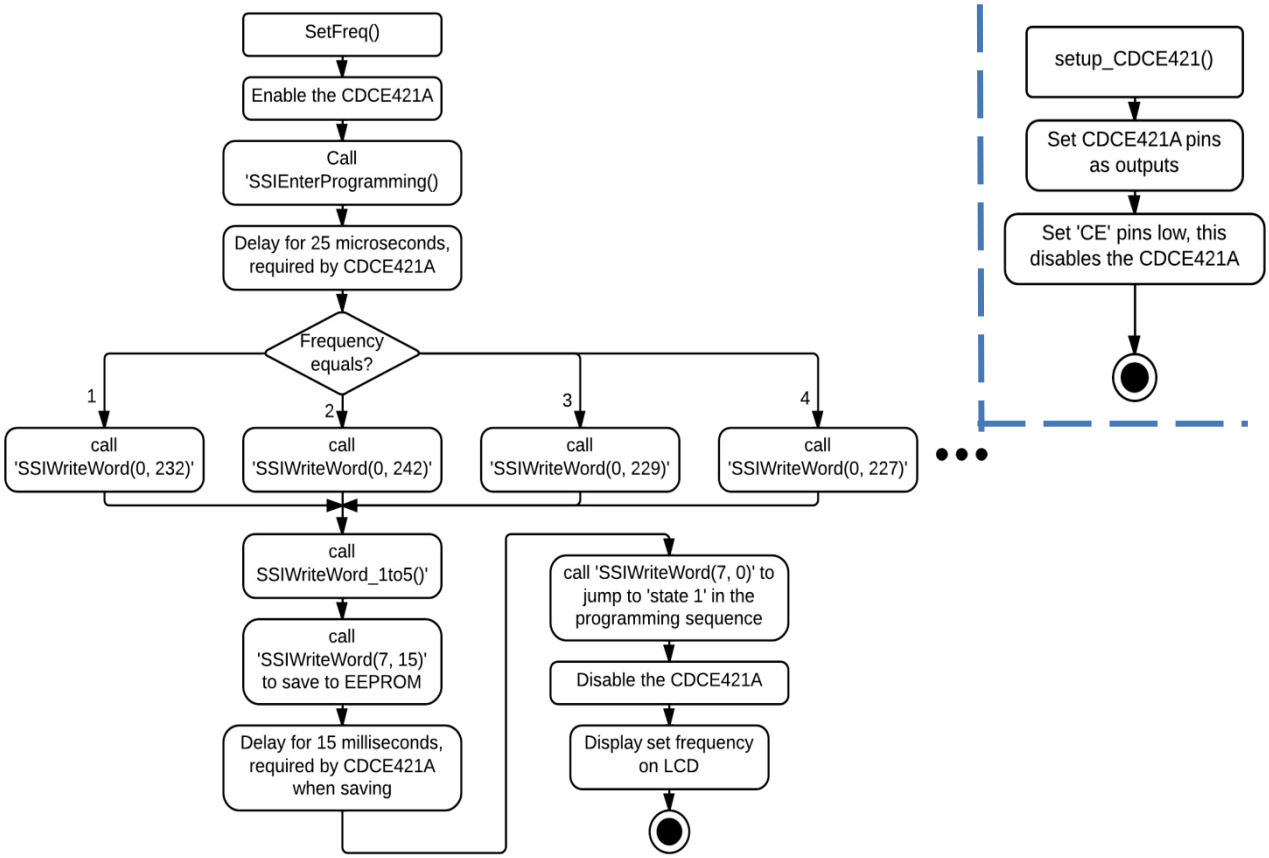

Figure 10-3. Showing SetFreq() and setup_CDCE421A functions.

iii. SSIWriteWord_1to5()

This function writes words 1 to 5 of the CDCE421A. It calls '*SSIWriteWord()*' for each word with the corresponding value for that word. A 30-microsecond delay is implemented between each write command as required by the CDCE421A. These words (or registers) are not explained in the data sheet further than the name of each bit and therefore the recommended values were used [76, p. 14].

iv. SSIWriteWord()

This function takes in two integers, '*wordNumber*' and '*input*' and then writes these bit by bit to the CDCE421A. If the LSB of the '*wordNumber*' is a logical '1' then it calls '*SSIOne()*' otherwise it calls '*SSIZero()*', this is repeated for each of the three word number bits and then for all eight data bits.

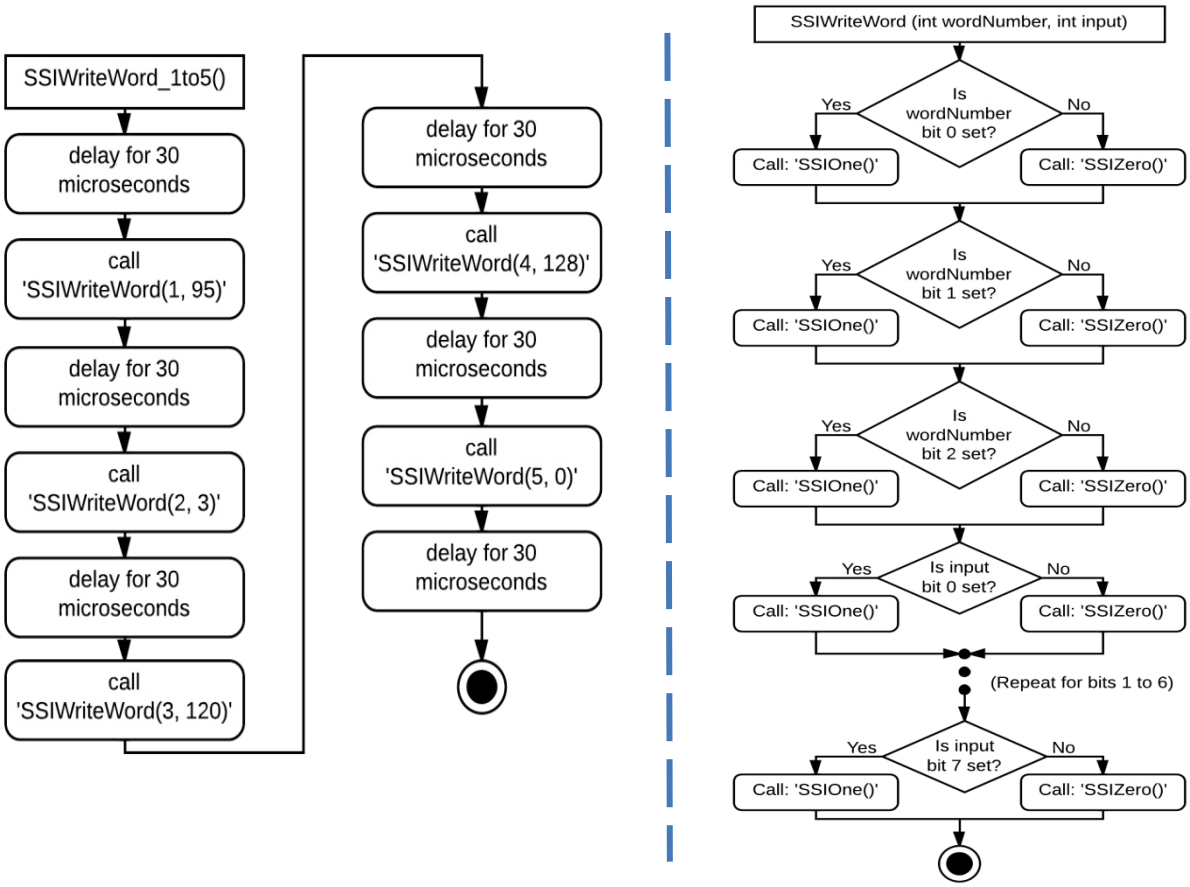

Figure 10-4. Showing the SSIWriteWord_1to5() and SSIWriteWord() functions.

v. SSIEnterProgramming()

This function enters the programming mode on the CDCE421A. It clears both the SSI and CE lines, waits for 160 microseconds, sets the CE line (to enable the CDCE421A), delays a further 6 milliseconds while the CDCE421A starts up and then transmits '001100' on SSI line by calling '*SSIOne()*' and '*SSIZero()*' respectively.

vi. SSIEnterReadback()

This function is very similar to '*SSIEnterProgramming()*' and only differs in that it transmits '111011' on SSI line and then a 60 pulse clock signal. This allows the current value of each register to be read on pin 'FOUT', the same output pin of the CDCE421A that it outputs the generated frequency during normal operation. This was only monitored with an oscilloscope for verification, as this feature was not required in the design. As such circuitry and wiring that would allow the Arduino to read these signals were not implemented.

vii. SSIOne()

This function sends a logical '1' over the SSI interface. It sets the SSI pin of the Arduino, waits for 4**t* microseconds then clears the SSI pin and waits a further 1**t* microseconds before returning

The variable *'t'* is a global variable that equals 2, this allows for easy transmission frequency tuning as the CDCE421A is very sensitive to transmission frequency which must be between 60 and 80kHz. Setting '*t*' equal to 3 gives a theoretical frequency of 67kHz, when only taking into account the delays,

but it was found that other code running between each bit transmission lowered this frequency to below 60kHz. When '*t*' was set to 2 the delays create a theoretical transmission frequency of 100kHz but the other software seemed to lower this into an operable frequency range. (Here frequency is analogous to data-rate and bit/s).

viii. SSIZero()

This function is very similar to '*SSIOne()*' but sends a logical '0' over the SSI interface. It sets the SSI pin of the Arduino, waits for 1**t* microseconds then clears the SSI pin and waits a further 4**t* microseconds.

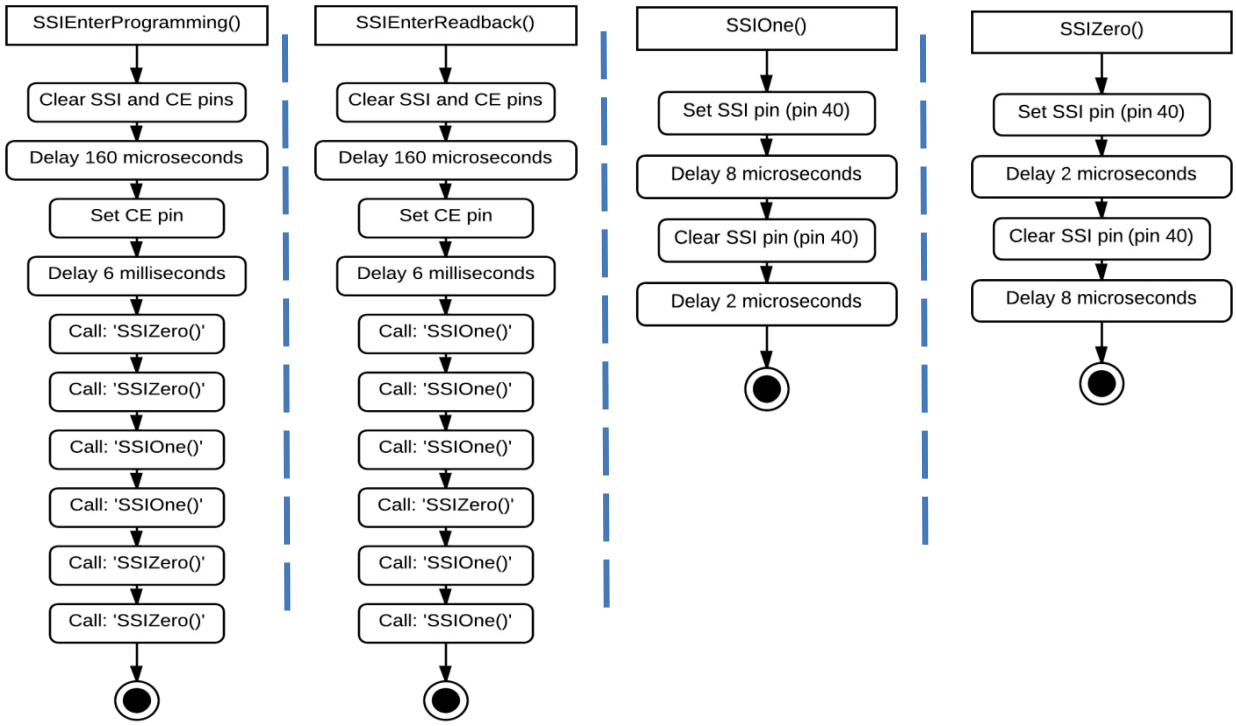

Figure 10-5. Showing the SSIEnterProgramming(), SSIEnterReadback(),SSIOne() and SSIZero() functions.

10.1.4 Communications with and control of TLV5618

The TLV5618 is a 12-bit DAC and has four control bits making up a total of 16 bits to be written with each write operation. The TLV5618 is communicated with by a SPI.

i. TLV5618_Write(char High, char Low)

This function takes in two character arguments that contain the data bits. Initially this function sets the TLV5618 '*slaveSelect*' line high, clears the 4 most significant bits of the '*High*' byte and then writes a 1 to bit 6 (in effect writing 0100 to the four most significant bits), this sets the DAC to output the voltage on pin B in fast mode. The '*slaveSelect*' line is then brought low to select the TLV5618 and the '*High*' and '*Low*' bytes are transmitted (these are transmitted twice as it did not work when transmitting once; this seems to be a common fault with the TLV5618 and was found in many internet forums when consulted [86]).

ii. setup_TLV5618()

This function is used to set up the GPIO pins used for the TLV5618's slaveSelect line and to set up the SPI bus. It sets '*slaveSelect*' and pin 53 as outputs (pin 53 is the master/slave control pin that controls whether the Arduino is a master or slave device, setting it as an output ensures that it will not toggle as a floating input). The SPI bus is then started, the '*SPI_CLOCK_DIVider*' is set to 64, the bit order is set to most significant bit first as this is what the TLV5618 requires and the data mode is set to *mode1* (this controls the clock polarity and phase). Finally '*TLV5618_Write()*' is called initialising the voltage output to 0v, this controls the laser current and sets it to 0 amps.

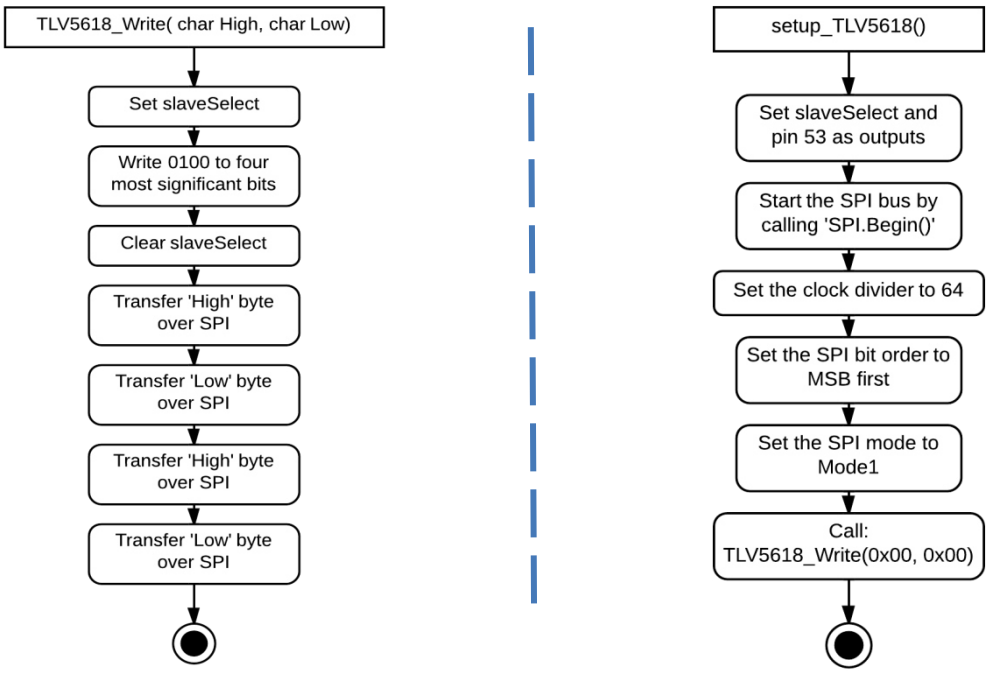

Figure 10-6. Showing the functions used to communicate with and control the TLV5618.

10.1.5 Measuring the voltage output of the AD8302 with the ADC

The AD8302 generated two analogue voltages that are proportional to the phase and magnitude of the received reflected signal relative to the reference signal. These analogue voltages have a range of 0-1.8V; this is multiplied by a factor of 2.4 by the TLV2372 rail-to-rail operational amplifier generating a voltage range of 0 to 4.4V.

i. ADC_Read()

This function is used to measure the ADC value multiple times as fast as possible and to save this result in a global array. This function initially calls '*ADC_Fast_Setup()*', if the ADC has not been set up in fast mode, it then delays for 1 microsecond to allow the ADC to settle after changing its setup. It then runs through a *for* loop that iterates as many times as there are elements in the array. Within this *for* loop it waits for the ADC to complete a conversion, reads the ADC value into the array, reads the *ADCH* register (needed to clear the conversion complete flag) and then clears the conversion complete flag to ensure that unique ADC conversions are read each time regardless of the conversion rate set in '*ADC_Fast_Setup()*'.

ii. ADC_Fast_Setup()

This function sets up the Arduino's ADC. 0x60 (or 0x40) was written to *ADMUX*; this set the voltage reference to 5V, 10-bit mode (or 8-bit mode), and using analogue pin A8 as the input (in order to use pin A9, when measuring magnitude, the least significant bit of *ADMUX* was also set). 0x08 was written to *ADCSRB*; this set the analogue input pins and the trigger source as the ADC interrupt flag, essentially enabling continuous conversion mode. 0xE3 was then written to the *ADCSRA*; this enabled the ADC, started conversions, set auto triggering, cleared the ADC interrupt flag and set a conversion prescaler of 8 (the prescaler was changed during testing to vary the sampling frequency). It then delayed for 20 microseconds to allow the ADC to settle.

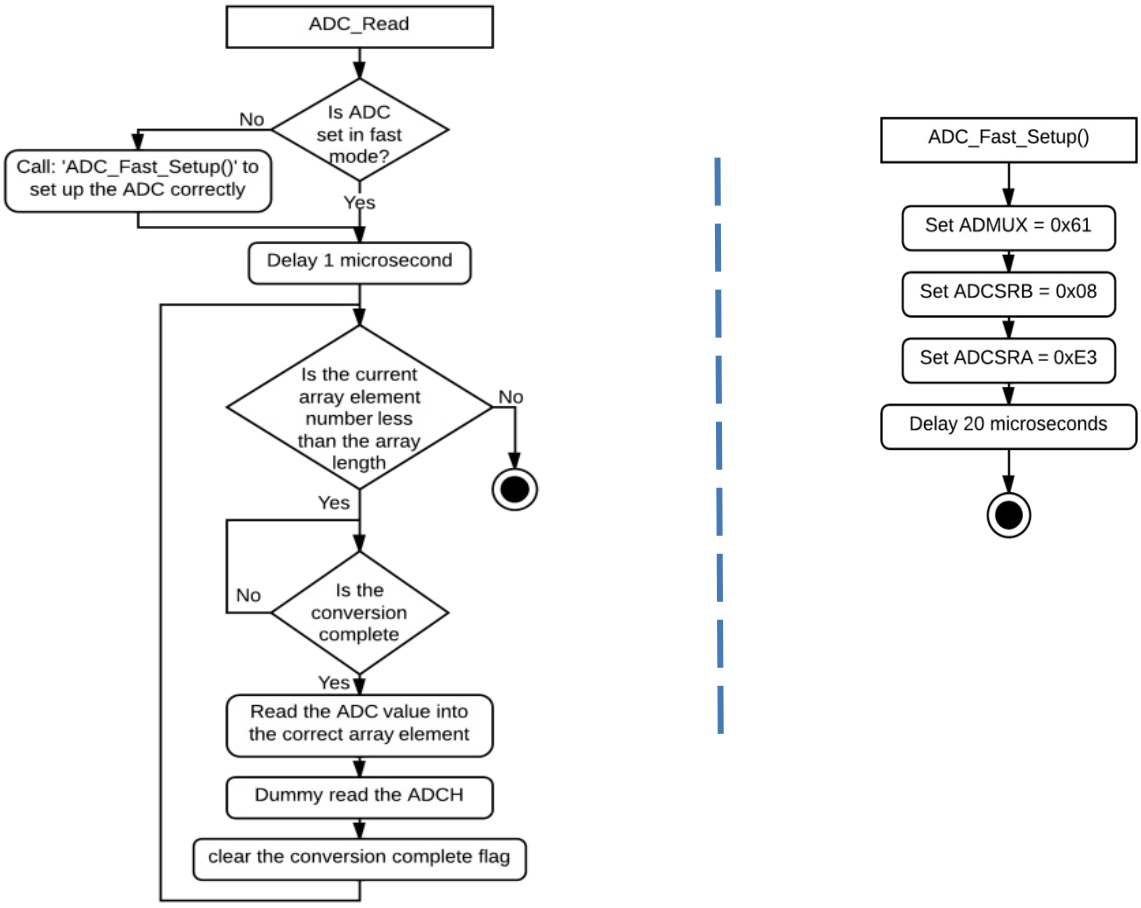

Figure 10-7. Showing the functions used to measure the voltage of the AD8302 with the ADC.

10.1.6 HMI communications and display

The HMI comprised of a LCD and six push buttons. The LCD is a 2x16-element display with each element made up of 8x5 dots. The LCD can be communicated with via GPIO pins and there is an LCD library in the Arduino development environment, which can be used when set up correctly. These buttons are made up of one reset button, which connects directly to the Arduino reset, and five buttons that assert a specific analogue voltage on pin A0.

i. LCD_ButtonRead()

This function reads analogue pin A0 and returns an integer corresponding to this button that is being pressed on the HMI. It initially sets the ADC in 5V reference, 8-bit, continuous conversion mode; and the analogue input pin to A0. It then waits one millisecond and reads the ADC value. The ADC value is

then compared with some predefined values in order to determine which button was pressed after which an integer is returned to indicate the button that was pressed (or '0' for no press).

ii. setup_LCD()

This function sets up the LCD. The "*LiquidCrystal.h*" library needs to be included for the LCD to work. '*LiquidCrystal lcd()*' is called to initialise the library with the pin numbers of the interface pins of the specific LCD model used. '*lcd.begin()*' is then called to set up the number of rows and columns on the LCD screen. Finally, "Home ↵ Starting" is displayed on the LCD screen.

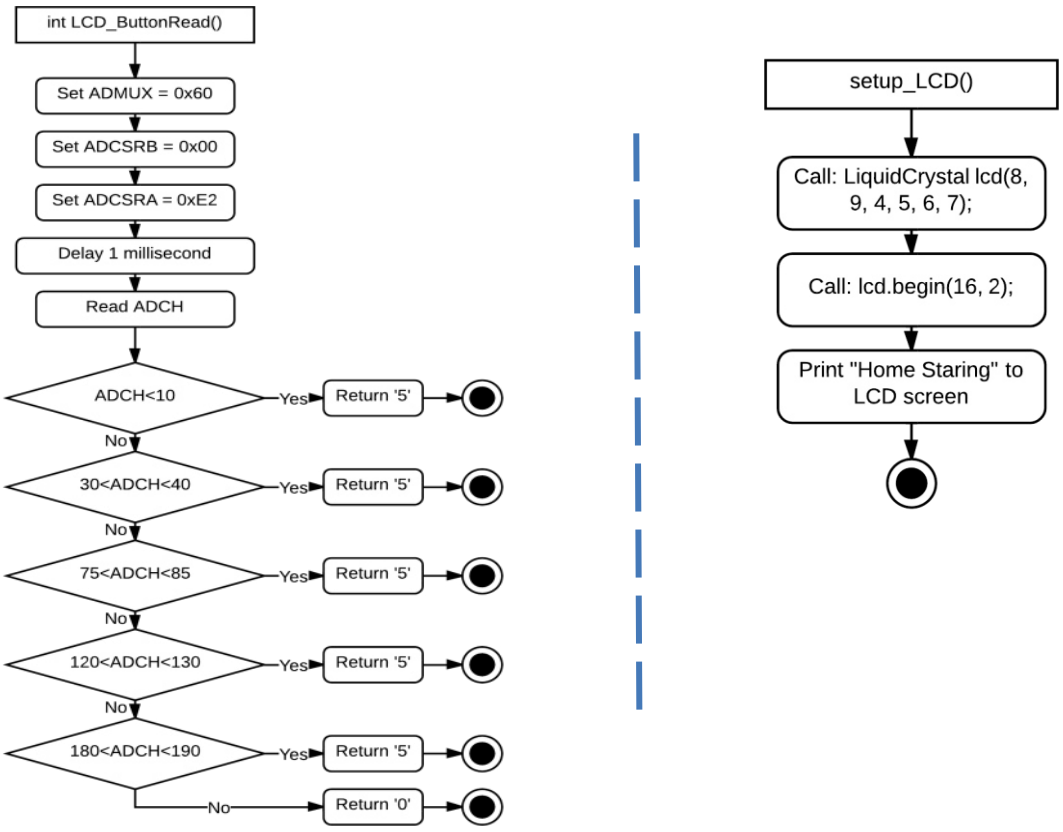

Figure 10-8. Showing the LCD_ButtonRead() and setup_LCD() functions.

iii. Current_Menu()

The current menu allows the DC current through the laser to be set via the HMI. When called, it runs a while loop that senses whether the 'up', 'down' or 'select' buttons are pressed, by calling '*LCD_ButtonRead()*'. If the 'up' or 'down' buttons are pressed if increments or decrements the global '*current*' variable and displays the current '*current*' value on the LCD. If the 'select' button is pressed, it checks whether the current setting is within an acceptable range and if not sets it to a default of three and displays an error message on the LCD. Finally, it prints the set current value on the LCD before returning.

iv. FrequencyMenu()

The frequency menu allows the frequency of modulation to be set via the HMI. When called it runs a while loop that senses whether the 'up', 'down' or 'select' buttons are pressed, by calling '*LCD_ButtonRead()*'. If the 'up' or 'down' buttons are pressed if increments or decrements the global

'*Select_Freq*' variable and displays the current '*Select_Freq*' value on the LCD. If the 'select' button is pressed, it calls '*SetFreq()*' to set the modulation frequency on the CDCE421A and prints the set frequency value on the LCD before returning.

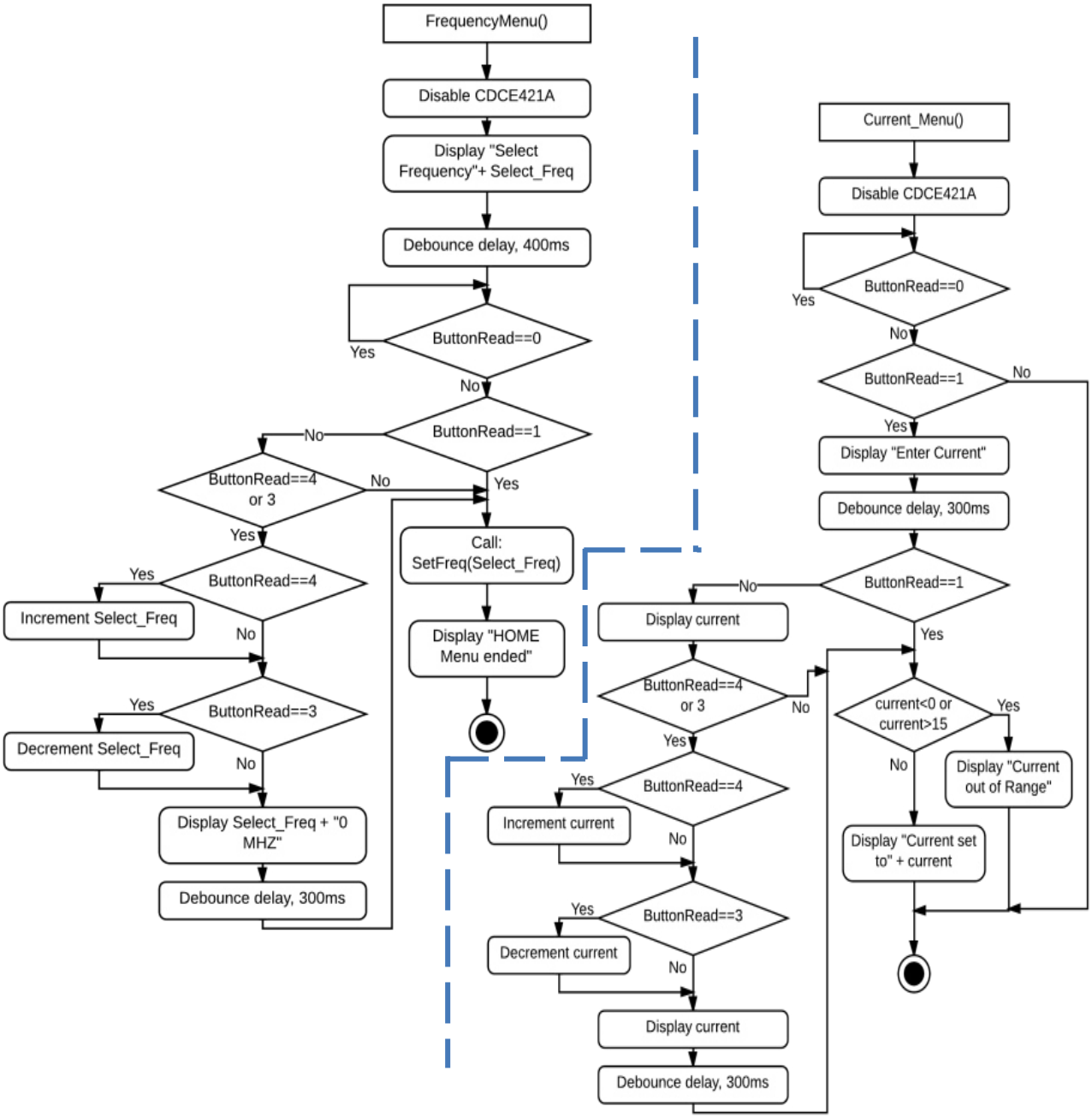

Figure 10-9. Showing the FrequencyMenu() and Current_Menu() functions.

10.1.7 Gantry testing program

In order to operate the gantry using the corresponding MATLAB program a corresponding *setup* and *main* program had to be written. This program was designed to communicate with the MATLAB gantry control GUI via G-code or to allow some operation of the gantry via the HMI buttons. This program initialised by including some libraries and declaring the necessary hardware setup pins and global variables. It then ran the '*setup()*' function, a necessity of the Arduino IDE, in which all the setup functions (described above) were called, the '*establishContact()*' function was called to connect to MATLAB as well as doing some hardware configuration. The main '*loop()*' function ran next. In this

loop, while any button on the HMI had not been pressed, it would check to see if the Arduino was operating in MATLAB mode (this was set in '*establishContact()*' function). If the Arduino was running in MATLAB mode, it would wait for serial data and then interpret this data when it was received, call the relevant functions and display the relevant data on the LCD screen. If the Arduino was not running in MATLAB mode, it would continue checking whether a button had been pressed; if it had, it would carry out a command that had been set up for that button. These button configurations were often changed during testing and mostly comprised of calling either the '*motor()*' or '*Home()*' functions or used for turning the laser on or off.

10.1.8 Phase and magnitude testing program

This program followed a similar structure to the Gantry testing program but called different functions depending on the command from MATLAB. The button configurations also changed often other than the '*Right*' button which was always used to enter into the '*FrequencyMenu()*' and '*Current_Menu()*' menus. This program was also able to run in either MATLAB or HMI modes depending on whether MATLAB was running on the host PC. Figure 10-10 shows the main loop, this is similar in structure for the gantry-testing program but the tasks carried out varied.

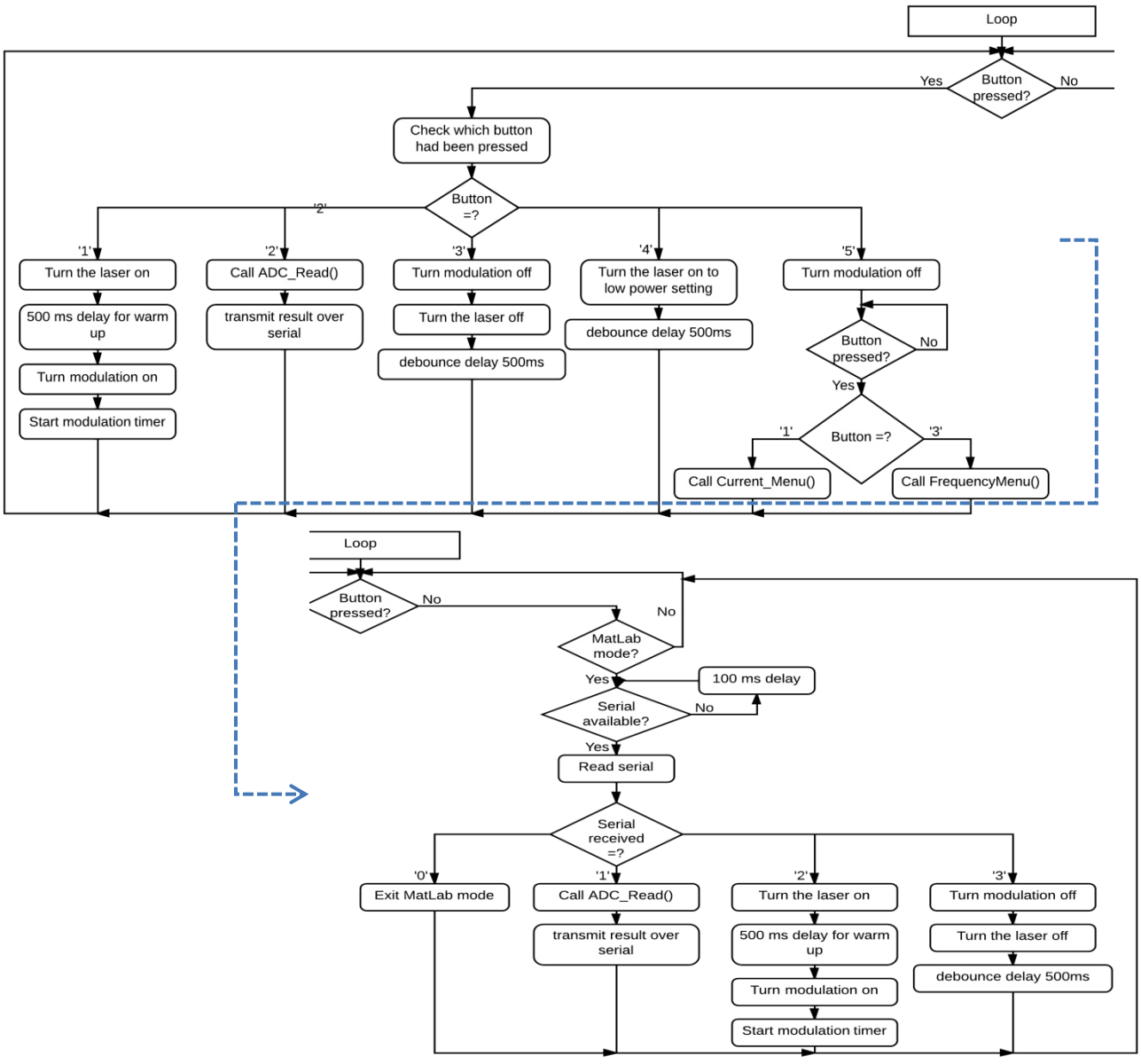

Figure 10-10. Showing the phase and magnitude testing program (lower portion fits on right).

10.2 Software Running in MATLAB®

The software running in the MATLAB environment is used to control the laser cutter and to gather the relevant data during testing. For this reason, the MATLAB code changed a lot depending on the test being run. The control interface used a GUI to allow the user to control the laser cutter and view results without going through code segments to alter individual variables. Two different GUIs were developed in MATLAB; one controlled the gantry and the position of the toolhead using G-code commands and the other was used to control the gantry and modulation for distance measurement testing. These two GUIs are shown below in Figure 10-11 and Figure 10-12 and are described in terms of the operation of each element within the individual GUIs. The complete MATLAB code can be seen in the attached CD.

10.2.1 GUI to control the gantry via G-code

The G-code GUI was used to send G-code commands to the gantry system and contained both a manual G-code entry area and a jogging area. Two large push buttons were also added for testing purposes. The only element in this GUI that was changed from test to test was the 'Run Test' button's call-back function as this was programmed to send a sequence of commands that depended on the test being performed.

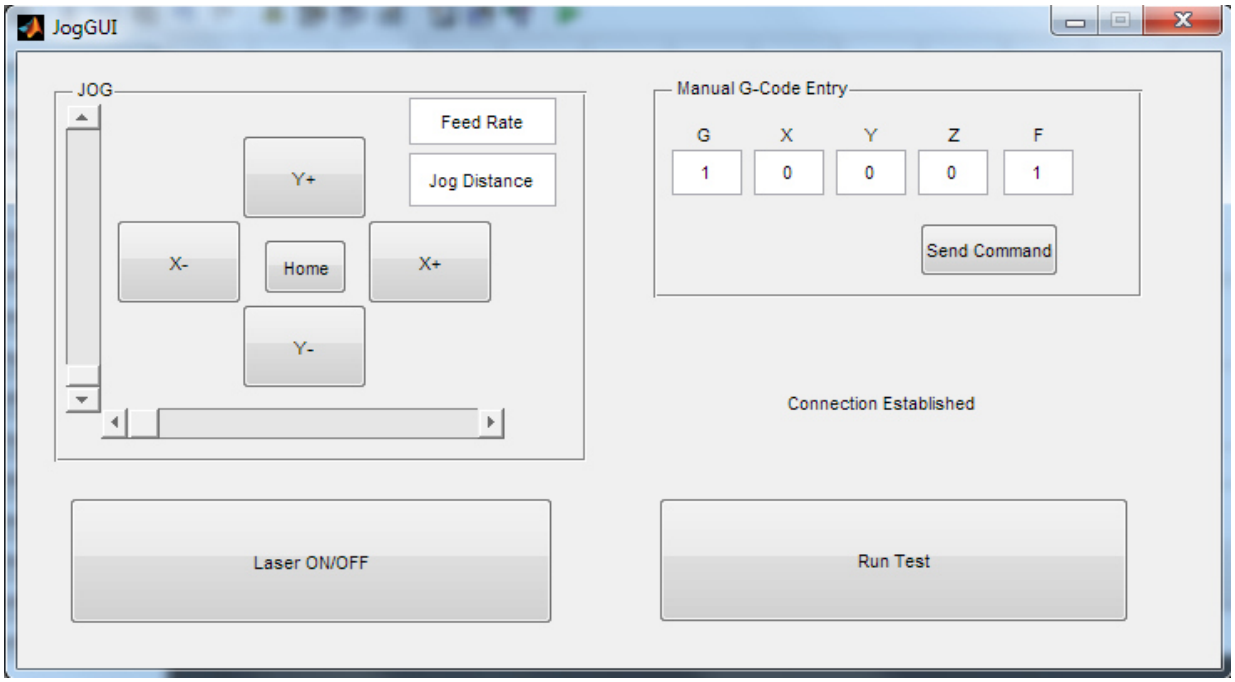

Figure 10-11. Showing the GUI used to control the gantry via G-Code.

i. Sliders

The sliders are used to indicate the current position of each axis of the gantry respectively and are updated each time the gantry is commanded to move. They are set up with a range equal to the gantry's physical limits. When the sliders are moved, by either pressing the arrows or dragging the slider bar, they send a new 'G1' command to move the motors. They initially get the current 'x', 'y', 'z' and 'f' ('f' is feed-rate) position data, then get the new slider position, augment this to the current position and send this in a correctly formatted 'G1' code. It then waits for and interprets the response form the Arduino and indicates this in the status box. If the movements were successful then it updates the current position to include the augmented slider value.

ii. 'X+, X-, Y+, Y-' buttons

These four buttons are used to jog the gantry the distance input into the '*Jog Distance'* edit text box (default of 1mm) at a feed-rate input into the '*Feed Rate*' edit text box (default of 1mm/s) in the respective direction. When the buttons are pressed, they get the current position, feed-rate and jog distance, calculate the new position and sent this via a 'G1' code to the gantry. It then waits for and interprets the response form the Arduino and indicates this in the status box. If the movements were successful then it updates the current position and the sliders to include the distance that had just been moved.

iii. 'Home' button

The home button is used to send the gantry to the home position. This is done so by sending the 'G28' command to the Arduino when the button is pressed. It then checks that the code was transmitted successfully and waits for the homing complete signal from the Arduino. Upon receiving this signal all the current distances and sliders are set to the zero position.

iv. 'Feed Rate' edit text box

This editable text box allows the user to specify a feed-rate when using the jog buttons or the sliders. The default value is 1mm/s.

v. 'Jog Distance' edit text box

This editable text box allows the user to specify the distance that should be jogged when using the jog buttons. The default value is 1mm.

vi. 'Manual G-code Entry' edit text boxes

These editable text boxes allow the user to enter the G-code parameters manually allowing diagonal movements that are not possible with the jog buttons.

vii. 'Send Command' button

This button sends the G-code entered into the manual G-code entry boxes above. If '28' had been entered into the 'G' box, 'G28' is sent (this commands the gantry to perform the homing routine), this is similar to the process called when the '*Home Button'* is pressed. If '1' had been entered into the 'G' box, a 'G1' command is generated similarly to the way it is when a jog button is pressed but in this instance the values that are entered into the manual G-code entry boxes are transmitted without consulting the current position. Once the movement complete response has been received from the Arduino the current position is set to that which was sent.

viii. 'Laser ON/OFF' button

This button sends either 'G3' or 'G5 to the Arduino in order to turn the laser on and off respectively. It also changes the colour of the button in order to give a quick visual indication of whether or not the laser is on.

ix. 'Run Test' button

The software that ran when this button was pushed was varied depending on what test was being carried out. Most of the tests entailed turning the laser on and off using 'G3' and 'G5' codes and moving the gantry using 'G1' codes in certain sequences controlled by different loops in the software. The methods used to transmit each code are similar to those that were used above and are not described again. The code that can be seen on the CD contains a loop that runs 10 times and within each iteration it turns the laser on, moves a set distance in the 'y' direction at a speed that increments on each loop iteration, turns the laser off and then moves back the set 'y' distance but also a set 'x' distance so as not to make the next cut in the same position. This creates a saw tooth travel pattern with the laser 'on' on the horizontal portions and off on the diagonals. The feed-rate on each cutting pass is set to increase on each iteration of the major loop in this test.

10.2.1 GUI to control the phase and magnitude testing rig and display the results

This GUI was used to test the phase and magnitude outputs while doing distance measurement tests. This GUI sent serial commands to the gantry in order to move the reflector attached to the toolhead a fixed distance, recorded the results and displayed them both graphically and tabulated. This GUI was also able to store the raw measurement data in a '.csv' file.

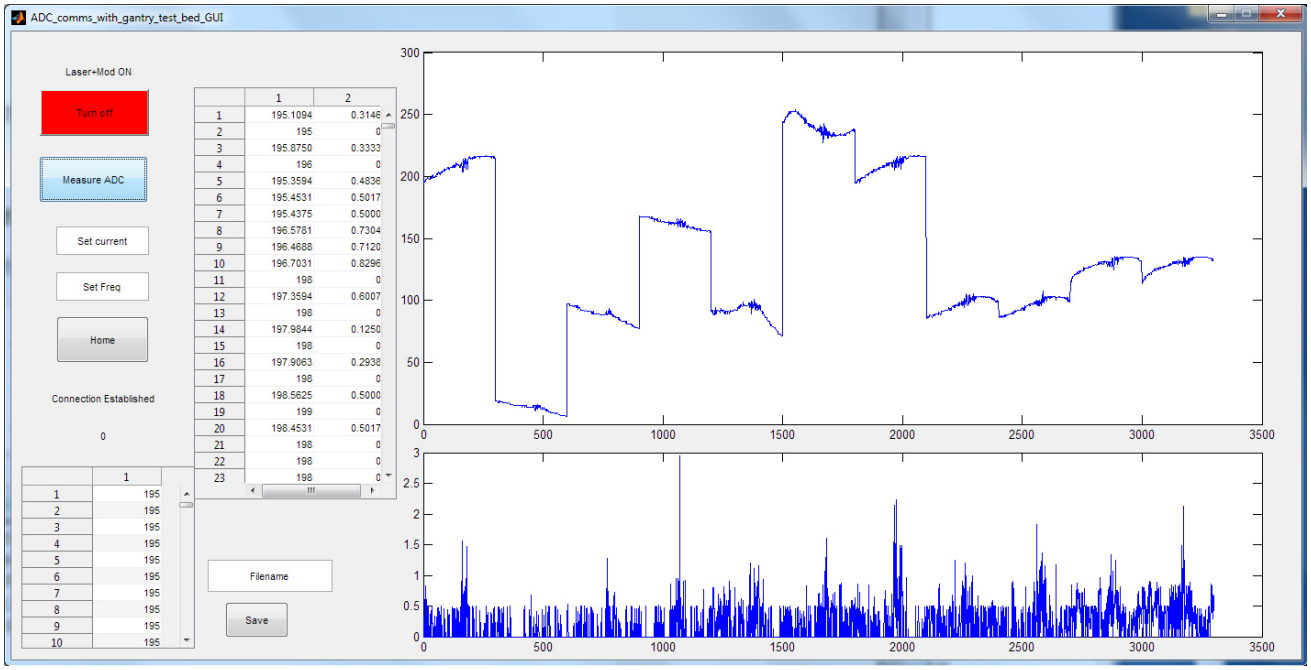

Figure 10-12. Showing the GUI used to control the phase and magnitude testing rig and display the results.

i. 'Turn ON/OFF' button

This button operated similarly to that described above in order to turn the laser on and off via G-code. It also sent current and frequency settings to the Arduino every time the laser was turned on, These current and frequency settings were sourced from the '*Set Current*' and '*Set Freq*' edit text boxes. These had default values set in the open_Function.

ii. 'Measure ADC' button

When this button was pressed, the main testing function was run. This call back function was changed depending on the test being performed but the routine described here produced the results shown in Figure 10-12. This was a test to see the effect of frequency on the phase shift. This function runs nested 'for' loops. The inner-most loop commands the Arduino to read the ADC a set number of times, reads these results into an array, shifts their values if necessary in 10 bit mode, calculates the mean and standard deviations and updates the respective matrices that contain the total data. It finally plots the data to the axes every 64th iteration. The middle loop runs once for each distance measured, it sets up the data variables, runs the inner loop, commands the Arduino to move the gantry 1 increment (the distance of each increment is set on the Arduino), plots the results on the axes, checks if the end distance has been reached and if so commands the Arduino to run the homing routine and finally it saves all the data to be used in other call-backs. The outer-most loop (commented out) is used to repeat the test and in this case, it incremented the modulation frequency with each iteration; in order to do this it needed to turn the laser off and on.

iii. Set current and SetFreq edit text boxes

These edit text boxes were to allow the current and frequency to be adjusted. These values were used when the '*Turn ON/OFF*' button was pressed.

iv. 'Home' button

This button sent '28' over the serial port to the Arduino. This would trigger the homing routine on the Arduino. No communication checks were performed as this GUI was only used for testing.

v. Display tables

The two tables were used to display the data. The lower table displayed the raw data and the longer table beside the axes was used to display the average and standard deviation of each data point.

vi. 'Filename' edit text box

This is where the desired filename is entered when saving data.

vii. 'Save' button

This function gets the filename entered into the '*Filename*' edit text box and the raw data that has been received, and then saves the data as a '.csv' file with the desired filename.

viii. Top axis

The top axis is used to plot graphs of the data, which were often averaged for each measurement while it was being acquired. This was done when the '*Measure ADC*' button was pressed.

ix. Bottom axis

The bottom axis was used to plot graphs of the standard deviation of each data point; this was done when the '*Measure ADC*' button was pressed.

11. Final Testing, Results and Discussion

This chapter aims to present some of the tests that were done in order to verify the operation of different aspects of the system. The chapter documents tests on how the different major parts of the project operate together. Each of the major parts of this project were previously tested in isolation and this was presented in the respective chapters. This chapter is broken up into two major sections, namely 'Laser Cutting' and 'Distance Measurement'.

11.1 Laser Cutting

The primary objective of a laser cutter is to be able to process materials for some sort of practical application. This laser cutter is ultimately intended for use as a prototyping platform and as a 3-dimensional printer of computer-generated models. Because this laser radiates infrared light, the way it reacts with different materials is not always as expected. Different aspects of this laser cutter's ability are tested here. The power of the laser is proportional to the current through the laser. All tests performed in order to measure the laser's cutting ability were done so at 2A (1.5W optical output) unless otherwise noted.

11.1.1 Different reflectivity or colour

This laser interacts with different colours of the same material in different ways. The energy needed to cut the workpiece is provided by the laser beam. Since this laser's radiation is in the near infrared part of the spectrum, it therefore has similar absorption properties to visible light. The more laser radiation that is absorbed the better the cutting ability of the laser. For this reason, darker coloured materials are expected to be cut more easily.

Some tests were carried out to test whether or not this is the case and if so demonstrate the impact colour has on the cutting ability.

i. White vs black paper

The first colour test was performed by cutting lines in a piece of white paper that had had black areas drawn onto it with a permanent marker. The results of this test can be seen in Figure 11-1. This test was conducted with the laser current set at 2A. In this test, the feed-rate was varied to show that faster feed-rates are still able to cut black paper but not white paper. The feed-rates used were 1, 2, 3, 4, 5, 6, 8, 10, 12 mm/s when viewing the image from left to right. Each line is 4mm apart (except between feed-rates 8 and 10, where it is 6mm). The cut direction is indicated by the arrow.

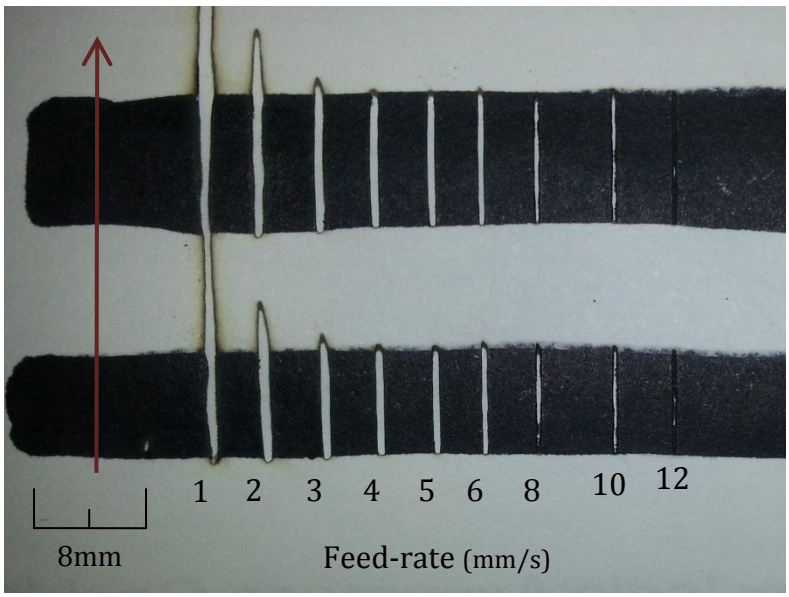

Figure 11-1. Showing the results of cutting black vs white paper.

Figure 11-1 clearly shows that the laser is able to cut black paper a lot more effectively than white paper. The cuts in the white paper for feed-rates 1 and 2 are only present due to the blackening effect on the edge of the paper when it is burnt. This allows the cut to continue into the 'white' paper when the feet-rates are slow. When the feed-rates are faster the laser moves past this narrow blackened area onto pure white paper and stops cutting.

It can also be seen in the figure that as the feed-rate increases the width of cut decreases. This is because the laser beam has a Gaussian power distribution and when the feed-rate is higher, only the centre of the laser beam contains enough power to cut the black paper. At a feed-rate of 12 mm/s the cuts do not reliably penetrate the paper but a surface cut is still visible.

ii. White vs black polystyrene

The second colour test was performed in the same way as the 'White vs black paper' test with slightly different feed-rates as indicated on the figure. In this test, polystyrene was cut rather than paper. The results of this test can be seen in Figure 11-2. The cut direction is indicated by the arrow.

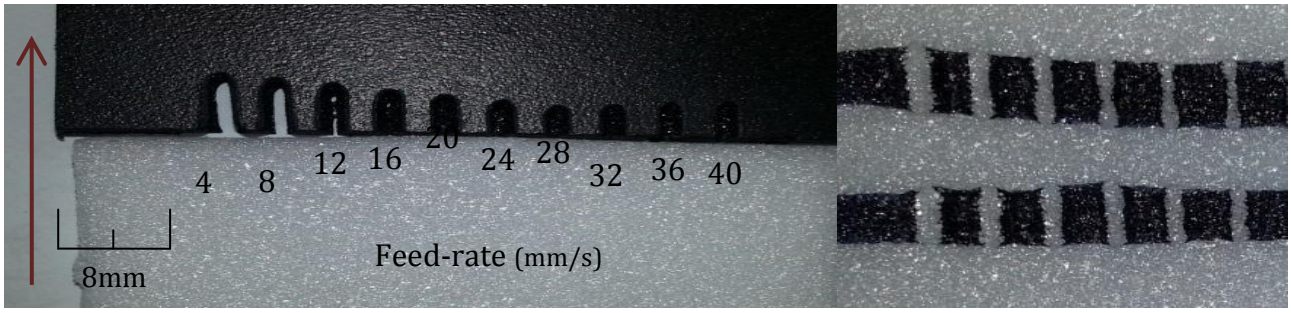

Figure 11-2. Showing the results of cutting black vs white polystyrene (LEFT) and white polystyrene with black areas drawn on (RIGHT).

In Figure 11-2 (LEFT), it can be seen that the white polystyrene was not cut at all whereas the black polystyrene was cut all the way through with feed-rates of 1 to 3 mm/s. Figure 11-2 (RIGHT) shows the same test but cutting white polystyrene which had had black areas drawn on with a permanent

marker. The black areas are cut but when the laser beam reached the white polystyrene, below these black areas, no further cutting occurred.

iii. Coloured foam

The third colour test was performed in the same way as the 'White vs black paper' test with feed-rates of 1 to 8mm/s. In this test three different coloured pieces of foam were cut; namely, red, green and blue. The results of this test can be seen in Figure 11-2. The cut direction is indicated by the arrow.

Figure 11-3. Showing the results of the coloured foam test.

In Figure 11-3 it can be seen that only the blue foam is cut. This is because blue will absorb most of the red spectrum and this seems to include near infrared for this type of foam. Interestingly it was observed that the red (and green to some extent) foam transmitted, rather than absorbed or reflected, a lot of the laser power and objects were able to be cut through it without any visible damage to the red foam.

11.1.2 Cutting depth vs speed

The depth of cut is very closely related to the feed-rate of the laser as the slower the laser moves the more energy is supplied to a certain area. The energy that is supplied to that area (ignoring dissipation) is what allows the laser to cut the material and hence the more energy the deeper the cut achieved.

The depth of cut test was performed by cutting lines in a 5mm thick piece of black polystyrene. This test was conducted with the laser current set at 2A. Each line is 4mm apart and the cut direction is indicated by the arrow. The polystyrene was then sliced across the cuts in order to show the depth in a photograph.

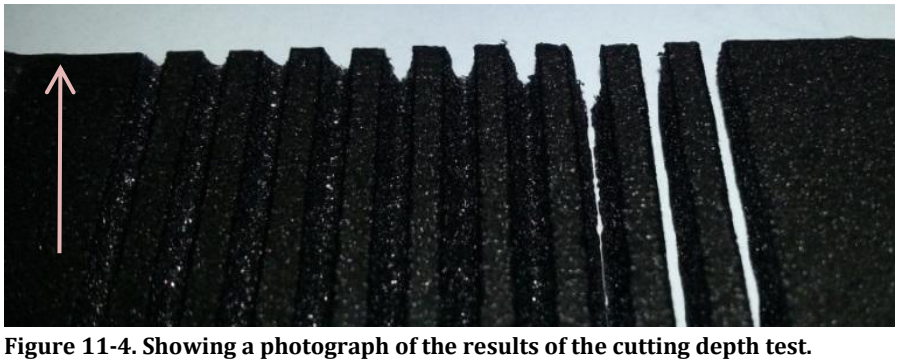

Figure 11-4. Showing a photograph of the results of the cutting depth test.

Figure 11-4 shows a photograph of black polystyrene cut at different feed rates. The feed-rates used decrease in increments of 4 mm/s and range from 40 to 4 mm/s (left to right). It can be seen that 4, 8 and 12 mm/s feed-rates are easily able to cut through the 5mm thick polystyrene sheet. At a feed-rate of 40 mm/s the cut depth was measured to be 1mm. From this and other tests it was found that the cut depth is inversely proportional to feed-rate.

11.1.3 Different densities

The density of the material will affect the amount of energy required to cut at material. In this test solid black plastic, plastazote foam (mouse pad) and black polystyrene (butcher's tray) were cut. These materials are all similar other than their densities. It is expected that the less dense a material the deeper the cut will be. The feed-rate was set to increase from 2 to 20 mm/s in increments of 2mm/s.

Figure 11-5. Showing results when cutting different densities. Top: solid plastic. Centre: plastazote. Bottom: polystyrene.

In Figure 11-5 it can be seen that the material density makes a significant difference to the cut depth. The deepest cut in the solid plastic was measured to be 0.4mm, in the plastazote was 3mm and the polystyrene was cut all the way through. The density of the material affects the cut depth in two ways; firstly, the higher the density the more material needs to be cut per unit depth and secondly the denser the material is more power is dissipated by the material.

11.2 Distance Measurement

In order to measure the change in distance, the phase between the reference signal and the reflected optical signal needed to be measured. The AD8302 IC performs this task and various tests were developed and conducted in order to ascertain the performance of the distance measurement component of this design.

11.2.1 Initial testing and verification

Initial testing and verification was performed in order to ascertain whether or not the system would perform as expected and to determine any areas that needed further testing and refinement. These

initial tests serve to prove that the different components of this system work together as expected but are not intended to be as accurate as possible. Final testing of individual aspects of the system can be seen in 'Final distance measurement testing' below.

i. Signal generator reference signal

A test using the signal generator to provide the reference signal was performed in order to test that the photo sensor and phase shift circuitry were operating as expected.

In the design of this laser cutter, the physical movement of the reflector or cutting surface is very slow relative to the high frequencies used and therefore the phase measurement output is seen as a DC voltage on an oscilloscope. If a signal that is of a different frequency to the laser signal is used as the reference signal the phase measurement output will be a triangle wave with a frequency equal to the difference in frequency between the two signals. For this reason, it was decided to test the operation of the photo sensor and phase detector circuitry using a reference signal generated by a signal generator. Unfortunately, the highest frequency signal generator available was only able to output signals up to 30MHz.

The laser driver circuitry was set to modulate the laser as close to 30MHz as possible (29.602MHz) and the signal generator was set to output a 29.607MHz signal. The phase output of the TLV2372 operational amplifier was monitored. This can be seen in Figure 11-6; where the yellow signal is the optical signal reflected back onto the photo sensor, the green signal is the output of the TLV2372 (and hence AD8302) and the purple signal is the FFT of the yellow signal.

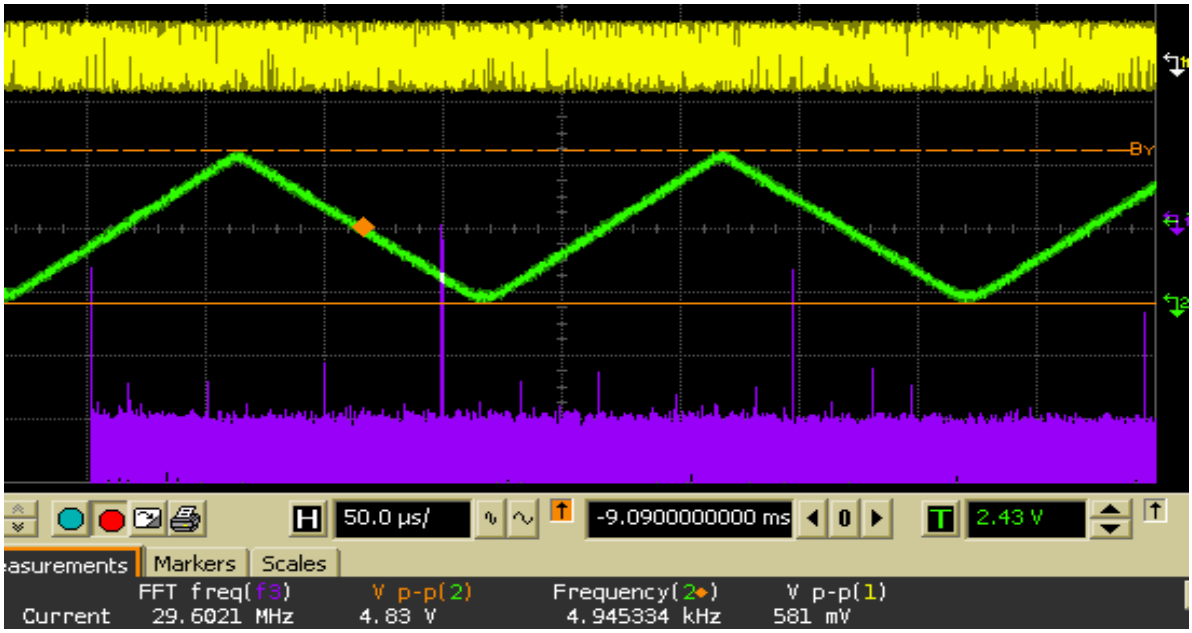

Figure 11-6. Showing the phase difference output of the AD8302 with a signal generator generated reference signal.

It can be seen from the measurements that the TLV2372 output is a triangle wave with amplitude 4.83V_{pp} voltage range from 0V to 4.8V and frequency 4.95kHz. This indicated amplitude is slightly larger than expected but this is because the oscilloscope measurement includes some noise at the extreme points (seen by orange marker lines). When measured by eye, knowing that the scale is 2V/div, it seems to be closer to the expected 4.3V_{PP}. The FFT of the optical signal clearly shows a large peak at 29.6MHz as expected with a smaller peak just below 60MHz, which is the second harmonic.

This shows the expected signal and proves that the photo sensor and phase detector circuitry operates as planned when an artificial reference signal is used.

ii. Oscilloscope phase detection

In order to prove that the signals entering the AD8302 were indeed experiencing a relative phase shift proportional to the distance of the reflector they were monitored with an oscilloscope and the phase shift was recorded. This was then repeated for different distances and the results can be seen in Table 11-1. Figure 11-7 shows how this phase shift was measured for each of the recordings shown in the table.

The test rig shown in chapter 5.8 ('Testing Rig') was used in order to set the distance of the reflector precisely. Six different distance settings were used, each 10mm apart, giving a testing range of 50mm. The laser was set to operate at 102MHz and at a current of 0.8A because these settings were believed to give the most accurate results. The distances shown indicate the distance between the reflector and the focusing lens as the reflector was moved toward the laser. It was initially hoped that the averaging function on the oscilloscope could be used in order to average the phase shift over many readings but the oscilloscope struggled to distinguish between positive and negative phase shift (and multiple cycles yielding phase readings 180° or 360° from the true reading) and hence the averaging function did not give accurate results. It was decided that at each distance, six recordings were to be taken. These were averaged and a standard deviation was calculated. Taking more readings at each distance would have yielded results that are more accurate but this proved tedious and the aim of this test was only designed to prove that phase shift proportional to distance was occurring.

The results of this test can be seen in Table 11-1 where all the readings can be seen, the average of the six readings at each distance and the corresponding standard deviation, the change in degrees and the change in distance calculated using Equation 2-7. These results show that there is phase shift present and it is proportional to the distance of the reflector from the focusing lens. It can be seen that the final step, from 15 to 5mm from the lens, is inaccurate by 2.2mm; it is thought that this is because the phase of the laser reflected off the reflector and off the leading face of the focusing lens are interfering with each other and this was observed in other testing as well.

Table 11-1. Showing the recorded phase shift between the reference and optical signals at different distances.

Phase shift (degrees)		Distance (mm)					
		55	45	35	25	15	5
Reading Number	1	80.37	76.35	72.09	75.21	74.86	68.98
	2	82.34	82.11	82.94	74.85	69.77	66.12
	3	79.94	81.16	76.89	78.61	72.27	73.16
	4	82.34	75.72	77.72	68.18	71.27	73.79
	5	80.12	83.33	71.49	74.7	72.13	68.07
	6	83.58	75.53	78.24	75.76	69.54	68.25
Average phase shift		81.45	79.03	76.56	74.31	71.64	69.73
Standard deviation		1.375	3.238	3.887	3.138	1.782	2.793
Change in degrees		-	2.415	2.471667	2.251667	2.67	1.911667
Change in distance from phase shift (mm)		-	**9.857**	**10.088**	**9.190**	**10.898**	**7.803**

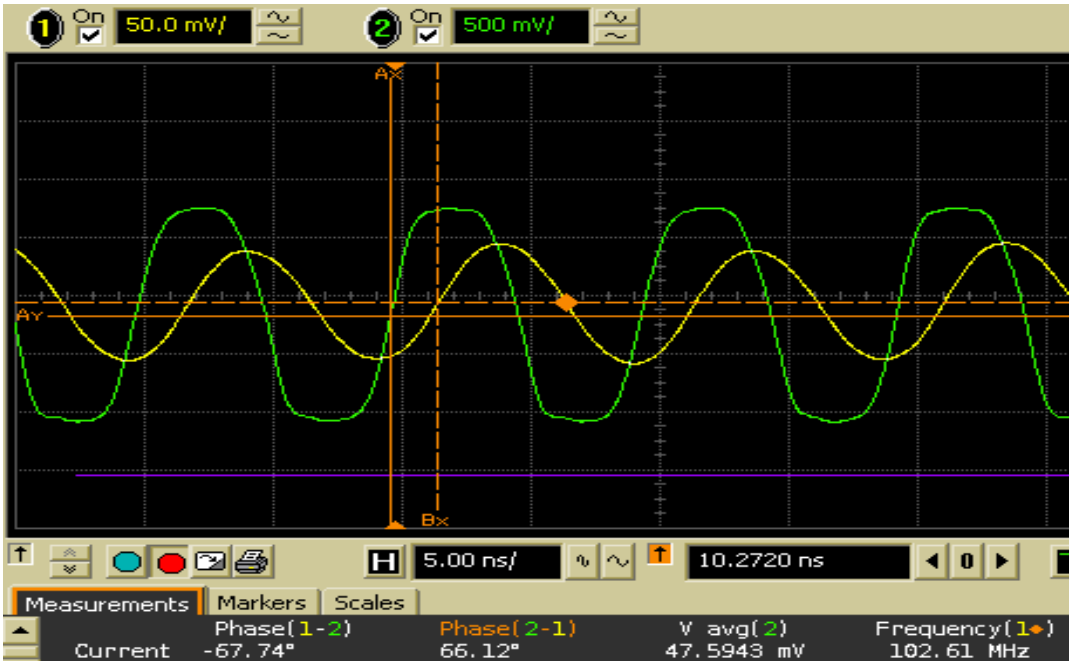

Figure 11-7. Showing how phase shift was measured on the oscilloscope.

iii. Initial system testing

In order to test the distance measurement system as a whole, the test rig shown in chapter 5.8 ('Testing Rig') was used initially as it provided distance measurements accurate to 0.02mm. This was expected to be a lot finer than what would be needed when testing, as the system was only designed to achieve an accuracy of 1mm. The tests shown in Figure 11-8, Figure 11-9, Figure 11-10 and Figure 11-11 show the results of the initial testing. The major drawback of the test rig was that it had to be moved by hand and although this was accurate, it was very time consuming. Software was written specifically for this testing phase and changed slightly depending on the test used. This software is presented in chapter 10 ('Software'). Each of these initial tests and their results are discussed here.

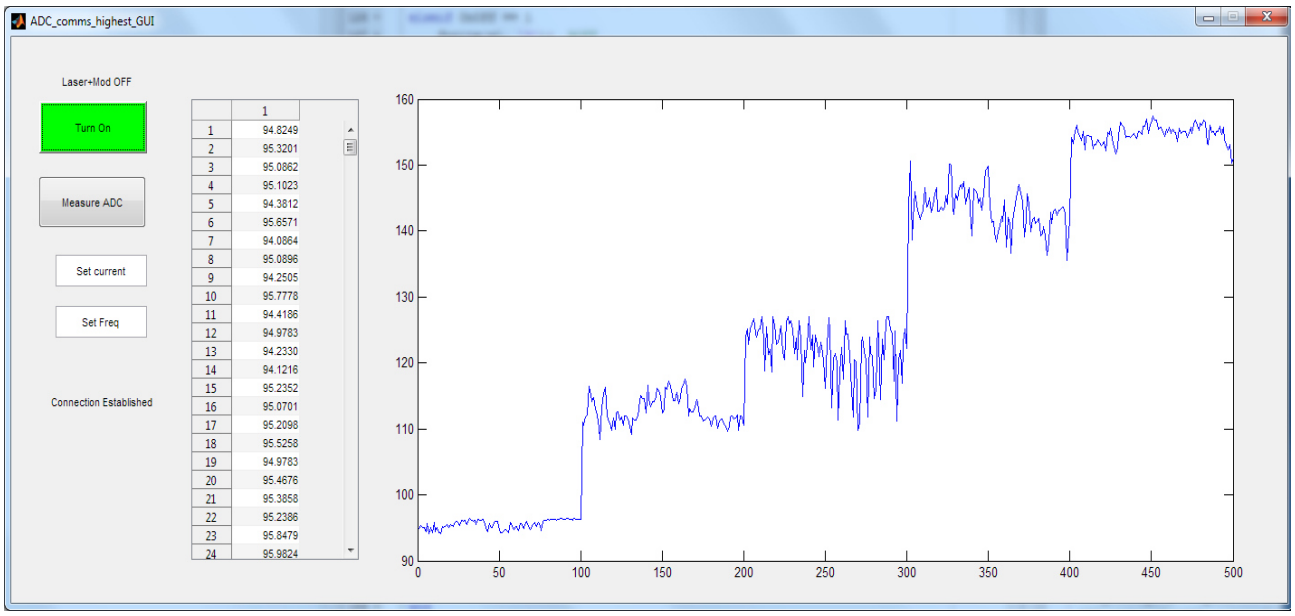

Figure 11-8. Showing initial testing results when moving the reflector 10mm at a time.

Figure 11-8 shows the results for the first test and was the first indication that this system would be able to measure distance using phase shift. The horizontal axis shows the reading number and the vertical axis shows the averaged 10-bit ADC value. In this test, the modulation frequency was set at 102MHz and the current at 0.8A. The reflector was moved 10mm at a time, visible as large jumps, and 100 points were sampled at each distance. Each point was made up of the average of 4096 ADC samples sampling at a rate of about 300 000 samples per second.

The distinct jumps on this test show that the system is able to distinguish between different distances but these do not seem to be particularly accurate. It was thought that this could be improved by using a slower sampling frequency and different averaging techniques. The following tests are similar but measured at 1mm distance intervals.

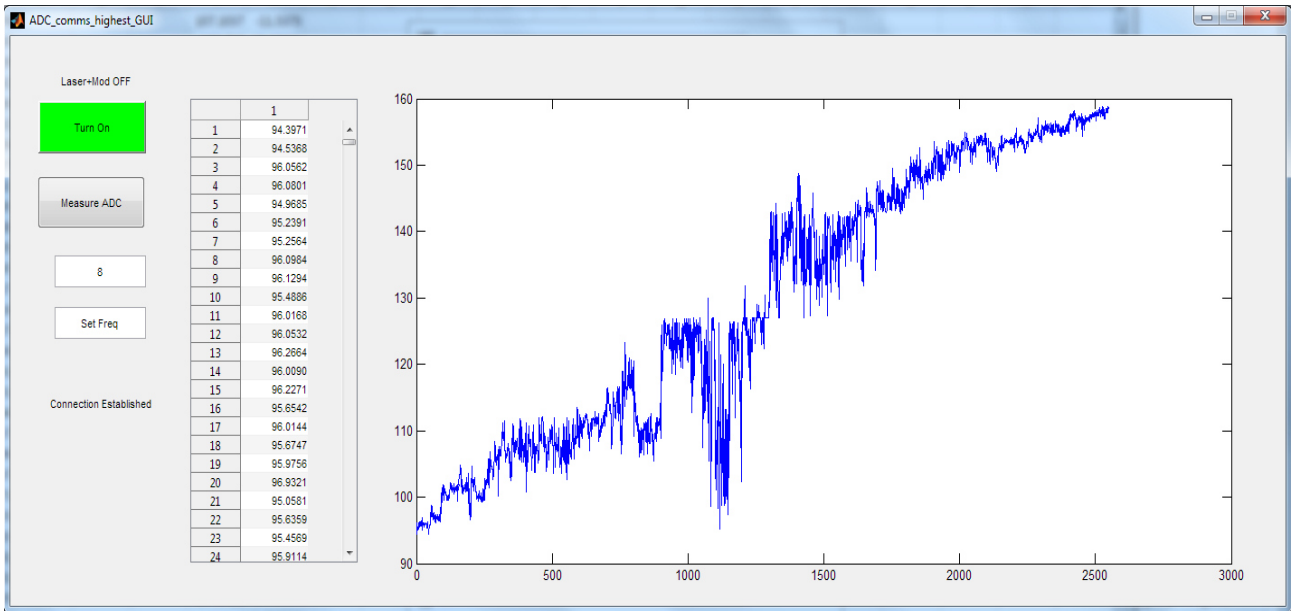

Figure 11-9. Showing initial testing results when moving the reflector 1mm at a time.

Figure 11-9 shows the results for the second test. The horizontal axis shows the reading number and the vertical axis shows the averaged 10-bit ADC value. In this test, the modulation frequency was set at 102MHz and the current at 0.8A. The reflector was moved 1mm at a time, and 50 points were sampled at each distance. Each point was made up of the average of 4096 ADC samples sampling at a rate of about 300 000 samples per second.

This test lacks the distinct jumps seen in Figure 11-8 as the distance was varied by 1mm at a time. The only other difference for this test was that only 50 points were sampled per distance therefore the 2500 samples represent a 50mm total change in distance. The general trend in this test is as expected with the 1.2 ADC units per millimetre expected slope observable. There are some large inaccuracies between samples 750 and 1500 (15 and 30mm) and this is discussed in the 'Focus irregularities discussion'. There is also an inaccuracy where the ADC seems to return '127' a lot more than should be statistically possible. This was thought to be a fault of the ADC built into the Arduino microcontroller and seemed to be a lot more prominent when operating at very high sample rates.

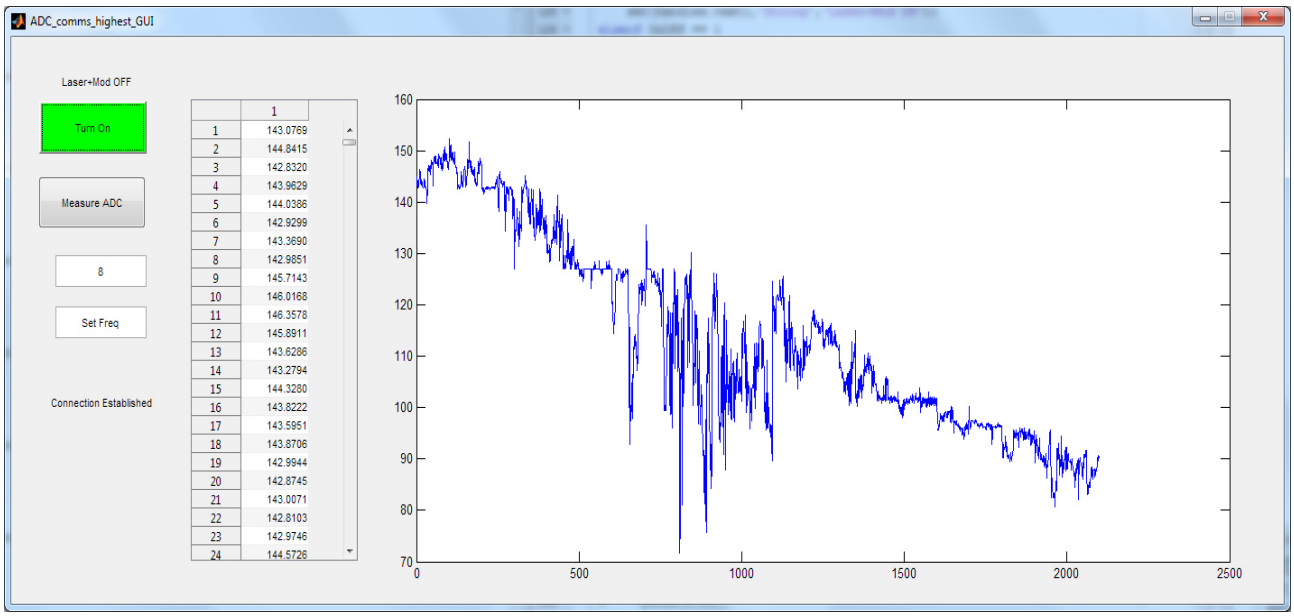

Figure 11-10. Showing initial testing results when moving the reflector 1mm at a time away from laser.

Figure 11-10 shows the results for the third test. This test was conducted in the same way as the second test, shown in Figure 11-9, but the reflector was moved away from the laser. Similar results were observed for both these tests although the expected negative slope in this test is obvious. This indicates that the system can measure distance changes in both directions as expected and further tests were only performed in a single direction.

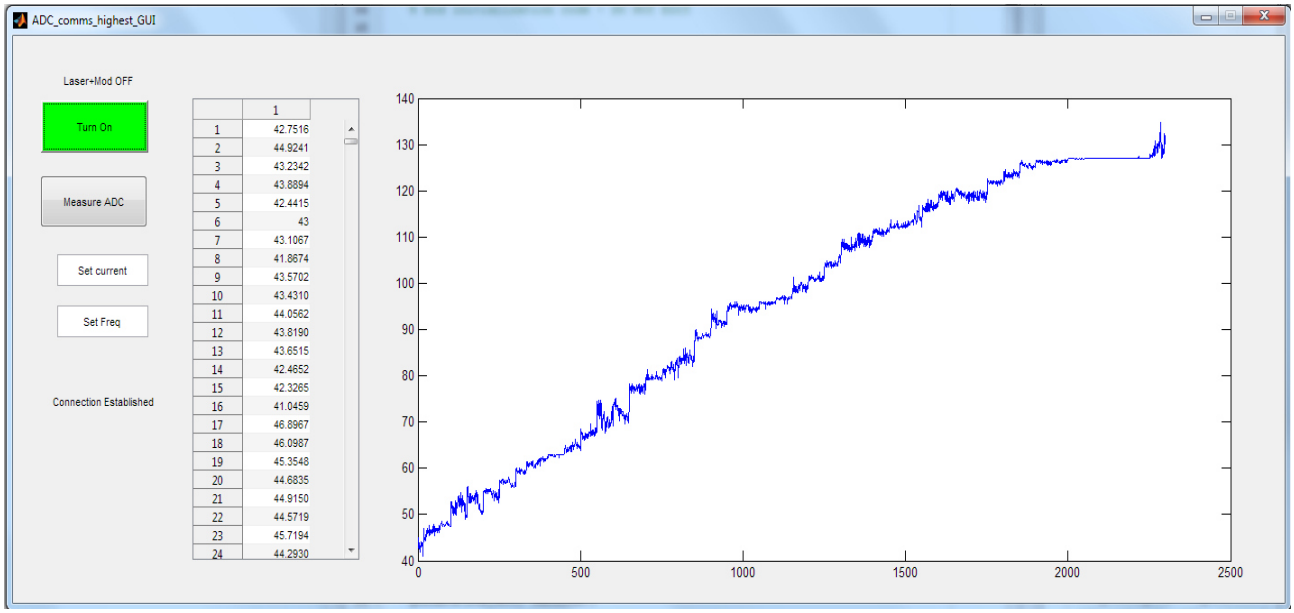

Figure 11-11. Showing initial testing results when moving the reflector 1mm at a time without focusing lens.

Figure 11-11 shows the results for the fourth test. This test was conducted under the same test conditions as the second test, shown in Figure 11-9, but the focusing lens was removed (the absolute distance of the reflector was also slightly further from the lens as can be seen by the lower ADC/vertical values). This eliminated the irregularities in the distance measurement and gave some indication that these irregularities arose when the laser was well focused as discussed in 'Focus irregularities discussion'. The '127 discontinuity' is also present in this measurement.

This initial testing proved that the system should work although some irregularities need to be accounted for and for detailed analysis to be performed. It was also found that moving the reflector by hand was tedious and presented the opportunity for human error. Further testing, designed to test specific parameters using an automated test platform, was conducted and can be seen below.

11.2.2 Final distance measurement testing

After the initial testing shown above further testing that was focused on specific areas and settings was performed. The test bed used in the initial tests was changed to the gantry system set up in such a way as to move the reflector towards and away from the laser (this had been constructed and tested previously and shown in chapter 5 'Mechanical Design'). This also allowed tests to be repeated as often as needed with certain settings changed on different iterations of the test. During this final testing, it was also decided to include a standard deviation plot alongside the results in order to determine the accuracy of each individual measurement (each measurement is an average of a number of ADC samples). During these results, take note that the scaling on all plots is automatic and varies considerably. The ADC values, when used in 10-bit mode, only include the lower 8 bits giving an unambiguous range of 1.25V; in some tests, where the results spanned two of these ranges but did not have a total span of greater than 1.25V, a constant was added to the lower readings for graphic clarity and this is discussed in 'Analogue to digital converter' below.

i. Magnitude output testing

The initial testing above proved that there was phase shift between the signals proportional to the distance but did not test the magnitude ratio of the two signals. Although the magnitude of the signals should not influence their phase considerably and it is therefore not required in a design such as this; the AD8302 provides a magnitude output and this was included in the circuitry. The magnitude of the reference signal was constant and set at 16.3mV$_{pp}$ (or -26dBm) as shown in 'Reference Signal Conditioning' on page 74. The AD8302 produces an output of 30mV/dB, which is then multiplied by a factor of 2.4 by the TLV2372 to produce an output of 72mV/dB and a midpoint of 2.16V (see Equation 8-5 and Equation 8-6). It should be noted that these equations predict an output proportional to power and because the reference signal is input-A the higher the received signal the lower the magnitude output.

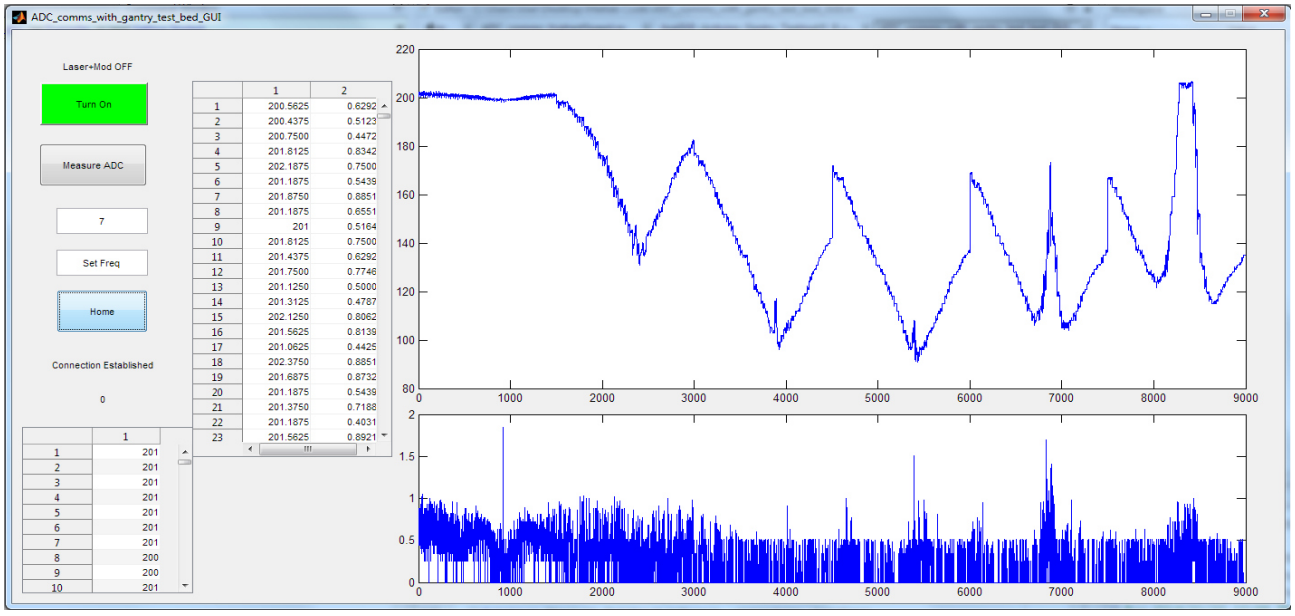

Figure 11-12. Showing magnitude testing results with the laser set at various current levels.

Figure 11-12 shows the results for the magnitude test. The horizontal axis shows the reading number and the vertical axis shows the averaged 8-bit ADC value. In this test, the modulation frequency was set at 102MHz. The reflector was moved 1mm at a time, and 25 points were sampled at each distance. Each point was made up of the average of 10 ADC samples sampling at a rate of about 300 000 samples per second. The reflector was moved over a distance of 60mm (with 25 points per mm) yielding 1500 points for the full distance covered. This test was carried out six times each with a different DC current in order to test the modulation depth at different DC currents.

In the first test (0 to 1500 points on the horizontal axis), the DC current was set at 0.25A. It can be seen that there is very little change in the magnitude ratio with the ADC value at about 205. This corresponds to a voltage of 4V and a magnitude ratio of -25.8dB which when added to the reference signal gives a received signal magnitude of -51.8dBm. This is the noise floor that is being sensed and is therefore expected not to show a change when the reflector is moved.

In the second test (1500 to 3000 points on the horizontal axis), the DC current was set at 0.4A. It can be seen the signal starts at an ADC value of about 200 that then drops to about 140 before rising again to 180. This indicated that when the measurement started the signal was still within the noise floor but as the reflector was moved toward the laser the signal strength increased as expected. The signal strength reached a maximum at the laser's focal point, as this was also the point at which the reflected

laser beam was focused onto the photo sensor. It then dropped off as the reflector moved past the focal point. The lowest point corresponds to a voltage of 2.8V, which gives a received signal magnitude of -34dBm.

In the third test (3000 to 4500 points on the horizontal axis), the DC current was set at 0.6A. It can be seen that the signal starts at an ADC value of about 180 that then drops to about 100 before rising again to 140 (the vertical jump at 4500 is due to the reflector position being reset and test four starting). The value starts below the noise floor and changes linearly with distance. The small peak that is present at about 3900 on the horizontal axis is due to there being a slight burn in the reflector, meaning that when the laser is well focused on the burn less light is reflected.

In the fourth test, a DC current of 0.8A was set and the results were very similar to the third although shifted down by about 10 ADC divisions indicating a slightly stronger signal. The maximum signal strength reached was 90 on the ADC; this corresponds to a received signal magnitude of -20.5dBm.

In the fifth and sixth tests, DC currents of 1A and 1.15A were set respectively. These tests show similar signal strengths to the forth test but also show much larger peaks in the focal point. This was because at these higher DC current settings the laser was able to burn the reflector when focused and hence did not reflect much signal.

The standard deviation plot shows that the standard deviation is normally below one unit, this is as expected when running the ADC in 8-bit mode. Slightly higher standard deviations were recorded during the first two tests due to the lower signal strength as well as during the peaks that were associated with the laser burning the reflector.

This test determined that for the best phase shift results a current of 0.8A should be used. This was used for all further tests unless otherwise noted.

ii. Effects of frequency

Both the laser driver circuitry and the photodetector circuitry were designed to operate at frequencies from 30MHz to 120MHz. The frequency generator could be commanded to generate frequencies within this range at about 10MHz apart. A higher frequency is expected to yield more phase shift for a similar change in distance. Equation 2-7 and Equation 8-4 predict that the phase shift should be linear for a linear change in distance and that the rate of change of phase should increase proportionally to frequency. Absolute phase shift is not important, as there are unpredictable sources of phase shift in both circuits. In the complete laser cutter, the system would need to calibrate itself with a known distance or be programmed in such a way that it only ever needs relative distance.

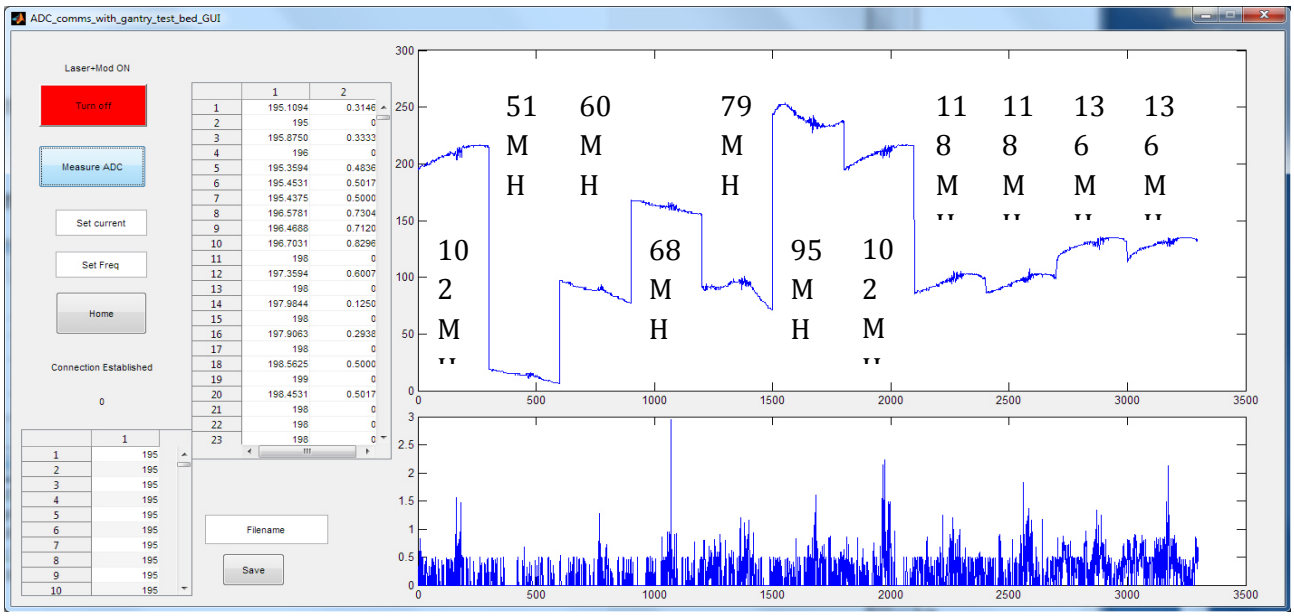

Figure 11-13. Showing frequency testing results with the phase output monitored at various frequencies.

Figure 11-13 shows the results for the frequency test. In the frequency test the phase output was monitored by the Arduino ADC running in 8-bit mode at 300 000 samples per second. The reflector was moved 1mm at a time with 5 points being measured at each distance; each of these 5 points was made up of an average of 64 samples. The reflector was moved over a distance of 60mm with the focal distance at about the centre of this range.

In Figure 11-13 eleven distinct regions can be seen, each of these was the same test as described above but with different frequencies. The frequencies were set as closely to 10MHz apart at possible and the frequency used for each part of the test can be seen in Figure 11-13.

The phase output of the tests with frequencies below 100MHz show a downward trend while for frequencies above 100MHz the phase output shows an upward trend. This is because phase shift within the circuitry is frequency dependant; at lower frequency settings the optical signal seems to be leading the reference signal while at others the optical signal seems to be lagging the reference signal. This does not pose a problem in determining the direction of distance change as the frequency selected for implementation would have a constant phase shift and it will be known if this is found to be a leading or lagging signal. The AD8302 is inaccurate at phase shifts that are multiples of 180°; this seems to have caused some distortion for the 95MHz test as the high voltage indicates 0° phase shift.

The expected and measured change in ADC units for each of the frequencies shown in Figure 11-13 is given in Table 11-2. From this table (and the figure), it can be seen that as frequency increases the slope of the phase output also changes. This slope did not seem to be particularly accurate for all readings but it is thought that this would be improved with repeated testing and averaging. The measured change at 95MHz is nearly half of the expected change; this is due to the 0° phase shift mentioned above.

Table 11-2. Showing the expected and measured change in ADC units for different frequencies

Frequency (MHz)	Expected change (ADC units)	Measured change (ADC units)
51	9	11
60	10.6	12
68	11.99	12
79	13.92	17
95	16.74	9
102	17.98	19, 17
118	20.80	21, 18
136	23.97	20, 21

The expected change in ADC units was calculated with the following equation:

$$\boldsymbol{Expected\ Change} = \frac{\frac{2*360*f*l}{c}*10*G_{TLV}}{\frac{V_+}{n}} = \frac{\frac{2*360*f*60*10^{-3}}{300*10^6}*10*2.4}{\frac{5}{256}} \qquad \textbf{Equation 11-1}$$

where f is the frequency (Hz)

l is the distance moved in m (=0.060m)

c is the speed of light in ms^{-1} (=$299.8*10^6$ ms^{-1})

$\boldsymbol{G_{TLV}}$ is the TLV2372 gain (=2.4v/v)

$\boldsymbol{V_+}$ is the ADC supply voltage in volts (=5v)

n is the number of ADC points (2^8 = 256)

The inaccuracies caused by the focusing of the laser are also visible in the frequency testing at all frequencies, although this seems to have less of an effect on the lower frequency signals. The standard deviation is normally below 1 unit as expected in 8-bit operation with peaks corresponding to the focused laser inaccuracies as before.

iii. Range

The range of the system was designed to be 50mm and this is easily met as most other testing was normally performed over a range that was either 60 or 55mm. Nevertheless, it was decided that the range in which the distance measurement is accurate would be tested. Figure 11-14 shows the phase and magnitude output of this test in blue and red respectively. The beam diameter range is not within the focal constraints set out in the specifications but this was ignored and the test performed for completeness as the range tested includes the cutting range within which the focal constraints are met.

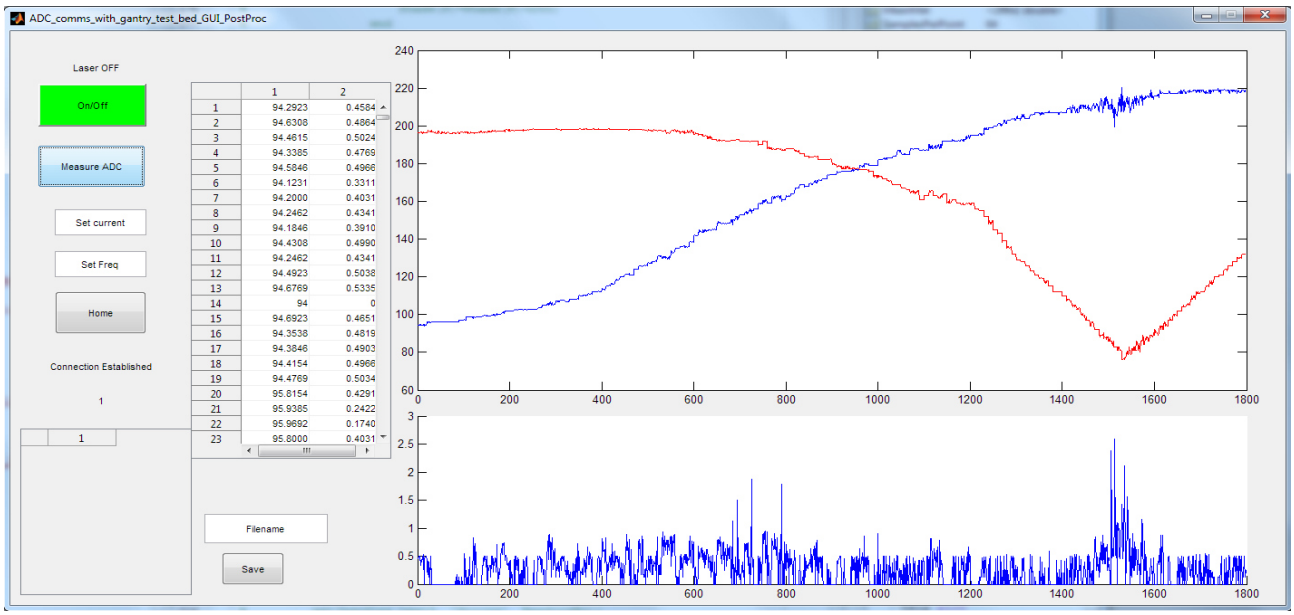

Figure 11-14. Showing the phase (blue) and magnitude (red) output of the range test.

The range test was carried out at a frequency of 102MHz and a DC offset current of 0.8A. The ADC sampled the outputs in 8-bit mode running at 152 000 samples per second. 64 samples were averaged for each reading and 10 readings were taken for each distance. The reflector was moved 1mm at a time. The reflector was moved over a range of 180mm, from 190mm to 10mm from the focusing lens.

The magnitude plot gives a good indication of the expected accuracy of the phase shift. While the magnitude output is at about 200, the signal is swamped by noise and therefore the phase output is unreliable. This occurs from reading numbers 0 to 600 (190 to 130mm). After this the magnitude output begins to drop off indicating that the reflected optical signal is beginning to become evident above the noise and the phase shift signal begins to become more reliable. After 800 readings (110mm) the received signal has a magnitude of -45dBm, it is thought that this is the point at which the phase shift signal becomes more reliable although the trend does seem to develop at about 400 readings (160mm) from the lens.

This tests shows that the system is able to measure distances over a range of at least 100mm and at most 150mm. This is twice as far as set out in the 'Design Specification'.

Interestingly in this test when the focal point was reached. Between 1500 and 1600 on the horizontal axis, there is no spike on the magnitude plot but similar focal point irregularities are observed in the phase plot. This is discussed further in 'Focus irregularities discussion'.

iv. Accuracy and precision

The Oxford English Dictionary defines *accuracy* as "the degree to which the result of a measurement conforms to the correct value" and *precision* as "the reproducibility or reliability of a measurement or numerical result" [87]. For this system, the accuracy is the difference between the distance measured and the correct value is the distance moved; whereas the precision is the reproducibility of individual measurements and is expressed by the standard deviation of that individual measurement.

The specification requires a system that is accurate to 1mm. Figure 11-15 and Figure 11-16 show two tests that were performed in order to ascertain the accuracy and resolution of this system. These are discussed below.

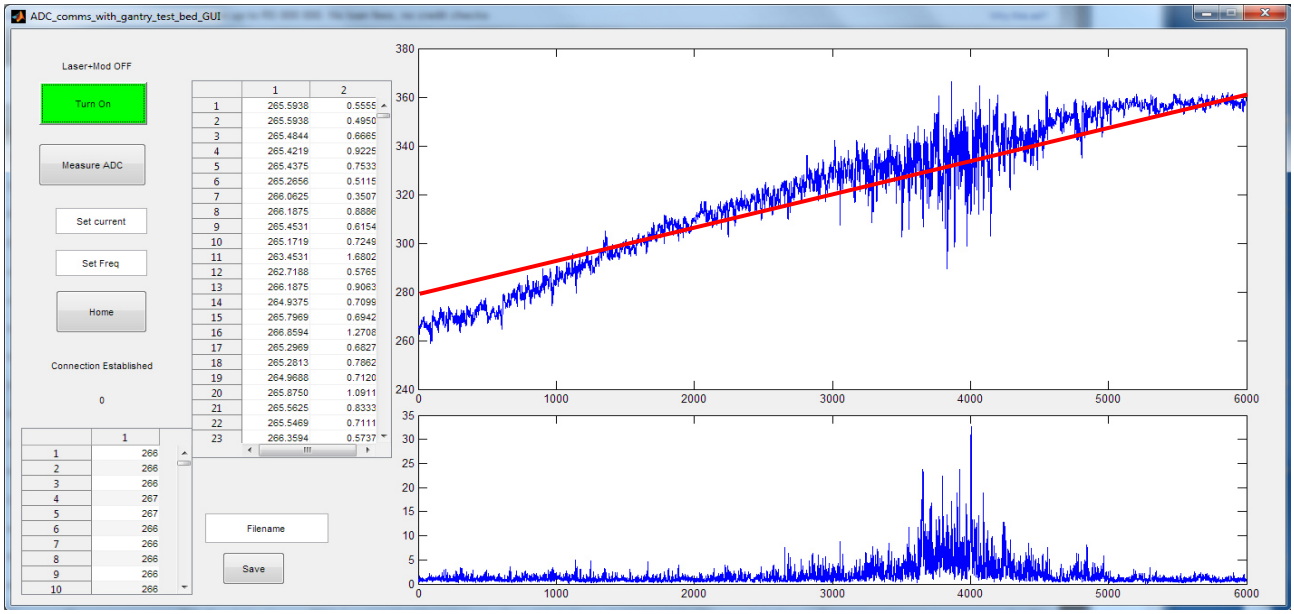

Figure 11-15. Showing the phase shift measured at 0.1mm increments.

Figure 11-15 shows the results for the accuracy test. The horizontal axis shows the reading number and the vertical axis shows the averaged 10-bit ADC value. In this test, the modulation frequency was set at 102MHz. The reflector was moved 0.1mm at a time, and 10 points were sampled at each distance. Each point was made up of the average of 64 ADC samples sampling at a rate of about 9 000 samples per second. The reflector was moved over a distance of 60mm (with 10 points per mm) yielding 6000 points for the full distance covered. Note a scaling factor was added to some points as the ADC values spanned two 1.25V ranges, see 'Analogue to digital converter'.

In Figure 11-15 the red line shows the expected phase shift values and the blue plot shows the measured values. It can be seen that the measured results generally follow the expected phase shift trend but do not form a completely straight line. The error on the further distances (lower horizontal numbers) is about 11 ADC units, which corresponds to an error of about 9mm. After 10mm (1000 on the horizontal axis), the maximum error is measured at 30mm (3000 on the horizontal axis) where it is about 6 ADC units or an error of 5mm.

The standard deviation for most of the readings is less than 4 ADC-units. This is expected when operating in 10-bit mode and indicates less than 20mV jitter on this signal. A small jitter is desirable as this allows ADC oversampling techniques to be used.

The focal point irregularities are still present in this plot although if these were to be averaged over a longer period the accuracy would remain within the 5mm band. The optical irregularity is also present in the standard deviation plot where it reaches a maximum of 30 ADC units, corresponding to 25mm, deviation within one measurement. This indicates that the focal point irregularity causes large variations, or noise, on the phase output signals. Each point takes 7.1ms to measure all 64 points and in order for this measurement to include such large deviations, the frequency of this noise must be higher than 0.5kHz. Longer sampling periods where more samples are averaged will yield better results, both in accuracy and resolution, at the expense of time and processing power.

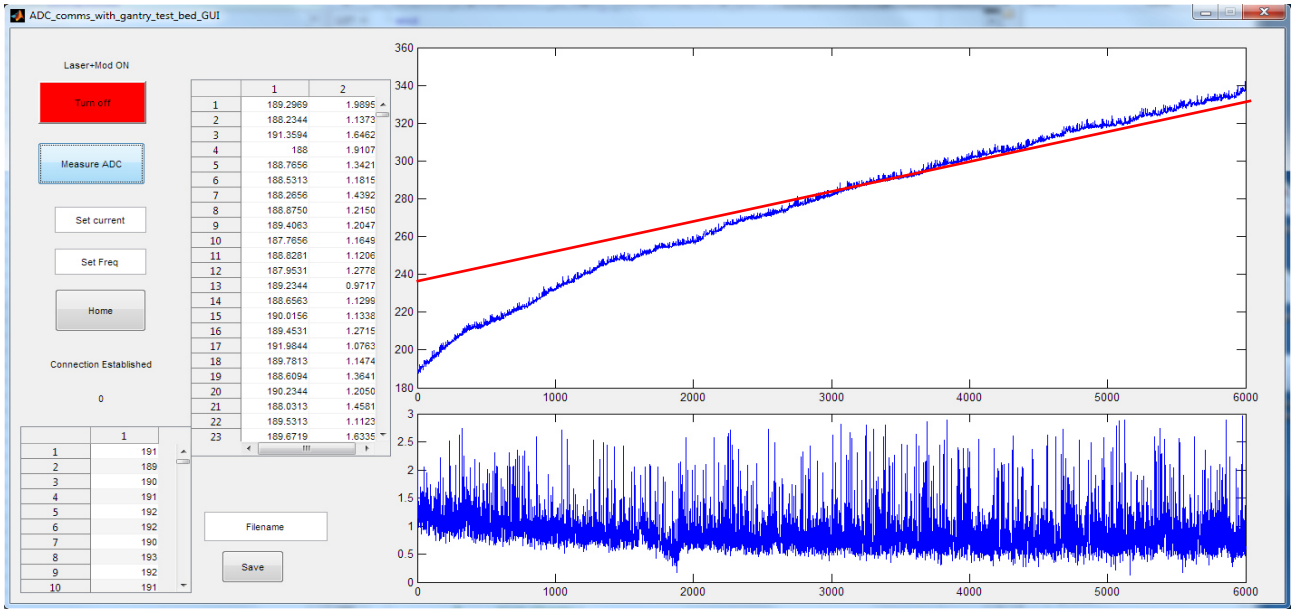

Figure 11-16. Showing the phase shift measured at 0.1mm increments without the focusing lens.

Figure 11-16 was acquired under the same test conditions as Figure 11-15 but the focusing lens was removed in order to remove the focusing irregularities and a modulation frequency of 118MHz was set. Again, the red line shows the expected results where the blue plot shows the measured results. It can be seen that the results from about 45mm to 10mm from the laser (1500 to 6000 on the horizontal axis) are within 5mm of the expected value, while the phase shift measured at lower frequencies is less accurate.

The focusing irregularities are eliminated in this plot and the precision of each measurement is consistent for different distances. This is also evident when looking at the standard deviation plot where the standard deviation of each point (made up of 10 averaged ADC samples) is never greater than 3 ADC units.

v. White paper

All the above distance measurement tests were carried out using a piece of reflective tape as the target or 'reflector'. This provided a much larger reflected optical signal for the photo sensor circuitry to detect. It was decided to test whether the system would be able to make accurate distance measurements with the target being a piece of white paper. White paper would reflect less light and therefore the magnitude of the received signal would be smaller. A single test was carried out, shown in Figure 11-17, and from this, it was evident that the gain of the photo sensor would need to be increased in order to detect a weaker signal. A further test can be seen in Figure 11-18 in which the gain was increased by 12dB.

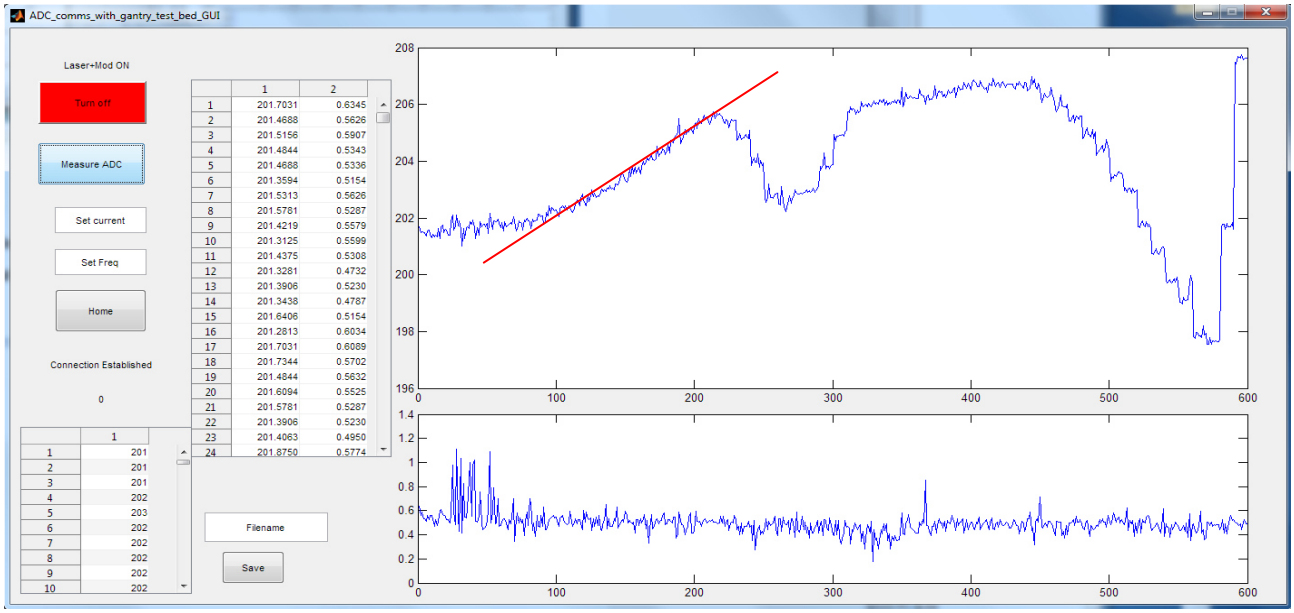

Figure 11-17. Showing initial white paper test.

Figure 11-17 shows the results for the initial white paper test. The horizontal axis shows the reading number and the vertical axis shows the averaged 8-bit ADC value. In this test, the modulation frequency was set at 102MHz. The reflector was moved 1mm at a time, and 10 points were sampled at each distance. Each point was made up of the average of 64 ADC samples sampling at a rate of about 150 000 samples per second. The white paper was moved over a distance of 60mm (with 10 points per mm) yielding 600 points for the full distance covered.

In the initial white paper test, it can be seen that the distance measurement shows very little correlation to the actual distance except for the region between 55 to 42mm from the focusing lens (100 to 230 on the horizontal axis). The expected slope of 3 ADC units per 10mm when using an 8 bit ADC is indicated in red and the plot shows that this is followed closely for this region. The amplitude of the signal was measured to be a maximum of -40dBm and this corresponded to 42mm from the focusing lens (230 on the horizontal axis). The signal was below the noise floor, at -47dBm, for readings outside this range. The large dip in the plot between 42 and 35 (230 to 300 on the horizontal axis) is thought to be due to the focusing irregularities but may also be caused by the misalignment of the photo sensor.

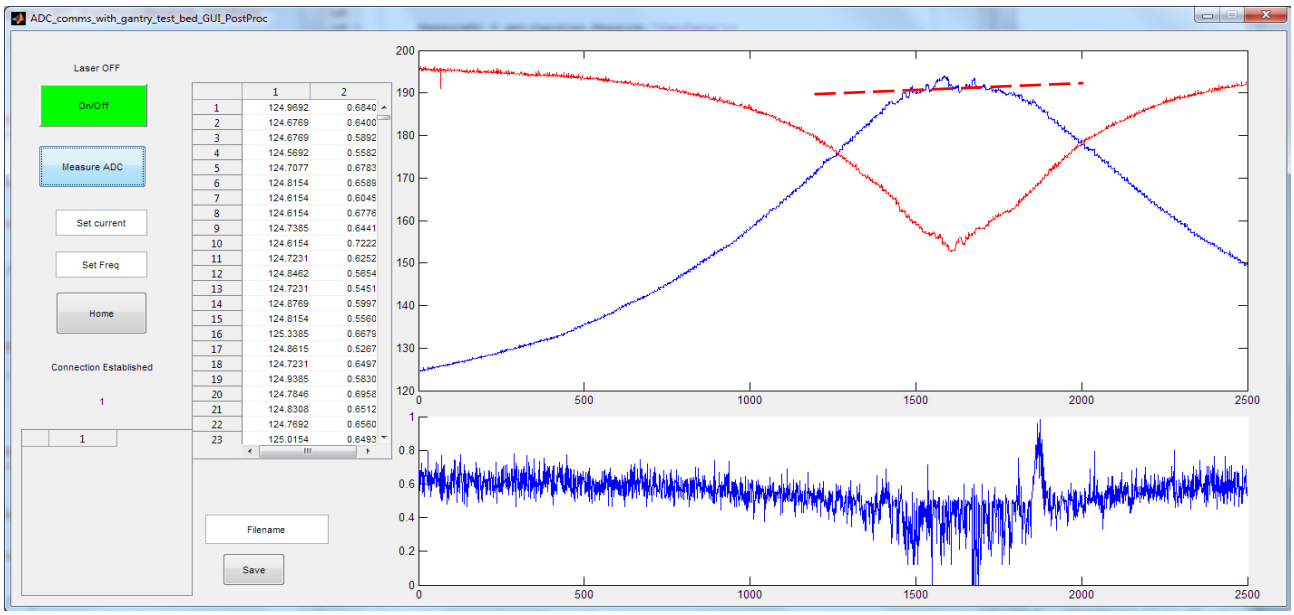

Figure 11-18. Showing white paper test with increased gain.

Figure 11-18 shows the results for the second white paper test after the gain of the photo sensor circuit was increased by 12dB. The horizontal axis shows the reading number and the vertical axis shows the averaged 8-bit ADC value. The blue plot is the phase output and the red plot is the magnitude output. The standard deviation plot is derived from the phase plot. In this test, the modulation frequency was set at 102MHz and the DC offset current at 0.8A. The white paper was moved 0.1mm at a time, and 10 points were sampled at each distance. Each point was made up of the average of 64 ADC samples sampling at a rate of about 150 000 samples per second. The white paper was moved over a distance of 25mm (with 10 points per mm) yielding 2500 points for the full distance covered.

In the second white paper test, both the phase (blue) and magnitude (red) plots were recorded. The dotted red line shows the expected phase output. The phase output shows the expected trend only for a very small portion of the measurement 1500 to 1750 on the horizontal axis, this is a 2.5mm range. This does correlate to the magnitude plot, which shows the highest received signal magnitude during this range. The magnitude plot indicates a maximum signal of -38dBm and this was verified by an oscilloscope, which measured a maximum signal of -37dBm. This signal is almost within the noise floor (which was now at -45dBm after the gain adjustment).

11.2.3 Notes on distance measurements

The following notes apply to the measurements done when doing the distance measurement tests. They affect most of the tests performed and it was thus decided to include them in a separate section.

i. Reflector

All the tests, except the white paper tests, were performed using a piece of reflective tape as the target. This produced a much larger optical signal for the photo sensor circuitry to detect and thus allow the distance measurements to be more accurate. This does not affect the theory of operation of the distance measurement circuitry other than requiring lower gains on the photo sensor signal path. A photograph of this reflective tape can be seen in Figure 11-19.

ii. Analogue to digital converter

The ADC used was the ADC built into the ATmega2560 microcontroller. This is a 16 channel, 10-bit ADC with a sample rate of up to 1 mega-sample per second for 8-bit accuracy (or 200 kilo-samples per second for 10-bit accuracy). It has an analogue input range of 0-5V.

10-bit mode

When the ADC was used in 10-bit mode, only the lower 8 bits were read. This allowed for faster processing and data transfer but meant that an unambiguous voltage range of only 1.25V was present after which the result would roll over back to zero. In some of the tests performed, the measured voltage range was less than 1.25V but spanned two unambiguous regions causing a sudden jump in the plots. In these cases, a fixed constant was added to values below that constant in order to provide a clean plot for analysis. This affects the values of the ADC but not the slope or relative change in measurements that this system would use.

Oversampling

In all the above tests, oversampling techniques were used. "By using a method called Oversampling higher resolution might be achieved, without using an external ADC." [88, p. 1]. The increased resolution is predicted by Equation 11-2. High frequency noise greater than 0.5 least significant bits is required in order to toggle this bit. "Noise amplitude of 1-2 LSB is even better because this will ensure that several samples do not end up getting the same value." [88, p. 3].

$$\boldsymbol{Number\ of\ extra\ samples = 4^n} \qquad \textbf{Equation 11-2}$$

Where n is the number of extra bits of resolution achieved. For example if 64 10-bit samples are averaged, the output (if jitter requirements are met) is accurate to 13-bits

The over sampling techniques served more as a high frequency filter than to increase the resolution of individual samples as the average over a longer time period was taken. In most cases, the resolution of the analogue signal sampled was lower than the resolution added by oversampling although some resolution was added. The over sampling also allowed standard deviations for each measurement to be calculated and this provided an indication of the higher frequency noise levels present on the analogue signals as well as the reliability of the measurement. The standard deviation also provided an indication of errors in the serial communications between the microcontroller and PC; this was evident when one or two random points had extremely large standard deviations.

Sample speed

The sample speed of the ADC is controlled by a prescaler, which divides the 16MHz ATmega2560 clock frequency. 13.5 of these divided clock cycles are need for one ADC conversion. For example for a prescaler of 128 the sample frequency will equal (16000000/13.5)/128 = 9.26 kilo-samples per second.

127 discontinuity

In Figure 11-9 to Figure 11-11 a slight discontinuity at 127 can be seen. In these tests, the ADC was operated in 10-bit mode, at 300 kilo-samples per second. This is above the recommended 200 kilo-samples per second that is specified in the datasheet and it is thought that this is the reason for the discontinuity. After these tests, it was decided to operate the ADC at half the speed when using 10-bit mode and this prevented future errors.

11.2.4 *Focus irregularities discussion*

During testing, there were often irregularities observed in the phase output and these were thought to arise from three possible causes. These are burning of the reflector, alignment of the optics and the possibility of reflections back and forth between the laser and reflector that could cause some sort of resonance and hence erroneous phase shift. These three irregularity sources are discussed here.

i. Reflector burning

It was observed that during some tests, the laser would burn the reflector, this would reduce its reflectivity and hence the ability of the photo sensor circuitry and AD8302 to perform the required phase shift measurements. The effects of burning on the magnitude of the received signal can be clearly seen in Figure 11-2 where, at higher currents, the magnitude output was not consistent when the laser was focused on the reflector. The increasing effect of this as current (and hence laser power) was increased and physical observations (seen in Figure 11-19) proved that reflector burning was a source of focus irregularities. This would not pose a problem if this system was sensitive enough to detect signals reflected from objects that were being cut.

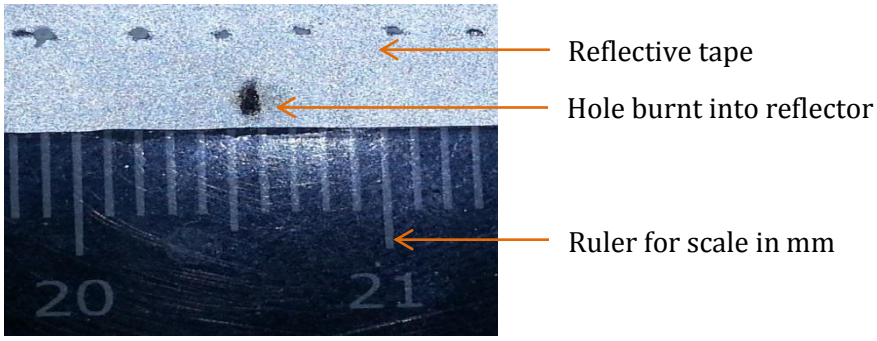

Figure 11-19. Showing reflector burning that was observed during 'Magnitude output testing'.

ii. Optics alignment

The SFH2701 photodiode and the photo sensor PCB as a whole were positioned in such a way that the reflected light would be focused onto the photodiode by the focusing lens when the laser was focused onto the workpiece. This would allow for the maximum range. As the reflector moved toward the laser's focal point the reflected light that is projected onto the photo sensor PCB becomes more focused (and less focused as the reflector is moved away from the focal point). It is thought that the photodiode was not perfectly aligned during some tests and that when the area illuminated by the reflected laser on the photo sensor PCB was focused to a small point the photodiode was no longer in the laser path (when the area illuminated by the reflected laser was larger, or unfocused, the photodiode was within this now larger projected area. Figure 11-20 illustrates how the photodiode can be illuminated when the reflector is not at the focal point but is not illuminated when the laser is at the focal point. Also, notice the elliptical beam profile with the major axis changing from vertical to horizontal due to optical aberrations.

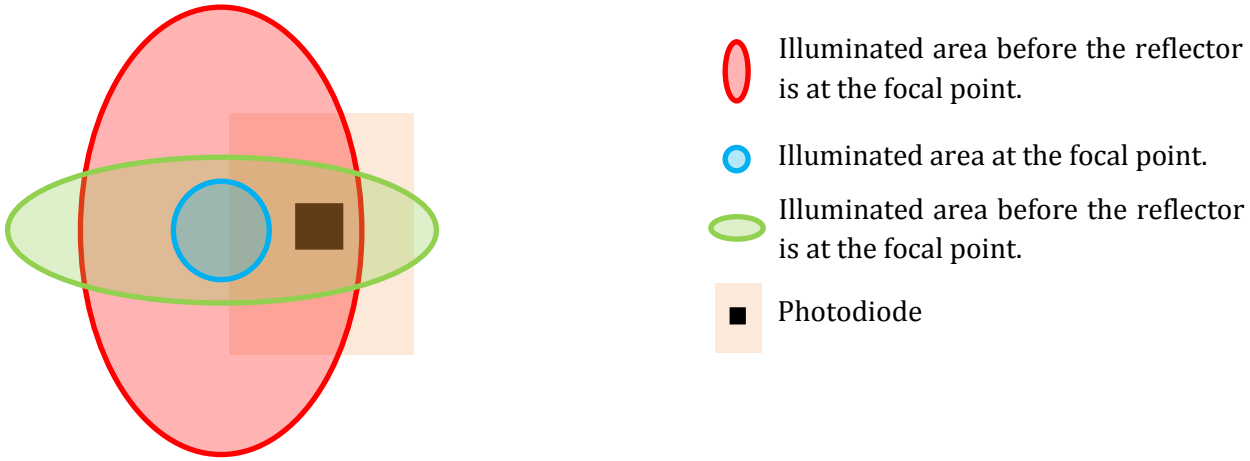

Figure 11-20. Showing the areas of illumination at different focuses.

iii. Reflections into laser cavity

The laser cavity has a mirror on either end with the mirror on the far end (of the cavity from the reflector) being nearly 100% reflective. If light is reflected from the reflector back through the lenses and into the laser cavity this may interfere with the lasing process (causing irregularities in the output signal), or be reflected by the mirror back onto the reflector. This reflection process could continue indefinitely with the distance travelled by the light increasing each time and hence the phase shift increasing. This light will combine with newly emitted light and this mixture of signals would reach the photodiode and eventually the AD8302, which would not be able to detect a consistent phase shift. This process was not well understood by the author and research into it was not part of the scope of the project.

12. Conclusions

During the course of this project the concept of building a three-dimensional laser cutter, using phase shift detection to measure the depth of cut, was proved possible.

An accurate gantry system was constructed that was able to move the laser cutting toolhead in an x-y plane to within 0.1mm and at speeds above 0.15m/s. This accuracy and speed was above that of the accuracy and cutting speed of the laser cutting toolhead and is thought to be satisfactory for future concept work.

Optics were designed and constructed in order to collimate and focus the laser onto the workpiece. The reflected light was then focused onto a photodiode using the same lens that focused the outgoing laser and a partial reflector. The optics performed as expected but the inaccuracies encountered in machining and the inability to measure the laser beam width reliably coupled with the small spaces and tolerances of diode laser optics proved to restrict the optics slightly.

Laser driver circuitry was designed that was able to drive a 3W laser diode and modulate it at 100MHz. The modulation depth achieved was ±334mA, enough to generate a considerable variation in the output power of the laser. The laser driver circuitry also provided a reference signal in order to measure phase shift. This circuit performed well although more modulation depth would have allowed for less sensitive detection circuitry. The major hindrance in achieving larger modulation depths was the inductance in the 1cm leads used to connect the laser. In future work these should be shortened or eliminated.

Photo sensor and phase detector circuitry was designed and built in order sense the received signal reflected off the workpiece. This signal was then compared to the reference signal in order to measure the phase shift between and magnitude ratio of the two signals. The change in phase shift was used to indicate the change in distance to the workpiece. This proved to be possible and results that were somewhat consistent with expectations were acquired. This was not as accurate as had been hoped for but could be improved if more sensitive and noise immune photo sensor circuitry is built.

An Atmel ATmega2560 microcontroller (Arduino) was used to control all the hardware during various stages of testing. Software running in MATLAB, on a PC, was used to communicate with and control the Arduino as well as to log data and results. This microcontroller had sufficient processing power and peripherals for this project and performed well overall.

The hardware and software of the laser cutter performed well enough to prove the concept but not at the level needed to build a functioning product. An improvement of all the different aspects would be needed in future designs. Major aspects to work on would be the photo sensor circuitry and the optics.

In conclusion, the system had an acceptable level of performance for the requirements of this project. Issues were encountered with modulation depth, photo sensor sensitivity, laser power and optical accuracies but these issues could however be significantly improved by implementing some of the recommendations suggested in the following chapter. Much work and research would still need to be done on this type of laser cutter to take it into a fully-fledged and useful tool found on design engineers' desks and eventually in industry.

13. Recommendations

A number of changes and improvements could be made to this laser cutter were it to be researched further.

Use a more powerful laser

The laser used was not powerful enough to cut most materials. 2W lasers were the most powerful commercially available lasers at the time this project was started but more powerful single emitter laser diodes have become available since.

Use different lasers for cutting and distance measurement

This would enable diode arrays or stacks to be used for cutting in order to achieve much higher material processing rates but smaller single emitters that can be modulated at the high frequencies required to be used for distance measurement.

Use fractional stepping stepper motor drivers

Using different stepper motor drivers that are able to perform fractional stepping would mean that the gantry system would be able to achieve finer step distances. This would also improve the speed of the motors as more effective acceleration routines could be used.

Increase 'z' axis range

This design was only intended to operate over a short cut depth but in order to produce a viable three-dimension laser cutter a greater cut depth range should be achieved. One way of increasing this is by focusing the laser at a longer range and hence a longer distance within the cutting width parameters. Another way would be by including some 'z' axis movement by raising and lowering either the workbed, toolhead or optics.

Increase the modulation depth

Increasing the modulation depth would mean that a larger signal will be reflected onto the photo sensor which will make the phase shift measurement more accurate. This could be done either by using more BUF602 ICs or by reducing the parasitic inductances of the wires connecting the laser to the laser driver PCB. Preferably the laser driver PCB should be arranged in such a way that the trace length from the buffers to the laser is minimised.

Increase modulation frequency

This would mean much higher distance measurement accuracies would be theoretically achievable as the phase shift for a set change in distance is proportional to the modulation frequency.

Improve the optics

The optics should be improved to allow more power to reach the workpiece but also optimise the reflected power reaching the photodiode. Using separate optics for the reflected beam should be reconsidered as focus irregularities could be omitted by using a different optical setup.

Implement a more sensitive photo sensor circuit

The photo sensor circuit could be improved in many ways both to increase the sensitivity and to decrease the noise. Tuning the system to a single frequency rather than having a range of possible frequencies will help to improve and simplify circuit design. It is recommended that future designs use a four layer PCB in order to improve circuit immunity to RF noise.

Use a dedicated two channel ADC

The use of a dedicated two channel ADC on the toolhead and preferably built onto the photo sensor board is recommended. This would improve the accuracy of the system, as any noise that is picked up on the long leads will be mitigated. It would also be possible to use an ADC with a lower analogue reference voltage that is just above 1.8V; this would remove the need for the TLV2372 operational amplifier. A 12-bit ADC could also be used to increase the accuracy without oversampling. This ADC would preferably communicate to the Arduino via the same IIC connection that the TLV5618 DAC is connected to (a connection between boards would have to be made) reducing the cable count to the toolhead.

Perform calibration routines

Calibration of the distance measurement circuitry will be necessary before each use. This could entail either a single point scaling or measuring the distance of a known profile. From the results obtained is clear that although the phase shift does is not perfectly linear it is repeatable. A lookup table created from a calibration profile could be implemented in software for much more accurate distance results.

Write software to control the laser cutter as a CNC machine

A lot of software needs to be written, for both the Arduino and PC, in order to allow the laser cutter to operate as a CNC machine. This would include software to calculate tool paths, calibrations, measurement frequencies etc. and then software on the Arduino to interpret all the commands commonly supported by CNC machines.

14. List of References

List of References

[1] J. C. Ion, Laser Processing of engineering materials, Oxford: Elsevier Butterworth-Heinemann, 2005.

[2] J. Hecht, The Laser Guidebook, 2nd Edition ed., McGraw-Hill, Inc., 1992.

[3] O. Dictionaries, Oxford Dictionary, Oxford: Oxford University Press, 2010.

[4] W. Koechner, Solid-State laser Engineering, Fifth Revised and Updated Edition ed., Springer, 1999.

[5] G. Brooker, "Introduction to Sensors for Ranging and Imaging," in *Introduction to Sensors for Ranging and Imaging*, Raleigh, SciTech Publishing Inc., 2009.

[6] T. H. Maiman, "Optical and Microwave-Optical Experiments in Ruby," *Physical Review Letters,* vol. 94, p. 564, 1960.

[7] J. Hecht, Understanding Lasers: An Entry-Level Guide, 3rd Edition ed., John Wiley and Sons, 2011.

[8] A. E. Siegman, Lasers, A. Kelly, Ed., Palo Alto: Miller/Scheier Associates, 1986.

[9] K. Boucke, "10.3 Diode Lasers," in *Tailored Light 2*, M. Prof. Dr. rer. nat. Reinhart Proprawe, Ed., Springer, 2011, p. 163.

[10] M. Physics, August 2012. [Online]. Available: http://www.miniphysics.com/2010/11/exciting-atom.html.

[11] E. Britannica, August 2012. [Online]. Available: http://www.britannica.com/EBchecked/topic/330874/laser.

[12] Laser2000, "Single Emitter Laser Diode F-Mount," Laser2000, [Online]. Available: http://www.laser2000.se/index.php?id=371924. [Accessed 12 12 2013].

[13] Coherent Inc., "1.6 mm Onyx MCCP High Power Array.," Coherent Inc., [Online]. Available: http://www.coherent.com/products/?1576/1-6-mm-Onyx-MCCP-High-Power-Array. [Accessed 12 12 2013].

[14] Jenoptik AG, "Bars & Single Emitters for High-Power Diode Lasers," Jenoptik AG, [Online]. Available: http://www.jenoptik.com/en-semiconductor-lasers. [Accessed 12 12 2013].

[15] Jenoptik AG, "Diode Laser Stacks & Assemblies," Jenoptik AG, [Online]. Available: http://www.jenoptik.com/en-laser-stack. [Accessed 12 12 2013].

[16] F. Bachmann, P. Loosen and R. Poprawe, High Power Laser Diodes, New York: Springer Science+Business Media, 2007.

[17] A. Instruments, "Single Emitter Diodes - Specification Sheet," 2012.

[18] J. c. Ion, Laser Processing Of Engineering Materials: Principles, Procedure And Industrial Application, Illistratuded ed., Butterworth-Heinemann, 2005.

[19] R. Wester, "Absorption of laser radiation," in *Tailored Light 2*, R. Poprawe, Ed., Springer, 2011, pp. Pages 15-16.

[20] L. I. o. America, August 2012. [Online]. Available: http://www.sintecoptronics.com/lasersafety.asp.

[21] Electrocorp, 4 September 2012. [Online]. Available: http://electrocorpairpurification.wordpress.com/2011/07/05/health-and-safety-concerns-laser-engraving-hazards/.

[22] Bofa, 5 September 2012. [Online]. Available: http://www.bofa.co.uk/LGACproblems.asp.

[23] U. o. Pensylvania, 9 September 2008. [Online]. Available: http://www.ehrs.upenn.edu/programs/laser/lasermanual/sect_xvii.html.

[24] F. I. U. -. S. K. Dua, "Laser Safety Manual," 2008.

[25] B. J. Neubert and W.-D. Scharfe, "Laser System Beam Characteristics, Metrology, and Standards," in *High Power Diode Lasers*, F. Bachmann, P. Loosen and R. Poprawe, Eds., New york, Springer, 2007, pp. 181-215.

[26] I. E. Commission, "IEC 60825-1, Safety of Laser Products," 2012.

[27] J. Byrnes, Unexploded Ordnance Detection and Mitigation, Springer, 2009.

[28] Alphas GmbH, "Infrared-to-Visible Converters, IR Laser Beam Visualizers, IR Detectors: IR-VIS Series," Alphas GmbH, [Online]. Available: http://www.alphalas.com/products/laser-diagnostic-tools/infrared-to-visible-converters-ir-laser-beam-visualizers-ir-detectors-ir-vis-series.html?gclid=CLH2l8yqqrsCFRLMtAod3kQAhg. [Accessed 12 12 2013].

[29] C. McFee, "An introduction to CCD operation," Mullard Space Science Laboratory, [Online]. Available: http://www.mssl.ucl.ac.uk/www_detector/optheory/ccdoperation.html. [Accessed 12 12 2013].

[30] Steven Winter Associates, The passive solar design and construction handbook, Canada: John Wiley & Sons, Inc, 1997.

[31] A. Mann, Infrared optics and zoom lenses, Second Edition ed., Washington: SPIE, 2009.

[32] Theil, "Introduction to the Aberrations of Optical Systems," Montanna State University, Bozeman, 1998.

[33] Thorlabs Inc., "355392-B," Thorlabs Inc, [Online]. Available: http://www.thorlabs.com/thorproduct.cfm?partnumber=355392-B. [Accessed 10 12 2013].

[34] R. Nave, "Coma," Hyperphysics, [Online]. Available: http://hyperphysics.phy-astr.gsu.edu/hbase/geoopt/coma.html. [Accessed 12 12 2013].

[35] "Sferische aberratie," Wikipedia, [Online]. Available: http://nl.wikipedia.org/wiki/Sferische_aberratie. [Accessed 12 12 2013].

[36] "Coma (optics)," Wikipedia, [Online]. Available: http://en.wikipedia.org/wiki/Coma_(optics). [Accessed 12 12 2013].

[37] OLYMPUS, "Common Optical Defects in Lens Systems (Aberrations)," OLYMPUS, [Online]. Available: http://www.olympusmicro.com/primer/lightandcolor/opticalaberrations.html. [Accessed 12 12 2013].

[38] R. M. A. V. P. Kai-Erik Peiponen, Optical Measurement Techniques: Innovations for Industry and the Life Sciences, Berlin: Springer-Verlag, 2009.

[39] Microsoft Corporation, Encarta Dictionary, Microsoft Corporation, 2012.

[40] Federation of American Scientists, "Continuous Wave Radar," Federation of American Scientists, [Online]. Available: http://www.fas.org/man/dod-101/navy/docs/es310/cwradar/cwradar.htm. [Accessed 31 1 2014].

[41] J. S. Parab, V. G. Shelake and R. K. Kamat, Exploring C for microcontrollers: a hands on approach, Dordrecht: Springer, 2007.

[42] Atmel Corporation , "ATMega2560," Atmel Corporation, San Jose, 2012.

[43] Freescale Semiconductor, "MCS08GT16A Data Sheet," 2006.

[44] ST Microelectronics, "The L297 Stepper Motor Controller," 2003.

[45] T. I. Incorporated, “DRV8818 : STEPPER MOTOR CONTROLLER IC,” Texas Instruments Incorporated, Dallas, 2013.

[46] S. Microelectronics, “L6208 : Dmos Driver For Bipolar Stepper Motor,” ST Microelectronics, 2003.

[47] S. Attaway, MATLAB : A practical introduction to programming and problem solving, Second Edition ed., Oxford: Butterworth-Heinemann, 2011.

[48] C. W. de Silva, Mechatronics : An Integrated Approach, Boca Raton: CRC Press, 2005.

[49] MathWorks, September 5 2011. [Online]. Available: http://www.mathworks.com/products/image/index_b.html?BB=1.

[50] S. G. Kochan, Programming in C : A complete intorduction to the C programming language, Third Edition ed., Sams Publishing, 2004.

[51] S. Ginsberg and R. Verinder, EEE3017W : Digital Electronics Course Notes, Cape Town: University of Cape Town : Department of Electrical Engineering, 2010.

[52] D. Shetty and R. A. Kolk, Mechatronics System Design, B. Barter, Ed., Boston: PWS Publishing Company, 1997.

[53] F. Cardarelli, Materials Handbook, Second edition ed., London: Springer-Varlag, 2000.

[54] MakerBot, “MakerBot products,” MakerBot, [Online]. Available: http://store.makerbot.com/. [Accessed 08 02 2014].

[55] voxeljet, “Systems,” voxeljet, [Online]. Available: http://www.voxeljet.de/en/systems/. [Accessed 08 02 2014].

[56] Wieser, “3D LASER MACHINE PROCESSING MACHINE FOR HIGH PRECISION,” Wieser, [Online]. Available: http://www.laserautomation-wieser.com/laser-machine/applications.html. [Accessed 09 02 2014].

[57] Haas Laser Technologies Inc., “Additional Laser Beam Delivery Components,” Haas Laser Technologies Inc., [Online]. Available: http://www.haaslti.com/laser-components/robotic-end-effector.html. [Accessed 08 02 2014].

[58] O. O. S. GmbH, “Laser Diode on Submount 2.0 W cw (C-Mount),” OSRAM Opto Semiconductors GmbH, Regensburg, 2010.

[59] C. W. d. Silva, Mechatronics : An Integrated Approach, Boca Raton, Florida: CRC Press, 2005.

[60] S. Holzner, Physics for Dummies, Hoboken, NJ: Wiley Publishing Inc., 2006.

[61] Mantech Electronics, September 2011. [Online]. Available: http://www.mantech.co.za/Stock.aspx?Query=stepper+motorand.

[62] C. F. M. Co., “1.8°Size 42mm High Torque Hybrid Stepping Motor,” Changzhou Fulling Motor Co., 2012. [Online]. Available: http://www.fullingmotor.com/en/ProductShow.asp?ID=246. [Accessed 05 12 2013].

[63] L. S. P. Frank L. Pedrotti, Introduction to optics, Prentice-Hall International, 1993.

[64] H. Sun, Laser Diode Beam Basics, Manipulations And Characterizations, Dordrecht: Springer, 2012.

[65] E. M. W. Masud Mansuripur, “The Optics of Semiconductor Diode Lasers,” *Optics and Photonics News,* vol. July, no. 1, pp. 57 - 61, 2002.

[66] M. J. Kidger, Intermediate Optical Design, Bellingham, WA. USA: SPEI - The International Society for Optical Engineering, 2004.

[67] P. D. A. J. J. Joseph Braat, “Diffractive read-out of optical discs,” Eindhoven, The Netherlands.

[68] Thorlabs, “Anamorphic Prism Pairs,” Thorlabs, [Online]. Available:

http://www.thorlabs.com/newGroupPage9.cfm?objectGroup_id=149. [Accessed 11 12 2013].

[69] United Detector Technology Inc., "Characteristics and Use of Photodiodes," United Detector Technology Inc., Santa Monica, CA. USA.

[70] M. M. H. e. al., "Gain-Bandwidth Characteristics of Thin," *IEEE TRANSACTIONS ON ELECTRON DEVICES,* vol. 49, no. 5, pp. 770-778, 2002.

[71] OSI Optoelectronics, "Photodiode Characteristics," OSI Optoelectronics, Santa Monica, CA. USA.

[72] V. Telefunken, "BPW43, Silicon PIN Photodiode," Vishay Semiconductor GmbH, Heilbronn, Germany, 1999.

[73] O. O. Semiconductors, "High Speed PIN-Photodiode," OSRAM Opto Semiconductors GmbH, Regensburg, 2007.

[74] O. O. Semiconductor, "SFH2701, High Speed PIN Photodiode," OSRAM Opto Semiconductors GmbH, Regensburg, 2008.

[75] Osram Opto Semiconductor GmbH, "Laser Diode on Submount 2.0 W cw," Osram Opto Semiconductor GmbH, Regensburg, 2010.

[76] Texas Instruments Incorporated, "Fully-Integrated, Wide Range, Low-Jitter Crystal Oscillator Clock Generator," Texas Instruments Incorporated, Dallas,, 2012,.

[77] Texas Instruments, "Dual, Ultra-Wideband, Current-Feedback OPERATIONAL AMPLIFIER," Texas Instruments, Dallas, Texas, 2008.

[78] Texas Instruments, "High-Speed, Closed-Loop Buffer," Texas Instruments, Dallas, Texas, 208.

[79] Texas Instruments Inc., "TLV5618A 2.7-V TO 5.5-V LOW-POWER DUAL 12-BIT 2.7-V TO 5.5-V LOW-POWER DUAL 12-BIT," Texas Instruments Inc., Dallas, Texas, 2002.

[80] STMicroelectronics, "L272," STMicroelectronics, Italy, 2003.

[81] OSRAM Opto Semiconductors GmbH, "SFH2701 High Speed PIN Photodiode," OSRAM Opto Semiconductors GmbH, Regensburg, 2008.

[82] Thorlabs, "Photodiode Tutorial, Theory of Operation," Thorlabs, [Online]. Available: http://www.thorlabs.com/tutorials.cfm?tabID=31760. [Accessed 12 1 2014].

[83] Analog Devices, "Choosing Between Voltage Feedback (VFB) and Current Feedback (CFB) Op Amps," Analog Devices, 2008.

[84] Texas Instruments, "LMH6609 900MHz Voltage Feedback Op Amp," Texas Instruments, Dallas, Texas, 2013.

[85] Analog Devices, "AD8302 : LF–2.7 GHz RF/IF Gain and Phase Detector," Analog Devices, Norwood, MA, 2002.

[86] S. Hobley, "The labratory : Technology Tinkering," [Online]. Available: http://www.stephenhobley.com/build/lh_arduino.html. [Accessed 13 02 2014].

[87] Oxford University Press, Oxford English Dictionary (OED), Oxford: Oxford University Press, 2011.

[88] Atmel, "AVR121: Enhancing ADC resolution by oversampling," Atmel, San Jose, CA, USA , 2005.

[89] J. D. Kramer and C. Jacky, "How to write biblos," vol. 1, no. 1, 2006.

[90] K. Stephan, "Radiometry before World War II: measuring infrared and millimeter-wave radiation 1800-1925," *Antennas and Propagation Magazine, IEEE,* vol. 47, no. 6, pp. 28-37, Dec 2005.

[91] A. Rogalski, “Infrared detectors: an overview,” Warsaw, Poland, 2002.

[92] T. Instruments, *TMP006 User's Guide - SBOU107,* 2011.

[93] September 2 2011. [Online]. Available: http://www.valuetesters.com/Extech-IR100-Infrared-Non-Contact-Thermometer.php.

[94] September 2 2011. [Online]. Available: http://www.parallax.com/tabid/768/ProductID/520/Default.aspx.

[95] Melexis, “MLX90614 family,” 2009.

[96] September 2 2011. [Online]. Available: http://www.fluke-direct.com/shop/itemDetail.do?itm_id=154660&itm_index=0&item=574.

[97] N. Bluzer, “Focal Plane Array”. United States Patent 4614960, 30 September 1983.

[98] J. A. Prescott, “Thermal Camera Arrangement”. United States Patent 5089914, 18 Feb. 1992.

[99] Unitemp, September 2011. [Online]. Available: http://www.unitemp.com/ThermalCameras?gclid=COWPoeSZgasCFUVMpgod_R7AzA.

[100] J. Lloyd, Thermal imaging systems, New York: Plenum Press, 1975.

[101] A. S. o. Photogrammetry, Manual of Remote Sensing, Second Edition ed., D. S. Simonett, Ed., Falls Church, Virginia: The Sheridan Press, 1983.

[102] Encyclopedia Britannica, “Planck's Radiation Law,” September 2011. [Online]. Available: http://www.britannica.com/EBchecked/topic/462936/Plancks-radiation-law.

[103] September 4 2011. [Online]. Available: http://www.google.co.za/imgres?q=dc+motor&hl=en&safe=off&sa=X&nord=1&biw=1333&bih=699&tbm=isch&prmd=ivnsrb&tbnid=E9oNN_YlPr_XdM:&imgrefurl=http://sgmadamotor.en.made-in-china.com/offer/WqtJZQndhYVC/Sell-DC-Motor-RF-385-.html&docid=UfdZixtOFokEuM&w=1186&h=.

[104] D. Cook, Robot Building for Beginners, Second Edition ed., New York: Apress, 2009.

[105] T. Miller, Electronic control of switched reluctance machines, Oxford: Reed Educational and Professional Publishing, 2001.

[106] L. M. Surhone, M. T. Tennoe and S. F. Henssonow, Parallel Communication, VDM Verlag Dr. Mueller AG & Co., 2010.

[107] D. M. Calcutt, F. J. Cowan and G. H. Parchizadeh, 8051 microcontrollers: an applications-based introduction, Oxford: Newnes, 2004.

[108] W. Dargie and C. Poellabauer, Fundamentals of Wireless Sensor Networks: Theory and Practice, West Sussex: John Wiley & Sons Ltd., 2010.

[109] Texas Instruments, “Infrared Thermopile Sensor in Chip-Scale Package,” 2011.

[110] Melexis, “MLX90614 family,” 2010.

[111] Fluke, *Better testing Better prices!,* 2010.

[112] RS Data Sheet, “Stepper motor driver IC SAA 1027,” 1997.

[113] SMBus, “System Management Bus,” 2000.

[114] Edmund optics america, Opticas and optical instruments catalog, Summer 2009 ed., Barrington: Edmund optics, 2009.

[115] Texas instruments, October 2011. [Online]. Available: http://www.ti.com/product/tmp006.

[116] Altuglas International, “plexiglas, Optical and transmission charecteristics,” 2000.

[117] RS Components (SA), October 2011. [Online]. Available: http://za.rs-online.com/web/c/?sra=oss&searchTerm=MLX90614&x=0&y=0.

[118] O. planet, August 2011. [Online]. Available: www.opticsplanet.net/heat-seakers-termal-imagers.html.

[119] nextag, August 2011. [Online]. Available: www.nextag.com/infrared-thermometer/shop-html.

15. Appendices

This chapter includes some things that were omitted from the chapters above but are considered relevant to the final design. Everything available here is also available on the attached CD.

15.1 Attached CD

The attached CD contains many files and folders considered relevant to this project. Please read the 'ReadMe' file in each folder for an explanation of that folder.

The following folders are presented on the CD:

- Electronics
  - *Altium*® files
  - Datasheets
  - *TINA-TI™* simulation files
- Raw ADC data
- Software
  - Arduino Code
  - MATLAB Code
- SolidWorks Files

15.2 Mechanical Design Appendices

Some drawings of the more complex and critical parts are presented here. All .prt, .asm, and .drw files are available on the CD.

15.2.1 Optics

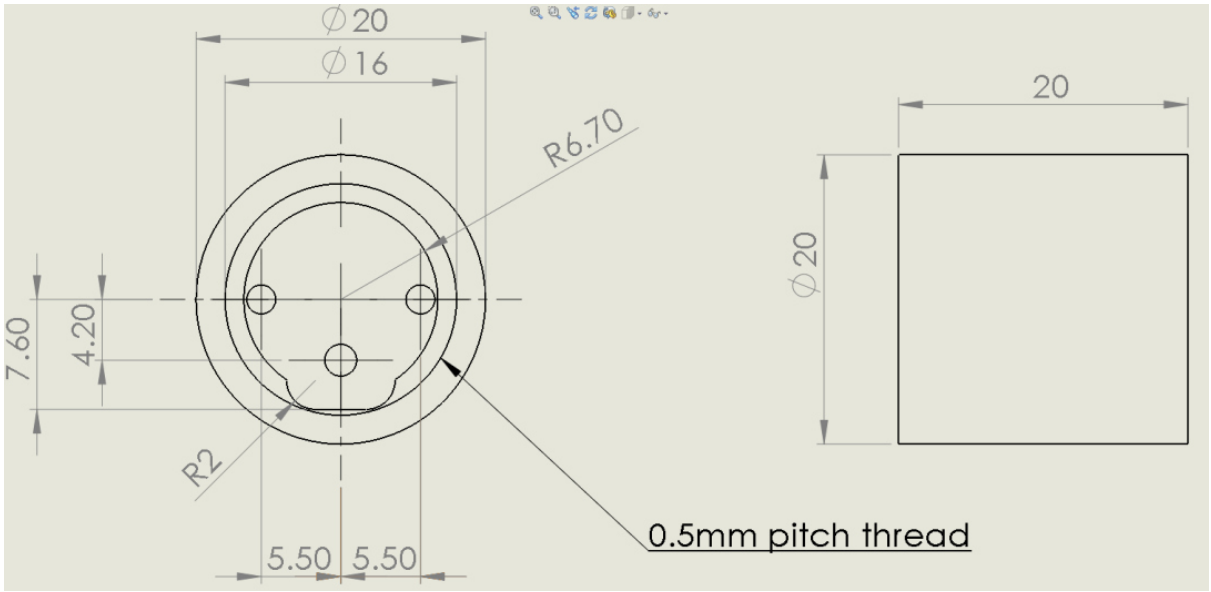

Figure 15-1. 'back mount'. Used to mount the laser and then screw optics into.

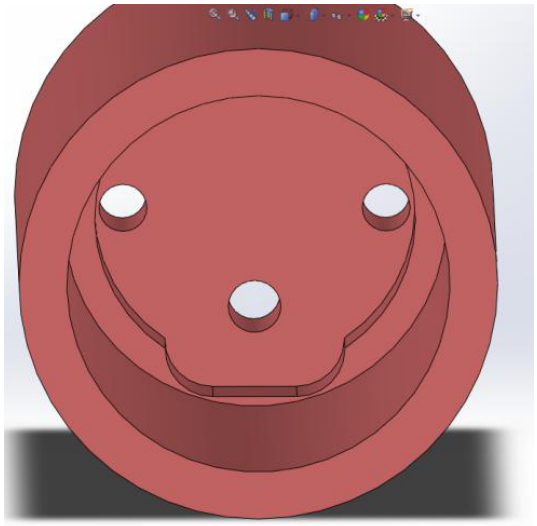

Figure 15-2. 'back mount'. Used to mount the laser and then screw optics into.

15.2.2 Gantry

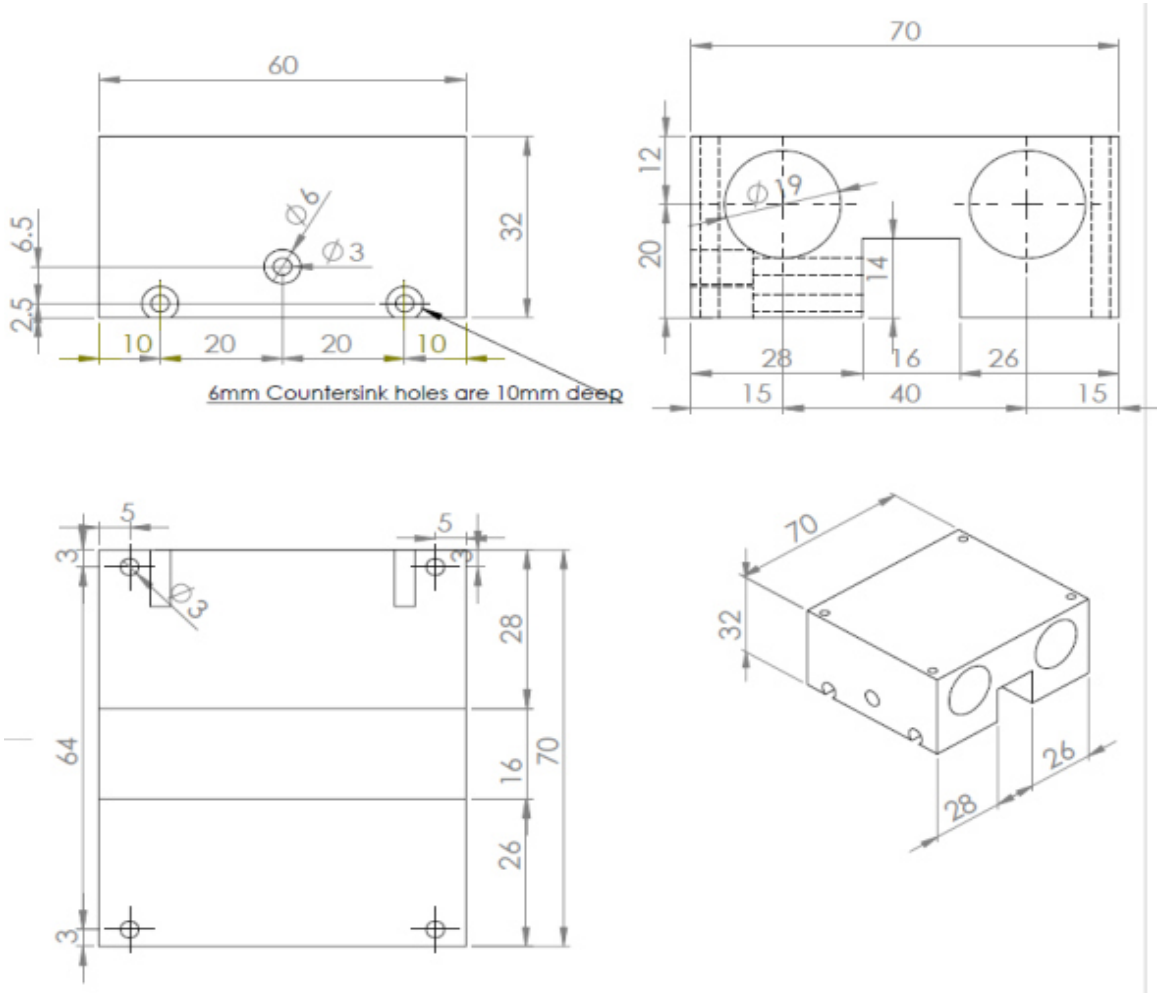

Figure 15-3. ' LaserBase v1'. This is the toolhead mounting platform.

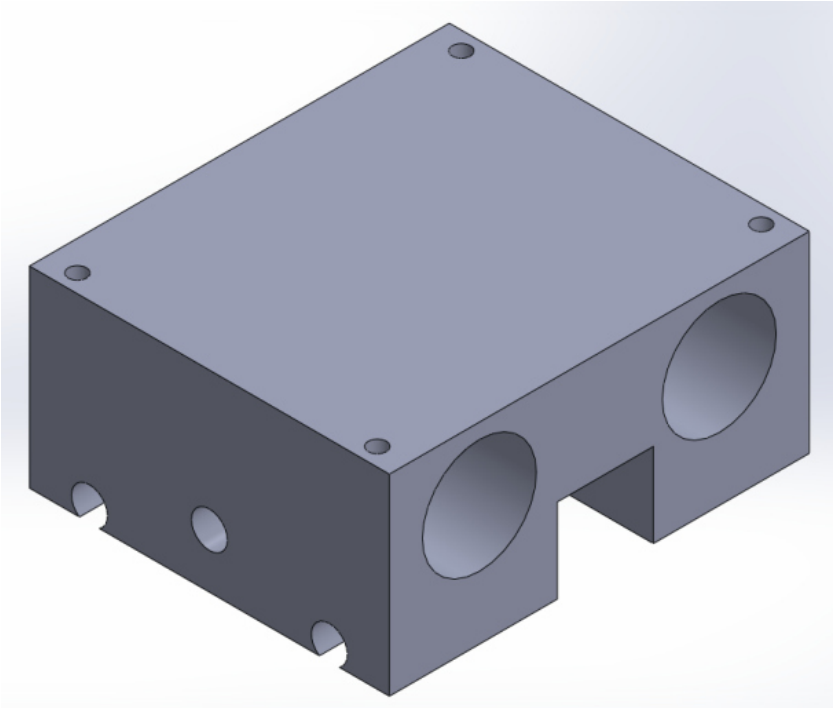

Figure 15-4. ' LaserBase v1'. This is the toolhead mounting platform.

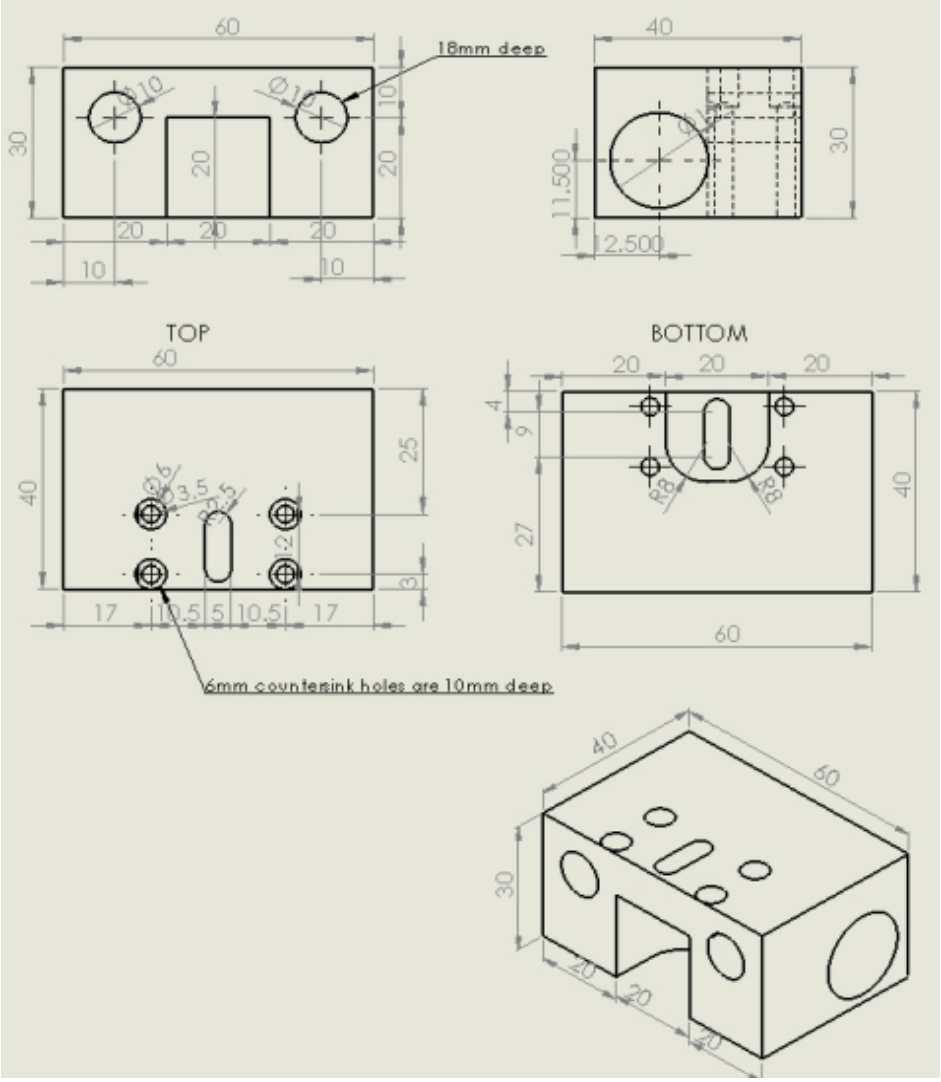

Figure 15-5. 'Endplate Pulley v1'. This is the pulley mount for the moving motor.

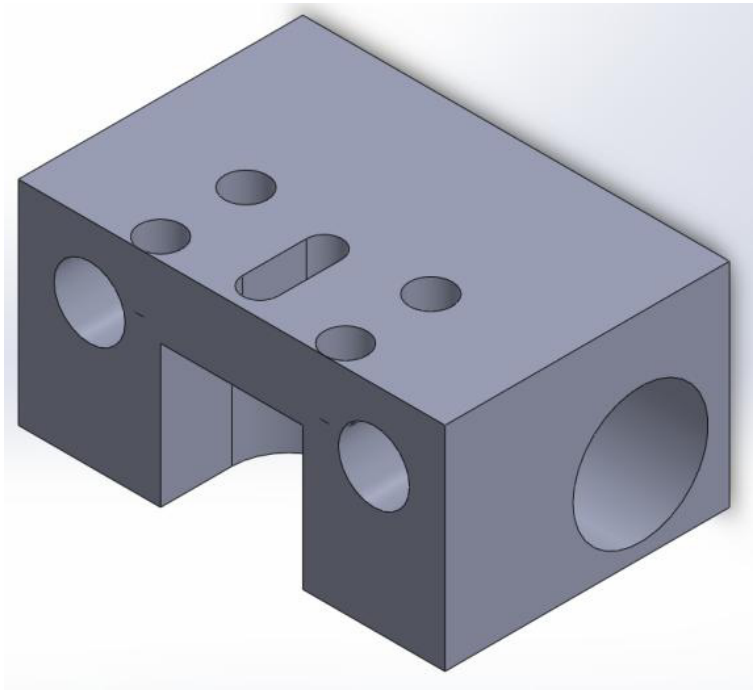

Figure 15-6. 'Endplate Pulley v1'. This is the pulley mount for the moving motor.

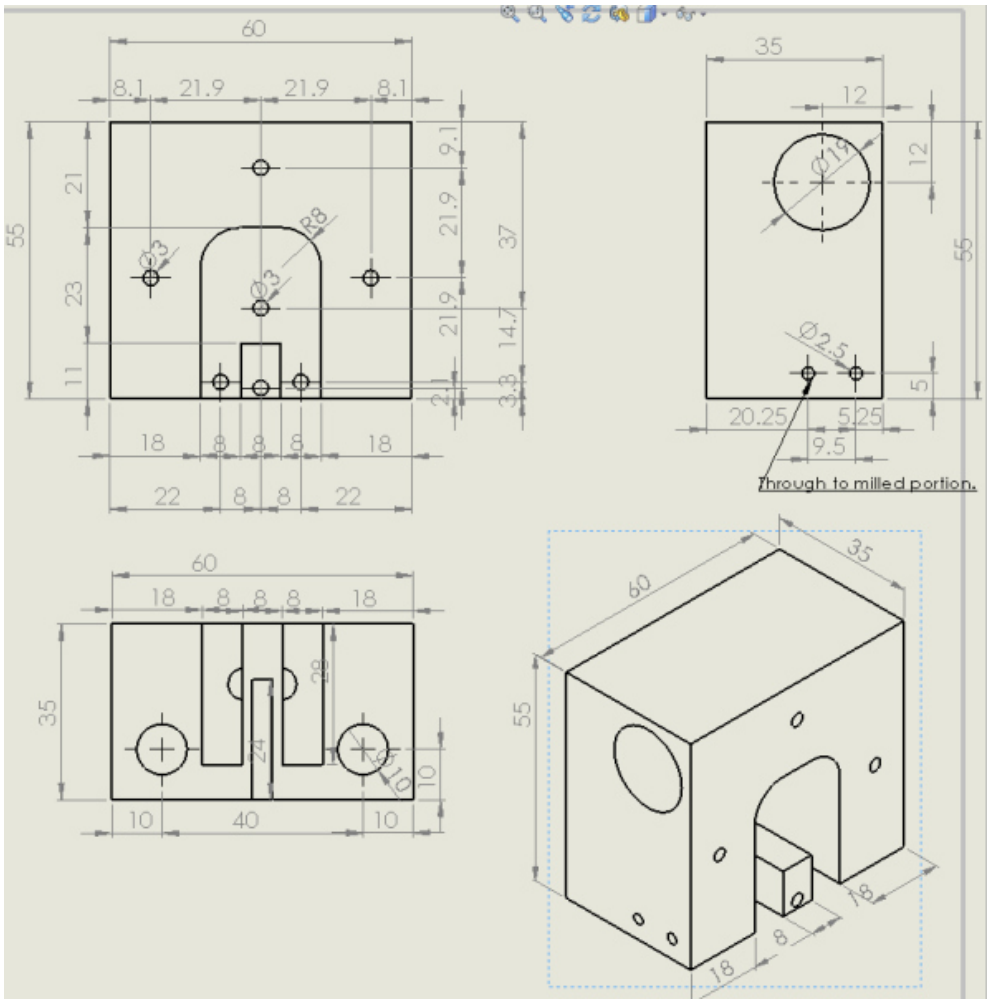

Figure 15-7. 'Endplate v1.1'. This is where the moving motor attaches onto. Also includes homing switch mounting.

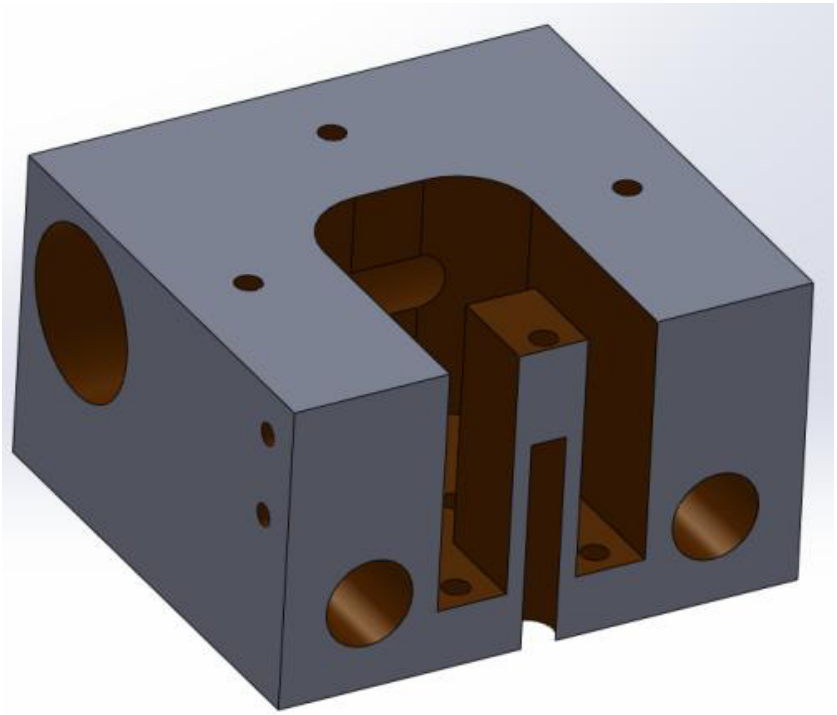

Figure 15-8. 'Endplate v1.1'. This is where the moving motor attaches onto. Also includes homing switch mounting.

15.2.3 Housing

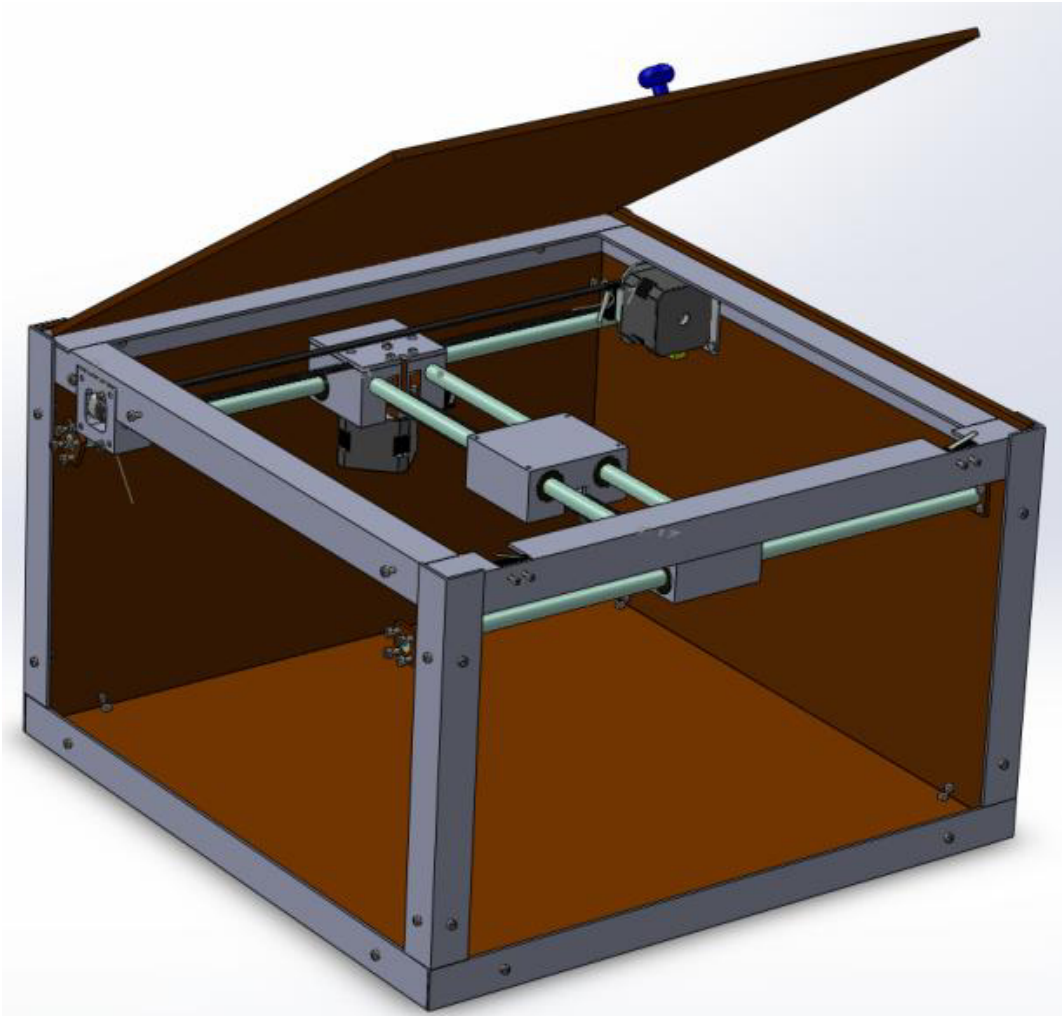

Figure 15-9. 'Assem 1'. A view of the gantry in the housing.

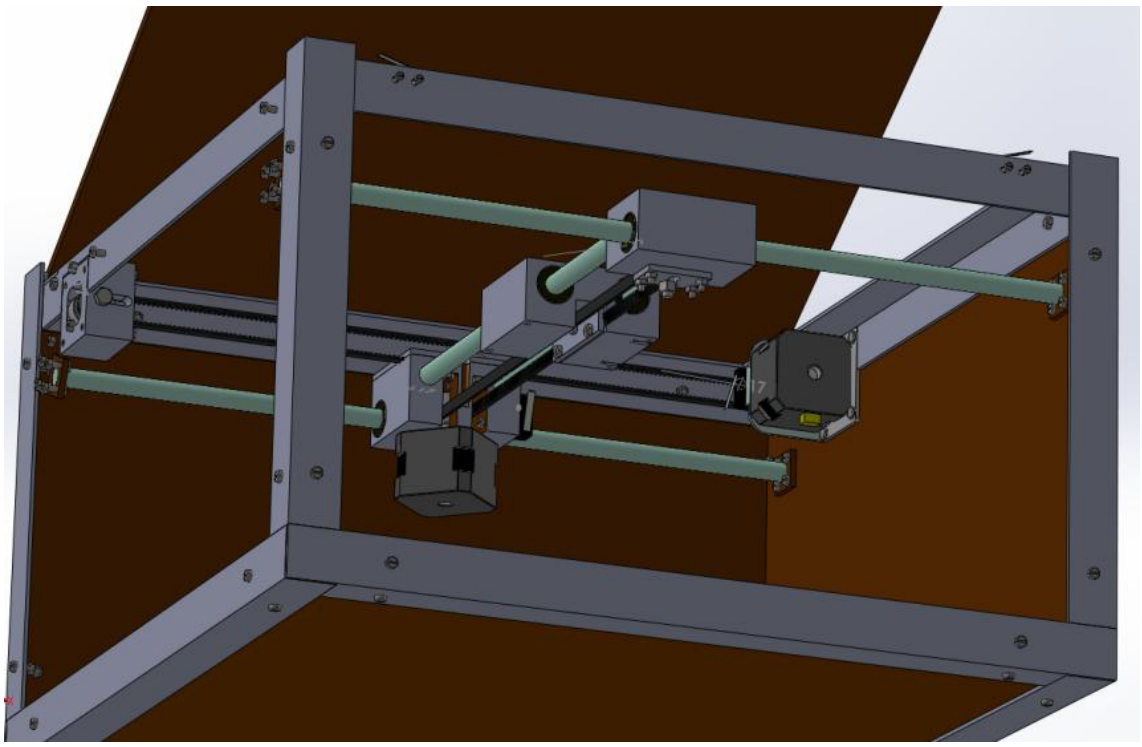

Figure 15-10. 'Assem 1'. Another view of the gantry in the housing.

15.2.4 Test Rig

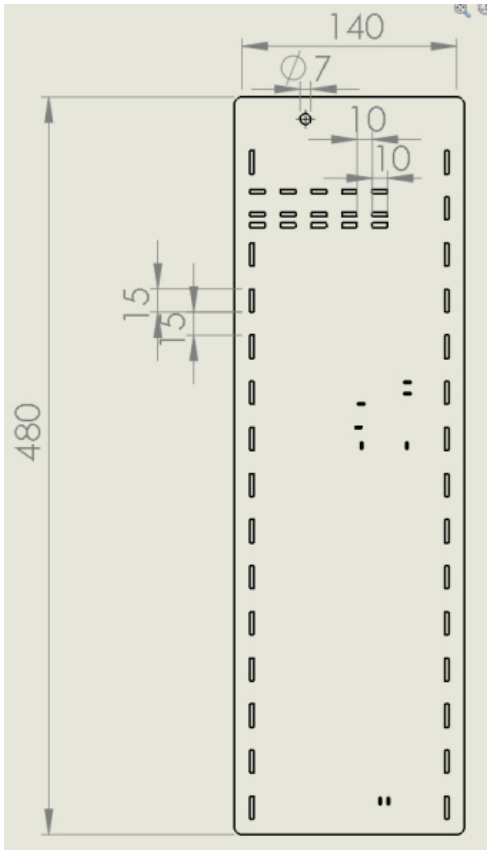

Figure 15-11. 'Testbench platform2'. Testbench mounting for toolhead and digital calliper.

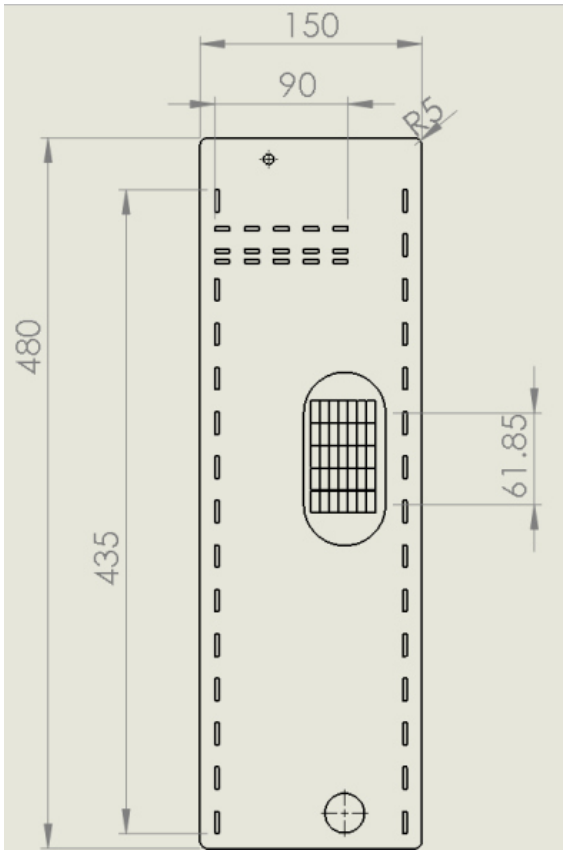

Figure 15-12. 'Testbench platform Under piece'. Testbench mounting for toolhead and digital calliper.

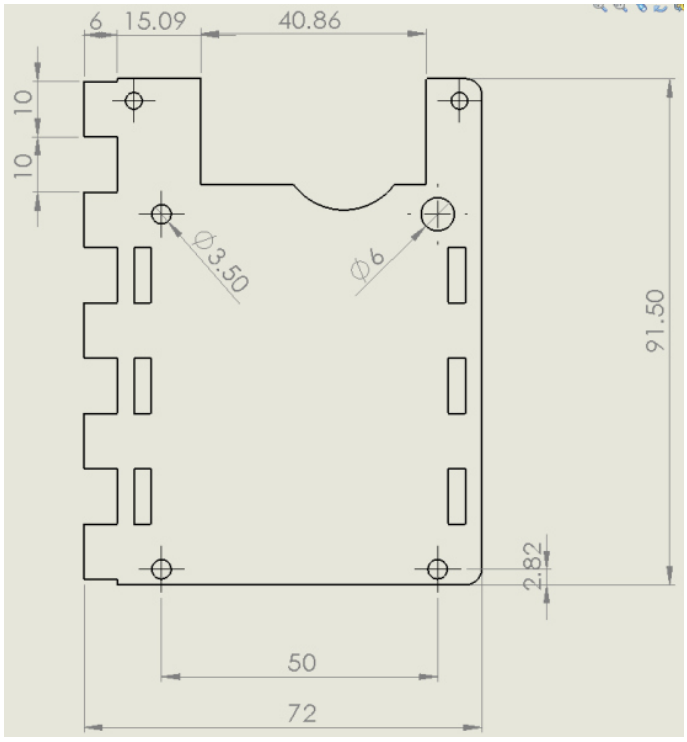

Figure 15-13. 'Testbench Upright 1'. Testbench dummy toolhead mounting platform

15.2.5 Toolhead

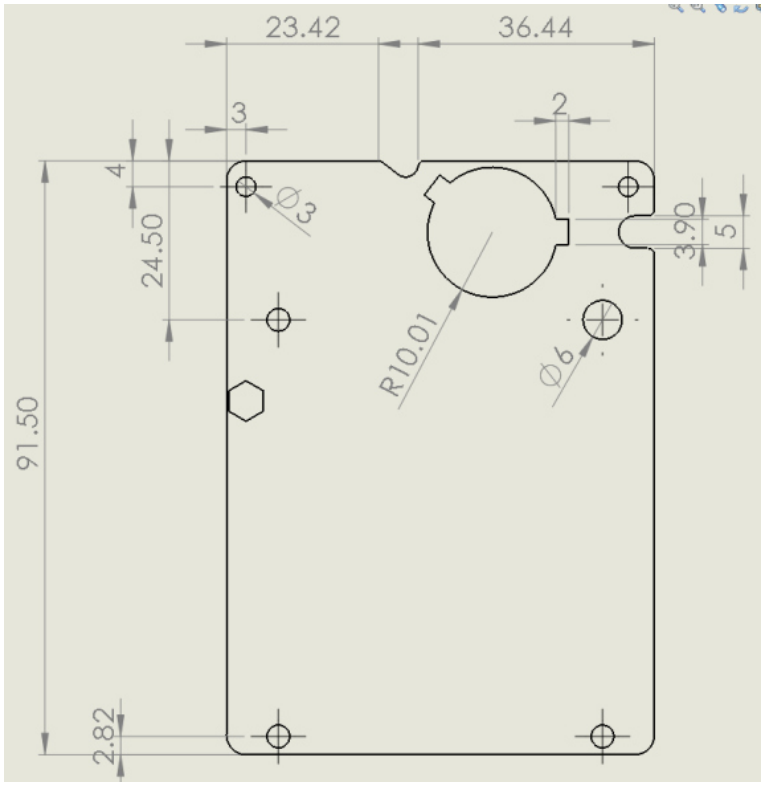

Figure 15-14. 'Driver to optics mount 4mm v3.1'. To mount the laser and laser driver to the toolhead platform

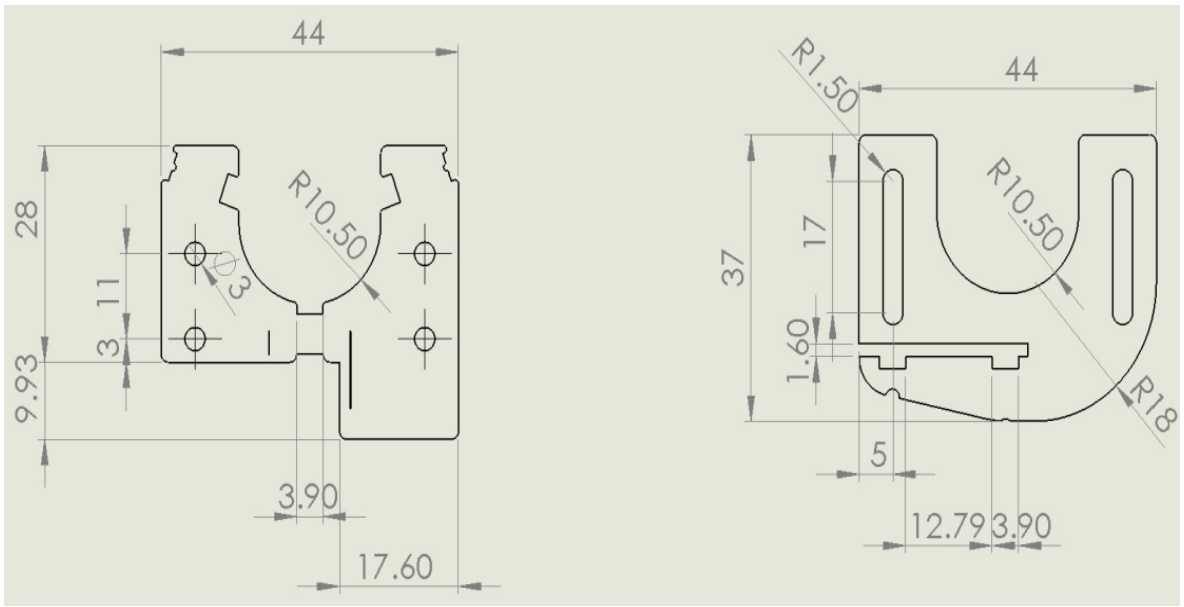

Figure 15-15. 'Photodetector Distance mount Adjustable'. To mount the phase detector board to the laser at adjustable distances

15.3 Software Appendices

The software is not available here, as this would add considerable bulk to the document. Please access the software on the attached CD.

15.4 Miscellaneous photographs

This section includes some photographs taken during design, construction and testing in order to give a general picture of the process. Some of these photographs contain work that was changed in the final design and where discrepancies between these photographs and the above document occur always follow what is stated in the document.

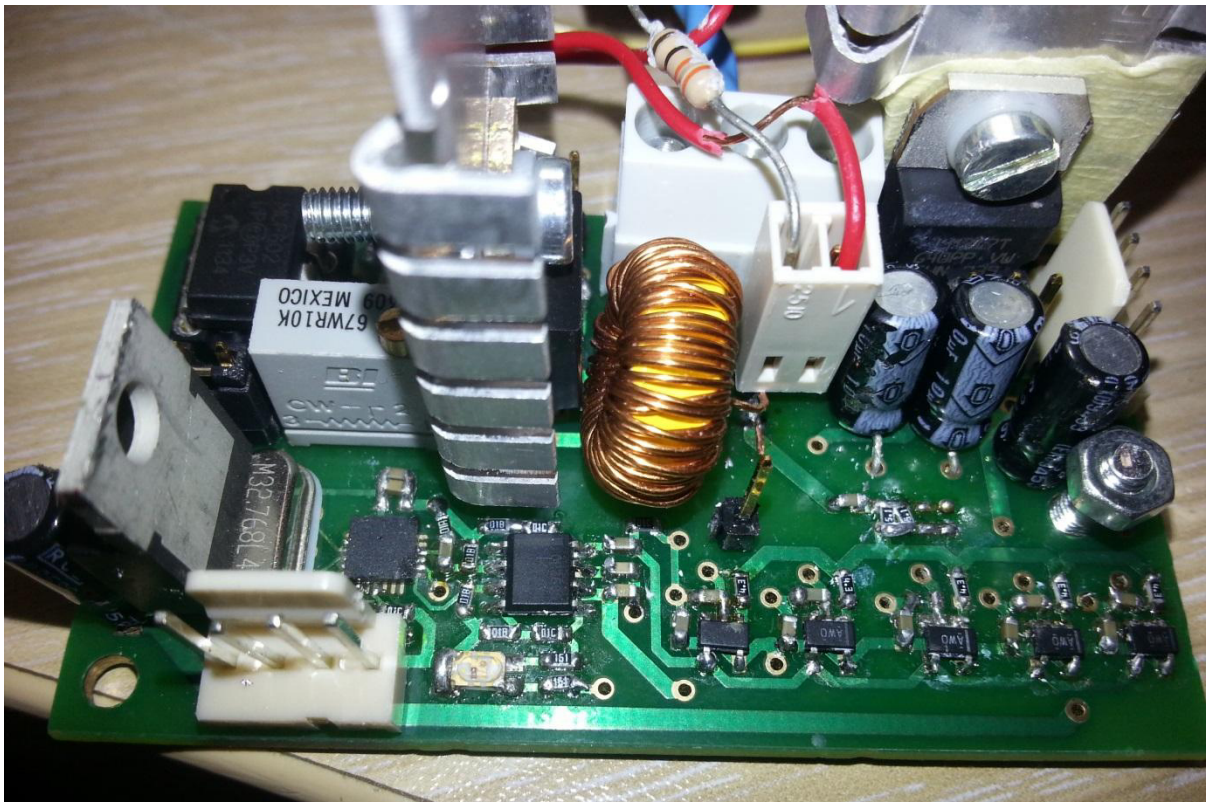

Figure 15-16. Laser driver PCB.

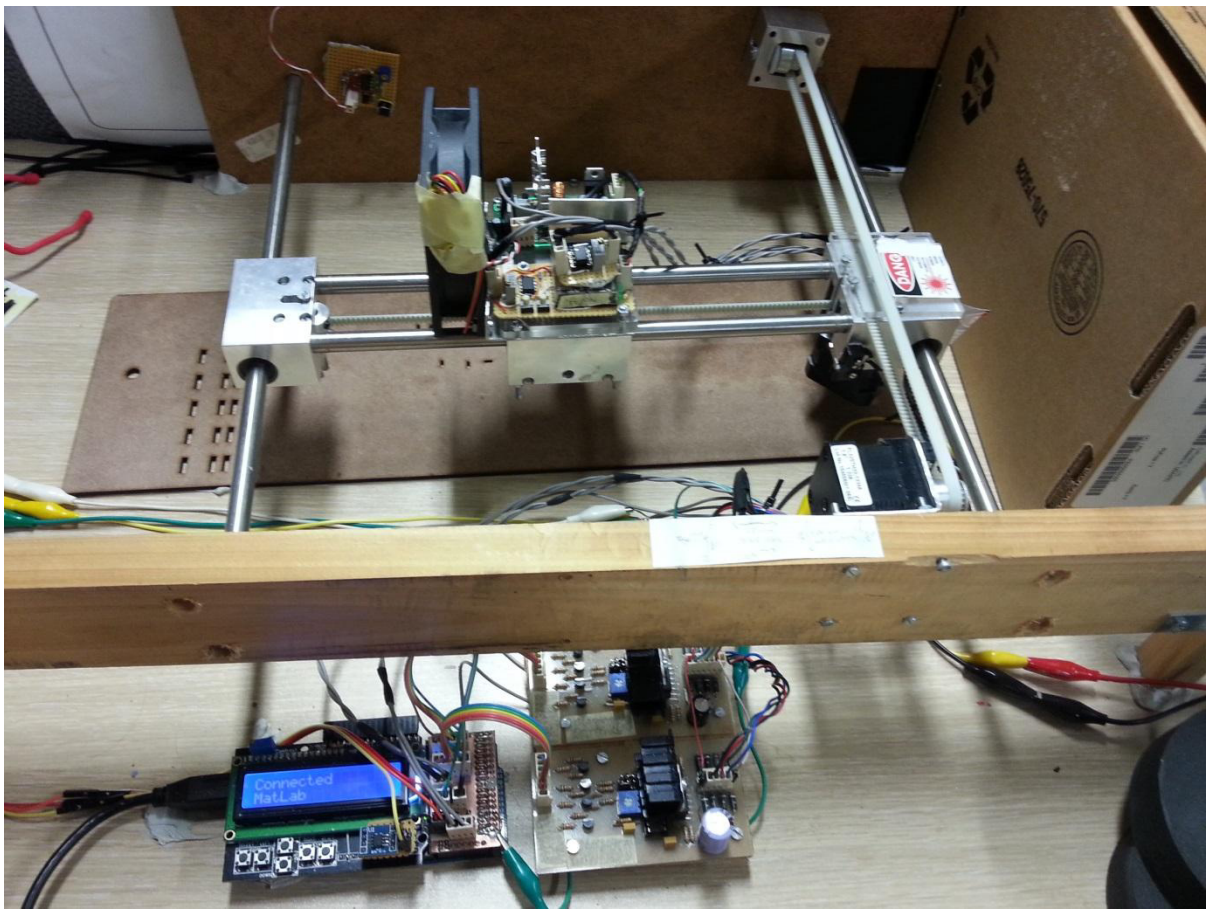

Figure 15-17. Gantry with toolhead mounted.

Figure 15-18. SSI readback from CDCE421a.

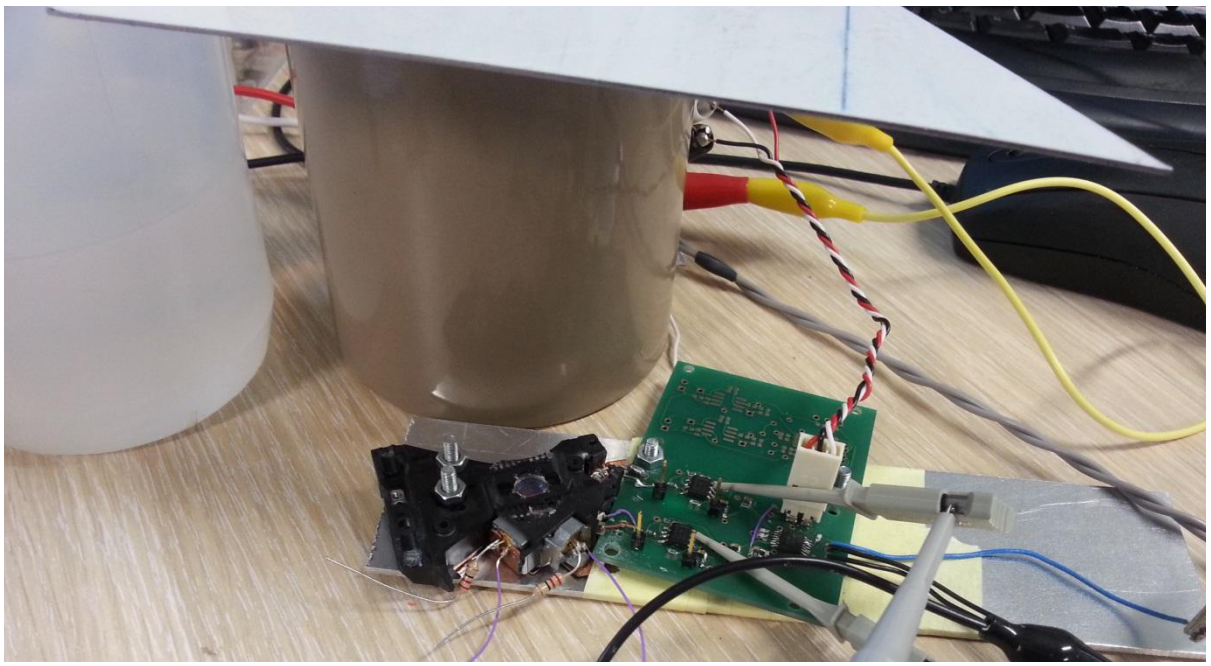

Figure 15-19. Initial testing with DVD optics.

Figure 15-20. Exploded view of optics assembly

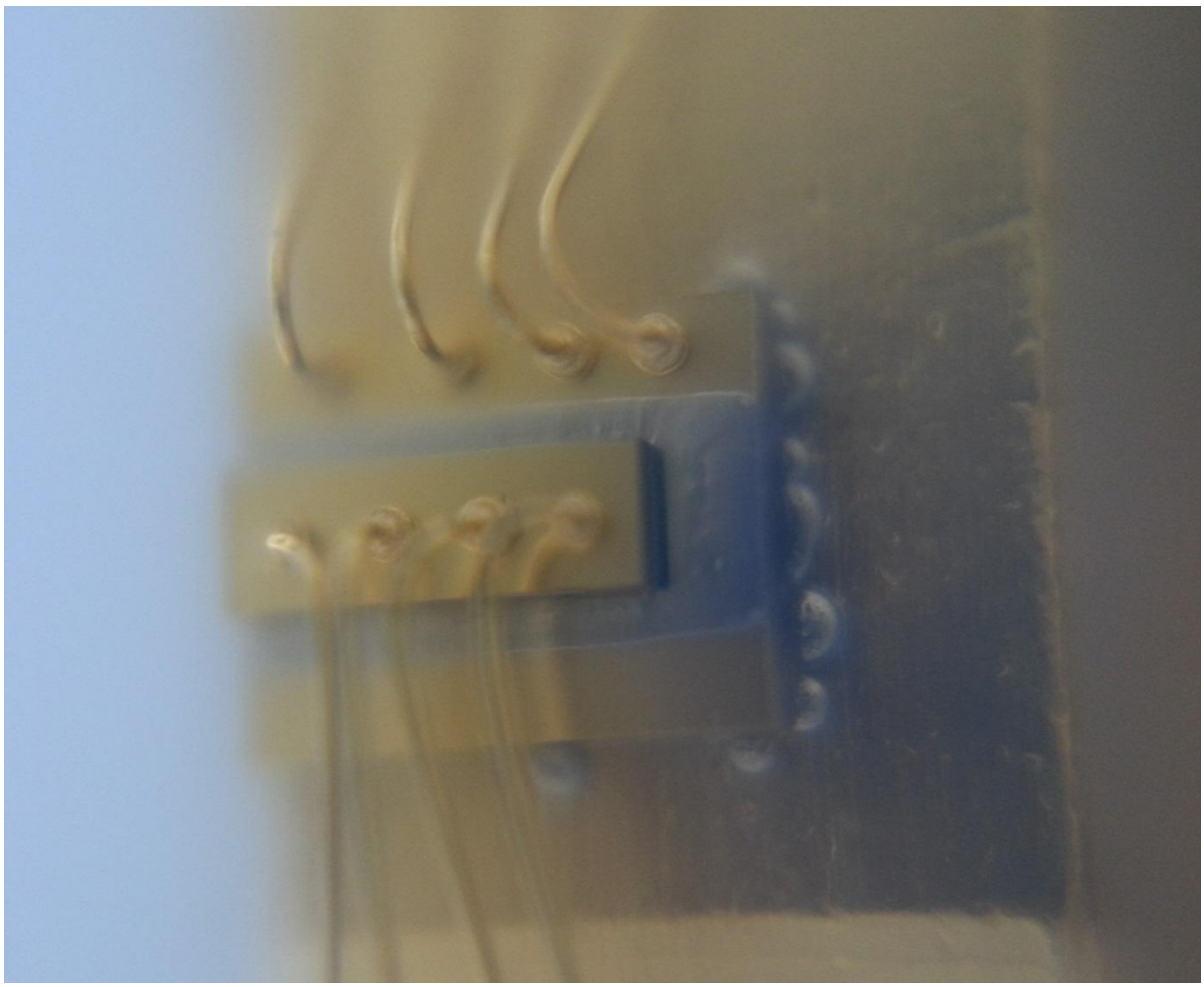

Figure 15-21. Laser Diode close up of lasing element.

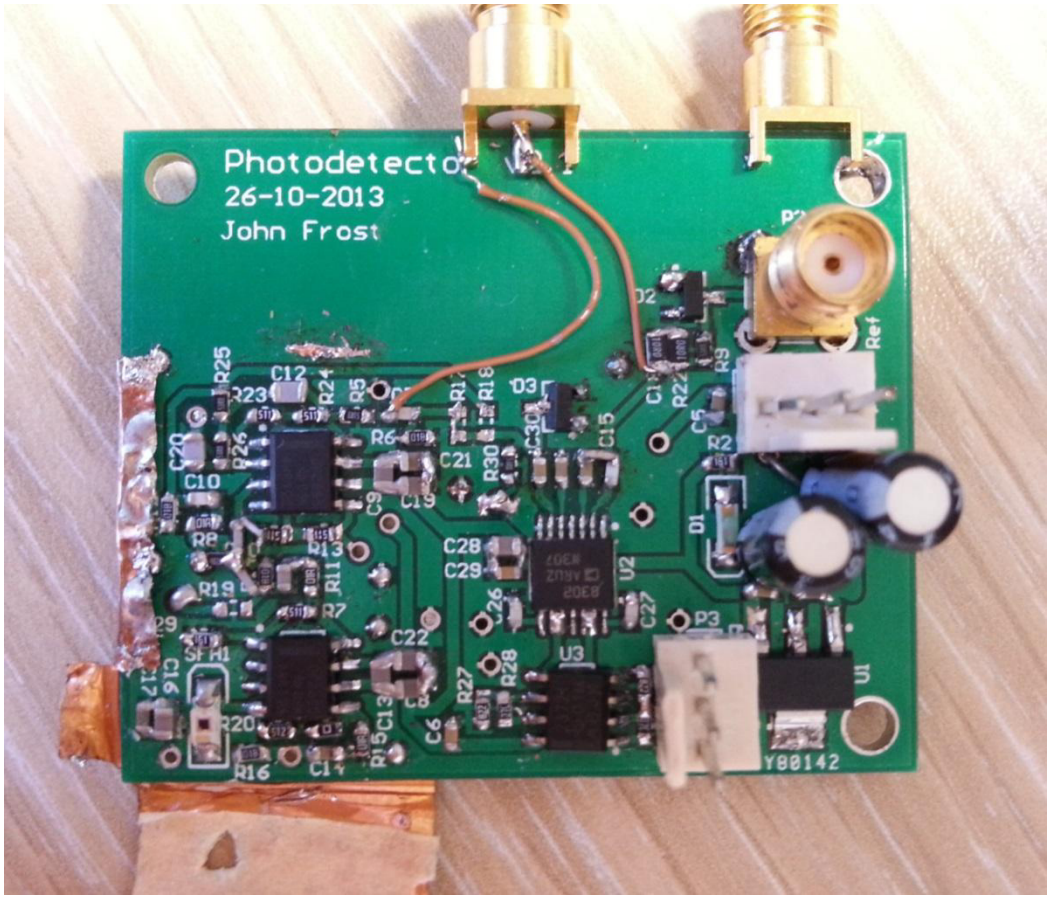

Figure 15-22. Photo sensor and phase detector PCB with SMA test points and shielding (folded back).

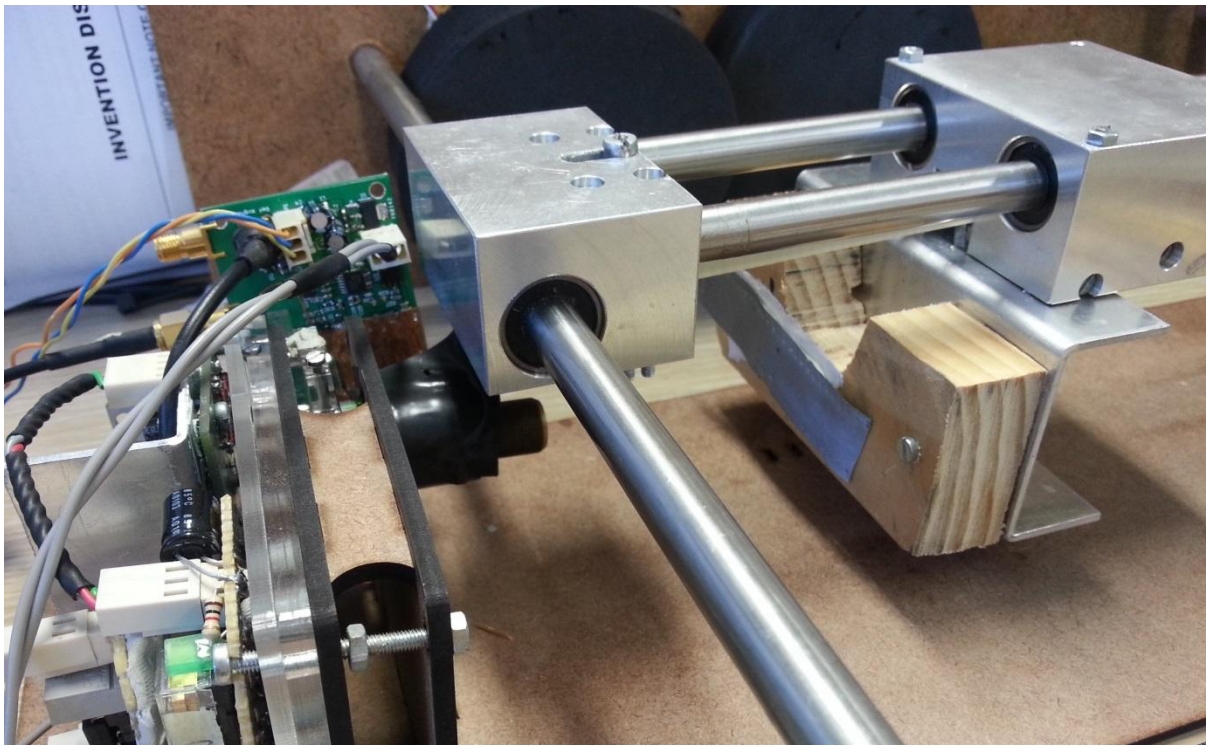

Figure 15-23. Automated test rig. Uses one gantry axis to move reflector.

EBE Faculty: Assessment of Ethics in Research Projects

Any person planning to undertake research in the Faculty of Engineering and the Built Environment at the University of Cape Town is required to complete this form before collecting or analysing data. When completed it should be submitted to the supervisor (where applicable) and from there to the Head of Department. If any of the questions below have been answered YES, and the applicant is NOT a fourth year student, the Head should forward this form for approval by the Faculty EIR committee: submit to Ms Zulpha Geyer (Zulpha.Geyer@uct.ac.za; Chem Eng Building, Ph 021 650 4791).Students must include a copy of the completed form with the final year project when it is submitted for examination.

Name of Principal Researcher/Student: Phillip John Lowne Frost **Department:** ELECTRICAL ENGINEERING

If a Student: YES **Degree:** MSc. Eng. Electrical **Supervisor:** Samuel Ginsberg

If a Research Contract indicate source of funding/sponsorship:

Research Project Title: Three Dimensional Control of a Diode Based Laser Cutter

Overview of ethics issues in your research project:

Question 1: Is there a possibility that your research could cause harm to a third party (i.e. a person not involved in your project)?	Yes	
Question 2: Is your research making use of human subjects as sources of data? If your answer is YES, please complete Addendum 2.		NO
Question 3: Does your research involve the participation of or provision of services to communities? If your answer is YES, please complete Addendum 3.		NO
Question 4: If your research is sponsored, is there any potential for conflicts of interest? If your answer is YES, please complete Addendum 4.		NO

If you have answered YES to any of the above questions, please append a copy of your research proposal, as well as any interview schedules or questionnaires (Addendum 1) and please complete further addenda as appropriate.

I hereby undertake to carry out my research in such a way that

- there is no apparent legal objection to the nature or the method of research; and
- the research will not compromise staff or students or the other responsibilities of the University;
- the stated objective will be achieved, and the findings will have a high degree of validity;
- limitations and alternative interpretations will be considered;
- the findings could be subject to peer review and publicly available; and
- I will comply with the conventions of copyright and avoid any practice that would constitute plagiarism.

Signed by:

	Full name and signature	**Date**
Principal Researcher/Student:	**Phillip John Lowne Frost**	24 May 2014

This application is approved by:

Supervisor (if applicable):	**Samuel Ginsberg**	24 May 2014
HOD (or delegated nominee): Final authority for all assessments with NO to all questions and for all undergraduate research.		24 May 2014
Chair : Faculty EIR Committee For applicants other than undergraduate students who have answered YES to any of the above		